THE BLENDING AND PERMEABILITY OF POLYMERS FOR PACKAGING APPLICATIONS

A Thesis submitted for the degree of Doctor of Philosophy

by

Ian MacIntyre Thomas

Brunel University of West London,
Department of Materials Technology

December 1995

PAGE
NUMBERING
AS ORIGINAL

ABSTRACT

In this study, commercially available isotactic polypropylene (PP) and nylon-6 (PA6) blends and laminates were prepared, to develop a material with optimal water vapour and oxygen barrier properties. The effect of compatibilizers on phase dispersion has been investigated using three commercial Polybond's, PB3002, PB1001, and PB3009. Three compatibilizers prepared in-house were also used as, maleic anhydride(MA) grafted on PP, MA and butyl methacrylate(BMA) co-polymer grafted on PP, and BMA grafted on low density polyethylene. The effect of two silanes(methacrylate functional and vinyl functional) on PP were also investigated and also the plasticization of PA6 with formic acid. The results were compared with a commercial blend of PP and PA6, Orgalloy R-6000.

Light microscopy with phase and fluorescence contrast has been used for morphological evaluation. Chemical changes were studied by Fourier Transform Infrared Spectroscopy and rheology by dynamic and steady state measurements. Barrier properties were determined gravimetrically for water vapour and organic solvents, and for oxygen by an Oxtran apparatus.

The results have shown that phase dispersion can be more easily explained by molecular interactions than by the rheological parameters. The blend slip factor has been improved however by compatibilizers and consequently the phase dispersion, which had little effect on the barrier properties of the blends and indeed the laminates were more effective water vapour barriers. The availability of particular functional groups, which can interact with the permeant is the most important parameter, which can be affected by processing and blending conditions. The addition of hydrophobic functional groups into polypropylene was therefore the most effective method for enhancing the barrier properties of polypropylene. Cross-linking of the matrix polymer has improved the barrier properties to a lesser extent. It has also been shown, that PP solvent permeability (particularly di-chloromethane) can be improved, by silane addition.

CONTENTS

ACKNOWLEDGEMENTS

I would like to thank my project supervisor, Dr Drahosh Vesely, for the encouragement, supervision and technical advice which he has given me throughout the term of this project.

I am grateful to CarnaudMetalBox, in particular to David Brooks, whose generous sponsorship enabled me to complete this thesis.

My thanks go to all the technicians and administrative staff of the Materials Technology Department, Brunel University for their kind assistance and guidance with my experimental work. Special thanks are also due to the research staff and students, especially my colleagues Patrick Morrissey, Yves Dutheillet-Lamonthezie and Paul Disley for their kind support and encouragement.

ABBREVIATIONS USED

AA = Acrylic Acid
AA-g-PP = Acrylic Acid Grafted on PP
ABS = Acrylonitrile-Butadiene-Styrene, ter-polymer
aPS = atactic Poly(styrene)
ASTM = American Society for Testing Materials
a_T = Temperature Shift Factor
ATR = Attenuated Total Reflectance
BA = Butyl Acrylate
BA-g-LDPE = Butyl Acrylate grafted on LDPE
Barrer = 10^{-10} x RPU's
BC = Block Co-polymer
BMA = Butyl Methacrylate
BMA-g-PP = BMA grafted on PP
BMAcoMAgPP/(BMAcoMA)-g-PP = Butyl Methacrylate co-polymerised with Maleic Anhydride grafted onto Polypropylene
BOPP = Bi-oriented Poly(propylene)
CGS = Centimetre Gram Second
CLS = Classical Least Squares
CTFM = Constant Thickness Filmaker
D = Diffusion Coefficient
DBP = Di-tert-Butyl Peroxide
DBTDL = Dibutyl Tin Dilaureate
DCM = Dichloromethane
DCP = Dicumyl Peroxide
DPBF = Diphenylisobenzofuran
D_M = Mutual Diffusion Coefficient
DMA = Dynamic Mechanical Analysis
DSC = Differential Scanning Calorimetry
D^* = Self Diffusion Coefficient
EAA = Ethylene Acrylic Acid co-polymer
EAAN = Poly (ethylene acrylic acid ester/maleic acid anhydride)
E_D = Activation Energy of Diffusion
EOS = Equation of State
EPB = Engineering Polymer Blends
E_S = Activation Energy of Sorption
ESR = Electron Spin Resonance
Eth-co-MA = Ethylene co-polymerised Maleic Anhydride
EVA = Poly(Ethylene-co-Vinyl Acetate)
EVOH = Poly(Ethylene-co-Vinyl Alcohol)
FTIR = Fourier Transform Infrared
G = Gibbs Free Energy

GC = Gas Chromatography
GLC = Gas Liquid Chromatography
GRP = Glass Fibre Reinforced Plastic
H = Enthalpy
HDPE = High Density Poly(ethylene)
HMD = Hexamethylenediamine
HeNe = Helium/Neon
IGC = Inverse Gas Chromatography
Inj. = Injection
ILS = Inverse Least Squares
IV = Intrinsic Viscosity
LCP = Liquid Crystalline Polymer
IPA = Isophthalic Acid
IPN = Interpenetrating Polymer Networks
IPGC = Inverse Phase Gas Chromatography
IRS = Internal Reflectance Spectroscopy
L = Time Lag in permeation
LCST = Lower Critical Solution Temperature
LDPE = Low Density Poly(ethylene)
LM = Light/Optical Microscopy/Microscope
LLDPE = Linear Low Density Poly(ethylene)
LVSEM = Low Voltage Scanning Electron Microscopy
MCT = Mercury Cadmium Telluride
MIR = Multiple Internal Reflectance
MA = Maleic Anhydride
MA-g-PP = MA grafted onto Poly(propylene)
MA-g-MSA = MA grafted onto Maleic-Styrene-Acrylic terpolymer
MAP = Modified Atmospheric Packaging
MD = Machine Direction
M_n = Number Average Molecular Weight
MW = Molecular Weight(average)
MWD = Molecular Weight Distribution
n = Number of Moles
η = Shear Viscosity
η^* = Dynamic Complex Viscosity
N = Polymer Index
NDB = Negatively Deviating Blends
Θ = Surface Interaction Ratio
ϕ = Volume Fraction
OPA6 = Oriented Nylon-6
OTR = Oxygen Transmission Rate = Permeability/film thickness
p^0_1 = Vapour Pressure
P = Permeability
PA = Polyamide
PA6 = Nylon-6 (Polycaprolactam)

PCL = Poly(caprolactone)
PCR = Principal Components Regression
PDMS = Poly(dimethylsiloxane)
PE = Poly(ethylene)
PEG = Poly(ethylene glycol)
PET = Poly(ethylene terephthalate)
PLS = Partial Least Squares
PMMA = Poly(methyl methacrylate)
PMS = Poly(Maleic acid-co-styrene)
PnBMA = Poly(n-Butyl Methacrylate)
PO = Polyolefins
PP = Isotactic Poly(propylene)
PPO = Poly(2, 6-dimethyl-1, 4-phenylene oxide)
Pr = Pressure
PS = Poly(styrene)
PVdF = Poly(vinylidene fluoride)
PVME = Poly(vinyl methyl ether)
R = Gas Constant, 8.31432 J/mol deg.
RDA II = Rheometrics Dynamic Analyzer
RI = Refractive Index
RPM = Revolutions Per Minute
RPU = Recommended Permeability Unit = **cm^3(STP) cm /cm^2 /s /cmHg**
R6000 = Atochem Orgalloy R-6000 (Commercial PA6/PP blend)
$\mathcal{S}$ = Entropy
S = Solubility Parameter
SAXS = Small Angle X-Ray Scattering
SAN = Poly(Styrene-co-Acrylonitrile)
SANS = Small Angle Neutron Scattering
SALS = Small Angle Light Scattering
SD = Spinodal Decomposition
SEBS = Styrene-ethylene/butylene-styrene triblock co-polymer
SEBS-g-MA = Maleic Anhydride grafted SEBS
SEM = Scanning Electron Microscopy/Microscope
SI = System International
SINC = Solvent Induced Crystallisation
SMA = Styrene-co-Maleic Anhydride co-polymer
SPE = Solid Phase Extraction
STEM = Scanning/Transmission Electron Microscopy/Microscope
St-MAA = styrene-methacrylic acid co-polymer
t = Time
T = Temperature
TD = Transverse Direction
TEM = Transmission Electron Microscopy/Microscope
THN = Tetrahydronaphthalene
T_g = Glass Transition Temperature, °C

T_m = Melting Point, °C
TPA = Terephthalic Acid
TPU = Thermoplastic Polyurethane
UCST = Upper Critical Solution Temperature
VCM = Vinyl Chloride Monomer
WVTR = Water Vapour Transmission Rate
X = Interaction Parameter
x = Spinodal Interaction Parameter
XLPE = Cross-linked Polyethylene
XLPP = Cross-linked Polypropylene

CHAPTER 1 - INTRODUCTION

1.0 Packaging Materials

The function of packaging is to protect the contents from the environment before reaching the customer. Polymers used for packaging have a shorter useage history than glass or metal. So, factors which promote polymers ahead of other packaging materials include, the economics of manufacture, the ability to print information on the package, processability into a variety of shapes, and lightness, the latter leading to economies of transport and storage. The majority of polymers fall into one of three categories[1]:

(1) Good barrier to water vapour but poor barrier to oxygen

(2) Good barrier to oxygen but poor barrier to water vapour

(3) Excellent barrier properties, but expensive

The barrier properties of tinplate, glass, aluminium (both sheet and foil), and ceramic materials are far superior to polymers. They are however, heavy and suffer from corrosion and brittleness, and their shapes are limited to cylindrical or rectangular. A survey of the properties and applications of the main polymers used in packaging is given in Table 1.

Nearly all polymers used in packaging have softening and melting temperatures in the range 70-270 °C, which allows them to be shaped by melting and then extruding from a screw extruder or by injection molding[2]. In both cases, extra strength is imparted to the material by stretching near the glass-transition temperature. This resultant extra degree of molecular orientation also improves in some cases the gas barrier properties.

1.1 Polymer Permeability

Transport of gas and vapour molecules is affected by several parameters. Temperature, the chemical nature of the matrix and the penetrant, as well as their molecular weights, matrix cross-linking, crystallinity, are some of the most important parameters which were considered in the past[3]. The temperature effects are particularly important since in the case of food packaging, containers are subject to high sterilization temperatures and low refrigeration temperatures.

Temperature changes have a major effect on barrier properties, with permeation normally

increasing with temperature and within the normal temperature range encountered by packaging, it is generally the case that[4] :

$$\log P \propto 1/T \text{ ---------- [1]}$$

It would of course be necessary to include a proportionality constant in equ'n.[1]. Polymer film permeation rate data taken at various temperature should give a straight line when the logarithmic form is plotted as a function of 1/temperature. Extrapolation to the temperature of interest, from data at other temperatures, is then possible. The slope is not constant for all films and gases and for vapours this relationship will not necessarily be true, particularly where known vapour/film interaction occurs.

Due to the chemical nature of O_2 and H_2O, the polar H_2O plasticizes polar high oxygen barrier materials like EVOH, making them poor H_2O vapour barriers at moderate humidities, and even diminishing their oxygen barrier capabilities above 60% RH. Similarly, non-polar O_2 permeates more rapidly through the non-polar, low oxygen barrier materials, due to the relative smallness of the molecule.

Polymer films are defined as being material of 0.25 mm or less thick, and the polymers used include, LLDPE, LDPE, HDPE, oriented/non-oriented PP, PA6, and PET. LLDPE is often the popular choice and when co-polymerized with EVA, such films will stretch elastically to over 100% and still recover. Oriented PP co-polymer with PE is reel fed, to give a heat sealable film[5]. Various factors such as appearance, transparency, sealability, cost etc., decide on whether or not co-extruded polyolefin/EVOH films are used instead of those based on aluminium foil (usually included for cosmetic reasons since production pin-holes are difficult to prevent) or PVdC.

In order to be a good all-round barrier material, the polymer must possess the following properties[6]:

(i) some degree of polarity such as found in nitrile, chloride, fluoride, acrylic, ester, hydroxyl or amide groups.

(ii) high chain stiffness.

(iii) inertness to the permeating species.

(iv) close chain-to-chain packing ability brought about by molecular symmetry or order,

crystallinity or orientation.

(v) some bonding or attraction between chains.

(vi) high glass transition temperature.

Linear polymers with a simple molecular structure lead to good chain packing and lower gas permeability than a polymer where the backbone contains bulky side groups. By increasing the crystallinity of LDPE from 50% to the 80% of HDPE, a four fold decrease in oxygen barrier can be achieved. By elongating a crystalline polymer, thus effecting the molecular orientation, reductions of 50% can be observed in oxygen permeability. This is particularly relevant in the bottle blowing process. Although humidity has no effect on the oxygen permeability of HDPE, or SAN, the PA6 oxygen permeability will increase five fold, when the humidity rises from 0% to 100%.

Some researchers suggest that since small molecules diffuse faster than large ones and streamlined molecules diffuse faster than bulky ones, the solubility of the penetrant will be greatly affected by steric factors. Polar molecules diffuse more rapidly than non-polar ones and the effect is more pronounced in polar polymers.

Unfortunately there are to many exceptions from the above guidelines to make them universally applicable, which reflects our lack of understanding of the complex polymer permeation process.

1.2 Objectives of the Study

The aim of the project was to design a packaging material which would have optimal water vapour and oxygen barrier properties, and possibly to organic solvents. A thermoplastic polymer blend of a commodity polymer to provide water vapour barrier with an engineering polymer for oxygen barrier properties, in which the phase dispersion was optimised for a barrier packaging application was selected for economic and recyclability reasons, instead of using a laminated/co-extruded structure.

For investigating in this work the resulting property, W, of a polymer blend, the property could be described by the following equation :

$$W = W_1 c_1 + W_2 c_2 + I_t c_1 c_2 \text{ ---------- [2]}$$

where W_1 and W_2 are the property values of the individual components and c_1 and c_2 their respective concentrations. I_t is an interaction coefficient that describes the level of synergism or thermodynamic compatibility of the components in the mixture. In this work, the final properties of polymer blends made with immiscible components, such as PP and PA6, are significantly affected by the size and shape of the dispersed phase. This depends upon several factors, including the melt viscosities of the components, interfacial tension, and adhesion between the two phases.

The necessary condition for miscibility is the free energy change in the mixture is ≤ 0, and also equal to the change in the mixture enthalpy minus the product of the temperature and the change in the entropy of the mixture. When the molecular weight of the blend polymers increases, the entropy change becomes small or zero. Phase separated immiscible blends can be defined therefore in terms of their properties being a function of volume fraction and a selected measure characterising the two phase structure. A third component compatibilizer can promote some miscibility of the phases and a compatibilized immiscible blend is termed a polymer alloy.

Hence, the prescence of a third component graft co-polymer of a similar structure to the matrix phase, could reduce the dispersed phase size, by lowering the interfacial tension between the two phases. In this work, an alternative compatibilizer was introduced, a polymer with a polar functional group, for modifying the viscosity of one of the phases, and hence the viscosity ratio, and thus improve the blending process. In order to improve the phase dispersion, which is important for maintaining matrix mechanical properties, and clarity, it was thought that the melt shear viscosities of the two components, PP and PA6, should be matched. Plasticization of the higher viscosity phase is one option or cross-linking the lower viscosity phase is another, or a combination of these, either before or during blending. Cross-linking or other chemical changes of the matrix could also significantly affect the blend oxygen permeability.

Development of a blend has a cost/benefit over a new homopolymer particularly if the new blend material can have several applications, which a new homopolymer is unlikely

Table 1 : Properties of Polymers used in Packaging[7]

Material	*Oxygen Permeability cm^3 mm m^{-2} d^{-1} bar^{-1} at 23 °C*	*Water Vapour Permeability g mm m^{-2} d^{-1} bar^{-1} at 25 °C*	*Solvent Chemical Resistance*	*Cost per kg £*
HDPE (film extrusion)	40	0.25	good except non-polar	0.49 [8]
PP (co-polymer)	60.5	0.55	good except non-polar	0.54 [8]
LDPE (film grade)	190	0.69	good except non-polar	0.50 [8]
LLDPE (film grade)	190	0.6	good except non-polar	0.49 [8]
PET	2.7 (amorphous) 1.4(crystal--line)	0.8	good	1.50[9]
PA6	0.98-1.02 (50% RH)	2.33-2.63 (50% RH)	excellent	2.10[9]
EVOH EVAL-F	0.003(RH 0%) 0.014(RH 75%) 0.30(RH 100%)	1.0 (50% RH)	good	5.00[9]
SAN	0.40	2.0	fair	1.50[9]
ABS	40	5.0	poor	1.65[9]
PS	160	2.0	poor	0.78[8]
Orgalloy R6000(pellets)	2.2 for a 72.2 μm film at 50% RH	1.55	good	2.80[9]
PVdC(Saran) Extra High Barrier MA co-polymer	0.02 at 75% RH	0.04 at 38 °C 90%RH	good	2.00[9] (non-MA co-polymer)

to have. Although the resulting blend may have several applications, compatibilizers are often specific, normally based on one of the components, usually the cheaper one, since the levels of grafting are low and also that the compatibilizer development costs are significantly high.

Polymer blends are used extensively for their cost effectiveness and optimisation of properties. The major problem however is to obtain a good dispersion of phases, so that the mechanical properties and clarity of the homopolymers are maintained. Polymers with dissimilar melt viscosities are often difficult to mix and for this reason the mechanism of phase dispersion has been extensively studied. There are several theories proposed to explain phase dispersion in uncompatibilized PP/PA6 blends, which form coarse mixtures, with large particle size, easily deformed into strings[10-12]. Nevertheless, PA6/PP blends offer lower moisture absorption, improved processability, good impact resistance, and good flexural modulus, compared to PA6.

The polymers used in packaging fall into two main price groups, depending on the complexity of their manufacture and the relative cost of the chemical intermediates used. The simpler and cheaper materials are the polyolefins, followed by PVC and PS. Next are the nylons, PET, EVOH, ABS, PVdF and PVdC. For this work, the vast choice of polymers for packaging was narrowed down within certain price margins, to a compromise between O_2 and H_2O barrier materials. Commercial considerations resulted in PP co-polymer, for water vapour barrier, and PA6 for oxygen barrier being selected. The environmentally friendly oxygen barrier materials are hydrophillic, but also provide good organic solvent resistance. PP was preferred over HDPE for water vapour barrier, because of easier processability, although PP is slightly more permeable to water vapour and slightly more expensive. PA6 was selected since it is cheaper than EVOH. PET is cheaper but requires orientation, an extra cost. PVdC is competitively priced but is environmentally undesirable, in Europe, due to the chlorine content, where burning can produce hydrochloric acid.

1.3 Research Programme

The following objectives for this research were therefore identified:

i. The selection and characterisation of suitable barrier polymer resins for pilot scale melt blending, within optimal barrier/cost constraints.

ii. The creation of a usable multi-phase material with H_2O and O_2 permeabilities equal or better than the homopolymers.

iii. The investigation of blend component melt viscosity ratio and the effects of blend compatibilization using FTIR, transport properties, LM and dynamic/steady state rheology, to establish a possible phase dispersion-concentration-permeability dependence.

iv. Investigating the effect of the microstructure produced, ie. the shape effect of the dispersed phase, the dispersed phase size concentration, and the chemical nature of polymer phase dispersion.

v. FTIR spectroscopy of bulk blend samples as an indication of the limited chemical interaction in binary blends compared with that in compatibilized blends, and for new functional groups investigation by blending compatibilizers directly with PA6.

vi. The effect on the permeability of, interfacial area, structural changes in the blends, and chemical modification, in the light of Orgalloy R6000 behaviour, where it has been found that the chemical changes to the blend components has changed by $< 3\%$.

vii. Comparison of blend barrier properties with those of laminated binary and ternary structures, made with the same components as the blends.

viii. Utilisation of the chemical/physical modification of the matrix, used to improve the H_2O/O_2 barrier, for organic solvent barrier improvement.

CHAPTER 2 - LITERATURE SURVEY

2a Polymer Blend Literature

2a.1 Introduction

Polymer blends comprise as much as 60-70% of the polyolefins market and 23% for other polymers. Generally, blends are defined as mixtures of at least two homopolymers or co-polymers, which can be miscible or immiscible. An alloy is an immiscible polymer blend with a modified interface and/or morphology, which may or may not contain a compatibilizer, a third component, for promoting some miscibility. Compatibilization is defined as the process of modification of interfacial properties of an immiscible blend, leading to polymer alloy formation[1].

Economics is the main reason for blending, in order not only to extend engineering resin performance by diluting it with a low cost homopolymer, but also for developing materials with properties desirable for a particular application, possibly by using recycled polymers. This work is concerned with simple immiscible polymer blends and alloys.

Blends of immiscible homopolymers and phase separated block and graft co-polymers generally exhibit additive specific volume, whereas densification is often observed in miscible polymer blends and is generally believed to be a consequence of specific interactions, often related to hydrogen bonding. For the barrier applications of this work, the gas permeability of a phase separated blend generally follows a sigmoidal relationship with composition, dependant upon the continuous-discontinuous phase structure of the blend. With miscible blends, a logarithmic relationship versus composition can be expected. Even in immiscible blends, there is evidence of some limited miscibility, where the dispersed polymer can reduce matrix swelling, or the permeant solubility. The partial miscibility of immiscible blends has been studied by electron beam damage and mass loss measurements on several systems[2,3,4].

Although there are more than 40 known miscible blends[5,6], this number represents but a fraction of the immiscible ones. Furthermore, the hetero-phased systems can exhibit not only advantageous barrier but also improved toughness of brittle polymers or reinforcement[7-11].

The droplet size is normally reduced by mechanical dispersion, in order to stabilize the morphology, for interlocking the components in a desired morphology. The stabilization is performed either by chemical (eg. cross-linking by electron beam irradiation) or physical means (eg. by controlled crystallization)[12].

Temporary or reversible cross-linking can be achieved by block polymerization[13] or by introduction of ionic interactions[14,15] or hydrogen bonding. Another way is to generate various types of interpenetrating polymer networks[16-26], (IPN) which are a special case of immiscible polymer blends where interlocking chains are achieved via cross-linking reactions. However, the most popular methods involve addition or generation of an agent which will modify the interfacial properties in polymer systems, which has been one aim of this work.

An excellent review of compatible and incompatible polymer mixtures, together with general theory and experimental methods in polymer blends, was performed by Paul and Newman, 1978[27]. Another review[28] updates and classifies the available information on the methods of blending. This is based upon the compatibilization method used (which in turn is related to the types of the blend components and additives), the assumed most probable compatibilization mechanism, and the types of chemical reaction involved. Thermoplastic composites are further covered[29], since reactive graft co-polymers and cross-linking agents are equally effective as adhesion promoters in blends containing a polyolefin phase. Likewise, for functionalized polymers, but coulombic interactions are not considered.

2a.2 Compatibilization Methods

Although there are various compatibilization methods, including high stress shearing, the compatibilizing agent acts as a polymeric surfactant, by lowering surface tension and promoting interfacial adhesion between the dispersed and matrix polymers. The gap that the current work tried to fill is the effect that the compatibilizer has on the individual phases, as well as in the ternary blend.

The only limitation of the bonds in the compatibilizing agent is that they remain intact during exposure to the blending, and may be preformed or generated in situ. The in situ

formation of a compatibilizing agent at the interface of two incompatible polymers, results in the generation of an adhesive bond between layers usually formed by extrusion lamination[30]. LDPE/PS are incompatible but a preformed hydrogenated butadiene-styrene block co-polymer, having the structure of a PE-b-PS co-polymer, is a compatibilizer. LDPE/PA6 were compatibilized with ethylene-methacrylic acid random co-polymer in the same work, to give organic fluid barrier properties.

ABS/PA6 blends are hydrogen bonded between the amide NH and acrylonitrile(AN) CN groups or between the amide C=O and the alpha-methylene group in AN[31]. Improved impact resistance is due to the addition of a carboxyl containing polymer, such as poly(St-co-AA), to the ABS/PA6, resulting from the presence of the carboxyl containing polymer. Hydrogen bonding between the carboxyl group and the amide and/or the alpha methylene group of the AN is accompanied by the reaction between the terminal amine group on the nylon and the anhydride, when present. Compatibilization of poly(esters) and poly(amides) via an exchange reaction was reported in the same work.

Block and graft co-polymers generated in situ[29] do not always give clearly determined reactions, ie., HIPS/ABS. For PET/HDPE, SEBS is an effective block co-polymer compatibilizer, as a result of the common aromatic character of PET and the SEBS end blocks.

A newer class of compatibilizer are poly(etherblockamides) (PEBA), which are used as a component of blends with ABS, poly(amides) etc. and it is clear from this paper and many others that compatibilization is a form of locally induced miscibility. Indeed, the miscible systems provide an important source of information on the possible methods of compatibilization[5,32-35].

Cross-linking via irradiation of LDPE/PP blends[36] follows on earlier works, where vulcanization has been used to stabilize polymer blends. Irradiative cross-linking is a free radical process resulting in a similar structure to that created by chemical cross-linking or vulcanization[37]. The aim of the process is first to generate the compatibilizing co-polymer which then provides the desired morphology. The continuous cross-linking stabilizes the system, by affecting the interphase, the phase existing between the

dispersed and matrix. The irradiative processing improves the mechanical strength, thermal stability, low temperature toughness, maximum strain at break, abrasion and solvent resistance. In fact, controlled cross-linking of the interphase in dispersed polymer blends, leads to a recyclable product. Cross-linking in fact of one phase results in IPN-type materials. In the current work, γ irradiation of each phase was attempted, but not on the mechanical blend. Physical cross-linking via crystallization of oriented blends was another method used to fix the performance of PET/PP[38] blends.

Two factors affecting miscibility are tacticity and the method of blend preparation. PE/PA6 blends were prepared with MA-g-HDPE compatibilizer[39]. The latter was synthesized by maleating the HDPE with DBP in 1, 2, 3, 4 THN solution initiator, and 1wt% of a 50/50wt% mixture of free MA in HDPE, within a twin screw extruder. Bound MA was estimated at 0.27wt%. The compatibilized ternary blends were processed identically. 88wt% HDPE/12wt% LLDPE was used as the PE phase, providing a route to vary the modulus of the PE phase. Storage modulus(G') increases were monitored for reactive blend compatibilization, and 10wt% of compatibilizer in 50/50 wt% blends reduced the dispersed phase size (identified with SEM) significantly, and also by lowering the compatibilizer M_n. Processability and multiaxial toughness were improved with the low M_n compatibilizer, at the sacrifice of notched Izod impact test results. In the current work, mechanical testing was not performed.

Tacticity studies were also investigated using low molecular weight models of PA6/PA66 amine end group and amide chain reactivity with MA modified materials[40], as a function of temperature. The conclusion was that both amine and amide functionalities can react with anhydrides. The analytical techniques involved were IR, MS, and NMR spectroscopies, whereas in the current work FTIR spectroscopy was used, and to a limited extent UV-VIS. Although the overall reactivity is more or less equal at 200 °C, in real polymer systems there is low chemical conversion, with imide and acid groups being hard to distinguish with IR spectroscopy. Evidence is given for the chain amide groups reacting as well as the amine end groups.

Another analytical technique involved both MA-g-PP and St-MAA compatibilizers with blends of PA6/PP and PA6/PS respectively[41], with the former compatibilizer being

prepared by xylene reflux, for 6 hours, using BPO initiator. The amount of reacted MA was 1.15wt%, based on polymer weight increase. Amino end group analysis showed that the amount of amino groups in the residue after Soxhlet extraction decreased with an increase in the equivalent ratio of MA in MA-g-PP to terminal amine groups of PA6. Further tests performed on the ternary blends were, DSC crystallinity, DMA, MFI, tensile, and impact. Note that even in the presence of the MA-g-PP, the mechanical properties of the 50/50wt% blend were poor, in which neither component could form a matrix, despite an improvement for the other ternary blends.

Where the MA-g-PP is blended directly with the PA6[42], this reactive blend, contained as a result, an interfacial PP-PA6 diblock co-polymer and showed positive deviation from the log-additivity rule, in contrast to the mechanical blend. The viscosity of the PP/PA6 systems increased remarkably with an increase in the amount of co-polymer, and with an increasing in M_n of PA6. This was not the case for the current work, since MA-g-PP containing free MA reduced blend viscosity for both high and low M_n PA6's. For the non-reactive blends, the viscosity change was small, with a decreasing in the dispersed particle size for the reactive blends.

Diverse and relatively stable morphologies can be obtained by other means as well. Of these, the whole domain of reactive processing[43], and solid state formation is where rapid technological progress must be expected[44,45]. An overview of the engineering polymer blend applications/compatibilizers for, PET, PBT, PA6, and PA66[46], including EAA, EAAN, and EVA has been written.

Current compatibilization efforts can therefore be summarised as follows. Polyolefin blend research is focused on low level grafted carbonyl functionalized polyolefins, depending on the barrier application. Organic fluid applications benefit from acid co-polymers, for example. For polyamides, engineering applications would involve block co-polymers, incorporating for ABS, a styrene grouping. In situ generation has been focused on interphase irradiation. Monitoring of storage modulus can give reactive blend compatibilization effectiveness. Caution when blending acid functionalized compatibilizers with PA6 should be practised, particularly if free MA remains, which can result in uncontrolled plasticization and molecular weight lowering.

2a.3 Thermodynamic Effects

The polymer self diffusion coefficient for miscible blends, where thermodynamic effects are valid, is very low[47,48]. For two component miscible blends, the mutual diffusion coefficient, D_M, can be calculated from the Flory-Huggins equation, controlling the rate of disappearance of a gradient in inhomogeneous systems towards homogeneity :

$$D_M = 2\phi_1\phi_2\left(X_s\text{-}X\right)\left(N_1D^*_1\phi_2 + N_2D^*_2\phi_1\right) \text{ ---------- [3]}$$

where ϕ_i, D_i and N_i (i=1, 2) are respectively, volume fraction, tracer diffusion coefficient and polymerization index (polymer chain degree of polymerization, related to the M_W and the average number of repeat units per polymer chains). The tracer diffusion coefficients refer to the diffusion of a low molecular weight diffusant which is mutually soluble in both polymers and is measured independantly by die tagging or radioisotope labelling. The value of the interaction parameter, X, at the spinodal is indicated by :

$$X_s = \left(1/\phi_1N_1 + 1/\phi_2N_2\right)/2 \text{ ---------- [4]}$$

Near the spinodal conditions, where X ---> X_s, the interdiffusion stops and the generated morphology tends to remain stable. An excellent review[49] of the miscible blend polymer interdiffusion was published.

For the study of interaction parameters discussed above, the capillary flow of immiscible PET/PA6 at 275 °C was studied by Dimov and Savov[50]. The authors reported that up to the phase inversion at w ≈ 40wt% PA6, the effective viscosity of blends was Newtonian for $\sigma_{12} \leq$ to 100 kPa. Blends of PET with PA6 showed negative deviation from the log-additivity rule (NDB) behaviour in the dependence of η on composition. However the depth of the NDB behaviour was found to be nearly independent of the shear stress. In contrast, the NDB character in the η vs. ϕ plot for PP/PA6[51] significantly deepen with increasing ϕ_{12}, which was the conclusion found during the current work.

IGC (Inverse Gas Chromatography), has been utilised to investigate thermodynamic miscibility in immiscible blends[52], by calculating X_{23}, for a binary system of polymer/volatile probe, and a ternary system of polymer blend/volatile probe. The

systems investigated were, oligomeric PS/PnBMA, PS/PPO, and PVdF/PMMA, using various probes and the data resulting were generally consistent with that obtained by other methods. The volume fraction of the blends were determined by assuming that the specific volume of the blend is the average of the specific volumes of the parent homopolymers, and could be used at temperatures above T_m, for crystalline blends.

From a study of the thermodynamics of the phase behaviour of polymer blends[53], , it was concluded that an increasingly positive volume of mixing is unfavourable for miscibility of polymers as it leads ultimately to phase instability, whereas for reactive blending of immiscible blends, volume reductions are often observed. It was found experimentally that shear flow elevates phase-separation temperatures, with the shear-induced phase change depending on the stored elastic energy excess. Theoretical and experimental results agreed quantitatively.

Paul and Barlow (1984)[54] considered the macromolecular chain of polymer or co-polymer as a sequence of interacting segments characterized by a value of X_{ij}. The miscibility in a two component system was assumed to result from a complex balance of interacting forces. Depending not on the sign but on the relative magnitude of various individual X_{ij}'s, the overall,X_{12}, in a blend could be positive, negative or zero, even when X_{ij} were all positive or all negative. The concept is useful in fine tuning of blend miscibility by slight variation of co-polymer composition or a degree of co-reaction during reactive processing. In particular, blends containing SAN co-polymer, can be successfully analyzed with this approach[55-58].

Summarising, for immiscible blends, thermodynamic effects have to be treated with some caution since the polymer interdiffusion coefficient is so small and the classical theories tend to have been applied to model miscible systems rather than commercial applications. Crucially, a thermodynamic terms should take account of the interphase, the third component, thought to exist as a core/shell morphology in compatibilized immiscible blends.

2a.4 Rheological Effects

One of the most serious obstacles in the phase equilibria studies of polymer blends is the viscosity of the system and matching the component viscosities is important, a consideration also pursued in the current work.

An emulsion model of viscoelastic liquids was used to interpret data from the linear viscoelastic behaviour of some immiscible blends, using PDMS/POE-DO, and PS/PMMA/PS-b-PMMA[59] systems for the experimental data. The experiments confirmed the model's validity, and showed that dynamic shear measurements can be used as a method to determine polymer melt interfacial tension, provided the volume-average (R_v) and number-average (R_n) radius of the dispersed particles is known and the polydispersity, R_v/R_n does not exceed ≈ 2.

Similarly, PP/PA6/PP-g-PA6 blends were examined[60], by rapid cooling of the specimen on the cone and plate rheometer, after shearing at 0.1 s^{-1} during three minutes and by examining the surface perpendicular to the radial direction of the cone and plate geometry. For PP, the low-frequency terminal zone is at $\omega < 0.2$ rads/s and for PA6, $\omega < 10$ rads/s. The size distribution of **d** was identical for the two systems investigated, ie. 60wt% PP/40wt% PA6, and 40wt% PP/60wt% PA6. From the equation, where K is $\eta_{o(dispersed)}/\eta_{o(matrix)}$:

$$G''(\omega) = \eta_o\left[1 + \left(5K + 2/2K + 2\right)\phi\right]\omega \text{ ---------- [5]}$$

experimental and theoretical values gave poor agreement at high frequencies and also underestimation of G"(ω) at low frequency/zero-shear viscosity. The model needs to be extended for undiluted systems, by taking into account the hydrodynamic interactions between neighbouring droplets. This gives the equation:

$$G''(\omega) = \eta_a\omega^2\left(h_1 - h_2\right)/1 + \omega^2h_1^2 \text{ ---------- [6]}$$

where η_a is the terminal zone viscosity and h_1 and h_2 are empirically derived from K, ϕ, η_0, σ, and R (the average dispersed particle size radius). Hence the blend zero shear viscosity, $\eta_{0(blend)}$ can be calculated as η_a, from : $\eta_{0(blend)} = (\text{as } \omega \text{ ---> } 0)\lim G''(\omega)/\omega = \eta_a$. A similar equation to equ'n.[6] can be derived to find G' as ω ---> 0, which shows that if the limit of G'/ω^2 in the terminal zone has been determined experimentally, it will

provide an estimation of R/σ. If R is taken as the largest particle radius, the interfacial tension can be calculated. It was found to be 8×10^{-3} N/m, the right order of magnitude for a compatibilized system, when compared to that for binary PP/PA6, which is 30-40 $\times 10^{-3}$ N/m[61].

A review of the effect of the interphase and deformability on the viscosity of blends[62] used a mechanical treatment to derive a symmetric mixture rule which predicts a positive deviation (synergistic) for a mixture with a disperse-phase viscosity greater than that of the continuous medium, and a much higher viscosity interphase. Negative deviation is to be expected when the interphase has a much lower viscosity than that of the two pure polymers in the blend. Blend systems data from Han[63-64], compatibilized and non-compatibilized, was compared favourably with this model. Utracki[65-66] and Willis/Favis[67], also observed an interphase with SEM, which reduced the effective volume of the blend components.

The slip factor, β[68], calculated for the current work, formally allows prediction of NDB behaviour, if $\beta_{1,2} \leq 0$. The interlayer slip factor β_1 is defined as :

$$\beta_1 = 1/\eta^* \left[w_1/\eta^*_1 + w_2/\eta^*_2 \right] \text{ ---------- [7]}$$

and the characteristic slip factor $\beta_{1,2}$ is defined as :

$$\beta_{1,2} = (1-\beta_1)(G'')/(w_1 w_2)^{0.5} \text{ ---------- [8]}$$

where w_1 and w_2 are the weight fractions of each component in the blend. G", the Shear Modulus of the blend, represents the constant stress level for Newtonian flow, and is used here instead of σ_{12}[69], the shear stress on the wall, and can be taken as constant in equ'n.[8].

A paper[70] not only considered β to have a maximum effect at $\phi = 0.5$, but also proposed two new relations for calculating the phase inversion concentration, ϕ_i. Firstly it is stated that ϕ_i depends not only on λ, the viscosity ratio, but also on the IV, $[\eta]$, and on the maximum packing volume fraction, $\phi_m = 0.84$. Secondly, that for systems where $0.1 \leq \lambda \leq 10$, $[\eta] = 1.9$ is valid. For the viscosity-concentration dependence of immiscible polymer blends, an increase of the relative blend viscosities occurs due to the

emulsion effect, with its maximum effect depending on the value of the "excess viscosity" parameter, η_{max}, occurring at the phase inversion concentration. As λ approaches zero, with the phase inversion concentration $\phi_{2I} \approx 0.5$, the maximum influence of these contributions occurs at the same concentration.

An equation[71] which was found valid for at least a dozen polymer alloys and blends, derived from the above work is :

$$\lambda = [(\phi_m - \phi_{2I})/(\phi_m - \phi_{1I})]^{[\eta]\phi m} \quad \text{[9]}$$

where I refers to the phase inversion concentration. Two mechanisms of flow were assumed, the first being the emulsion like blend behaviour, controlled by the relative polymer concentration, ϕ_i/ϕ_{Ii}, where ϕ_i is the volume fraction of polymer i in the blend. The second mechanism included β, where:

$$\log \eta = \log \eta_L + \Delta \log \eta^E \quad \text{[10]}$$

and where, $$\log \eta_L = -\log[1 + \beta(\phi_1\phi_2)^{1/2}] - \log(\phi_1/\eta_1 + \phi_2/\eta_2) \quad \text{[11]}$$

and, $$\Delta \log \eta^E = \eta_{max}\{1-[(\phi_1 - \phi^2_{1I}/(\phi_1\phi^2_{2I} + \phi_1\phi^2_{1I})]\} \quad \text{[12]}$$

$\Delta \log \eta^E$ is an excess term derived from the emulsion like blend concept. Maxima in viscosity-volume fraction relationships for polymer blends are due to the second term in equ'n.[10]. Minima can be explained by interfacial slippage and expressed through the term log η_L. Hence it was concluded that, β increases with temperature and shear stress, and that η_{max} decreases with temperature and shear stress, but increases with molecular weight.

Paul and Barlow[72] also attempted to correlate with blend interfacial tension lap shear adhesion test data, for immiscible polymer pairs, bonded with two different compatibilizers. The results were inconclusive.

Current rheology research is focused on the shape development of dispersed particles, dispersed particle dimensions, interfacial tension, shear rate, and processing cycle duration, to establish the function responsible for the phase dispersion mechanism. Empirical evaluations are made under given processing conditions.

2a.5 Polyolefin Blends

Approximately 44% of the world market for polymers is polyolefins, of which 60-70% of LLDPE enters the market as blends, usually with other polyolefins. The rheology of polyolefin blends has been reviewed by Plochocki[73-75] and by Utracki[76-78]. There is also more specific extensive literature on PE/PP blends [73,79,80]. The main thrust of polyolefin blend research has been in the selection of appropriate compatibilizers, as summarised below.

In order to enhance the blend ultimate mechanical properties, 5% ethylene-propylene rubber(EPR) has been used as a compatibilizer for HDPE/PP blends[81,82], whereas the formulation of dispersing agents, comprising functionalized PP or propylene block and graft co-polymers can essentially be done by one of three routes. They are, direct co-polymerization of functional co-monomers, post-polymerization chemical modification of PP, and formation of precursors which are readily converted into various functional groups[83]. In the second approach, for reactive extrusion, the functional groups either are attached to their chain end or statistically distributed along the PP chain, in the range of 2-10wt% grafted co-monomer. Carboxylic acid terminated PP was prepared using thioglycolic acid and AIBN, to give 0.56 mol/kg functional carboxylic acid.

Again, PP/PA6 systems were investigated and this system was emulated during the current work. The grafting of maleic anhydride onto PP was achieved in the above paper by reacting $\approx$ 18wt% MA at 225 °C, for four hours, purified using hot cyclohexane in anhydrous acetone. Characterization was performed with IR spectroscopy, end group analysis by titration and ^{1}H NMR, giving anhydride functionality of 0.84 mol/kg. A similar grafting was achieved in xylene[84], with benzoyl peroxide, using 10wt% MA, at 120 °C, under nitrogen, for four hours and purified using methanol. FTIR showed a grafting ratio of $\approx$ 3wt% of polymer.

In contrast to the above work, the MA-g-PP was used for binary blends with PA6[85]. Preparation was conducted with BPO in a single screw extruder, to which the PA6 was subsequently added, without any PP homopolymer. The impact strength improvement of the PA6 with the addition of the MA-g-PP was monitored by Stress-Strain curves, Tensile Strength, Tensile Modulus, Elongation, Flexural Strength/Modulus, and Charpy

Impact. Predicted values were evaluated using regression of the experimental data.

Rather than looking at mechanical properties, the dispersed phase for PA6/PP blends was found to have a core-shell morphology, in which the shell was a co-polymer[86]. This had a compatibilizing affect and was examined in terms of the influence it had on the rheological properties of the blends. It was found that at low shear rates the blend viscosity was higher than the matrix viscosity, with a nodular morphology, while at high shear rate, the contrary is observed and the morphology was lamellar. The two-phase Oldroyd model[87] was used to analyze the low shear rate behaviour. For the high shear rate analysis, a shear thinning model was derived with alternating layer of blend components surrounding a nodular core. The coefficients of the power law used were computed and compared with experimental data, which gave a good fit. An arbitrary concentric layered structure was assumed, and that each phase viscosity obeys a power law.

A further compatibilized polyolefin system was initiated by grafting BA onto LDPE[88], as an LDPE/PA6 blend (PA6 matrix) compatibilizer. Grafting yield was optimized for, initiator concentration, temperature, time, and LDPE/BA ratio. The percentage grafting efficiency was determined on the basis of changes in LDPE weight during reaction[89], to form BA-g-LDPE. The optimum conditions were found to be, ratio of LDPE:BA $\approx$ 0.7, BPO concentration 0.012mol%, and reaction time of 10 hours. This gave an 11wt% grafting, better than that of the MA-g-PP, commonly used for PP/PA6 blend compatibilization. The C=O and C-O stretch wavebands appearing on the LDPE IR spectra after grafting were identfied. Further testing[88] included tensile, Izod, flexural, Rockwell, torque, SEM, and water absorption.

A second compatibilizer[90] was prepared as (BA-co-MA)-g-LDPE using a similar method to above, and since the double functionality will reduce the number of free amide groups in the ternary blend, lower water absorption results were obtained. The grafting was found to be $\approx$ 7wt%, containing 4.7wt% MA.

Experimentally obtained morphologies[91] are related to predictive equations for co-continuity and are presented in a paper where MA-g-PP is used for compatibilizing

PP/PA6 blends. Moisture absorption, dimensional stability, mechanical properties, and morphology, are related to blend composition. The optimum PP : compatibilizer ratio was found to be 4:1, using 5wt% compatibilizer. For the same system as above, the interfacial adhesion core-shell morphology is examined in relation to other compatibilizer systems, classified in terms of the domain size produced. TEM was used to examine the degree of dispersion. The low functionality MA-g-MSA was found surprisingly to produce good mechanical properties and a fine dispersion[92]. Note that the reactivity of the anhydride grafted compatibilizers was greater than that of the acrylic acid grafted PP due a greater -carboxylic group concentration.

Direct measurement of interfacial tension for several ternary blends, using various compatibilizers[93], showed significant reductions when compared with those of comparable binary systems. ie. for HDPE/PA6, a reduction from 12.5 to 2.0 dynes/cm, with MA-g-PP compatibilizer resulted. Tensile elongations and Izod impact tests were also performed on compression and injection molded blends.

A second HDPE/PA6 system was investigated by compatibilization with a 40wt% PB, PA6-PB multiblock co-polymer. The compatibilizer effect on the binary blend, was reduction of the PA6 disperse phase size, as observed by TEM. This showed the compatibilizer at the interfacial areas, slightly inside both the homopolymers, and also forming a separate phase[94].

Compatibilizers blended directly with PA6 were discussed through the blend rheology-structure[95] relationship for (1)PA6/EVA, (2)PA6/CXA 3101(DuPont de Nemours Co.), and (3)PA6/Plexar 3(Chemplex Co.) blends. DSC, DMA, IR, and rheological results are presented, since the CXA 3101 and Plexar 3 resins are an ethylene based multifunctional polymer and chemically modified polyolefin, respectively. The CXA, according to the manufacturer, when co-extruded, has good adhesion to a number of polymers, including PA6, PC, LDPE/HDPE, PP, PS, and HIPS. This was verified by the authors but they could not verify the adhesive structure or composition. Plexar 3, according to patent literature, is a blend of EVA with PP. onto which unsaturated carboxylic acids or anhydrides are grafted. IR Spectroscopy showed that the CXA contained 18.1 wt% VA and 2.1 wt% -COOH groups and that the Plexar contained 6.5 wt% VA and 0.1 wt%

-COOH groups. Both are normally used as co-extrusion, multilayer, tie-layer adhesives, an application involving high scrap rates. Economics suggests that these scrap materials be recycled as blends and upon comparison of the dispersed phase size(d) of the "tied" blends, blend (2) appears to be substantially reduced compared to blend (1), probably because CXA 3101 contains about 3 times as much vinyl acetate as Plexar 3, and about 20 times as much -COOH groups as Plexar 3, the latter being a blend of EVA with PP onto which unsaturated carboxylic acids or anhydrides are grafted.

SAN (75wt%) blends with PP were investigated[96] using a PP-b-SAN compatibilizer, containing, PP segments which co-crystallise with PP and styrene/acrylonitrile segments. This resulted from interaction of the polar components of the blend. Only 10wt% of compatibilizer reduced the average size of the dispersed phase by more than one order of magnitude. The mechanism of how Styrene-MA co-polymer is found more effective than SAN as a compatibilizing agent for PE/PA6 and PS/PA6 blends is critically discussed[97]. Indeed the phase morphology effect of the compatibilizing agent is associated with interfacial tension, where blends with high interfacial tension give coarse, unstable phase morphologies that tend to coalesce.

Two papers[98,99] set out to characterize Orgalloy R-6000 (R6000), a commercial blend of PP and PA6, under solid state and shear flow regimes. The first suggests that the possible compatibilizer may be formed by reacting an acidic co-polymer with an oligopolyamide[100], and estimated the interfacial tension coefficient as, $\nu_s \leq 2$mN/m. The alloy was dried at 90 °C for 7 days, and tests included, DMTA, SEM, and impact. The 13-14wt% insoluble non-crystallisable fraction was observed to increase upon heating[101], containing the branched PA-PP co-polymer. The free volume fraction f_g and thermal expansivity, α_f of the alloy PP are significantly increased as compared to the homopolymer, in both the TD and MD, the former being the higher. The PA6 T_g was 3 °C more than for PA6 homopolymer.

The second paper[99] discussed the extended drying time necessary for the alloy, due to the PA6 hydrophilicity, ie., a water vapour permeability $\approx$ 20 times that of PP. Hence, extracting moisture from the PA6 matrix involves the relationship where diffusivity is inversely proportional to the tortuosity. Microdrops of PA6 were also observed in the PP

ellipsoids of the processed material. The moisture permeability was estimated as being 2.07 times larger than PP and 10 times smaller than PA6, giving a rate of moisture absorption/desorption of one order of magnitude smaller than that of 100% PA6. It was finally concluded that capillary flow measurements (steady state) should not be used for characterization of melt flow behaviour of immiscible polymer blends, due to non-repeatability of the data. Parallel plate measurements (dynamic) should be used instead.

The main thrust of polyolefin blend research is clearly in their immiscible combination, including a third component compatibilizer and also in trying to emulate the phase dispersion, chemical, and physical properties of existing commercial blends. Identifying the interphase, if any, is also prevalent, assuming that the compatibilizer is concentrated at the interface, and not in the bulk of the blend. PA6 and PP feature prominently for many disclosed and undisclosed applications, for cost reasons, either together or with a different partner.

2a.6 Infrared Spectroscopy(IR)

2a.6.1 IR Spectra and Polymers.

The infrared spectrum is a property of the molecule that is determined by short range relationships between atoms. Given a large enough polymer molecule, one can rearrange it in such a way that all the short range relationships between the atoms remain constant, and only the long range ones move, in which case the mid-infrared will show practically no change. Polymer chemists often encounter such situations when looking at sequence pattern variations.

Dispersive spectra of most commercial polymers have been recorded[102], hence qualitative identification of unknowns can be frequently be accomplished by comparison, including those having varying stereochemistry or monomer sequence distribution. Insight into polymer structure may be gained by consideration of functional group absorption bands, or by comparison with low-molecular weight model compounds of similar structure. Differences that will occur, for example, would be in the aromatic C-H bending region (650-900 cm^{-1}), arising from para-disubstituted versus monosubstituted benzene rings. FTIR allows studies of polymer degradation, and less easily cross-linking. Coupling with a microscope allows analysis of highly localised sections of polymer

samples. Digital subtraction allows the generation of otherwise hidden spectra[103].

HDPE, when irradiated from a ^{60}Co γ source, in the absence of oxygen, will cross-link[104], and FTIR showed the appearance of the ketonic carbonyl group stretch at 1716 cm^{-1} and at 965 cm^{-1}, the C-H out of plane deformation of the trans-vinylene groups, trans RCH=CHR'. A psuedo "internal standard" method was used for subtraction, by eliminating the absorption bands in the 1800-2400 cm^{-1} region.

Discrete particles and bow-tie water trees[105] can be identified using a combination of FTIR Spectroscopy and Light Microscopy. For the former, a defect was found to be PET in an LDPE matrix, due to low a recycling reprocessing temperature. For the latter, subtraction of the area adjacent to the matrix shows ester functionalization and that of a carboxylate ion, consistent with that obtained from water trees in unfilled XLPE, obtained by masking off the defect with a pinhole, or by IR microscopy[106,107].

2a.6.2 Internal Reflectance Spectroscopy

The internal standard method is a variant on the band ratio procedure, in which, another material, which is not part of the system being analyzed, is added, at a known concentration, to the standards and the sample. A knowledge of the concentration of the reference band permits the back-calculation of an equivalent to the pathlength which can be applied to the standards and sample alike. This method only works for polymer films, if sample thicknesses are accurately known. For all methods that use a band as a thickness reference, it is essential that the reference band selected is well defined, preferably isolated from other absorptions, and free from interference[108].

When looking at the potential of polypropylene films as membrane separators in small capacitors, the films are tested by looking at them in oxidised and unoxidised states. Computer selection of bands that showed significant change, in terms of oxygen uptake, found that the ratio of the C-O stretching band height at 1020 cm^{-1} to that of the methylene ($-CH_2-$) band at 1450 cm^{-1} could be correlated with oxidation properties. By examination of these calculated ratios vs. sample number, it was possible to pick out the film properties. Hence, computer analysis of large data sets allows easier interpretation, from which improved deductions can be made[109].

For concentration profiles on the scale of fractions of a μm (nm), as might occur in polymer-polymer blend interfaces, IR-IRS (Internal Reflectance Spectroscopy) is suitable. IR microscopy has the requirement that the region examined spectroscopically coincides with the optical image, and once this is achieved, concentration profiles at a polymer blend interface can be obtained, if the dimension of the compositional change exceeds the minimum IR sampling dimensions. A diffusion coefficient of triphenylphosphine in PP[110], was obtained that way, where spatial resolution is a few micrometers, after deconvolution from the slit function.

IRS has been used to characterize the interphase region in polymer composites[111, 112](Garton, 1984; Garton and Daly, 1984). The method can be extended to immiscible polymer blends. The total depth of penetration[113] varied from 300-500 nm. In one of several possible variants of the method, a sandwich of two polymers was placed on the IRS element, with the first polymer about 100-200 μm thick. For several pairs, the first homopolymer had large enough "windows" in the IR spectrum through which the characteristic bands of the second one could be observed. Comparison of these for neat homopolymers and for the sandwiched ones gave information on the interactions[114].

2a.6.3 IR Spectroscopy and Polymer Blends

The application of IR Spectroscopy in characterization of polymer blends is extensive and this review includes only those works published after 1979, starting with[82,55,115,116] (Olabasi et al., 1979; Robeson, 1980; Coleman et el., 1981; Coleman and Painter, 1984). The latter two authors have published several papers and two books, "Theory of Vibrational Spectra and its Application to Polymeric Materials"[117], and "Specific Interactions and the Miscibility of Polymer Blends"[118], but only those papers of direct relevance to the polymers used in this work have been cited. An introduction to various modern spectroscopic methods for polymeric systems was published by Klopffer(1984)[119], with the applicability of each of these methods being clearly presented. The fundamental aspects as well as principles of experimentation using IR dispersive double beam instruments (IR) or computerized Fourier Transform Interferometric (FTIR) instruments were discussed.

The IR spectrum exhibits, for an immiscible blend, a super imposition of the two

homopolymer spectra, whereas the spectrum of a miscible blend is the superimposition of three components, spectra of the homopolymers and the interaction spectrum. The idea of using small shifts (<10 cm^{-1}) in characteristic absorptions of polymers as a probe of miscibility and interactions became established in the 1970's. Allara[120], pointed out that the IR spectra of an immiscible polymer blend may differ from the spectra of the constituent polymers because of the effect of RI (Refractive Index) dispersion on reflection at interfaces.

Local mixing at the interface of an immiscible blend can occur, when free energy minima exist, with attendant spectral shifts, but the blend will retain a phase separated morphology. Clearly[121], the effects of RI dispersion are appreciably smaller than small spectral shifts, supported by spectroscopic examination of immiscible blends. The difference between the spectrum of the blend and the pure polymer was small relative to the shifts which occur on mixing.

FTIR was used to study hydrogen bonding in polymer blends[122-128](Ting et al., 1980; Cangelosi, 1982; Moskala, 1984;Moskala et 1985;Pennacchia, 1986; Coleman et al., 1988; Painter, 1988). These interactions not only affected the -OH absorption region (3500 to 3600 cm^{-1}) but also the C=O stretching (1737 cm^{-1}), the -CH_2- symmetric stretching (2886 cm^{-1}) as well as the fingerprinting frequency region (1300 - 650 cm^{-1}) and others. The results show that macromelecular conformation in hydrogen bonding blends is affected. Where the blend system shows UCST, only a small effect of blending was observed in the carbonyl stretching frequency region around 1735 cm^{-1}, since there is no reason to expect strong interactions of this type.

FTIR spectroscopy will remain a useful tool for identifying the functional groups present in a polymer molecule, which essentially are the same as those to be found in a simple aromatic/aliphatic molecule. Potential specific polymer immiscible blend interactions can be identified with FTIR spectroscopy, especially where semi-crystalline materials exhibit hydrogen bonding disruption.

2a.7 Microscopy

The main application of polymer blends microscopy is to study morphology, rather than miscibility. The five microscopy categories are, optical or light microscopy (LM), scanning electron microscopy (SEM), transmission electron microscopy (TEM), scanning/transmission electron microscopy (STEM), and finally low voltage scanning electron microscopy (LVSEM). Sample preparation involves, staining, swelling, fracturing, or etching. Microscopy techniques are well reviewed(Hemsley, 1989)[129].

LM is a simple, cheap, and versatile technique, with the resolution being dependant upon specimen thickness as the field depth is small. Specimens of $\approx$ 0.5 μm are required, and the 1 μm resolution being suitable for most blends, but phases cannot be stained. For LM, in descending order of reliability and convenience, the techniques used are: phase contrast, polarized light, reflected and transmitted light[130,131](Karger-Kocsis et al., 1984; Dumoulin et al., 1984) and fluorescence, the latter technique having been extensively used in this work.

SEM sample preparation of tough blend materials, having small phases, results in broken fibrils of a spherical craze. In addition, the conductive material coating is grainy, and with resolution only $\approx$ x10 better than LM[132](Vesely and Parker, 1990). However, SEM is becoming the most popular method of polymer blend observation because of its rapidity, range of readily accessible magnifications, depth of field and, the ability to perform back scattered electron imaging and X-ray elemental analysis of the observed surface. The latter, largely eliminates the need for sample preparation. Several reviews on advances of SEM in polymer characterization have been published[133-138](Thomas, 1977; Roche and Thomas, 1981;Vesely and Lindberg, 1982;Michler, 1984;White and Thomas, 1984;Shaw, 1985).

Etching of PE/PA blends[139,140,141] (Kamal et al., 1984;Dumoulin et al., 1985; Utracki et al., 1986) and of PE/PET blends (Pillon and Utracki, 1985, 1986)[142,143] not only allowed clear identification of the composition and shape of the dispersed phase (rods vs. spheres) but also demonstrated the physical presence of a block polymer, generated in exchange reaction between two components of the blend. PP/PE blends were also observed under SEM, using freeze fracturing with or without n-heptane (Noel and Carley, 1984)[144]. The

effects of concentration, compatibilization and annealing for PA blended with either PS or PE were studied by SEM (Chen et al., 1988)[97]. Either MA-g-PP or SMA, were used as compatibilizers, at the 5wt% level. Addition of these ingredients reduced the diameter of the dispersed phase by x10 and stabilized the system against coalescence, when annealed at a temperature of 200-230 °C for at least 1.5 hours.

Influence of process variables on resulting morphology in model PS/PE blends was also investigated by SEM[145-147] ,(Elemans et al., 1988; Meijer et al., 1988;Valsamis et al., 1988) polymer viscosity ratio, component concentration, type of compounding equipment, processing conditions and compatibilization methods.

TEM sample preparation is more tedious and exacting. The specimens have to be hardened and stained with Br_2, OsO_4, or RuO_4, ultramicrotomed into $\leq$ 20 μm slices, mounted on a grid/polymeric film support, and measured. Cutting of glassy polymers is relatively easy but not of semi-crystalline material, and the samples need a fine coating of carbon, with the minimum of heat damage. Beam damage weakens the already weak contrast, as a result of differential mass loss. The double bond formation, from chlorosulphonic acid etching, for ease of staining, is unsuitable for blends. The surface morphology can also be observed under TEM by cryogenic shadow casting and/or replication methods. Here also etching is frequently used to enhance the morphological details[148,149](Rybnikar, 1985; Eastmond and Phillips, 1985).

Microscopic methods are frequently used in parallel, the SEM/TEM pair being the most frequent. In all cases, microscopy is considered but one method of polymer blend characterization[150-154] (Lars et al., 1983; Yang et al., 1984;Karger-Kocsis and Kiss, 1987; Kyotani and Kanetsuna, 1987;Hsu and Geil, 1987).

There are numerous sources of artifact introduction into electron microscopy, which should be avoided[134,135](Roche and Thomas, 1981;White and Thomas, 1984). In particular, SEM metallization, and TEM OsO_4 staining may introduce an artificial grain structure observed under greater magnification. Serious errors can be made in cases where the domain size are comparable[155]. Hardening of liquid blend samples is another source of artifacts, alleviated by experience gained with biological specimens or

emulsions[156]. Staining and hardening may also engender chemical changes in the system, which in turn can be expected to promote phase separation.

STEM uses ≈ 200 nm thick hardened and stained cast films. The method allows for three techniques of image enhancement which lead to a few nm resolution[157]. The advantages of LVSEM is the ≈ x10 increased image contrast (in comparison to conventional SEM) with almost no charging problem[158]. Due to the high value of the secondary electron coefficient, even small compositional changes show up in the image. Owing to shallow sampling depth, and low energy of the secondary electron coefficient, even small compositional changes show up in the image. Owing to shallow sampling depth and low energy of the secondary electrons, conductive coating is not required, with flat ultramicrotomed specimens being used. The blends investigated included, PP/PA, and PE/PS with the quality of LVSEM being found comparable to TEM.

Binary and ternary blends of PP and PA6 (majority phase), compatibilized with functionalized elastomers (SEBS-g-MA) were not only studied by TEM[159], but also by Izod Impact, tensile stress, elastic modulus, DMTA, and Capillary Rheology. Cellular structures of compatibilizer in the PA6 for both the binary and ternary systems were observed. The SEBS-g-MA formed the continuous phase, for a 10-20wt% elastomer content. Impact strength was improved, elastic modulus reduced and viscosity of the binary PA/compatibilizer mixtures increased.

Staining of PMMA, PVC, SAN, PS, PBD, and PC solvent cast thin films was achieved using OsO_4 staining of the unsaturated double bonds, after polyene formation via STEM electron beam damage[160]. Immiscible blends of PS, PMMA, and PC were irradiated, and the phases identified using the same technique. Furthermore, staining can reveal polymer melt fusion boundaries, which have no diffusion or intermixing, for PMMA and SAN blends, whereas the technique showed this not to be the case for a PVC and SAN blend.

The conclusion to be drawn from polymer blend microscopy is the focus on morphology research, and the potential for examining the interphase, using STEM is a direction worth pursuing. Solvent extraction, for removal of the dispersed phase, has to be performed

with caution, since the resulting structure could quite easily have also been produced by solvent extraction of a homopolymer. Homopolymer fracture surface examination could also show a surface remarkably like that which a blend would produce. In other words, the portion of the blend being examined has to be carefully identified, particularly near the interface.

2a.8 Dispersed Phase Size and Shape

Low permeability polymers are usually expensive or their mechanical properties are undesirable. Hence, by blending them with engineering polymers, an economic compromise is reached, more suitable than layered barriers, since in the latter case, reprocessing and manufacturing are difficult. Clarity can only be attained by good dispersion and matching refractive indexes.

Since by experimentation it has been established that permeability is not necessarily purely additive, ie. not a linear function of component concentration, then an explanation of reducing permeability by reducing cross section is incorrect. Because permeability is a product of solubility of the penetrant and its diffusion through the barrier material, then reduction of solubility or increase of the diffusion path (tortuosity) caused by the lamellar blend structure can decrease permeability. For semi-crystalline PE, PA and PET, the optimal pair was found to be HDPE/PA6[161], for O_2 and H_2O barrier, at the same volume fractions.

The flow behaviour and the flow-imposed morphologies in the HDPE/PA6 were again studied by Dumoulin et al(1985)[140] and by Utracki et al(1986)[141], during which, no compatibilizer was used. Blend dynamic and capillary flow data could not be superimposed, but the dynamic data were highly reproducible and measurements at T = 150-250 °C could be superimposed on a time-temperature master curve. However, since T_m(PA6) = 219 °C, the a_T vs. T plot did not follow any simple relation, but SEM indicated that HDPE/PA6 sample morphology was not affected by a low strain dynamic test. Dynamic flow measurements therefore were found not to affect HDPE/PA6 morphology, whereas the steady state flow through a capillary generated diverse structures, depending on the flow conditions[162-165].

Co-extruded bottles resulted in Monsanto licensing its process for producing hydrolysed ethylene vinyl acetate (EVOH) resins to Kuraray and Nippon Synthetic of Japan. The Kuraray product is called EVAL and is used as an oxygen/solvent barrier in association with LDPE, PP, and PA6[166].

As discussed earlier, polyolefins, as the major component have been used to extend the performance of more expensive polymers,[167,168,169], including those with enhanced barrier properties, such as, EVOH, poly(amides), PVdC, or PET. Such blends are immiscible, requiring a degree of compatibilization, but the immiscibility is precisely the reason for selecting the ingredients. Only additive permeability could be expected if the blends were miscible but since they are immiscible, the generated overlapping dispersed phase lamellae create surprisingly high barrier properties. Biaxial stretching of the poly(amide) drops, will significantly reduce the oxygen and/or solvent permeability, but not necessarily water vapour permeability. The size of PA6 drops and the resulting lamellae thickness can be controlled by the amount of compatibilizer[170]. DuPont's Selar RB-214 is a patented PA6, modified for polypropylene compatibility, when the two are melt blended[171]. PA6 is then dispersed in the PP matrix with a unique laminar arrangement of discontinuous overlapping platelets, which serve as a series of barrier walls arranged parallel to the surface of the container wall. This technology is cost competitive with metal and glass containers, and naturally provides a lower oxygen barrier than 100% PP.

The physical properties, permeability, and morphology[172], of PET/polyolefin blends is discussed, in relation to thin, large, laminae, for hydrocarbon barrier applications. PE modified with carboxyl groups or anhydride groups, either by co-polymerization or grafting, was used as the compatibilizer. The coupling agent compatibilizer chosen for a 60/40 wt% blend of PET/PP[173], was the co-polymer of propylene-acrylic acid, on the basis of solubility parameters. The conclusion was to increase the compatibilizer percentage and reduce that of the PET, for water vapour barrier applications.

Reprocessing of a five layer LDPE/PA6 film to produce a barrier blend[174], containing a tie layer adhesive compatibilizer was investigated, using both minimal and extensive processing in a Brabender, followed by compression molding. The former processing produced better tensile test, and oxygen permeability barrier material than 100% LDPE.

Photoxidised LDPE for 24, 48, and 72 hours was used to produce material for blending with 75wt% PA6, with the LDPE carbonyl concentration being evaluated for the peak at 1718 cm^{-1} and an extinction coefficient of 300 L mol^{-1} cm^{-1}. The Molau test[175] results suggested that the suspension turbidity increased with the growth of the C=O groups between chains of soluble PA6, and insoluble LDPE homopolymers.

A finely dispersed phase structure is the aim of the formulator of immiscible blends, via a compatibilizer[176]. Here the compatibilization of PP/PET blends is described, both in the laboratory and in an extruder, using AA-g-PP compatibilizer (6wt% AA). A relatively small 4 fold decrease in interfacial tension is calculated and the PET did eventually slowly crystallise to about 30%, as in the non-compatibilized blends.

In all probability, capillary flow rheology would produce disc or cigar shaped dispersed ellipsoid particles, depending upon the viscosities of both the polymers, providing that the viscosity of the particles is not much greater than that of the matrix[132], and depending on a processing parameter. This only applies to immiscible blends, for which the interfacial interaction is small and negative. The resulting particle size distribution is a statistical compromise between the surface tension and the ability of the particles to join. Experimental measurements using systems of four blends were correlated with processing conditions.

For barrier organic solvent liquid applications, dispersed particle size and shape are vitally important, due to the molecular concentration effect, and is a major factor for vapour barrier. Generally, large overlapping dispersed phase laminae provide the necessary increased tortuosity for inhibiting the passage of the permeant. Size and shape is clearly not a factor for water vapour barrier of blends, as the above literature has shown. A finer dispersion could be a factor for oxygen barrier applications, but the evidence for this is not conclusive, particularly if the oxygen interacts with the matrix.

2a.9 Theoretical Approaches

For immiscible polymer blends, a third component which is miscible with both components is often used as a compatibilizer, to promote some miscibility across the phase boundaries. The theories of miscibility have been based on the thermodynamical

approach and five theoretical approaches are worthy of mentioning[177].

The first is that of Flory-Huggins[178], which is a description of the miscibility conditions using an interaction parameter, but the theory ignores volume changes during blending. For many blend systems, LCST behaviour is observed, which is not predicted by the Flory-Huggins theory, unless the interaction parameter is assumed to be temperature dependent. The second are EOS (equation of state) theories, allowing for the compressible nature of the systems[179]. These theories consider the volume changes and pressure dependence, as enthalpic and entropic contributions to the interaction parameter, and are consequently more versatile. These theories always favour immiscibility and cannot be a driving force for mixing. The stability condition for a binary miscible mixture however, may be written as equ'n.[13]:

$$(\delta^2 G/\delta\phi_i^2)_V + (\delta V/\delta p)_{T,\phi i} (\delta^2 G/\delta\phi_i\, \delta V)^2 > 0 \text{ ---------- [13]}$$

where p is the pressure, V the volume of the mixture, and G the free energy. The first term is the only one treated by Flory-Huggins type theories, applying only at constant volume. The second term is from the compressible nature of the system, estimated by EOS theories. Since the first part of the second term is always negative, the term tends to destabilize the mixture, as the second part of the second term is always positive or zero.

A third theory is the Gas Lattice Model[180], which considers the blend as a ternary system, where the third component is the free volume. This theory can predict both the upper and lower critical temperature. The fourth theory is the Cell-Hole theory[181], which is even more complex, as it again considers free volume, as well as pressure and temperature. Low molecular weight systems are also covered by it, since it can predict liquid ageing and viscosity, and also liquid/vapour equilibrium, making it the most universal system. The fifth Strong Interaction Model[182] uses the original Flory-Huggins theory and, but replaces the interaction parameter with enthalpy and entropy dependant parameters and has a special application for systems with chemical interaction.

Gain in entropy does not drive homopolymers to mix, as it does in low molecular weight systems, but specific interactions between them does, making the term ΔH_{mix} negative[183]. Change in the packing of the homopolymer chains on mixing, and relative viscosity

matching are also important and this paper describes not only the phase separation mechanism, in terms of spinodal, binodal, critical point, nucleation growth, but also the techniques of detecting miscibility. These include, T_g, DSC, mechanical methods, SALS, SAXS, SANS and TEM. Pressure effects on miscibility are discussed, along with shear, as future research directions.

Summarising, the most widely used Flory-Huggins theory has severe limitations for polymer blends, as it cannot predict the LCST, and considers the interaction parameter to be constant. The most universal and complex is the Cell-Hole theory.

2a.10 Polymer blend literature summary

The phase dispersion in binary immiscible blends is dependant not only on the blend rheology but mainly on the interfacial properties, which in most systems are important not only for a good dispersion, but also for the stability of the dispersed phase.

2b Polymer Permeability Literature

2b.1 Fundamental Principles

Polymer permeability is the transport of mass through a matrix of finite thickness. In the absence of microvoids, permeation of gas through a polymer film, is considered to be controlled by the sorption of gases into the film. The gas from the high-pressure side dissolves in the single phase film (adsorption) and later diffuses down a concentration gradient by step-wise mechanism, to the low pressure side of the film, where it is desorbed until thermodynamic equilibrium with respect to the polymeric interfaces is attained. The interfacial sorption and desorption are therefore rapid as compared to the rate of diffusion through the film. Two assumptions have been made, that firstly, all the permeant reaching the surface can be collected, ie. that the rate of removal of the permeant from the surface must exceed the rate of transport, and secondly, that there is only a small percentage of immobile permeant mass, of which only a small fraction would permeate through the matrix.

Unlike diffusion, which is a dynamic process, permeability is steady state, and is therefore a less fundamental process, the data being dependant largely upon the method used for its measurement. Nonetheless, for many practical polymer packaging applications, permeability data is preferred, providing the measurement conditions are identified.

2b.2 Polymer Barrier Property theories

In terms of Fick's 1st and 2nd and Henry's Laws respectively, polymer diffusion of small molecules is shown by[1] :

$$\delta Q / \delta t = -DA(\delta C / \delta x) \quad \text{[14]}$$

$$\delta C / \delta t = D(\delta^2 C / \delta^2 x) \quad \text{[15]}$$

$$C_1 = Sp_1;\ C_2 = Sp_2\ ;\ S = C_1/p_1 = C_2/p_2 \quad \text{[16]}$$

where Q is the amount of permeating gas, D is the diffusion coefficient, A is the area of permeation, x is the distance of penetration from the upstream surface, C is the concentration at x, p_1 and p_2 are the permeant partial pressures at the upside and downside of the film respectively, S is the solubility coefficient (defined from Henry's Law as C/p), t is time and $(\delta Q/\delta t)/A$ is F, the flux (rate of transfer of penetrant per unit

area expressed as quantity of diffusant per unit area per time). Since Henry's Law is assumed to apply at the interfaces (film surfaces) then concentrations can be replaced by pressures and applying the steady state conditions, when $Q \propto t$, equ'ns.[14]-[16] can be solved to give Q at time t as :

$$Q = -D\,S\,(p_2 - p_1)\,A\,(t - L)/l \quad \text{---------- [17]}$$

where l is the film thickness and L is the time lag in permeation, the time elapsed between the test start and the intercept of the projection of the steady state portion of the transmission curve onto the time axis. The negative sign can be removed by rearranging the pressure term and also p_2 can be ignored when $p_1 >>>> p_2$, which is often the case.

Using the quasi-isotactic method, in which the permeant is accumulated as a function of time, C_0 is the initial uniform film diffusant concentration, and C_2 is the inner film surface emerging concentration, which are kept at zero. C_1 is the permeant concentration inside the face of the film adjacent to the high concentration chamber and it is assumed that equilibrium is established instantaneously at the interface. Barrer presented a solution of equ'n.[15] for quasi-isotactic conditions, assuming that the polymer film is initially free of permeant and the downside volume is maintained at zero concentration relative to the upside volume (total extraction of the permeant from the outside of the downside face of the film) with which D can then be correlated to L by[2], :

$$D = l^2 / 6L \quad \text{---------- [18a]}$$

By measuring Q, p_1, A, l, and t, L can be estimated by the least-squares method from a plot of Q as a function of t; D and S are calculated from equ'ns.[18a] and [17], respectively[3,4]. The permeability coefficient, P, is additionally defined as[5]:

$$P = DS \quad \text{---------- [19]}$$

and can then be substituted into equ'n.[17].

It has been shown that[6] the folowing inequality exists for a large number of fundamental depndancies of D, the mean Fickian diffusion coeficient, on penetrant concentration :

$$1/6 < D\,L/l^2 < 1/2 \quad \text{---------- [18b]}$$

This relation indicates that using equ'n.[18a] to estimate D may lead to a value three times smaller than it should be, due to the difficulty in maintaining negligible penetrant

concentration in the reciever as compared to that in the reservoir.

The activation energy, E_p , for the permeation process can be calculated from the Arrhenius equation :

$$P_T = P^* \exp(-E_p/RT) \quad \text{[20]}$$

The plot of ln P_T as function of 1/T gives a slope of $-E_p$. P^* is the value of P at a standard temperature such as 293K, and P_T is experimentally obtained. The quantity E_p can be separated into activation energies of diffusion, E_D , and sorption, E_S, as :

$$D = D^* \exp(-E_D/RT) \quad \text{[21]}$$

$$S = S^* \exp(-E_S/RT) \quad \text{[22]}$$

From equ'ns.[21] and [22], we get :

$$E_P = E_D + E_S \quad \text{[23]}$$

E_S is also referred to as the enthalpy of sorption, designated by ΔH_S.

The activation energies for the permeation process is in the case of oxygen, for example rather small, and largely depends on the nature of the polymer-gas interaction. However, it has been shown that D^*, P^*, and S^* in equ'ns.[21]-[23] are related to the density and size of the free volume available within the polymer matrix[7,8], at the standard temperature, with the free volume being defined as a favourable distribution of localised excess volume to allow a diffusive jump.

Polymer permeability[9] is comprehensively treated in an early review, and also the derivation of activated diffusion. The observations of Frisch[10] are discussed and also the Laidler, Shuler[11], Herrick, McNeil, Bennet, and Leininger hydrostatic/osmotic theories. The dimensional dependence, swelling and "skin" vs. bulk theories of Baddeur et al, Barrer[2], and Crank and Park[12,13,14] theories are included. A notable conclusion of this review was that the rate of permeation for some systems, instead of varying linearly with concentration or pressure differential, were found to vary exponentially with the concentration or pressure at the ingoing surface. Therefore, these systems were independent of the pressure gradient or the pressure at the outgoing surface[15,16,17], ie. for the permeation of n-heptane through PP[18].

Summing up, the permeability is related to the quantity Q of penetrant molecules passing through a sample of given surface area A and thickness l during a fixed amount of time t, when the partial pressure difference between the film surfaces is Δp by :

$$Q = P A \Delta p t/l \quad \text{---------- [24]}$$

to give the permeability as :

$$P = Q l/A t p_1 \quad \text{---------- [25]}$$

where $p_1 >>>> p_2$. Clearly, phenomenological approaches have been made for the solution-diffusion mechanism for permeation which are largely, the free volume, interchain cohesive forces, and solubility theories.

2b.3 Units of Permeation

Innumerable techniques have been devised to measure the permeation of gases and vapours through polymer films and, thus, a number of units have been used to express the data[19]. An interconversion to standard units may be very convenient for comparison of published data. The RPU either in CGS or SI may be considered for the sake of simplicity as the :

cm^3(STP) cm /cm^2 /s /cmHg (atm.)

since it has been employed by the majority of researchers working in this area. If it is multiplied by 10^{-10}, then it is 1 barrer. For oxygen, the values of P ranges between 0.1 for highly impermeable polymers, such as PVdF, to 500 barrers for one of the most permeable polymers, PDMS. In this work, as required by the sponsors, the units used for vapour permeability are g mm/m^2/day/bar and for gases, cm^3 mm/m^2/day/bar.

2b.4 Selective Permeability

Polymer membranes for selective gas separation[20,21] and applications of polymer membranes in the preservation of food[22,23] are receiving a great deal of attention. Earlier reviews include that by Felder and Huvard[24], on gases/vapour transport through polymer membranes and gas separation by the same method[25-27]. A review of the patent literature in this area has been prepared[28-31] and selective oxygen permeable membranes have been reviewed[32]. Koros et al[33] compared dense walled and different types of asymmetric structures in describing the advantages/disadvantages of different gas separation membranes.

Moving to the area of food packaging, there has been a dramatic growth in the use of polymeric films, asserting their many inherent advantages over other materials[34]. However, such undesirable transport phenomena during storage as, permeation of oxygen, moisture, and organic vapours, through the film, do occur, and knowledge and control of them become critical. These transport processes are effected by the thermodynamic compatibility between the polymer and the permeant, the occurrence of active sites, in addition to the structural and morphological characteristics of the film material.

The latter point was raised in a paper describing the effect of polymer molecular structure on the gas permeation behaviour of the materials used as gas separation membranes. In this pursuit, Paul, et al[35,36], investigated the effect of stereoregularity on the permeation characteristics of oxygen through PMMA membranes, at 35 °C, 1 atm. pressure. For three different films. P, D, and S increased with an increase in syndiotactic sequences content, and a 50:50wt% blend of syndiotactic/atactic PMMA was also studied. A similar application was envisaged by Haraya et al[37,38], who reported the permeation results of various gases through a polyimide and syndiotactic/atactic PMMA blend membrane. He observed an oxygen permeability of 2.5 x 10^{-11} RPU for a 50:50wt% material.

The conclusion is that unlike the last two applications, the best separation membranes are examined from the combined high selectivity and reasonably high permeability aspects. Polymers deviating significantly from a simple coupling of the permeability and selectivity are often therefore the materials of choice.

2b.5 Molecular Orientation

Touched upon in the last section is the increased use of polymers in the food packaging and beverage bottling industries and PET has been used for the bottling of carbonated drinks. The transport of oxygen through oriented PET films at 25 and 60 °C has therefore been studied by using the dynamic diffusion method[39]. The permeation results showed a lowering of O_2 permeability upon drawing. The Fickian diffusion coefficients obtained at 25 °C ranged from 6.5 x 10^{-9} cm^2/s for the isotropic feedstock to 4.0 x 10^{-9}

cm^2/s for the most highly drawn films. The corresponding D for the highly drawn films at 60 °C was 35 x 10^{-9} cm^2/s. The transport properties of a number of homo and co-polymer films of PET for O_2 have also been studied[40]. The influence of molar mass and annealing temperature on crystallinity and subsequent resistance to oxygen permeability was studied for biaxially oriented films of PET[41], with the annealing temperature showing a direct positive influence on permeability.

The significance of draw ratios's for biaxially oriented PET and HDPE,[42], using for the former oxygen and water vapour penetrants, and for the latter, helium and oxygen, were investigated. HDPE is used as a food container and the helium permeability was largely unaffected until after a draw ratio of 10 is achieved, upon which some reduction in permeability was observed, reinforcing the lack of interaction between the gas and polymer theory. The HDPE **D** for oxygen was however, significantly reduced, with draw ratio, suggesting that the permeation path for oxygen was made more tortuous upon drawing. Biaxially oriented PET oxygen permeability was correlated with the degree of orientation, measured using FTIR microscopy, but there was no correlation for water vapour.

Conversely to the above work, the orientation of LDPE film[43] was used to assess its transport properties to DCM, a common component of paint stripper, at various draw ratios, before and after annealing. By suspending the polymer in the solvent vapour and measuring weight gain with time, **D** was calculated from the initial slope of a plot of $\mathbf{c(t)/c(\infty)}$ **vs.** $\mathbf{t^{1/2}}$, at varying vapour activities, $\mathbf{p/p_0}$, where **p** is the total pressure and $\mathbf{p_0}$ is the equilibrium vapour pressure at the experimental temperature. Similar work was done[44] with aPS and it has been reported[45], that with PP, ordered domains of 10 nm were impermeable to DCM at low vapour activity, but the permeability increased with vapour activity.

PE was again the focus of earlier work on the sorption and flow of N_2, CO_2, He, and O_2 in the range 0-50 °C[46]. A series of carefully prepared HDPE and LDPE samples were used, of crystallinity 43-82%. Branching indices and density were also monitored, for calculating tortuosity. Diffusion and solubilities were determined by time-lag and by an

accurate static method[47], respectively, and found to obey Henry's Law. For each gas at constant temperature, the solubility constant is directly proportional to the amorphous volume fraction of the amorphous phase, justifying that the crystallites are an impermeable second phase. The conclusion was that the combined influence of crystallinity on solubility and diffusivity, permits as much as a tenfold variation in gas permeability of PE, depending on polymerization method and fabrication process.

For products containing fats and oils, such as fried snacks and meats, protection against the effects of oxygen and light (photoxidation) is required[48]. In certain cases, a cosmetic package may have to contribute toward oxygen barrier properties. In a paper by Dong et al., O_2, N_2 and other gases passing through a PMS + PEG complex membrane was discussed[49], with these films having relevance in the preservation of fruits and vegetables.

The mobility of oxygen in polymer films is once again addressed as the predominate controlling factor in the photoxidative degradation and photoprocessing of materials. In most cases, the transport of oxygen is rapid compared to the movement of polymer chains, and the rate of transport is controlled entirely by the type of polymer matrix, which is expected to provide valuable information about the movement and structure-property relationships of polymer chain segments. This method has been employed in correlating thermal treatment T_g shifts with oxygen permeability, for different PP/alicyclic oligomer wt% blends[50].

Courtaulds PP[51] Films are producing, it is reported, an easily printable, white, 5 layer, sealable OPP, giving, water vapour permeability of 0.2 g mm m^{-2} day^{-1} bar^{-1} at 38 °C and 90% RH and oxygen barrier of 59.2 cm^3 mm m^{-2} day^{-1} bar^{-1} at 23 °C and 0-90% RH. These figures compare favourably with PP homopolymer values of 0.55 and 61 respectively, see Table 1 of Chapter 1.

Although extra processing is involved, clearly, sorption and transport is a function of cross-linking in non-crystalline polymers. Usually, the solubility is proportional to the amorphous volume fraction, and similarly for diffusion, except that the amorphous

volume fraction is raised to a parameter m, varying between 0.3 and 1. Cross-linking has little effect on solubility, except at high degrees or when the polymer swells, and diffusion decreases approximately linearly with cross-link density. Shape factors related to the axial ratio, the magnitude of which decreases as departure from sphericity increases, are used to define the tortuosity of the penetrant path in cross-linked and semi-crystalline materials. Segmental mobility of the polymer make the diffusion process more dependant on the size and shape of the penetrant molecule. Orientation to produce an asymmetric structure by relaxation recovery generally reduces diffusion both parallel to and perpendicular to the orientation axis.

2b.6 Experimental Methods

2b.6.1 Introduction

A number of experimental techniques have been developed and used by many scientists working in this area, with the details being available in the original literature. Several modifications and newer approaches are available in ASTM manuals[52]. Many techniques for measuring the permeation of gases and vapours through polymer films and thin sheets have been reviewed in detail by Lomax[53].

2b.6.2 Oxygen Permeability Methods

2b.6.2.1 Introduction

Molecular transport of oxygen through polymer barriers has been a major thrust area of research for several years, with the increasing demand for use of polymers in engineering, medicine, separation science, agriculture and food industries. In technological areas an understanding of polymer film gas transport phenomenon is vital in view of the development of a wide variety of packaging applications, surface protective coatings, drug delivery membrane systems, artificial organs, etc.[54,55].

The MOCON OXTRAN 100 permeability tester is becoming the de facto standard for measuring the oxygen transmission rate of polymer films, as per an ASTM method[56]. This is a coulometric fuel cell method, allowing for different or the same RH's to be specified on both sides of the film. A diagram of a twin cell system is shown in Figure 1 below. For controlling a pair of OXTRAN 10/50 instruments, a PC and Camile data

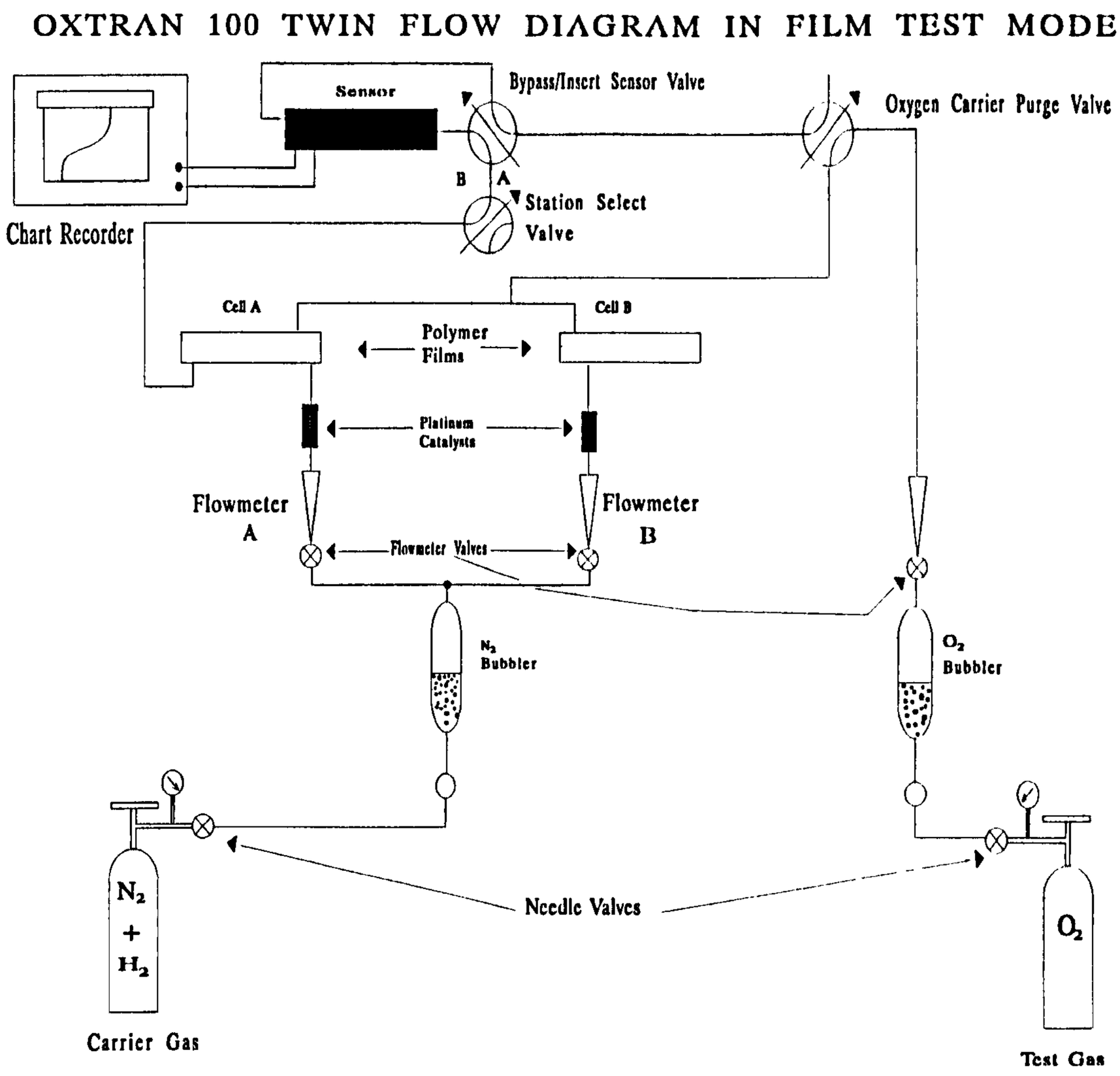

Figure 1 : Oxtran 100 Twin

acquisition/control system is described in a paper[57], where a Fortran program sequences the analysis, increasing productivity by 250%. Automated models are now available from the manufacturer.

Another electrical signal change polarographic method is based upon the Clarke electrode principal[58]. A steady state current generated between a platinum cathode and silver anode is related to the oxygen permeability of a polymer film. The latter is placed on an aqueous sodium chloride solution which is covering the cathode. The number of moles of oxygen necessary to sustain the cathode reaction, $4e^- + O_2 + 2H_2 = 4\ OH^-$, is four. The method is more applicable to semi-soluble and semi-permeable membranes.

2b.6.2.2 Chemical Instrumental Methods

Comparative data is often sufficient for practical packaging situations and a device for measuring the permeability of polymer films used for food products packaging[59] simulates the shelf environment. A Teflon jointed cell, with controlled humidity, and GC detector, detects carbonic anhydride and oxygen. Relative values of oxygen permeability were measured for double LDPE and double LDPE/aluminium breathing bags[60], using water to displace oxygen free gas from an airtight container into the test bag, on which was connected a septum, through which oxygen concentration was measured with time, by syringe and GC. The final gas volumes in the bags after 2 weeks was also measured, using the reverse procedure to that of filling them. Barometric pressure differences gave the exact volumes. Although the aluminium/double LDPE bag was only 4% as permeable as the double layer LLDPE bag, pin holes in the aluminium are difficult to prevent, since for lightness the metal layer has to be thin, and is often there for design and cosmetic reasons only.

Another method for measuring the overall polymer bag permeability is colourimetric and one of many novel instrumental chemical methods. A saturated aqueous solution of ammonium hydroxide (NH_4OH) and ammonium chloride (NH_4Cl) is mixed with finely divided excess copper[61]. The copper forms a complex with the ammonia, $Cu(NH_3)_2^+$, the colourless cuprous ammonia ion, under the influence of oxygen permeating into the atmosphere above the solution, through the wall of a polymer bag holding the solution. At the end of the test, upon exposure to the air outside, the blue $Cu(NH_3)_4^{++}$ complex is formed and the degree of blueness can then be monitored colourimetrically. This is directly related to the amount of oxygen which had entered through the bag. Also based on colourimetrically measuring a change in blueness[62] is that involving the indicator indigo-carmine. A solution of the indicator is oxidised to blueness with sodium sulphite, reduced to colourless with sodium hydrosulphite, and then back to blueness by atmospheric oxygen permeating through the polymer film. The latter is clamped to the top of the reaction tank fitted with a mechanical stirrer, and the bottom surface is in contact with the liquid. The tank is replenished through a valve by gravity, from a higher level reservoir, after aliquots of liquid are taken by syringe, through a septum, for colourimetric analysis.

A third method for polymer bag permeability measurement involves luminous marine bacteria confined in the bag[63] for O_2 permeability determination. Light is emitted *in vivo*, the intensity of which is directly proportional to the O_2 concentration, and hence the polymer oxygen transmission rate. The method is reported to be fast, and the results for six of fifteen commercially available films were compared with those obtained using an ASTM 1971 permeation cell, with a thermal conductivity detector GLC. The bags were held in the bioluminescence cell to allow a photomultiplier to detect the output. Calibration was achieved by injecting different amounts of oxygen saturated NaCl solution into a cell and plotting the change in light intensity as a function of moles of O_2. Ratios of OTR's were produced, compared to an LDPE film of known OTR, rather than O_2 permeabilities.

A third colourimetric method involves supported manganese (II) oxide (MnO)[64]. This changes colour from a bright green to brown upon oxidation, being completed in less than one minute, forming manganese (IV) oxide (MnO_2), which can be regenerated many times. The MnO is formed by starting with hydrated manganese acetate supported on Celite ceramic chromatography support material and decomposed to the (II) oxide, followed by activation. At least 1 part of oxygen in 10^8 is removed/detected, with the removal taking place until the brown zone has reached about 1mm from the end of the mixture. The rate of movement of the brown/green boundary can be used to measure the rate of oxygen uptake, from which the proportion of oxygen in the gas can be deduced. By mounting a polymer film between atmospheric oxygen or pure oxygen and the MnO_2, it would be possible to relate the rate of movement of the colour front to the oxygen permeability.

The quenching of the delayed fluorescence of pyronine B[65] molecular probe was used to determine oxygen P and D at low partial pressures, allowing the oxygen content of the films to be determined, but only for semi-permeable polymer contact lense materials.

Petrak and Bumfrey [66],used a spectrophotochemical method to evaluate D and P of oxygen in water soluble polymer films at a given relative humidity. The singlet excited oxygen indicator involved was Rose Bengal and the singlet oxygen acceptor was DPBF.

They claimed[67] that this method eliminates many of the disadvantages of the conventional methods, and Petrak and Pitts continued[68] by reporting their work on determining the permeability coefficient and diffusion coefficient of oxygen in hydrophillic polymers, at a given relative humidity. The effect of film thickness on the transport parameters was also investigated.

2b.6.2.3 Diffusion Methods

The Fickian diffusion mechanism is assumed for most of the methods described below, which necessarily need not be the case. A new technique, based upon manometry, used to study the diffusion coefficient of oxygen from the dynamic response of films initially saturated with ambient oxygen has been described[69]. However, the authors sound a note of caution, to ensure that steady state has been reached before taking a reading.

An apparatus based on ASTM D1434-1958[70], the pressure decay method, was modified to include a quick opening assembly, permitting easier installation of and removal of the test specimen, and also the test area of the specimen can be changed quickly by simply using a different size O-ring and filter disk. Most of the apparatus is metal, with glass being used for the capillary and plate through which it protrudes.

An all glass system[71] is described, with an improved diffusion cell clamp, sealing agent, and small 200 cm^3 capacity cell. Sealing was provided by four circular collars machined from a flat sheet of 1/8" thick GRP. Tests were conducted with PVdC film, giving oxygen permeability results close to those previously reported.

Plasma-Deposited siloxane coatings[72] were used in different thickness with HDPE, to improve the latter oxygen barrier properties, with measurements being made using a Lyssy GPM-200 analytic gas permeability fractioner[73]. Similarly,[74] PET membranes were deposited with SiO_2 were used for He permeation selectivity, with the permeabilities determined by the steady-state diffusion method[2].

The oxidation processes in irradiated PE films have been studied by the ESR method[75]. Diffusion coefficients were determined at various temperatures in the crystalline region,

with the E_D of oxygen in this region proving to be 32 kcal/mol.

Electron Spin Resonance Spectroscopy[76](ESR) was used to determine the diffusion coefficient of O_2 in PVA, by irradiating the polymer in vacuum, producing free radicals, the concentration of which decreased, upon exposure to air. Optimum doses of radiation were identified, and curves were fitted to the data points using the equation :

$$R_t = R'_0 \exp(-D\pi^2 t/a^2) \quad \text{---------- [26]}$$

where R'_0 an R_t are the radical concentrations at time t and initially, respectively, and a = polymeric sphere radius.

ESR was used[77] again to monitor the permeation of oxygen, with a moving boundary diffusion model in a cross-linked co-polymer of MMA/EGDMA(40, 55, 70, 85, and 100% EGDMA). Decay in concentration of trapped radicals in the temperature range 110-180 °C, was used as an indicator, since permeated oxygen will consume them. Final residual radical concentrations were calculated, as well as measured, with good agreement, indicating that they should not experience bimolecular termination (radical/radical) during oxygen permeation, but rather react with oxygen only. ESR spectra strength decreased with permeation time, and decay rates calculation involved double integration of them. If one oxygen molecule terminates one radical, and if the equation for polymer rod diffusion is assumed, with initial boundary conditions, the permeability coefficient is estimated by regressing the average radical concentration vs. t. In this system, oxygen permeation is mainly affected by the microstructure of the network, with peak permeability at 70% EGDMA, the most porous structure. The permeation of oxygen into the polymer was much slower below the T_g, and the T_g value obtained from the permeability data was similar to that obtained by DSC.

2b.6.2.4 Summary of Oxygen Permeability methods

Of the various methods of measuring oxygen permeability reviewed above, the most accurate methods are costly and time consuming, particularly for the high barrier materials. Oxygen detection based on fuel cells and gas chromatography are the most accurate. The commercial OXTRAN apparatus measures to 0.001%. For comparative semi-quantitative purposes, cheap chemical colourimetric detection, if reliable, could be suitable for high barrier materials, since the sensitivity is good.

2b.6.3 Polymer Permeability for other gases

BOPP methane permeability has been measured using a twin cell method, in which each cell has a polymer film sandwiched between "o" rings. One side of the test cell has the permeant gas flowing over it and the other side has pure nitrogen, directed to the detectors. The reference cell has nitrogen gas flowing on both sides of the film. The detectors are Flame Ionisation (FID), with the system modified for an absorption/desorption cycle. The permeant on the downside is swept to an absorption tube. After a preset time interval, heating causes desorption from the tube, with the slug of permeant vapour causing a sharp peak, rather than a slight offset over a long period[78].

GC was also used for determining the nitrogen permeability of PA6 films, to control their quality[79], after orientation uni-axially and bi-axially. The permeability results were favourably compared to those obtained using a pressure decay method.

The structure-property relationship for model polyurethanes was investigated[80] mainly for CO_2 permeability. The CO_2 latter was the in situ generated blowing agent, used in producing foamed materials, instead of environmentally suspect CFC's. Oxygen permeability was also measured. The Mocon OXTRAN and a PERMATRAN W modified for carbonic acid detection, discussed above and below[56,81], were used.

2b.6.4 Water Vapour Permeability

Like the OXTRAN, the Mocon PERMATRAN W water vapour permeability tester has become the industry standard method, and uses an infrared sensor for detecting water vapour downstream of a polymer film[81].

Gravimetric water vapour permeability[82] determination of polymer films is based on the ASTM Standard E96-80 (ASTM 1983), in which the mass loss of permeant with time is monitored, from a glass water filled container, over the mouth of which is mounted with hydrophobic adhesive or wax a polymer film. The test temperature and relative humidity are carefully monitored and reported. Alternatively, the uptake of water vapour is monitored similarly for a hygroscopic material in glass container, over the mouth of

which is placed in similar fashion the polymer film. A constraint on this latter method is the maximum mass percentage absorbent uptake (2 wt%) allowed by the standard.

Water vapour permeabilities were determined, with a method similar to that used by Banker et al[83] and Patel[84]. A 10 cm^3 glass bottle contained 5 cm^3 of saturated ammonium sulphate solution, giving a constant 81% RH, corresponding to a water vapour pressure of 19.2 mm Hg at 25 °C. Five specimens of each sample were fixed to the top of the bottles, using a concentrated solution of the polymer in butanone as an adhesive. The bottles were left for 3-4 hours to allow solvent evaporation and then re-weighed and stored in a desiccator at 25 °C, giving an RH of zero. The bottles were intermittently reweighed and the weight loss vs. time plot was used to determine the permeability coefficient. The adhesive showed negligible permeability. An obvious shortcoming of this method is that by keeping the RH at zero, the data is not relevant to practical polymer packaging applications, but measurements at various RH's would suffice.

For monitoring the plasticization effects of water, methanol and ethanol, in PA6, the differential sorption method was applied[85], using an electrobalance with ±0.01mg accuracy, in a vapour atmosphere (vapour pressures measured by mercury barometer to within ±0.5 mm), at constant temperature and pressure. The sorption/diffusion behaviour were interpreted in terms of clustering theory, in view of penetrant molecular size, and hydrogen bonding capability. The transport and mechanical properties indicated dependence on penetrant concentration. The decrease in the hydrogen bonding capability with the alcohols affected both mechanical properties and diffusion, caused by penetrant cluster formation at characteristic concentrations of sorbed penetrant. Water only affected mechanical properties. DSC, XRD, and density measurements (benzene displacement at ±0.001 gm/cm^3 accuracy) were also taken. Sorption isotherms were analyzed by using a clustering function, the cluster integral divided by the partial molar volume of the penetrant as a function of sorbed concentration. The Boltzmann solution[86] for the penetrant mass uptake with time is applied for diffusion determination :

$$M_t/M_\infty = (4/\pi^{1/2})\,(D_t/l^2)^{1/2} \quad \text{[27]}$$

giving a diffusion coefficient of :

$$D = (\pi/16)\, K^2 \text{ ---------- [28]}$$

where

$$K = \delta(M_t/M_\infty)/\, \delta(t^{1/2}/l) \text{ ---------- [29]}$$

is the initial slope of the sorption curve, calculated by the least squares approximation. The mean diffusion coefficient ($D(c_2)$) was calculated from the average value, ($D(c_1, c_2)$), using equ'n.[30], where c_1 and c_2 are the initial and final equilibrium concentrations, and $D(c_1)$ is the mean diffusion coefficient calculated from the previous concentration increment, using the equation :

$$c_2D(c_2) = c_1D(c_1) + (c_2-c_1)D(c_1, c_2) \text{ ---------- [30]}$$

PA6 when exposed to water and methanol vapour showed identical sorption and desorption isotherms. However, ethanol vapour exposure produced non-identical isotherms , indicating that structural changes were induced. Penetrants are sorbed in the amorphous regions, and the factors responsible for the non-Fickian behaviour are reversible structural relaxation processes and the concurrent immobilization of the penetrant. A "γ" to "α" crystalline form change was also observed with ethanol vapour.

Moving to hydrophobic polymers[87], water molecules tend to cluster together in partially oxidised PE since the cohesive hydrogen bonding between them is stronger than the interaction force with the polymer. Oxidation by shearing in a two roll mill of an LLDPE and two different LDPE's of differing melt viscosity was conducted at 160 °C, followed by saturating in water. Water desorption was monitored with both an electromagnetic microbalance (sensitivity 2 ppm) and moisture analyzer (coulometry, sensitivity 5 ppm). The ability of oxidised sites to trap or bind water was modelled in terms of alcohol, hydroperoxide, and carboxylic acid groups being more effective traps than ketone groups, with ester groups having a negligible effect. The experiments, conducted by neutron analysis for oxygen content, gave values in the ppm range and correlated the concentration of oxidised functionality with water vapour permeability.

The theory of active site occurance[88], endorsed in[87], involved PP films which had been γ irradiated and subsequently grafted with AA. Water vapour permeability for the films was found to increase only for the PP from which the antioxidants had been extracted.

Water permeability is measured at high hydrostatic pressures on PVdF, PA's and elastomers with liquid or gaseous permeation cells rated at 100 MPa and ≤ 200 °C at MERL[89]. Certain elastomeric permeability has been found to reduce at pressures of approximately 45 Mpa, at constant temperature.

Of the methods outlined above, for economy and the number of tests performed simultaneously of ASTM E96-80 is excellent, providing the test conditions, usually 25 or 38 °C and 50% RH, are maintained constant throughout. Alternative systems incorporate a humidity sensor in a second dry chamber above the polymer film, for detecting small humidity changes in a dynamic flow of dry air. The time dependence of RH also being monitored.

2b.6.5 Organic Solvent Permeability

For polymer organic vapour permeability[90], the attributes of various permeability cells is discussed, namely, single chamber, evacuated chamber, pouch, and two-part cell. The latter method was preferred for the referenced permeation of styrene through PA6, which gave more realistic mass vs. time curves, when GC is used to analyze the permeant. The same paper discussed a variable humidity OXTRAN Oxygen Permeability Cell, see ref.[56].

Theories were developed which allow calculation[91] of permeability coefficients using the boiling point and molecular volume, applied to the permeability of homologous series's of alkanes, alcohols, and esters, measured through co-extruded PP. Downside organic vapour detection was achieved using GC in the so called continuous/isotactic method, incorporating an adsorption/desorption cycle. Effective molecular volumes were determined by making space filling models of the individual odourant molecules and for measuring their molecular dimensions, assuming ellipsoid shaped molecules.

Another cosmetics packaging application is an isotactic method again used for d-limonene vapour permeability determination of various polymer films[92]. The same permeant was detected with photoionization and atmospheric ionization methods[93]. Similarly, a Barrer[2] type cell, also with a GC FID detector[94], was validated by measuring the permeation of

d-limonene across BOPP and comparing the data with literature values. The permeant was placed in a container below the film, and above the film nitrogen eluted the transported permeant to a commercial SPE column adsorption trap. After a time t_1, the column is changed for another, prior to the contents of the first being extracted with n-hexane, which is analyzed by GC. The high sensitivity of the method was tested using the same permeant through acrylic coated BOPP and PET films, and also permeants with different polarity and volatility, menthol and citronellol. The diffusion and permeability coefficients of the coated BOPP were found to be three or four orders of magnitude smaller than for the uncoated material.

Hernandez and Baner et al[94,95], employed isotactic techniques for organic vapour permeability determination, using an FID GC. They reviewed[96] aroma barrier property determination methods and results. Baner[97], had previously applied equilibrium vapour pressure and microbalance gravimetric technique (sorption) to study the diffusion of toluene in OPP and Saran (PVdC from DuPont) films, as a function of penetrant concentration, by suspending the polymer film directly from one electrobalance arm, with a constant concentration of penetrant vapour flowing over the polymer.

Chlorinated monomers present a particular hazard for polymer food packaging, since they are carcinogens. Desorption of VCM from PVC and AN from PAN were detected with IPGC, at very low concentrations, as migratory non-linear diffusion[98]. The VCM content of the plasticised and unplasticised PVC was reduced to $<$ 5ppm and the GLC was calibrated with VCM solutions in oil and water. These two solvents were then equilibrated with masses of the polymer, so as to limit third phase headspace effects, and predetermined amounts of VCM in N_2 added through a septum cap. For AN/PAN, PAN was coated onto the GLC solid support. Varying the VCM concentration for the polymer/food simulant system was equivalent to varying the initial VCM concentration. The partition coefficient K_p showed a concentration dependence which was lower than that established by earlier researchers[99], for a corn oil system. For water, however, the data are not adequate for evaluation of partition distribution, at low migrant levels.

The absolute adjusted retention times support different modes of interaction

predominating in the two monomer/polymer systems. The retention volume of the monomer increases as the amount of monomer injected onto the unplasticised column is decreased, indicative of sorption of the monomer onto active sites in the polymer. For AN/PAN, the exponential trend of V_g as a function of solute concentration below T_g, suggests that at some finite low concentration, the retention is so prolonged as to represent immobilization. These molecular probe techniques are of great importance when safety from the potential for migration is concerned.

The transport properties of DCM[100] , a component of paint stripper and a rapid permeant, were measured using the gravimetric sorption method. This enabled the differences in the crystalline structures of a quenched and annealed film to be evaluated. The fraction of sorption in and transport through the smectic phase was compared to that of the crystalline film free of the smectic phase. The smectic phase is an oriented structure in which the polymer macro molecular folded chains are ordered in layers head to tail. The sorption data gives the fractions of smectic and amorphous phases in a quenched sample, and the density of the phase that does not sorb the penetrant, which is not easily achieved with other techniques. Later work[101] on the same system focused on DCM with smectic PP, at temperatures higher and lower than 25 °C, to determine the permeability and the process of SINC, with the conclusion that the smectic phase becomes permeable at 25 °C after DCM activity a = 0.5. In all the range of activity at 5 °C and in the range of activity in which the smectic phase does not sorb the penetrant at 25 °C, it was shown possible to derive the amorphous sorption in a smectic sample by comparison with the sorption of the crystalline sample. Although many anomalies were observed in the sorption curves at very low or high penetrant activity, the activation energy derived by the variation of the zero concentration diffusion coefficient with temperature is 21 kcal mol^{-1}. This is high although still in the Fickian controlled process range.

Branching and orientation, it is suggested, supports non-Fickian behaviour, with cross-linked PE resistance to DCM being not surprisingly less than that of drawn, branched LDPE[102]. In terms of industrial polyolefins, which feature significantly in this work, applications, such as cable coverings, landfill and automotive applications, are included in this review of small molecule diffusion. The review addresses morphology, molecular

interactions, and macroscopic parameters and looks at previous polyolefin transport property research. The relevant diffusion models are examined and the role of stabilisers/antioxidants is related to the penetrants. Temperature dependence, co-solvents, carbon black additives, are also included, in addition to polyolefin jelly-filled cable coverings, and swelling behaviour with organic solvents.

2b.7 Multiphase Systems

The high barrier materials such as EVOH and PVdC, are costly and inorganic fillers and commodity polymers frequently dilute them for cheapness. Inert fillers in polymers can either increase or decrease their barrier properties, depending on the degree of compatibility and adhesion between the polymer matrix and filler. Such additives as plasticizer, impact modifiers, etc., generally seem to increase permeation rates. Some of these effects were studied many years ago by Meyers et al[103], and more recently[104] by Bissot. The latter discussed the beneficial effect of mica blended with EVOH on oxygen barrier, for melt phase thermoforming, solid phase thermoforming, and co-extruded blow molding applications, but not for flexible films, or where the platelets are oriented perpendicular to the direction of gas permeation.

A more quantitative approach to aspect ratio is the prediction of permeability changes with concentration of the filler "flakes", as discussed by Cussler et al[105], where experimental data is compared with four models. The second phase is of mica or PA6, the former in PC and an unspecified phenolic polyester (the source of this mixture is cited), of density 1.35 g/cm^3 and the latter in LDPE, both as "flakes", or lamellae.

More recently[106], five grades of a nylon-clay hybrid have been developed as an oxygen barrier packaging film which can also be much thinner and stronger. One nm clay particles uniformly dispersed in the resin as 2wt%, gave half the oxygen permeability of PA6. The PA6/PA66 co-polymer with the clay gave the best oxygen barrier.

A PA6 combination again featured in various wt% blends with amorphous PA[107], containing HMD, IPA, and TPA, and claimed to have the unique property of decreasing oxygen permeability with increasing RH. This is most likely due to water molecules

filling the free volume in the microvoids, since the polymer is mainly hydrogen bonded. It also has a ten fold better CO_2 barrier performance than PA6, useful for future MAP work.

PA6, PA66, and elastomer modified PA66, were blended at with HDPE, LLDPE and LDPE and the blend oxygen and water vapour permeabilities measured[108], with the conclusion that HDPE/PA6 was the best combination because HDPE oxygen barrier of HDPE was improved by a factor of 3.6 and the water vapour barrier was worsened by a factor of only 2.6. At < 20wt% PA, the Maxwell and Rayleigh models fitted the experimental data. The general equation is :

$$P = P_1\{ [1 + (f+1)(P_2/P_1 - 1)c]/[P_2/P_1 + f) - (P_2/P_1 - 1)c]\} \text{ ---------- [31]}$$

where c = 1 - α, and α = volume fraction of conducting phase,

f = a shape factor = 1 for the cylinders relationship of Rayleigh

and = 2 for the spheres relationship of Maxwell

and the subscripts 1 and 2 refer to the continuous and dispersed phases respectively.

PA66/PA6 co-polymer, Selar RB 214, also featured for organic solvent barrier applications in HDPE matrix polymer blends[109]. Toluene, xylene, and a 90wt% unspecified hydrocarbon/10wt% methanol mixture permeants were used. The well mixed material containing 10wt% unspecified compatibilizer gave superior toluene barrier properties to the poorly mixed compatibilized material or either of the uncompatibilized blends. This result is contrary to that found for oxygen barrier of EVOH/PP blends[110], made by co-extrusion with a slit die to produce laminar EVOH in a PP matrix. Theoretical calculations for up to 20wt% EVOH show an oxygen permeability reduction following the homogeneous system predicted value, with at 25wt% a considerable decrease. The trend for higher EVOH content was toward multilayer system behaviour. Tie layer adhesives, both based on MA-g-PP were incorporated into the blends, one with 0.29 wt% MA(1) and the other 0.25 wt% MA(2), calculated from titration[111]. Binary PP/EVOH blends, ternary with (1), and binary with EVOH and latter (2) were prepared. The 70%(2)/30% EVOH material showed good phase bonding from SEM, but this resin had inferior oxygen barrier. The transport data showed that large numbers of small platelets of EVOH are more effective in reducing the permeation rate than thicker ones

in smaller numbers, and SEM studies show optimum EVOH content as 25 wt%, where the predominant platelet structure changes into a layered structure.

More often than in blends, EVOH features in multi-layer, pressure-forming (retortable) hot fillable containers, tied using CXA adhesive resin[112]. An 8 oz. can is shown to be 39% below the price of metal cans. The shelf life is two years where they are filled with food and thermally sterilized, including an HDPE water vapour barrier layer, a Plexar adhesive, and a drying agent.

Contrarary to previous results, it has been found[107] that EVOH exhibits a minimum oxygen permeability at approximately 50% RH, when contained in a LLDPE/tie layer/EVOH/tie layer/LLDPE structure, since water molecules are thought to occupy the free volume.

LCP's have been used in a high barrier co-extrusion film, called Superex[113], consisting of a tough bi-axially oriented LCP layer, a unique tie-layer, and a PET base. Based on equivalent oxygen barrier performance, the LCP layer may cost up to 55% less than EVOH and 40% less than PVdC systems, with simplified recycling. Films of between 50-100 μm thick and 500 mm width have an oxygen permeability of 0.094 cm^3 $mm/m^2/day/bar$. Development of 7 μm films is under way.

More unusually, for amorphous barrier blends, Chiou and Paul[114] reported oxygen and nitrogen gas permeation data through miscible blends of PMMA and SAN, with the composition dependence of gas transport properties being attributed to the weak interaction between PMMA and SAN segments, produced by repulsions between styrene and acrylonitrile units in SAN random co-polymers. Poorly mixed phase separated blends showed similar sorption and permeation properties to those of the corresponding homogeneous blends.

Semi-crystalline blends, co-extrusions or laminates generally include a tie-layer or compatibilizer as shown above. The cost/effectiveness of blend vs. co-extrusion/laminate is often the criteria for selecting the type of multiphase system in a barrier application.

2b.8 Theoretical Permeability Measurement

2b.8.1 Introduction

The majority of theoretical polymer permeability approaches can include as parameters, component permeabilities, component concentrations, dispersed phase shape factors, permeant activity coefficients, permeant/polymer interaction coefficients, permeant/system path coefficients, and environmental coefficients. Some of the more relevant systems are outlined below.

2b.8.2 Environmental Methods

In a study by Chao and Rizvi[34], the study of oxygen and/or water vapour transport through hydrophillic or hydrophobic films was studied in terms of the environmental conditions established within the film during storage was discussed and analyzed.

Looking again at the end use of polymer packaging, Pappas and Khanna[115] proposed a mathematical theory applicable to all types of gases and polymers by incorporating the sorption process in this analysis. The object was to establish a single polymer-food system parameter, including water vapour transport systems where the polymer swells. Pappas[116] in later work used partial differential equations for the three step, transient, Fickian Diffusion moisture transport through the film, Langmuirian adsorption upon the food surface, and Fickian through the food. The modifications this approach allowed the actual RH value near the food to be applied.

Food/polymer interaction again resulted in mathematical models for the simultaneous permeation of moisture and oxygen through packaging polymer films and subsequent adsorption onto the food surface. These were presented for the case of competitive adsorption of the two diffusing species[117] and the models were good in predicting the internal packaging conditions during exposure time, for a variety of selected food products. The contents surface oxygen and moisture transport competition was described by the Langmuir adsorption isotherm.

The permeation of modified atmosphere gas mixtures through LDPE film was modelled mathematically[118], using mixtures of CO_2, N_2 and O_2. When the three component

mixture was humidified, the O_2 permeability decreased almost ten times.

The prediction of barrier again looks at environmental factors for the oxygen transmission rates of multilayer packaging materials containing water sensitive layers under humid conditions[119]. An equation was derived for validating this procedure and it was used to compare the predicted rates with measured rates on a specially prepared multilayer material, giving excellent agreement between the two. The materials used were a sandwich of LDPE surrounding EVOH and the equation derived for the average partial pressure of water vapour at the centre layer, p_c is :

$$p_c = \frac{p_i(t_c / P_{w_c} + 2\ t_o / P_{w_o}) + p_o(t_c / P_{w_c} + 2\ t_i / P_{w_i})}{2(t_i / P_{w_i} + t_c / P_{w_c} + t_o / P_{w_o})} \quad \text{----- [32]}$$

where, t = thickness

P_w = water vapour permeability coefficient

p = partial pressure of water vapour

i = inside layer subscript

c = centre layer subscript

o = outside layer subscript

The %RH can be substituted for partial pressure, at a constant temperature. It is assumed that the transmission rate is inversely proportional to the thickness and that the non-water sensitive layers have an oxygen transmission rate change which can be neglected. For a particular film thickness of the water sensitive layer, a graph can be plotted of OTR vs. the %RH, from which the OTR can be predicted. The effect of several layers can be calculated using the inverse summation equation, where the OTR units are similar to those for permeability but do not include film thickness :

$$1/OTR_t = 1/OTR_1 + 1/OTR_2 + 1/OTR_3 + \text{etc.} \ldots\ldots \text{--------} \quad [33]$$

A computer simulation of the transport properties of a semi-crystalline/amorphous interpolymer membrane is considered as a three component system, ie. the crystalline portion of the matrix polymer, the amorphous part of the same, and the amorphous polymer with ion exchange groups[120], where the influence of crystallinity and crystallite size on percolation threshold and permeability is considered. The conclusion was that the system includes excluded volume, due to the crystallites, and that the critical

concentration of permeable(amorphous) polymer at which a percolation transition appears decreases with increasing crystallinity/crystallite size. The permeability coefficient of the membrane increased with increasing crystallinity/crystallite size at constant concentration of permeable component.

Brown and DeLassus[121], in contrast, compared on the basis of various environmental factors including cost, the choice between High Barrier Saran (MA/PVdC co-polymer), EVOH, SAN, and PET, since the oxygen barrier properties of polymers are described adequately, by their permeabilities. The problem of selection is however, complicated by their variety. Hence, a model for describing their cost effectiveness should take into account, cost/kilogram, density, temperature of interest, and permeability. Since the permeability is based on the thickness and area, thus the material volume determines the cost of raw material involved and so the permeability must be multiplied by the density and raw material cost.

2b.8.3 Blend theories

Theoretical calculations for blends rather than layered structures have been made for permeability, describing the effect of a conducting spherical filler on the overall composite permeability, using Robeson's[122] equation, to give :

$$P_c = P_m[P_d + 2P_m - 2\varnothing_d(P_m - P_d)/P_d + 2P_m + \varnothing_d (P_m - P_d)] \text{ ----- [34]}$$

where, P_c = Permeability of the blend

P_m = Permeability of the matrix

P_d = Permeability of the disperse phase

$\varnothing_d$ = Volume fraction of dispersed phase

The corresponding Maxwell[123] series and parallel equations, normally applied to laminates/co-extrusions or co-polymers are respectively :

$$P_c = P_1P_2 / (\varnothing_1P_2 + \varnothing_2P_1) \text{ ---------- [35]}$$

$$P_c = P_1\varnothing_1 + P_2\varnothing_2 \text{ ---------- [36]}$$

where P_1 and P_2 are permeabilities of the respective phases, with $\varnothing_1$ and $\varnothing_2$, being the corresponding volume fractions.

From an approximate solution of the Laplace equation, applied to the effective dielectric

properties of powders and suspensions :

$$F_d = [3P_m/(2P_m + P_d)]F_m \text{ ---------- [37]}$$

where, F_d and F_m are the average activity gradients of the permeant at the steady state stage of permeation (when the concentration of the permeant in the film is no longer changing) in the dispersed and matrix phases, Higuchi et al[124] developed an equation similar to equ'n.[34] for polymer blends. His equation is thus :

$$P_c = (3P_mP_d\varnothing_d + 2(P_m)^2\varnothing_m + P_mP_d\varnothing_m)/(3P_m + \varnothing_m(P_d - P_m) \text{ ------ [38]}$$

sometimes quoted[125] in the form :

$$P_c = P_m\left(P_d - 2P_m - 2\varnothing_d (P_m - P_d)/P_d + 2P_m + 2\varnothing_d (P_m - P_d)\right) \text{ ------- [39]}$$

Ottino and Sax[126], investigated small permeants diffusing through polymer blends, as morpholological probes, in steady state. Effective Medium Theory, produced a co-ordination number (z), with accurate predictions of effective diffusivity being made for the conducting component volume fractions between 0.3-0.8, by letting z = 6.

In contrast to the above mechanism, the many parameters influencing the permeability of both homopolymers and blends is reviewed[127] from a practical point of view. The optimum barrier polymer is described and also the short comings of the current polymers. The meaning of permeability and how it cannot be derived from D are also included. The propagating wave theory of diffusion, the dependence of permeability on swelling, the density effects on penetrant concentration, and finally molecular transport in polymer blends are highlighted.

2b.8.4 Water Vapour Transport

Shwartzenberg addresses several issues[128] for modelling transport through hydrophillic films with highly non-linear water sorption isotherms and diffusivities which depend strongly on the films water content. Mass transfer resistances in adjacent gas layers and materials, strongly effect mass transfer resistances in the film itself. He presents methods for separating upstream and downstream resistances from that of the film by incorporating diffusivity terms for swollen films, as proposed by Doolittle and Fujita[129] into Fick's first law and also water activity coefficients (a_w). The latter must fall on the same straight line region of the water sorption isotherm, and the flow diagram for

calculating the diffusive flux through the film is presented. For gases and vapours, their permeation rate will tend to increase as the humidity and moisture contents on the downstream side of the film increases, but selectivity will diminish in the case of pervaporation. He also questions the neglect of the mass transfer coefficients in the ASTM Standard E96-80(ASTM, 1983) test calculations.

In a later chapter from the above volume[130], the relative humidity on the upstream side of the polymer packaging film is considered to be the a_w of the product packaged, and is correlated with the water vapour permeability for various hydrophobic and hydrophillic packaging materials, together with the difference in partial pressure across the films, at various temperatures and RH's. For OPP the equation was proposed :

$$\mathbf{P_{water} = a_w \Delta p + b} \quad \text{---------- [40]}$$

where P = permeability, in units of mass or volume $mm/m^2/day/bar$ and for OPA6 :

$$\mathbf{P_{water}/external\ RH = a_w \Delta p_{f(t)} + b} \quad \text{---------- [41]}$$

when $\Delta p > 10$ mm Hg and $\Delta p_{f(t)}$ is the partial pressure change at a particular temperature. Below 95% RH, OPA6 was also shown to be a better oxygen barrier than PET. The way in which water is fixed to the polymer chain of hydrophillic high oxygen barrier materials such as EVOH was established by correlating the equation :

$$\mathbf{X = a_w \log(-\log a_w) + b} \quad \text{---------- [42]}$$

with experimental results, and the fit was excellent. However, for experimental permeability determination, a laminated structure of OPP/EVOH/LDPE was used, and due to the differences in the water vapour permeabilities of each layer, the rule of reciprocals :

$$\mathbf{1/P_{water} = l_1/l_tP_1 + l_2/l_tP_2 + l_3/l_tP_3} \quad \text{---------- [43]}$$

gave erroneous results. Ignoring the water uptake of the polyolefins, the structure showed a perfect correlation with that of pure EVOH. Between a_w 0.0 to 0.85, it was found that the multiphase system oxygen permeability closely followed the equation :

$$\mathbf{\log(P + P_2 + 0.53) = 1.373\ a_w - 0.32} \quad \text{---------- [44]}$$

where P is the overall permeability and P_2 is the oxygen permeability of the EVOH layer.

A finite element analysis incorporating material geometry and using the Luikov coupled partial differential equation[131] again addresses water transport. It includes, transient flow

of moisture, heat and pressure potentials as variables and a method[132] computes the moisture permeability of barrier films using this equation. The solution proceeds step by step with time, with an update of material parameters at each time step. Chemical interaction and swelling are ignored, and a non-symmetric stiffness matrix is produced, with a symmetric matrix resulting if certain material properties are constant. Designed primarily for construction materials simulation, the preprocessor includes a special modelling feature for thin moisture barrier films, although small elements are not easily introduced and solved, and are therefore modelled as local moisture resistance between coincident nodes, thus avoiding numerical difficulties in the solution. A database of moisture related material properties is included and the postprocessor presents colour diagrams, and the software is written in FORTRAN. The author shows an example of moisture flowing through a PMMA plate sealed with a nitrile rubber seal, and suggests further enhancements for moisture related material properties at different temperatures and also linear and non-linear elasticity theory.

By complete contrast to the above civil engineering application, FTIR spectroscopy studies of sorbed water molecules[133] in polymer matrices were correlated with the shifts of the three bands corresponding to the normal vibrational modes of an isolated π water molecule, and hence the heat of water sorption was deduced. It was concluded that almost exclusively for both hydrophobic and hydrophillic polymers, sorbed water molecules form strong or weak hydrogen bonds. The atom with the largest electronegativity in the polymers increases the bending frequency shift more than the stretching frequency shifts, indicating that a water molecule associates itself with a particular site such as a polar atom or group (X) in the polymer. The interaction becomes stronger with increasing polymer hydrophilicity. The lowering of the ν(OH) frequencies increases according to the following order : F < Cl < C(aromatic π-electron)< COO < O < NHCO < NH. A Water Affinity Parameter (WAP) is defined as the frequency shift of ν_a(OH), with the reciprocal representing the hydrophobicity of the polymer.

2b.8.5 Group and Graph Theory

Using polymer molecular structure functional groups (group theory), Salame[134] introduced a new physical parameter for which he coined the name (specific) Permachor

(Π), an additive molar function for the estimation of amorphous polymer permeability. He in fact correlated polymer structure and morphology and gas permeability and the Permachor is defined by the equation :

$$\Pi = -1/s \ln P(298)/P^*(298) = -2.3/s \log_{10} P(298)/P^*(298) \text{ ---------- [45]}$$

where, P(298) is the permeability of an arbitrary simple gas in an arbitrary polymer, $P^*(298)$ is the permeability of the same gas in a chosen standard polymer and s is a scaling factor, determined by the choice of the second fixed point on the Π scale (x axis) of a plot of Π vs. log of permeability, for various polymers. This point is normally a very impermeable polymer and s for oxygen has a value of 0.12 at 298K.

The disadvantage of the permachor method is that in the case of different gases, a set of values for $P^*(298)$ and for s should be known. Therefore, log P(298) for nitrogen is first of all calculated (taking this gas as the standard gas) and then the relative P-values obtained from tables calculated by Stannett and Szwarc[135], Rogers et al.[136], and Frisch[137] are applied to find s. Estimations can also be made for other temperatures, if E_P is known. Corrections for α_c and draw ratios can be applied to the amorphous Π-values, for semi-crystalline and oriented crystalline polymers.

Salame finally found[138] that Π is a linear function of $\log(e_{coh}/f_v)$, where e_{coh} = cohesive energy density and f_v = fractional free volume of the polymer. For miscible polymer blends[139], the permeability was usually lower than the predicted value, and with immiscible blends, the permeability was always higher than the permachor prediction. He attributed the better than predicted values with the miscible blends to a loss of free volume and the worse than predicted results for immiscible blends being due to a lack of adhesion between the disperse and matrix phases. He feels that permeability might be a good way of assessing polymer blend compatibility.

Bicerano[140] cited another method of predicting the oxygen permeability of polymers by a functional group contribution method, using the "newchor", v, including corrections for hydrogen bonding contributors like -OH and CONH functional groups. The equations generated for N_2 CO_2 and O_2 can be used to obtain a rough order of magnitude estimate of P for all polymers built from the elements C, N, O, H, F, Si, Cl and Br, without

being limited by the lack of group contribution data. For the calculation of v the following equation was used:

$$v \equiv E_{coh1}/V - 196\ V/V_w + 110\ N_{rot}/N - 57\ N_{per}/N \text{ ---------- [46]}$$

where E_{coh1} = is the Fedors-type cohesive energy[141,142]

V = the molar volume

V_w = the van der Waals volume

N_{rot} = the rotational degrees of freedom parameter

N = the number of vertices in the hydrogen-suppressed graph of the repeat unit

N_{per} is defined to improve the correlation by including corrections for different substituent groups, and hydrogen bonding effects

Thence, the permeability is estimated from :

$$P_{O2} = 4991.6 \times \exp(-0.01762 \times v) \text{ ---------- [47]}$$

Equ'n.[47] has a standard deviation of 0.7159, indicating that approximately two thirds of the fitted P_{O2} values are within a factor of $\exp(0.7159) \approx 2$ of experimental values, ie. between $0.5 \times P_{O2}(exp)$ and $2 \times P_{O2}(exp)$. The correlation coefficient of equ'n.[47] is 0.9685, indicating that this equation accounts for 93.8% of the variation of $\ln(P_{O2})$ in the data cited. Tables of the experimental and calculated values from equ'n.[47] are included. Equ'n.[47] is in fact analogous to Salame's permachor equ'n.[45]. The limitations of such a simplistic approach, where the permeability is treated in terms of a single parameter, is also discussed.

Graph theory methods were shown to complement group additivity methods of predicting oxygen permeability in certain types of polymers[143]. Graph theory is a topological approach that assigns a set of indices (Randic Indices) to a molecule to describe its structure, in this case via a modified representation of the monomer unit. A 3.2% average relative error value of the molar indices used to describe the log of the oxygen permeability was achieved, showing good agreement with the permachor method. But this corresponds to an average error of 22% in P. By selecting data from only one experimental method for comparison, the variation can be minimized. The correlation coefficient was 0.91, with the remaining 9% of data scatter probably due to the graph theory model not having any crystallinity terms. Accounting for the free volume or the

van der Waals or excluded volume may be useful to quantify the crystallinity of the polymer systems.

Oxygen permeability prediction from T_g of PA6 and PA66 at different RH's[144] produced good agreement between experimental and theoretical results. Both the permachor parameter from[134] and in order to incorporate the effect of moisture, the CED, FV, V_m,[145] and E_v, were also included. Using the E_v, the mobility parameter n, is calculated from the equation[146]:

$$E_v = (0.5\ RT_g - 25)n \quad \text{---------- [48]}$$

presuming n does not change below the T_g. The equation represents the variation in the cohesive energy E_v, with the change in T_g as a function of the moisture content,

where, CED is the cohesive energy density, E_{coh}/V_m,

E_{coh} is the cohesive energy per mole

V_m is the molar volume

and FV is the free volume

2b.8.6 Polymer Permeability Literature summary

The theoretical approaches for barrier properties prediction presented above are many and varied. One conclusion is however clear, that the model selected will be dedicated to a particular system and largely empirical, but should include as many polymer physical, chemical, structural, transport parameters as possible, in order that the model is valid.

CHAPTER 3 - EXPERIMENTAL PROCEDURES

3a Preparation and Characterization of Polymer Multi-Phase Systems

3a.1 Introduction

A series of thermoplastic polymer blends were prepared in the melt, using a laboratory scale blender, at a fixed temperature for each system, and with a fixed rotational speed. The blender residence time was optimised for the best phase dispersion (by measuring the dispersed phase size after different blender residence times) and minimum polymer degradation.

3a.2 Blend Components

PP homopolymer, ICI grade PP-A PXC 21369, with a crystalline melting temperature(T_m) of 153 °C and MFI of 9 g/10 minutes (230 °C/2.16 kg) was initially selected as the water vapour barrier blend component. ICI Melinex PET, with a T_m of 241 °C, injection grade Isotactic PP co-polymer (DSM Stamylan 48M10), spinning grade PA6 (BASF Ultramid B5), and spinning grade PA6 (EMS-Chemie Grilon A23), were later used for blend compounding, the first two being supplied by CarnaudMetalbox. The A23 was supplied directly from EMS. PET is cheaper than PA6 but only provides better oxygen barrier after biaxial orientation, at moderate RH, see Table 1 in Chapter 1. The PA6 was chosen eventually for blending with the PP. The injection grade of Orgalloy R-6000(Elf-Atochem)(R6000), a commercial PA6/PP blend, was also studied. The two PA6's and R6000 were dried at 80 °C under reduced pressure for 48 hours.

Prior to blending, Differential Scanning Calorimetry(DSC) was conducted on the homopolymers to establish their T_m, using a Perkin-Elmer DSC-2B, in accordance with ASTM D 3417, "Standard test method for heats of fusions and crystallisation of polymers by thermal analysis". Between 5 and 10 mg duplicate samples of the homopolymers were heated from 40 °C to 280 °C at a rate of 10 °C min^{-1} by heating the samples in closed aluminium pans, under a nitrogen blanket. Reproducibility of the results was estimated to be ± 0.5 °C.

The blend components were also characterized by FTIR (Fourier Transform Infra-Red) Spectroscopy, Steady State/Dynamic Viscosity, density and have the following physical

properties.

Table 2 : Selected Polymer Properties

Material	*T_m °C*	*MFI g/10 minutes*	*Density gm cm^{-3}*	*Relative Viscosity cm^3/g(in 1wt% aqueous H_2SO_4)*
PP (DSM 48M10)	163.3	14	0.902	———
XLPP(silanated PP)**	153	0.5	0.893	———
PA6(B5)	221	1.4	1.130	315
PA6(A23)	225	48.7	1.163	0.23
Orgalloy R-6000	161.8(PP) & 221(PA6)	8.4	1.030	———

**** Note that the PP used is DSM 48M10 and is silanated with 2wt% Union Carbide A174 silane, using a method described in Section 3a.8.1**

The MA (Maleic Anhydride) and BMA (Butyl Methacrylate), both used later, were BDH 99% grade, and the hydroquinone stabilizer was removed from the latter by washing with 30wt% sodium hydroxide solution. BPO (Benzoyl Peroxide) was BDH 97wt% grade and DCP(Dicumyl Peroxide) BDH 98wt% grade. Both were purified by dissolving in chloroform at room temperature, followed by precipitation in methanol. The BP (British Petroleum) Polybond PB1001, PB3009 and PB3002 compatibilizers were used without further treatment.

When it was decided to focus on blends of polyolefins and PA6, grafted PP compatibilizers were used, such as, MA-g-PP(Maleic Anhydride grafted onto PP). These are well known interfacial agents (compatibilizers)[5], so called because it is thought they promote some partial miscibility and greater homogeneity in immiscible polymer blends. The PB3002, PB3009, and PB1001 are commercial BP Polybond compatibilizers. The PB3002 is PP functionalized with Maleic Anhydride, the PB3009 is HDPE functionalized with Maleic Anhydride, and the PB1001 is PP functionalized with Acrylic Acid. BA-g-LDPE[7], has been formerly used in polyolefin blends and the preparation of BMA-g-LDPE is described in Section 3a.7.

The melt shear viscosity of the PA6(B5) was reduced from an MFI of 1.6 to 16.7 by suspending PA6 in formic acid vapour (plasticization), at 90 °C, under reduced pressure, for 3 hours. The material was dried after plasticization in a similar way to the homopolymer, to ensure that residual formic acid vapour was removed. FTIR spectroscopy of the plasticized B5 (plast.B5), showed no evidence of residual formic acid. A granule of PA6(B5) was found to dissolve completely at the T_m of liquid MA, 68 °C. Plasticization of PA6(B5) was thence performed by melt blending 95wt% PA6 and 5wt% MA and examined by FTIR spectroscopy. See Section 3.9. MA-g-HDPE (PB3009) and BMA-g-LDPE (synthesised in-house) were not found to be more effective compatibilizers for PP/PA6 blends, despite each having an MFI closer to that of the PP than PB3002, and were abandoned.

3a.3 Mechanical Blending

Polymer melt blending, to make 5 g amounts, was performed using a heated mechanical blender, rotating at approx. 105 rpm and fitted with Gulton West 3400 Temperature Controller, operating at ≤ 280 °C. A controlling Iron-Inconel thermocouple was mounted between the outside wall of the blender and mixing vessel insulating jacket. A supplementary Iron-Constantan thermocouple, inserted into the blender lid was connected to a Digitron 3750-K digital thermometer. The shear generated by the blender was similar to that of a twin screw extruder, ie. a rate of 10^2-10^3 s^{-1}, as estimated from the angular velocity of the rotating blender cupola. Veins in the stationary blender lid distributed the materials evenly during residence time. A schematic diagram of the blender is shown in Figure 2.

The order of blending was governed by the temperature having to be above the T_m of the highest melting component. Hence, the PA6 was added first, followed by the PP and a compatibilizer, if included. The higher viscosity material, has a tendency to be enfolded by the lower viscosity material, when it is the minor component.

3a.4 Sample Preparation

Homopolymers and blends for FTIR analysis were hot pressed , using a 15 μm washer, one of six, on the SPECAC CTFM (Constant Thickness Film Maker), under the SPECAC 15.011 Press, fitted with a Gulton West 3400 temperature controller. To ease

the cleaning of the highly polished and machined anvils of the CTFM, circles of aluminium foil were placed above and below the polymer granules and these also produced smooth films of uniform thickness. The thickness of the films was measured in μm with a Mercer 122D pneumatic gauge fitted with a hemispherical non-invasive probe, by taking the arithmetic mean of sixteen measurements of the material, where the permeability effective cross-sectional area diameter is located. Silicon free proprietary mold release was placed on the aluminium foil in contact with the polymer. It was

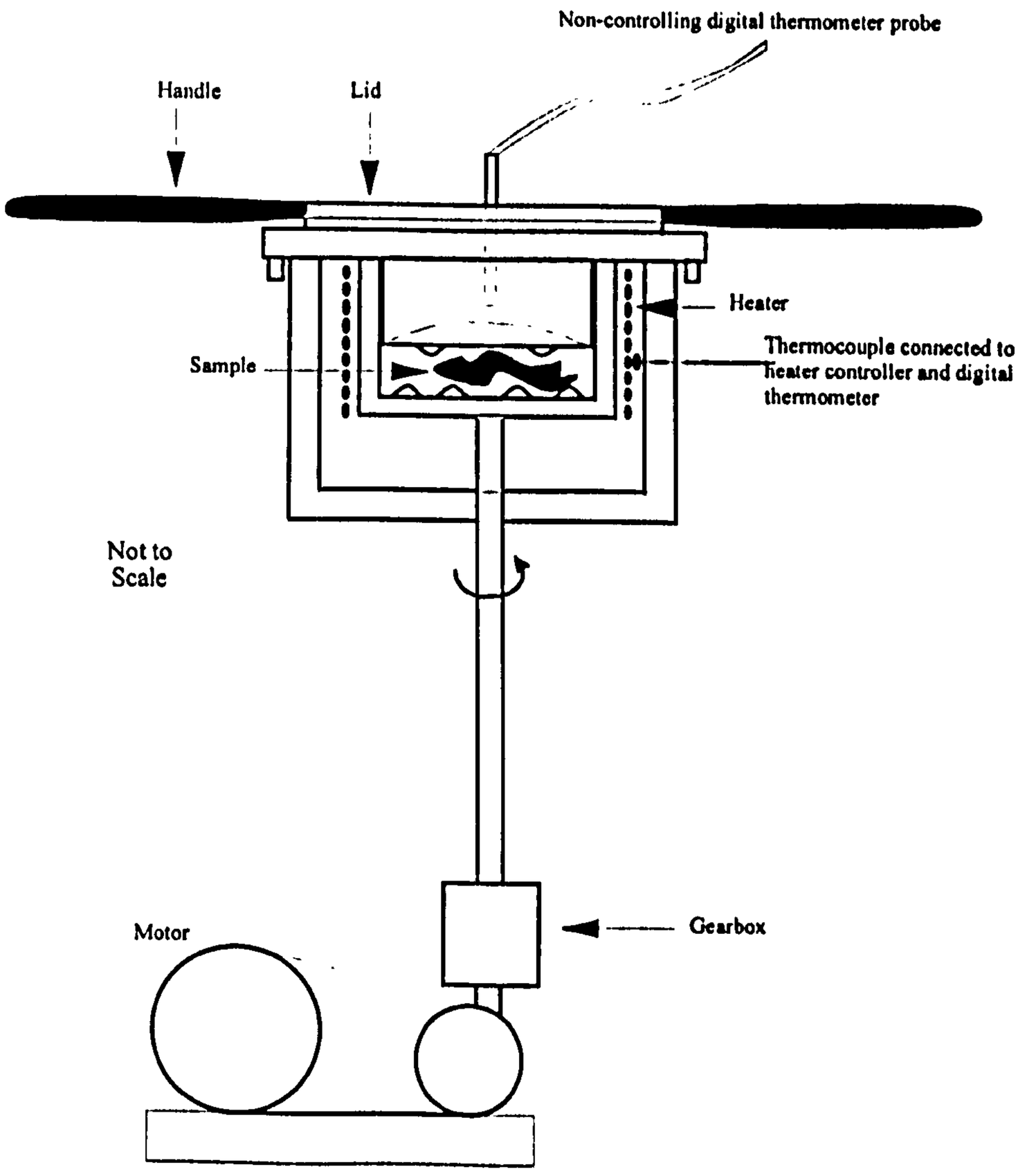

Figure 2 : Schematic Diagram of Laboratory Mechanical Blender

difficult to separate the PA6 films from the aluminium foil, which was subsequently removed with NaOH solution. Some samples were microtomed with a glass knifed Cambridge/Shandon instrument, both for FTIR and LM. For permeability measurement films, the CTFM was also used, generally with washers larger than 15μm.

3a.5 Light Microscopy (LM)

Blend morphology was studied using LM with a Leitz Laborlux S light microscope and Zeiss M35 camera. The latter was also fitted with a Zeiss MC63A exposure meter, Hobut intensity meter and Reichert turntable. The microscope was equipped with a Phaco phase contrast lense and Leitz fluorescence source, with, red, green, and blue filter blocks. Blend morphology was examined using light microscopy , under, transmitted light, phase contrast, polarized light, fluorescence, and differential interference contrast (DIC). High contrast micrographs at x700 magnification, similar to those in Figures 27-56 were obtained. From the micrographs, the particle size distribution and average particle size was evaluated, by direct manual measurement, classified into categories of 0.5μm step size, with the range of particle sizes being from 0.5-70 μm. The phases are identified in this work by using the LM UV fluorescence source, since with a blue filter, the PA6 phase fluoresces.

3a.6 Interfacial Tension

Phase dispersion is dependent on the interfacial tension of the phases in the melt, which cannot be easily measured. Analogous however, is the surface tension of low molecular weight liquids with solid surfaces at room temperature. Dynamic surface tension was therefore performed and contact angle measurements were made on a CAHN DCA-322 instrument, and the receding angle data is reported in Table 5, section 4.2, since this is a more accurate measure for polymer films, than the entering angle.

6 4.4.2

The instrument was operated within the plate range, at a sensitivity of 0.1 mg and maximum force of 750 mg. The wetting force at the solid/liquid/vapour interface is automatically recorded with an electrobalance as a function of time and immersion depth. The meniscus formed at the interface is characterised by Θ, the dynamic contact angle or tangent at the interface, which is an experimental representation of the Young's equation[8], relating the angle to the interfacial free energies of the three interfaces, solid/vapour(sv), solid/liquid(sl), and liquid/vapour(lv). At equilibrium :

$$\cos \Theta = (\gamma_{sv} - \gamma_{sl})/\gamma_{lv} \text{ ---------- [49]}$$

γ_{lv} is the known surface tension of the liquid and by transposing the equation, γ_{sl} can be calculated. The difference between the two extreme contact angles, as the stage moves up and down is known as contact angle hysteresis, and is a universal property of most

surfaces. The Wilhemy hysteresis technique of measurements were made for the polymer films by running the samples in and out of the liquids in triplicate. By ensuring a wet-out condition (zero contact angle) of the liquid against a known high-energy solid glass surface, the exact surface tension for the liquids was determined from the equation :

$$\cos \Theta = F/ p \gamma_{lv} \text{ ---------- [50]}$$

where F is the force in dynes measured by the balance, p is the perimeter of the sample in cm, and γ is measured in dynes cm^{-1}.

The solvents selected were, xylene, methanol, and water, each with varying degrees of polarity. The values obtained, see Section 4.2, are close to those quoted literature values, but do not give an indication of the interfacial tension between the blend components.

Due to the inconclusiveness of the surface tension data, and lack of high temperature equipment, an alternative method was sought for measuring the contact angle, by heating pieces of PP and/or compatibilizers onto films of the two PA6's and also onto films of the PA6's blended with 8wt% of each of the four compatibilizers used in this work. This was achieved at 190 °C, under reduced pressure. The melted material also included PP blended with 8wt% of compatibilizer used. However, for incompatible materials, a negative angle would be expected, but largely, a positive angle was observed. The exceptions were for the (BMA-co-MA)-g-PP and PB1001 compatibilizers, where the measurement of a negative angle was obscured forthese materials since they appeared not to melt onto the PA6 films at this temperature, despite having high MFI's(low melt viscosities).

Laminated structures were prepared as an alternative to dispersed phases, since they are commonly used as polymer packaging films. This was accomplished in one of three ways. Firstly, by melting PP or XLPP(2wt% A174 silane) films onto either PA6(A23) and PA6(B5) films, under reduced pressure, at 190 °C. Secondly, by following a similar procedure as the first, but also including a compatibilizer layer in between the homopolymers. Thirdly, by "tying" the homopolymer layers together using one of either Scotch Grip 4235, Fastbond 30, or Durotak 380-1846 commercial tie adhesives. The thickness of the films before and after laminating was measured, from which the average thickness of the tie layer was calculated. Tie layer laminated films were also prepared

using XLPP, and ternary laminates were made without a tie layer but including instead a compatibilizer layer.

Mechanical testing of the strength of the bond between the layers[9], would give an indication of the interfacial tension, which could be estimated from the Taylor's theory relationship, applied to dispersed particle deformation[10] :

$$k = \eta_2 \gamma d / \nu \quad \text{---------- [51a]}$$

where k is the capillarity number, η_2 is the viscosity of the matrix, γ is the Newtonian shear rate, and d is the dispersed phase size, and ν is the interfacial tension. Providing the dispersed phase is not perfectly spherical, which is often the case, k can be found from[10] :

$$k = \{((L - B)/(L + B)).(16\lambda + 16)\}/(19\lambda + 16) \quad \text{---------- [51b]}$$

where λ is the viscosity ratio, and L and B are the mean major and minor diameters of the deformed dispersed phase particles.

3a.7 Compatibilizer Synthesis

The MA has a tendency to absorb atmospheric moisture to form the acid, which would prevent the grafting reactions. Therefore, prior to reaction, the MA was dried in reduced pressure at 80 °C. The grafting of MA onto PP[11] was achieved by mixing 8.99wt% of PP with 0.90wt% of MA and 89.93wt% of xylene, with agitation, until homogenized, at 120 °C,under nitrogen, followed by the addition of 0.18wt% of BPO. The mixture was refluxed for a further 4 hours, washed with methanol several times, to remove excess reactants, and dried to constant weight in vacuum. The evidence of the 1.5wt% grafting ratio was obtained from FTIR of the graft co-polymer, MA-g-PP, based on polymer weight increase. See Figure 3 for the probable reaction scheme. In addition to the PP radical shown, there are other possible "unzipping" and chain scission reactions, which result in a lowering of PP molecular weight.

It was thought that MA could also be grafted onto PP by melt blending them together, as 0.5 wt%, 1wt%, 5wt%, and 10wt% MA. However, MA has a melting point of 68 °C and volatilised rapidly with molten PP, prior to sealing the blender. Only the 0.5% blend showed strong FTIR spectroscopy evidence of C=O and C-O-C stretch. BPO was also included in a further blend, prepared with the same wt% as the solution grafting method

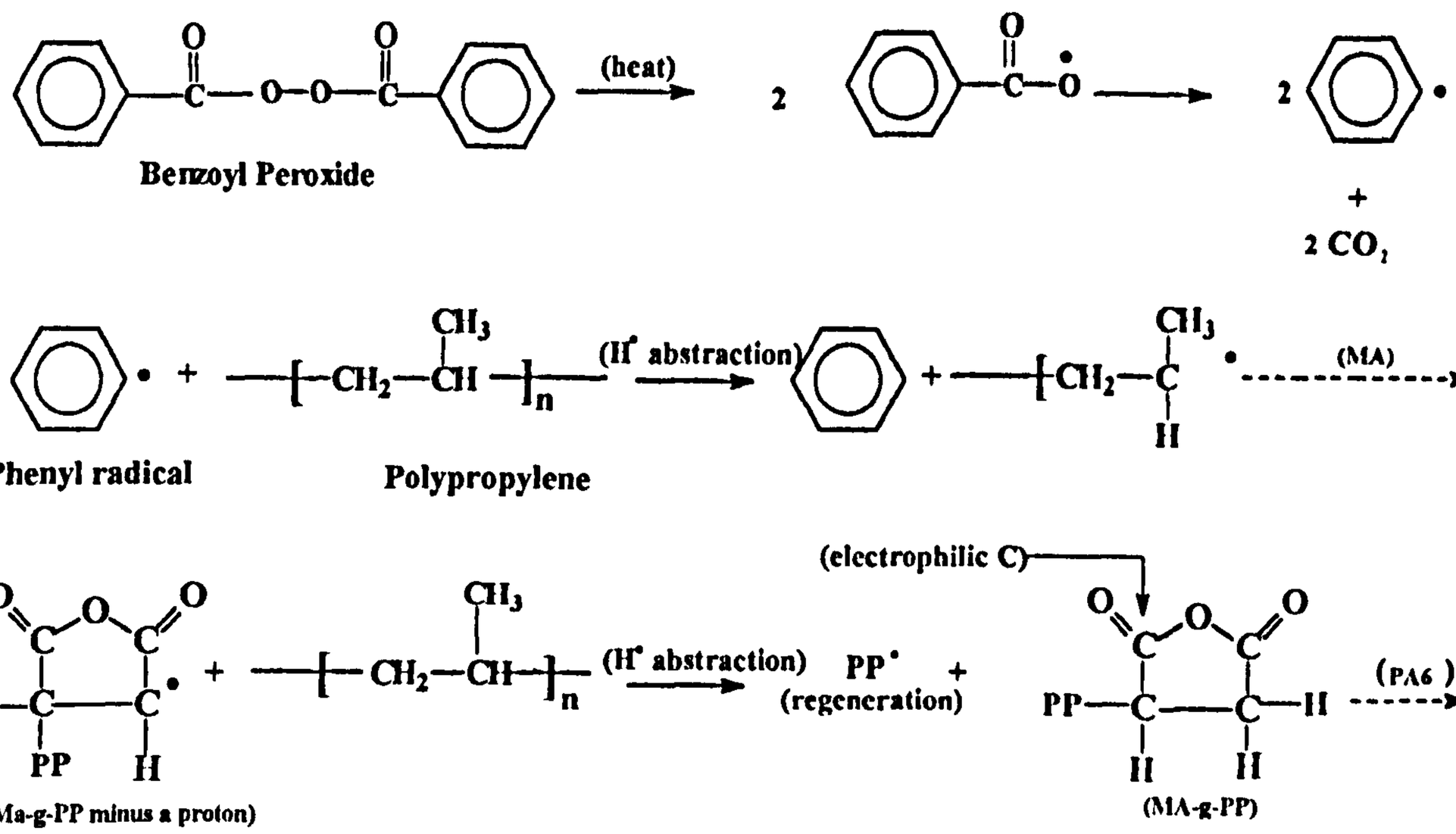

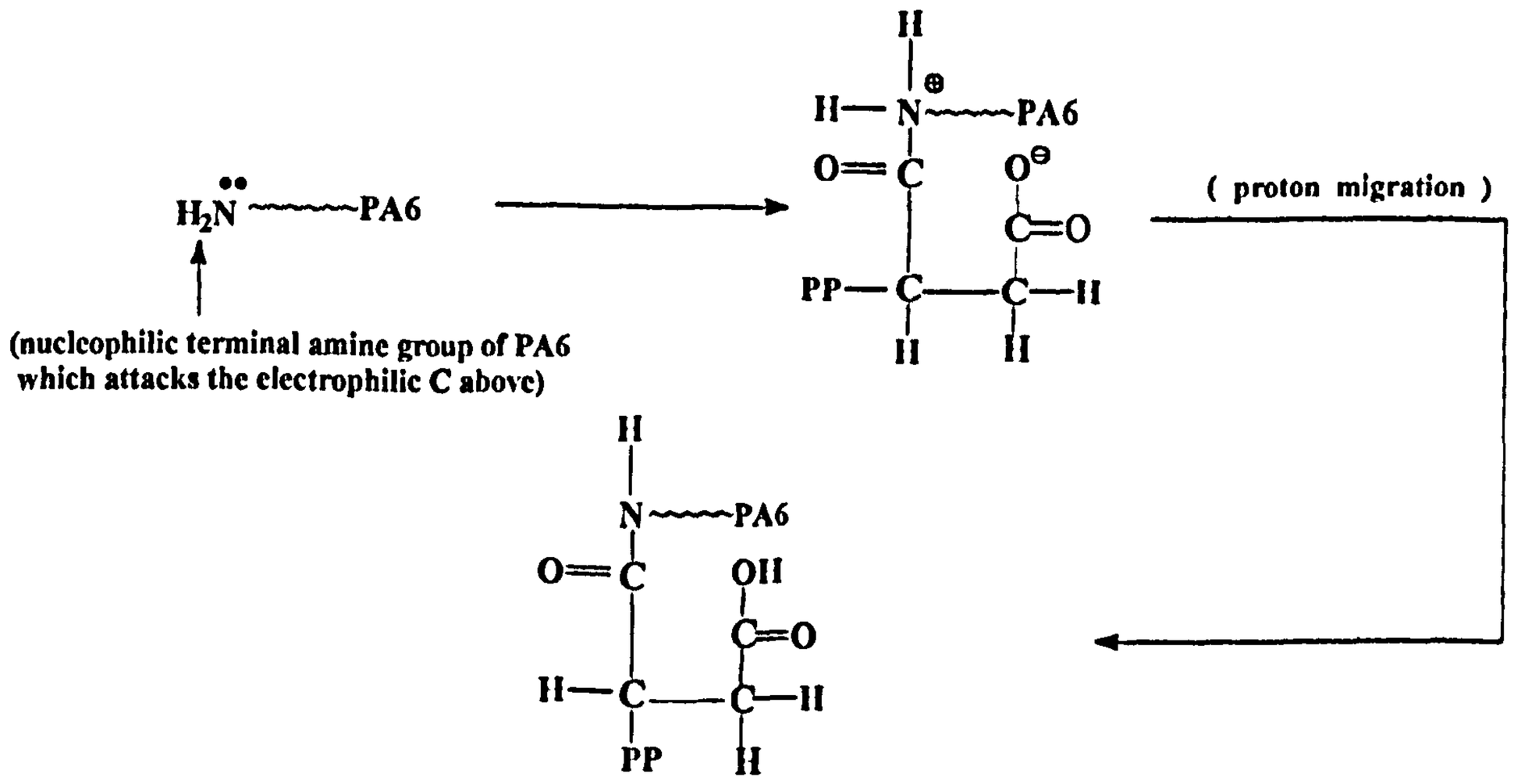

Figure 3 : Possible MA-g-PP formation reaction scheme and subsequently with PA6

and this material showed no discernable difference from the 0.5wt% MA blend, based on FTIR spectroscopy.

The grafting of BMA on LDPE (BP Novex)[7] was performed by mixing 9.64wt% LDPE, and 83.60wt% toluene, under nitrogen at 90 °C, for ten minutes, to remove dissolved oxygen. 0.96wt% of DCP was then added, and after a ten minutes agitation, 5.80wt% BMA was added. Refluxing continued for a further 15 hours, the product cooled, washed with 2 litres of acetone, to remove unreacted reactants, and dried under vacuum at 50 °C to constant weight. The percentage grafting efficiency was determined on the basis of changes in LDPE weight during reaction[12], to form BMA-g-LDPE, showing a grafting ratio from FTIR spectroscopy of ≈ 2wt%. The optimum conditions were found to be a ratio of LDPE : BMA of ≈ 0.7, BPO concentration 0.012 mol wt%, and reflux time of 10 hours. This gave an 11wt% grafting, better than that of the MA-g-PP, but unfortunately in this work the BMA-g-LDPE was not found to be a suitable compatibilizer for the PP/PA6 blends.

A third compatibilizer was prepared as (BMAcoMA)gPP by heating 9.03wt% PP, with 78.31wt% xylene, under nitrogen, at 110 °C, followed by the addition of 0.013wt% of DCP. After 10 minutes of stirring, 6.32wt% each of MA and BMA were added and the refluxing continued for 12 hours[13]. The resulting precipitate, after pouring into 1 litre of acetone, was washed, and dried under vacuum to constant weight, at 50 °C. The grafting was found to be approximately 7wt%, of which 4.7wt% was MA. The reaction scheme for BMAcoMAgPP preparation and the subsequent compatibilization reaction with PA6 is shown in Figure 4.

BP quote the grafting ratio's of the Polybond's[14] as 3wt% for PB3002 and 6-10wt% for PB1001 (See Section 4.5.2.3 for FTIR spectra, where the former grafting ratio is shown to be < 1wt% and the latter 8wt%). The commercial blend, R6000, has a composition of approximately 40wt% PP, 48 ± 2wt% PA6, and 12 ± 2 wt% of compatibilizer[15]. The compatibilization results in reduction of the blend crystallinity by 13-14wt%, representing, it is thought, the compatibilizing co-polymer of PA6 and PP. Since the PA6(B5) dissolved in the liquid MA, at 162 °C, MA was blended directly with PP and PA6, in the melt, to form 65wt% PP, 30wt% PA6(B5) and 5wt% MA. The LM

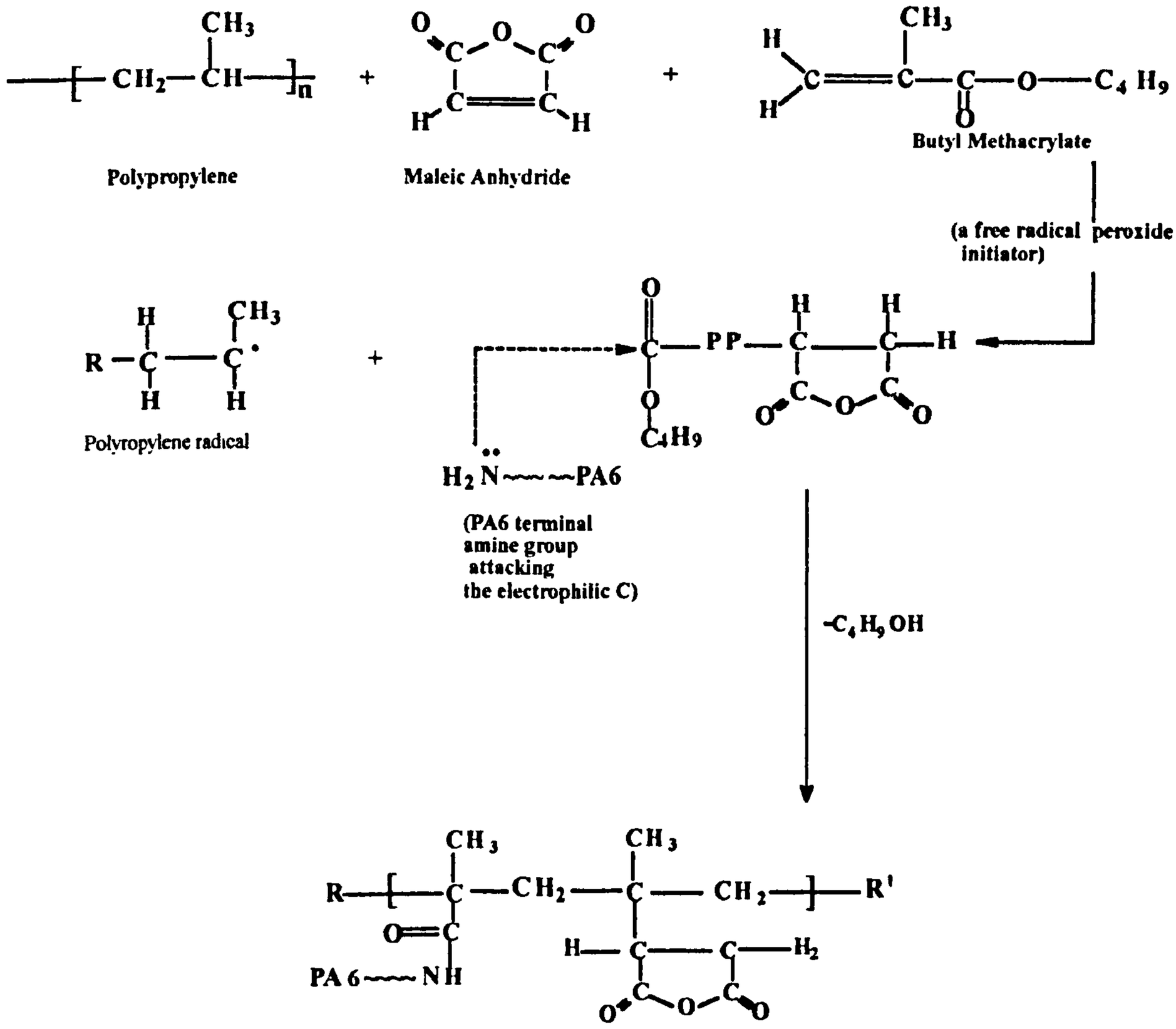

Another possible reaction product of PP with MA and BMA is shown below

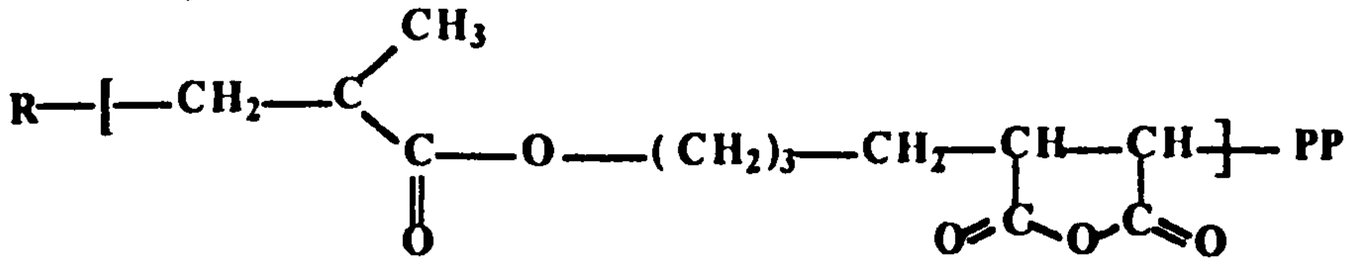

Poly(butyl methacrylate-co-maleic anhydride)-g-PP

Figure 4 : Possible reaction scheme of MA/BMA with PP forming (BMAcoMA)-g-PP and subsequently with PA6

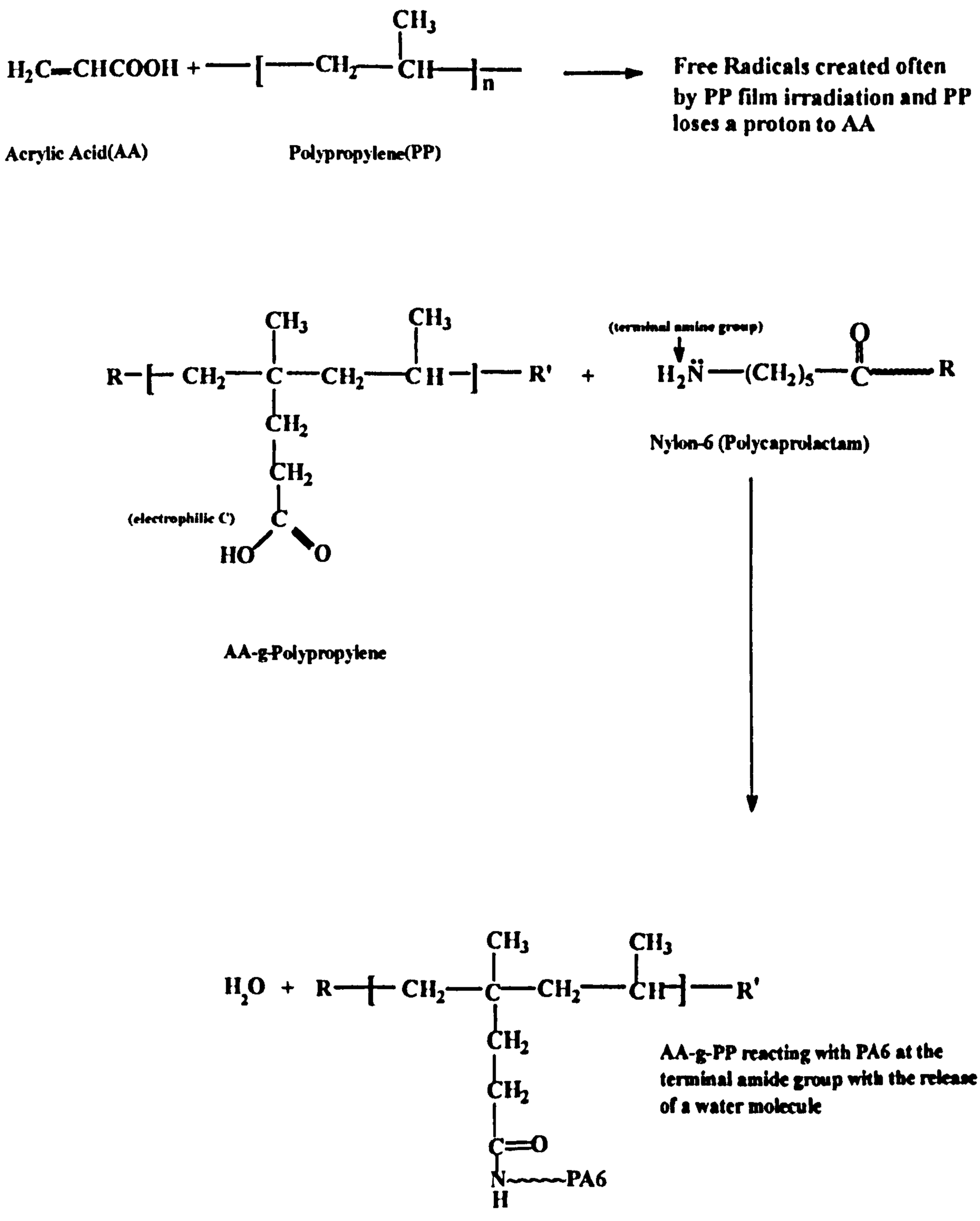

Figure 5 : Possible reaction scheme of AA with PP forming AA-g-PP and subsequently with PA6

microstructure was found to be a slight improvement over that of the binary 70wt% PP/30wt% PA6(B5) blend, as discussed in Section 4.3.1.

Films of PP which had been γ irradiated at 9.63 kGy/h for 96h and also annealed at 130 °C in a reduced pressure N_2 atmosphere, were treated with 10, 20 and 30wt% aqueous solution of Acrylic Acid(AA), in order to functionalize the PP as AA-g-PP[16], in a similar fashion to BP PB1001. The method involved immersing the films in glass tubes containing the solutions, into which nitrogen was bubbled for 15 minutes. After closure by means of screw caps, the tubes were rotated in an oven at 90 °C for 2 hours. Removal of the residual monomer and homopolymer was achieved by washing thoroughly in running water.

The surface adhesion properties of the PP are thus thought to be enhanced, with the preferred method of characterization being the FTIR. It is very important to know whether the grafting occurs at the surface, to a given depth, or in the bulk. The possible reaction of the PP with the Acrylic Acid is shown in Figure 5. It was thought that without extraction of the PP additives, grafting can only occur on the film surface, after physical adsorption of the monomers, with the polymerization continuing here as long as the monomer is unable to diffuse into the film. As the grafting goes on, the polarity of the grafted chains increases simultaneously with their loss of cohesion, allowing monomers to penetrate the deeper film chains, with diffusion being limited to the surroundings of the already grafted chains. Grafting also involves only the amorphous part of the PP.

With an increased radiation dose, polar functions could improve the hydrophilicity of the PP. Water Vapour Permeability tests have been performed on these grafted films, with the results being shown in Section 4.6. Where the apparent grafting rate is high, it is thought that cross-linking can occur between the various layers involved. Indeed, PAA branches can be generated in the PP-AA reaction, but the most likely reaction is shown in Figure 5.

3a.8 PP Cross-linking

3a.8.1 Silane Cross-linking

Organic chemistry predicts the formation of chemically covalent bonds between the organofunctional group of the silane and the reactive species in the polymer matrix, particularly the polymerization of vinyl and methacrylato silanes. Another important feature is the formation of an IPN of the silane and polymer, by the condensation of the silanol group to siloxane linkages.

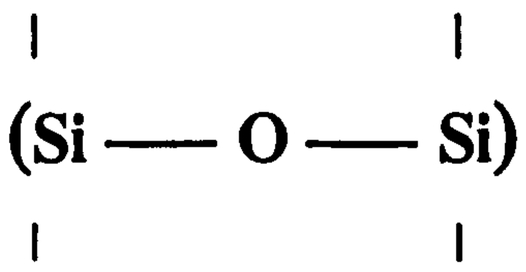

Any feature in the silane structure that contributes to greater hydrophobicity or to greater cross-linking will be beneficial.

Effective coupling requires that one or more of certain conditions are met:

1. Chemically reactive groups must be available in the polymer.
2. Silane functional groups must be matched to the type of reactivity in the polymer.
3. The solubility parameter of the silane network should be similar to that of the polymer.
4. The hydrophobic character of the silane network should be maximised.
5. Cross-linking in the silane structure should be maximised.
6. The silane organofunctional group rate of reactivity must be similar to that of the matrix polymer so that it will be bound to the polymer before the latter's reactive groups are largely consumed or immobilized.

Since polyesters cure by copolymerization with a free radical-initiated chain reaction, the use of a methacrylate functional material like Union Carbide A174 with PP meets condition 3 above. The PP used for reaction with the A174 is the DSM Stamylan 48M10 co-polymer. The systematic name for this material is methacryloyloxy propyl trimethoxysilane, $CH_2=C(CH_3)COO(CH_2)_3Si(OCH_3)_3$. If V is taken as the co-polymerization product of the Methacryl functional group and the PP then the following polycondensation reaction occurs:

$$V\text{-------}Si(OCH_3)_3 \quad + \quad {}_3(H_3CO)Si\text{-------}V$$

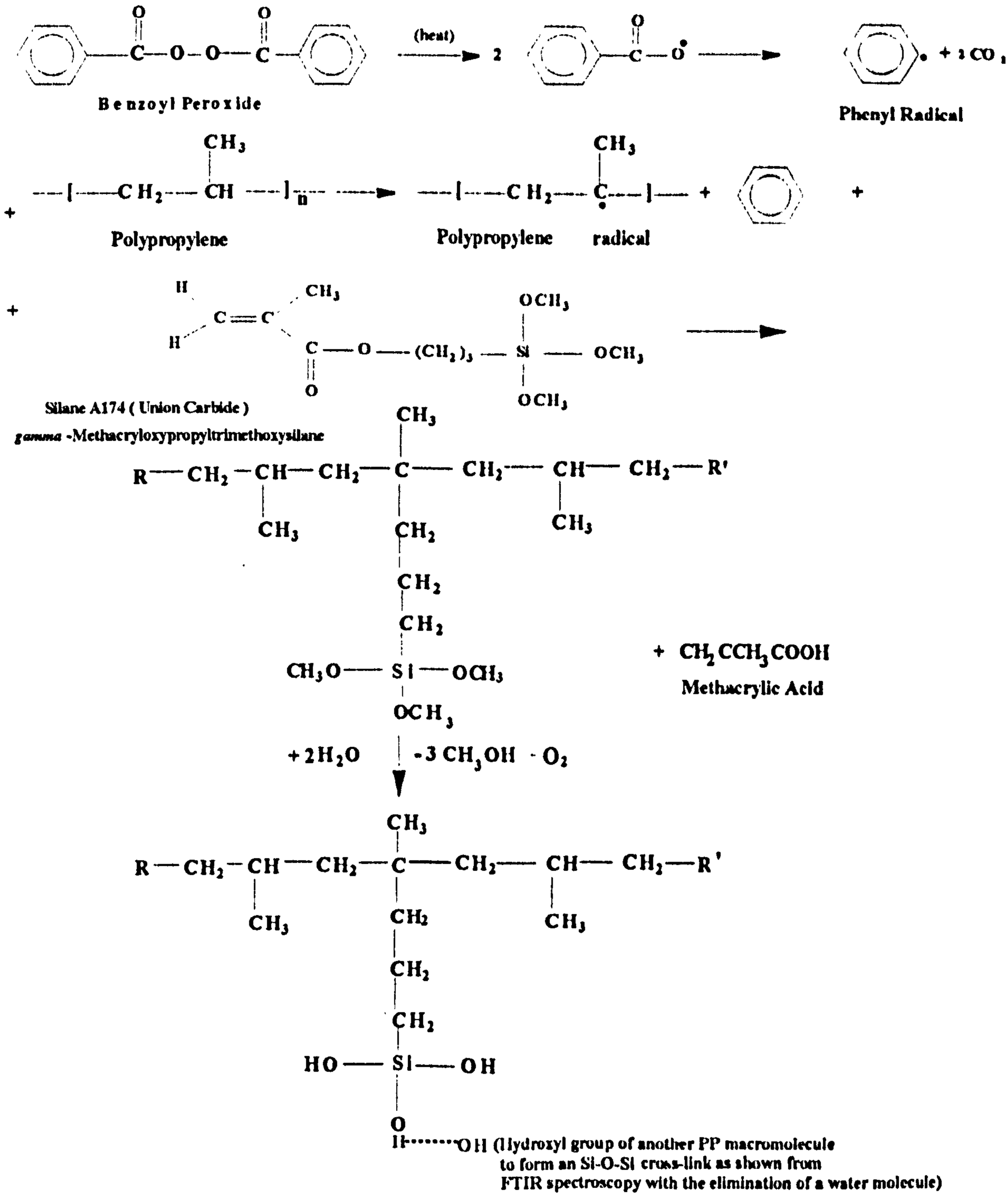

Figure 6 : Possible reaction scheme of A174 Silane with Polypropylene

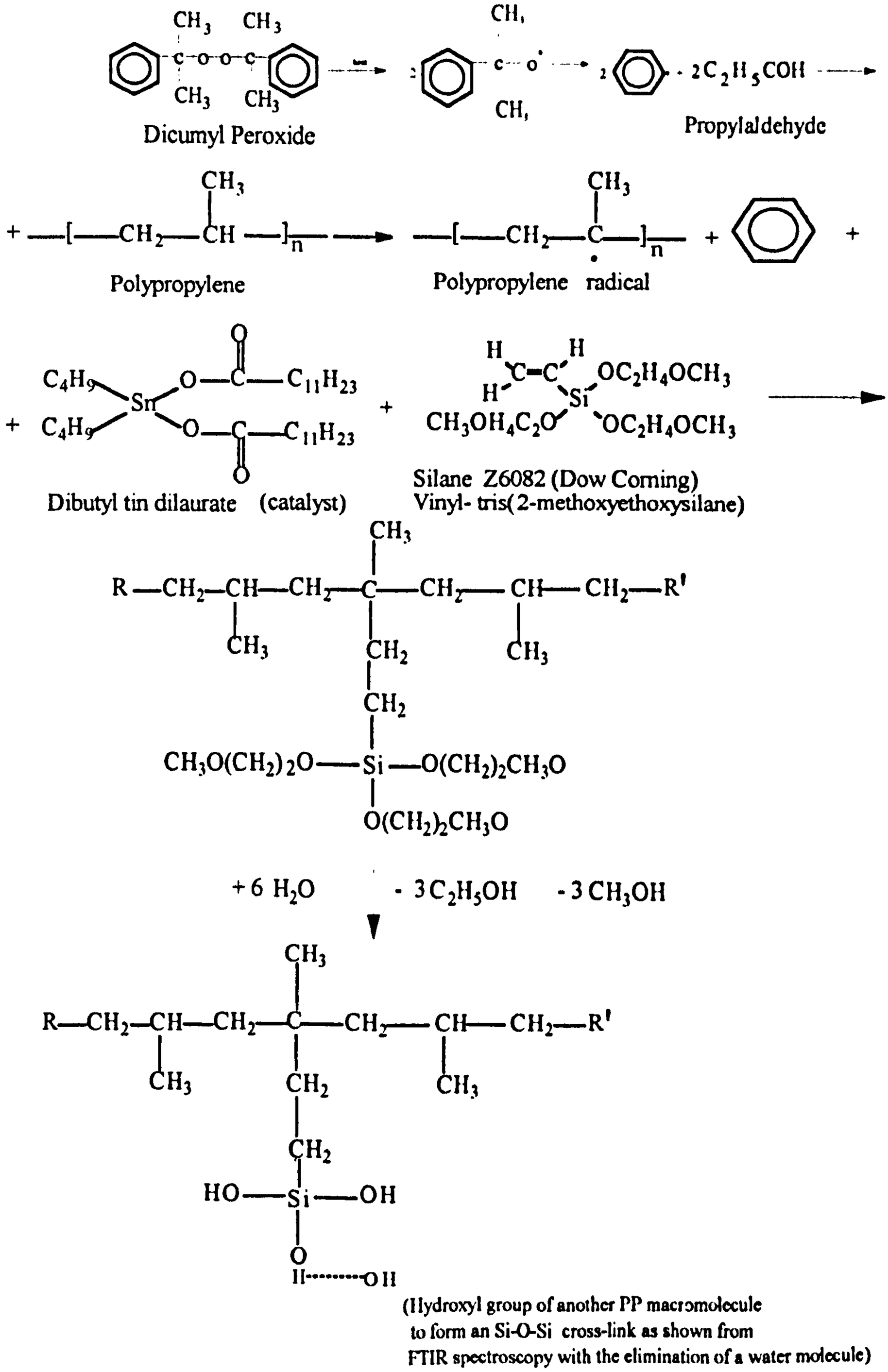

Figure 7 : Possible reaction Scheme of Silane Z6082 with Polypropylene

$$\text{(Catalyst)}CH_3COOH \quad \downarrow \quad \text{H-O-H(Water)}$$

$$V\text{-------}Si(OCH_3)_2\text{-----}O\text{-----}_2(H_3CO)Si\text{-------}V \; + \; 2CH_3OH\text{(Methanol)}$$

A more comprehensive reaction scheme is shown in Figure 6 with the shear viscosity dependence on silane concentration and shear rate being shown in Figure 8.

In the case of non-polar Silanes, like A174, precipitation can occur whilst they are in an aqueous solution at a pH greater than 7, promoting self condensation of the silanol form to form siloxane polymers. Methanol, the hydrolysis product of methoxysilanes, improves the solvent activity of the aqueous medium. High dilution in fact reduces the condensation rate and improves solution stability, but where the solutions are prepared daily, such as in this work, a 95wt% Ethanol solution has been used, acidified to a pH of 4.00-4.50 with acetic acid[17].

A 2wt% blend of A174 with PP was prepared in the melt using the solutions described above, in the laboratory blender, with cross-linking achieved by immersion in water overnight(hydrolysation). The degree of cross-linking was determined by uptake measurements using various solvents (see Section 4.8.3), by changes in G" from uncross-linked to cross-linked material, and by changes in melt viscosity. The 2wt% material been used in this work for blending with PA6. In order to assess the optimal dosage of this cross-linking silane, further blends of A-174 with PP were prepared similarly as 1wt%, 3wt%, 5wt%, and 10wt%.

Dow Z-6082 silane is bi-functional, containing both vinyl and trialkoxysilyl groups and has the formula, $[CH_3O(CH_2)_2O]SiCH{=}CH_2$ and designated as vinyltris (ß-methoxy-ethoxy)silane[18]. In this work, Z6082 was compounded with dicumyl peroxide (DCP) and dibutyl tin dilaureate (DBTDL), to accelerate the moisture activated cross-linking mechanism of PP. The PP used for reaction with the Z6082 is the DSM Stamylan 48M10 co-polymer. Further enhancement is achieved by air forming trace quantities of peroxides, similar to the air oxidation of organic ethers. Distillation of such a mixture may result in a violent exotherm, so compounding is less hazardously achieved in the melt, which in this work was performed in the laboratory blender, at 190 °C. In silane cross-linking, every alkoxysilane group has the same chance of becoming a cross-linking

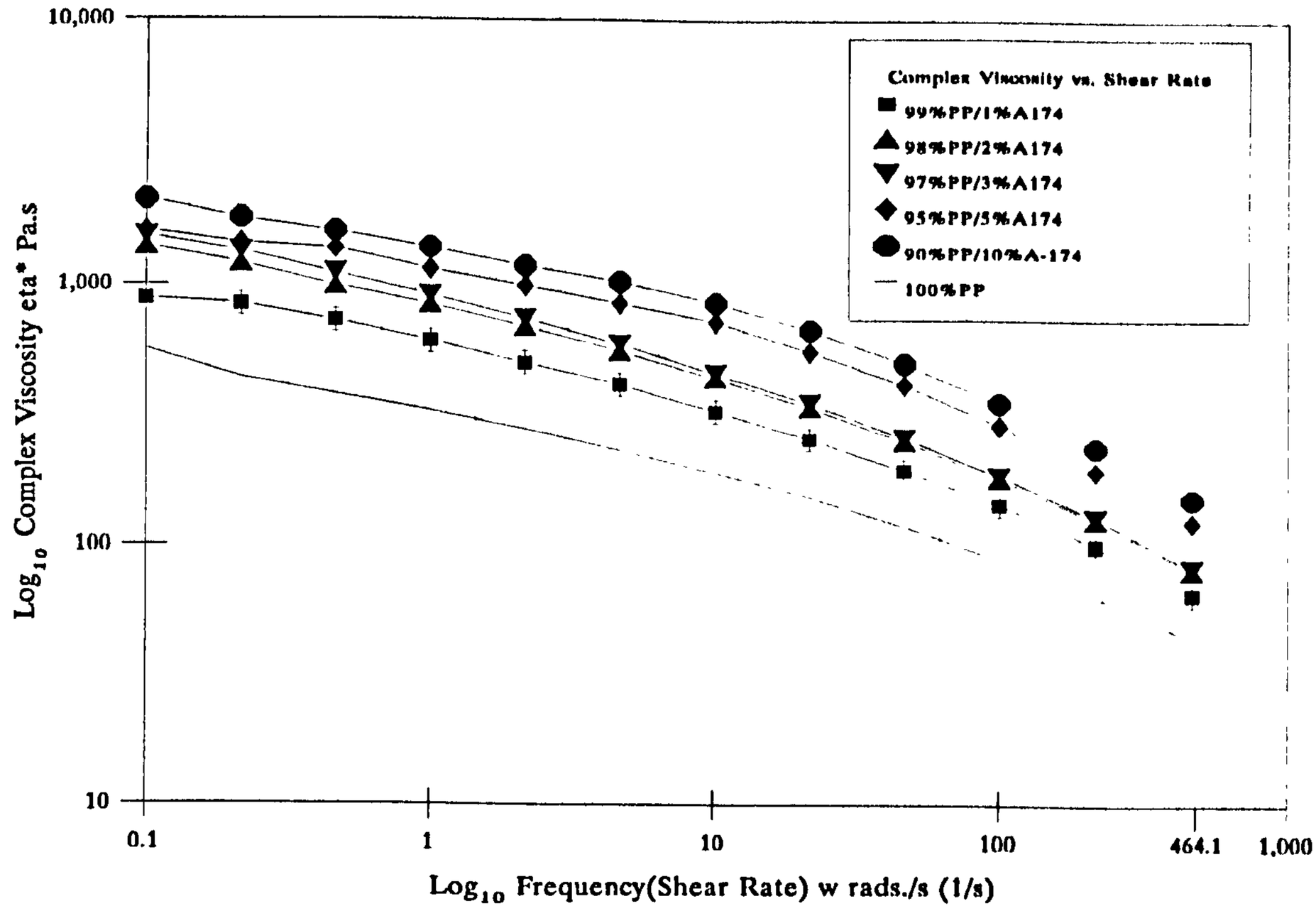

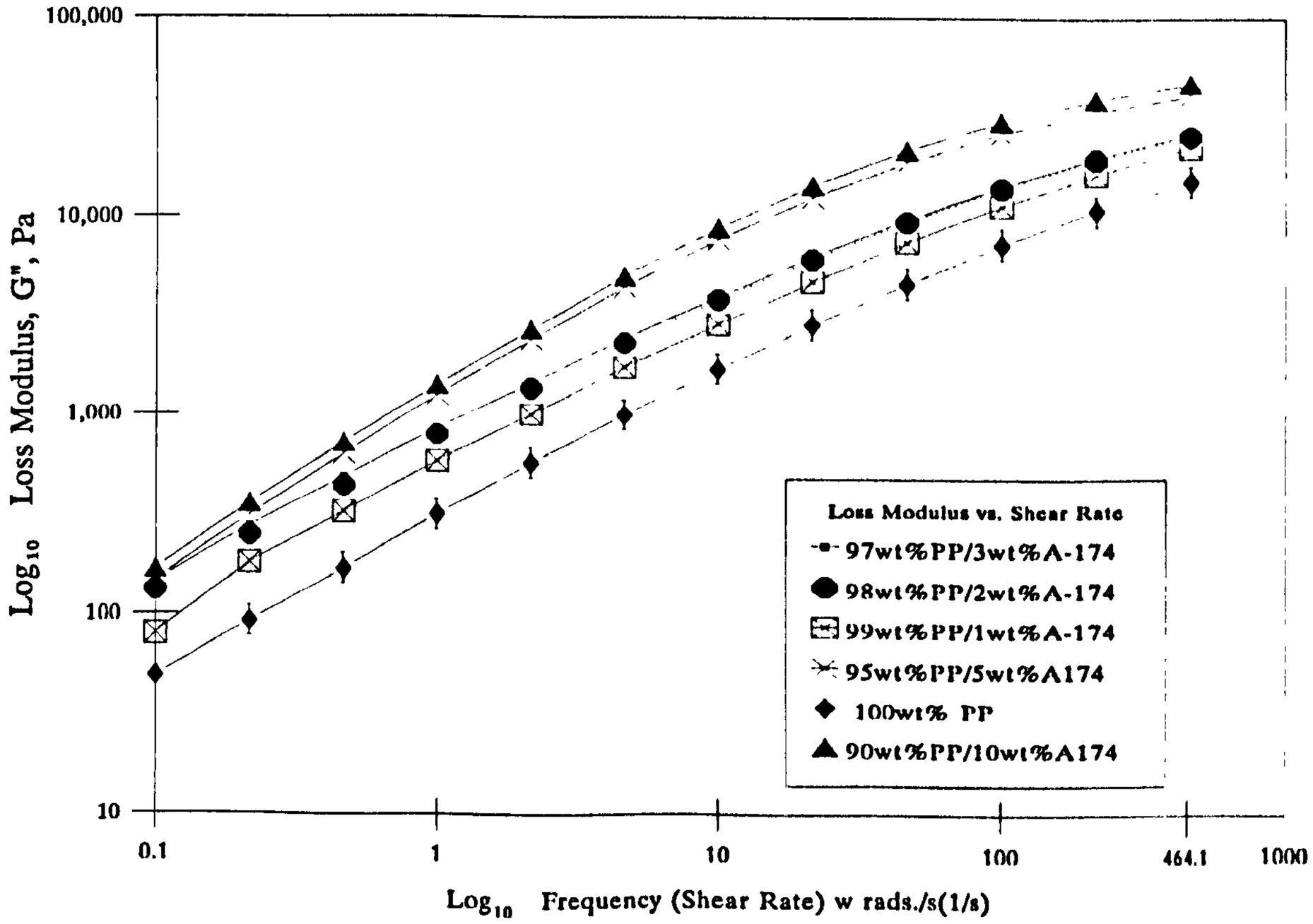

Figure 8 : Rheology at 230 °C of Silane A174 Xlinked PP (XLPP)

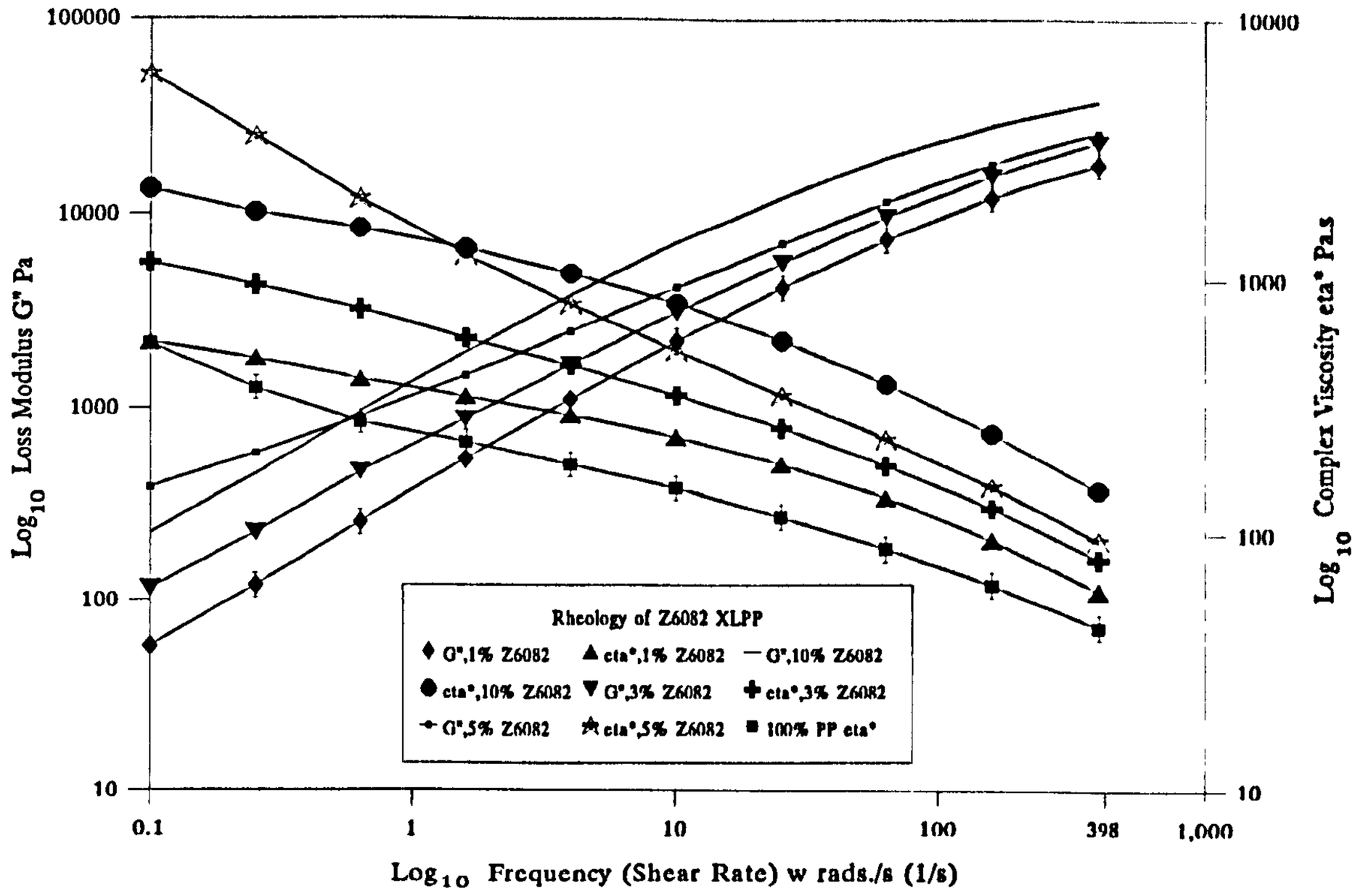

Figure 9 : Rheology at 230 °C of Silane Z6082 Xlinked PP (XLPP)

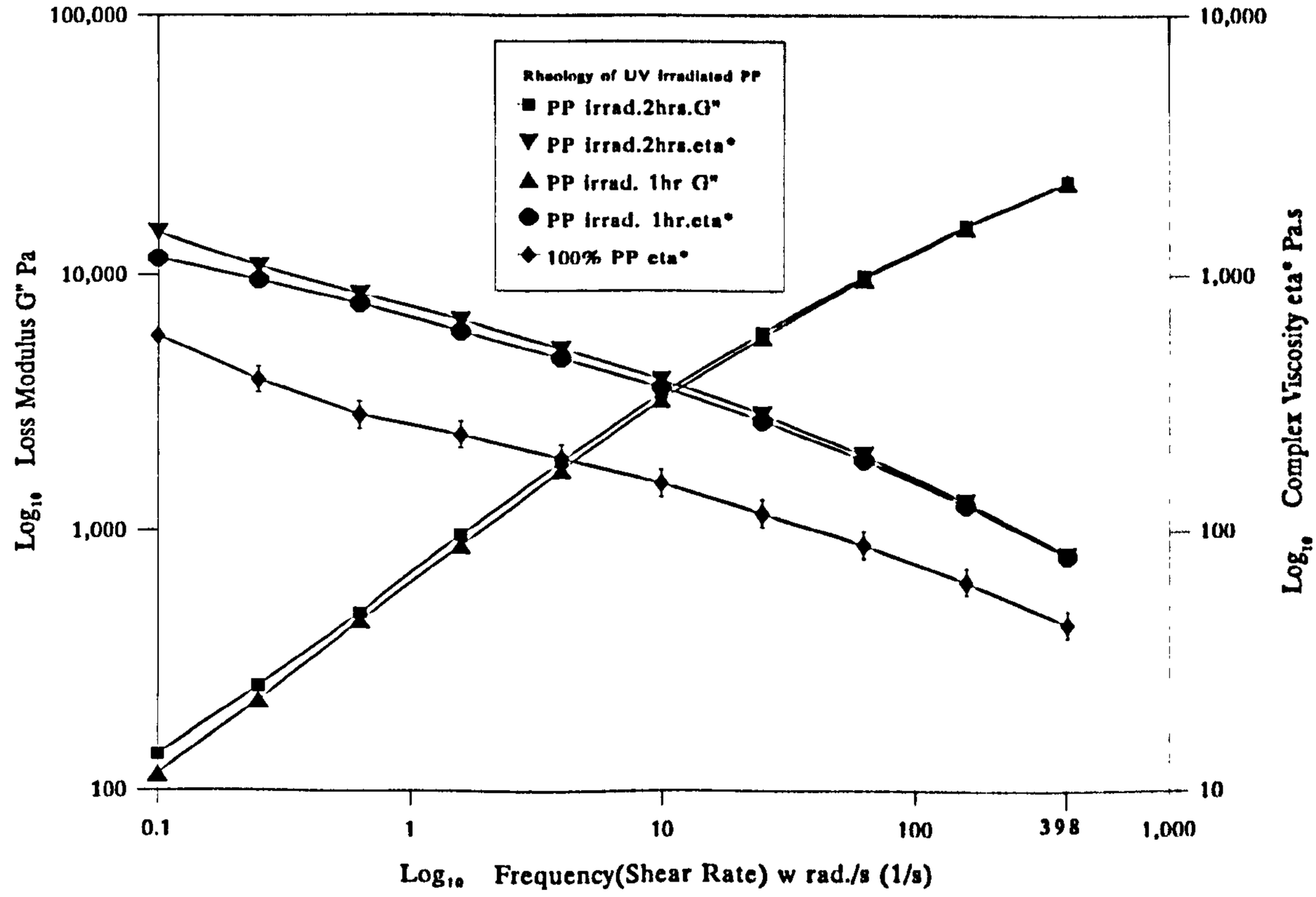

Figure 10 : Rheology at 230 °C of 50 mW/m² UV irradiated PP

site for several PP chains. The reaction scheme for Z6082 silane is shown in Figure 7 and the shear viscosity dependence on silane concentration and shear rate being shown in Figure 9.

The DCP molecule breaks on heating at the -O-O-, to form two identical radicals which can fragment to yield propaldehyde and a phenyl radical. Each of the phenyls can then abstract a terminal H atom from the PP single unit, leaving a propyl radical, for possible reaction with the silane. At an appropriate time, as indicated in the reactions,the methoxy-ethoxysilane groups are hydrolysed, with an alkyl group (butyl) being donated from the catalyst to the chain radical, and also with the loss of ethanol and methanol molecules.

Silane cross-linking is chemically complicated, but is relatively easy in practice since modified PP is purchased, mixed with a master batch containing a catalyst, in this work, DBTDL, and processed. The resulting molded part is not yet cross-linked but subsequent diffusion of water initiates the reaction, which is the rate determining step. This proceedure was followed by making a stock solution of 5wt% of the Z6082 in 95 wt% aqueous C_2H_5OH, acidified to pH 4.00-4.50 with CH_3COOH. To a portion of this was added 0.15wt% of DCP and 0.05wt% of DBTDL and a blend of 5wt% of this liquid was made with PP, by melt blending at 190 °C, and subsequently cross-linked by immersion in water overnight (hydrolysation). Cross-linking effectiveness was again determined, by changes in G" and in melt viscosity, both as a function of shear rate, at a fixed temperature, using dynamic viscosity. Further mixtures of Z6082 with PP as 1wt%, 3wt%, and 10 wt% were also prepared.

3a.8.2 PP Cross-linking by ^{60}Co γ Irradiation

PP films were irradiated with γ radiation from two different sources. The first was a 3.6 Ci ^{60}Co source at distances of 3cm and 30cm for 3 hours, 24 hours, and 96 hours. These films were untreated. The second was a 400 Ci ^{60}Co source, at distances of 32mm and 20cm for, 24 hours and 96 hours. Other PP films were treated with Acetophenone/DCP (Dicumyl Peroxide), all irradiated for 24 hours. Both 64.5 μm and 416 μm films was also irradiated for 96 hours at 32mm by the 400 Ci source. In this work, further γ irradiation was also done as a control experiment on PP films which had been swollen

in acetophenone and dicumyl peroxide solution, for 12 hours[19], giving a total dose of 3.36 Mrads, when exposed for 24 hours.

It was thought that the dose rate from the more powerful γ source of 1.40 kGy/h would be suitable for the olefinic cross-linking, since a 1.22 kGy/h source had been used previously[19]. The samples were irradiated initially by a UV source (see Section 3a.8.3). In parallel with this experiment, the 99wt% PP/1wt% Sorbitol material was irradiated, for the same length of time, since it is thought that the clarity and radiation stability would reduce, with a nucleating agent[20]. The dosage received was 33.6 kGy. Irradiated material can be blended with PA6, and possible initiators for the radiation cross-linking of PA6 were investigated, but without success. PA6(A23) was irradiated with the 400 Ci source, for 96 hours.

3a.8.3 PP Cross-linking by UV Irradiation

PP films were exposed to UV irradiation for, 1 hour, 2 hours, and 4 hours without further treatmen. Films were also exposed for 10 hours, with and without swelling in Acetophenone for 24 and 60 hours. The UV irradiation rate was 50 mW/cm^2, achieved in this work with 8W tubes, at a distance of 30 cm, over a CSA of 7.12 cm^2. An FTIR spectra of a 205 μm film swollen in acetophenone for 24 hours and UV irradiated for 10 hours, showed minimal evidence of C=O carbonyl peak development from FTIR. The 60 hour acetophenone swollen material was also exposed to UV radiation for 10 hours, since it was thought from the evidence of mechanical testing[19] that the optimum exposure time was between 7 and 16 hours, for HDPE. Material which had and had not been cross-linked with UV radiation was also exposed to γ radiation, after acetophenone treatment, as a comparison.

The radiated samples were annealed at 80 °C for 8 hours in a nitrogen atmosphere. The samples were subsequently tested for dynamic viscosity and water vapour permeability. The results of the latter tests are discussed in Section 3b and the former are shown in Figure 9.

3a.8.4 Conventional Chemical PP Cross-linking

DCP is often used as a cross-linking initiator[21], by heating the PP in chloroform, under nitrogen, for 30 minutes, at 170 °C. In this work, the DCP was refluxed in xylene with the PP, under nitrogen, for 30 minutes, at 85 °C. Materials of 1wt% (yield 96.9wt%), 0.5wt% (yield 99.3wt%), and 0.1wt% (yield 93.8wt%) DCP were prepared by this method, and also 0.5wt% DCP with 2.5wt% DMF. As expected, an increase in melt flow was experienced, rather than cross-linking, due to the disproportionation of polymer radicals in lieu of coupling. However, when DMF is present[22], the degradation is minimized, which can be shown by a higher intrinsic viscosity, ie. from 0.8 to 1.3 dl/g in the cited paper. In this work, the effectiveness of cross-linking was measured using dynamic viscosity. However, the MFI increased from 16.1 for the 99.5wt% PP/0.5wt% DCP material, to 18.9 for the 97wt% PP/2.5wt% DMF/0.5wt% DCP material. See Section 4.4 for the complete dynamic and steady state results. Cross-linking can be enhanced in this type of work by the presence of the co-agent PETA, and the soluble part of the cross-linked material can be examined by IR spectroscopy, which is a possibility of further work in this direction.

3a.9 Fourier Transform Infrared(FTIR) Spectroscopy

Similar thin sections to those used for LM were prepared for FTIR spectroscopy, performed primarily on a Nicolet 60SXB and some on a 710 spectrometer. For the 60SXB two different Mercury-Cadmium-Telurium liquid nitrogen cooled detectors were used. One for use with an experimental stage had a resolution of $4cm^{-1}$, within the waveband range 4500-400 wave numbers(cm^{-1}), and the other, used with the microbeam detector stage had a resolution of $2cm^{-1}$ within the same band-width. For the 710 instrument, a room temperature DTGS detector with a resolution of $4cm^{-1}$ was used. The laser accuracy for both instruments FTIR spectra obtained were corrected for water and CO_2, by subtraction. Polymer film absorbance spectra were obtained of all PA6/PP binary and ternary blends/homopolymers, compatibilizers, various blends of LDPE, LLDPE, PS, HDPE, EVOH, R6000 after exposure to glacial (saturated aqueous) acetic acid for 6.5 hours (to establish whether or not the PA6 phase could be dissolved by the acid, in a similar fashion to the homologous series formic acid), Poly(ButylMethacrylate), silanated PP (both in bulk and film samples) before and after water exposure for approximately 20 hours and also after refluxing in water for approximately 20 hours.

FTIR absorbance spectra using KBr discs were obtained for ϵ-caprolactam, xylene, MA, silanes, butyl methacrylate, and White Spirit(Stoddards Reagent).

3a.10 Differential Scanning Calorimetry(DSC)

DSC experiments were conducted on R6000 pellets and injection molded, PP, XLPP (2wt% A174 silanes), PA6(B5), PA6(A23), PET, and EVAL-F(EVOH). The results are tabulated in Table 3.

3a.11 Rheology

For investigating the viscosity ratio of the blend components and the overall blend viscosity, rheological measurements were made of the polymers being studied. Steady state flow is represented by Capillary Rheometry and Dynamic Response by rotational parallel plate rheometry, using a small gap, and low shear rate. The uniformity of stress and strain rates should both be linear for the dynamic method, where the large strain shear viscosity is within the low range of deformation rates, at $\gamma \leq 100\ s^{-1}$.

Table 3 : Differential Scanning Calorimetry of Homopolymers and Orgalloy R6000

Material	*Scanning Rate* $^{\circ}\ min^{-1}$	*Mass mg*	T_m ^{o}C
PP	20	0.49	163.25
XLPP(2wt% A174 silanes)	20	1.32	153.32
PA6(B5)	20	0.81	221.25
PA6(A23)	20	0.92	217.6
R6000 Pellets	10	9.38	161.81(PP) 220.74(PA6)
R6000 Inj. Molded	10	7.65	160.76(PP) 221.21(PA6)
EVOH (EVAL-F)	20 5	2.36 0.98	181.02 183.45
PET (Melinex)	20	3.21	241.26

The PA6 and Orgalloy R6000 were dried under reduced pressure for 48 hours at 80

°C[23], and cooled in a reduced pressure desiccator, prior to charging in a rheometer. Steady state melt viscosity was measured using a Davenport Melt Flow Indexer (MFI) at 230 °C, and dynamic viscosity on a Rheometrics RDA II parallel plate dynamic mechanical analyzer, at the same temperature. On both instruments duplicate samples were run within standard deviation limits of ± 2%, and the RDA II was operated under dry N_2. However, the PA6 samples and blends showed a yellowing at the edges of the parallel plate. The MFI was operated using a 2.16 kg mass and the RDA for frequency sweeps (increasing shear rate). Dynamic viscosity measurements when compared to MFI, for a particular material, are quoted at the corresponding MFI shear rate, in order that the two parameters are consistent. However, for comparing the viscosity of different materials with each other, the shear rate used is that of PP MFI, 2.67 s^{-1}. The following equation used to calculate the MFI shear rate at the wall of a Newtonian fluid[24], in sec^{-1} is :

$$\gamma_N = 4Q / \pi R^3 \text{ ---------- [52]}$$

where Q is the volume throughput in cm^3/sec and R is the radius of the MFI capillary(0.059 cm). Q was calculated from the average mass output from the MFI in gms divided by the density, in gms/cm^3. Since the MFI is measured as a mass per 10 x minute, a factor of 600 is used to convert to sec^{-1}.

3a.12 Polymer Density

The densities of the homopolymers and blend samples were measured in triplicate, using displacement of C_2H_5OH in a calibrated density bottle to a deviation of ±0.05%.

3b Barrier Properties Determination of Homopolymers, Blends, and Laminates

3b.1 Water Vapour Permeability Determination

Water vapour permeability[1] determination of homopolymer, blend and laminated films is based on the ASTM Standard E96-80 (ASTM 1983). The water is placed to a standardised level below the rim of a glass ampoule which has been carefully ground to flatness with 4 μm paste. The rim is sealed with a polymer film, held in place by Crodamelt wax. The test conditions were controlled at 23 °C and 50% RH. Periodically, the ampoule is weighed and the time from the start of the test is noted. From the linear steady state portion of the curve obtained by plotting the mass lost (Q) as a function of elapsed time (t), the water vapour permeability can be calculated, by placing the slope, Q/t into equ'n.[25] of Section 2b.1, defining the permeability P.

This gives the water vapour permeability at a particular temperature and relative humidity(RH), and one bar. Although the test is slow, it is cheap and reliable. The water vapour permeability of the wax was tested over a three year period, by waxing a glass slide to the mouth of an ampoule containing water. The weight loss of water from the ampoule during this period was 2.09 g. A schematic diagram is shown of the ampoule in Figure 11. A correlation was sought between the PA6 concentration in all the binary and ternary blends and the water vapour permeability. The results are shown in Chapter 4, together with those for laminated structures, the preparation of which is described below.

Binary laminated PP/PA6 films were prepared, using both PP and silane cross-linked material, with both B5 and A23 PA6's, by melting PP films onto PA6 films, under dynamic reduced pressure at 180 °C. In addition, ternary laminated PP/PA6 films were prepared either by including a compatibilizer film in between the PP and PA6 films or by using one of four tie layer adhesives. They are as follows, National Starch and Chemical Ltd. Durotak 380-1846, 3M Scotchgrip 4235 and 3M Fastbond 30.

The thickness of each polymer layer was measured prior to heating and hence the wt% contribution of each material calculated from the film cross sectional area (giving the volume) and density of each layer. That of the tie layer adhesives contribution was

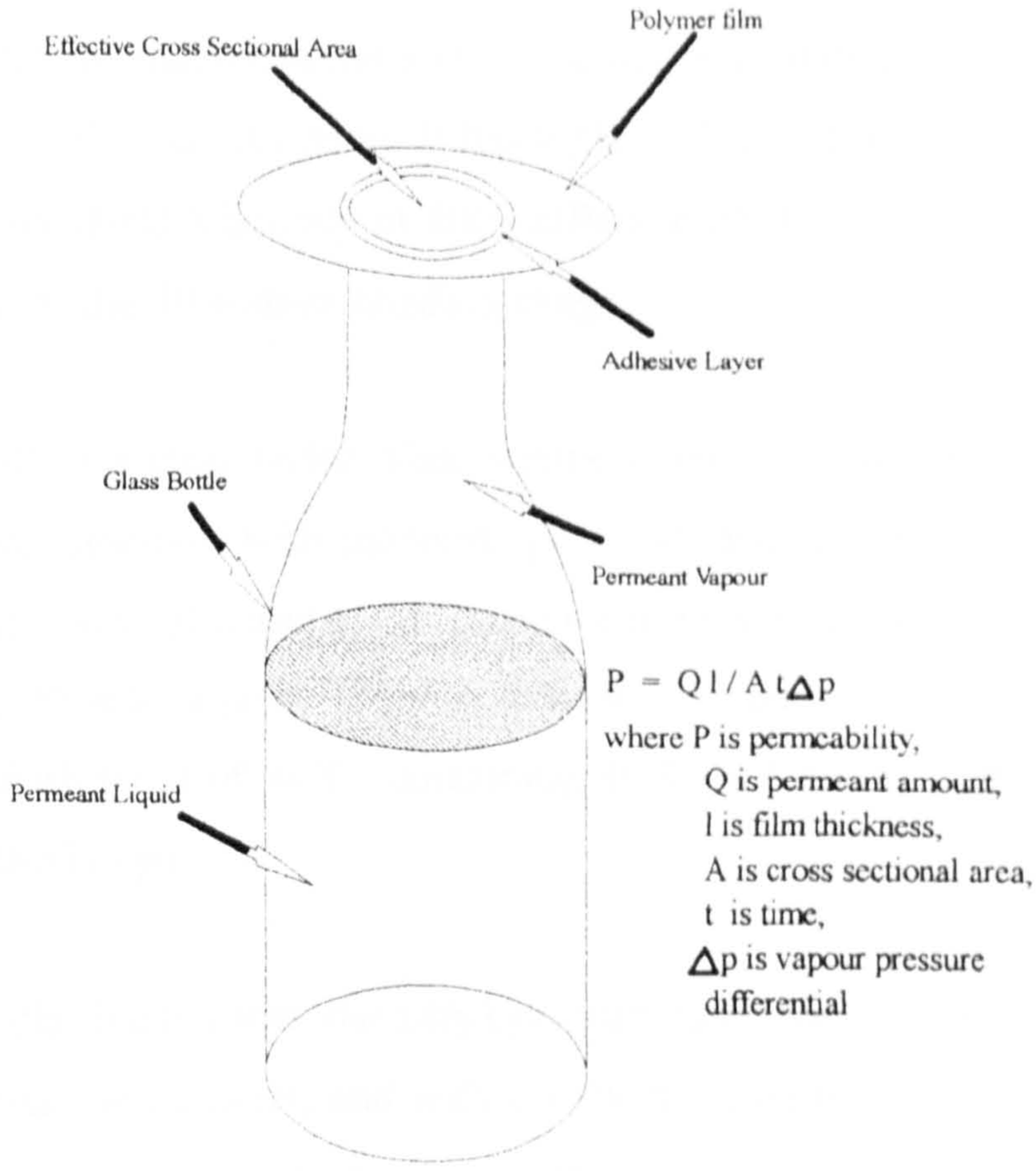

Figure 11 : Gravimetric Vapour Permeability Ampoule

calculated by difference from the combined thicknesses of the polymers and that of the final laminates, from which the mass percentage was calculated by again using the volume and density of the tie layer.

The properties of the tie layer adhesives are as follows. Fastbond 30 is non-flammable Polychloroprene based, with high immediate bond strength and a long bonding range. The solvent is a $>$ 95wt% water/$<$ 5wt% toluene/ethanol mixture, changing colour from turquoise to green on curing. It has a pH of 10.5, contains $\approx$ 50wt% solids, Brookfield Viscosity of 300 mPa.s at 26 °C, has an SG of 1.09, and a T-Peel strength of 6.8 daN/cm at 24 °C after 21 days.

Scotch-grip 4235 is non-flammable Acrylate based, pressure sensitive, with moderate

tack, to allow for immediate repositioning. The solvent is water, with ≈ 55wt% acrylics, < 0.2wt% acrylate/methacrylate monomers, < 0.2wt% ammonia, and changing colour from white to colourless upon curing. It has a pH of 7.2, contains 55wt% solids, has an SG of 1.07, a Brookfield Viscosity of 4000 mPa.s at 26 °C and a 180 ° peel strength of 1.12 daN/cm, after the 30+ days bonding range.

Durotak 380-1846 is a clear water white solution, self cross-linking acrylic copolymer pressure sensitive adhesive, with moderate peel and tack, ensuring excellant shrinkage resistance/cohesive strength, and good resistance to plasticizer migration. The solvent is 57wt% toluene, 22wt% heptane, 18wt% isopropanol, and 3wt% urethane grade ethyl acetate, with a flash point of -4 °C, containing 29-31wt% solids, and with a Brookfield Viscosity of 250-350 cps.

Tufloc TLC06 adhesive is a low viscosity cyanoacrylate adhesive, designed for materials with relatively inactive surfaces, and with excellent humidity resistance. With EPDM it exhibits after 10 seconds a tensile shear strength of 3 N/mm^2. The monomer is modified, colourless, Ethyl Cyanoacrylate Ester, with an SG of 1.05, a Brookfield Viscosity at 25 °C of 15-30 cPs, is non-toxic, RI(ND 20) of 1.46 when cured, Rockwell Hardness of 85 when cured, Specific Resistance of 8×10^{12} OHM/cm, and a softening point of 150 °C, after curing. Only a limited number of laminates using this particular adhesive were mounted for water permeability determination and the results are not reported.

3b.2 Free Volume Effect on Permeability

3b.2.1 Introduction

It was thought that the free volume polymer theories of Vrentas and Duda[2,3,4,5] could be applied to the transport of water vapour through the materials investigated, since, as mentioned in reference [104] of Section 2b.7, water molecules thought to be trapped at free volume sites in the matrix can reduce oxygen permeability. Hence, the volume thermal expansion, α, was measured for selected polymers, because the availability of free volume is related to α.

3b.2.2 Volume Thermal Expansion

Polymer water vapour permeability, is temperature dependant, just like the thermal expansion behaviour, which is directly related to the polymer free volume. The free volume is defined[6] as the availability of a favourable distribution of localised excess volume to allow a diffusive jump. The volume thermal expansion coefficient, α, was thus determined for, PP, PA6(A23), PA6(B5), XLPP(2 wt% A174 Silanes), Orgalloy R6000(R6000), 70wt% PP/26wt% B5/4wt% PB3002, and 56wt% A23/36wt% PP/8wt% BMAcoMAgPP, using a Perkin-Elmer TMS I instrument.

A uniform geometrically shaped polymer sample is enclosed by a sliding, thermocouple controlled, cylindrical, dewar furnace, which can operate from -150 °C to 325 °C. The samples were prepared as cylinders of 0.5cm length and 3mm diameter, with similar thermal history on the motorised, 12.7 cm platen, 80 ton Moore Press. The linear thermal expansion coefficient, ß, was obtained, representing a pure length change of an isotropic sample. A linear variable differential transducer (LVDT) serves as a displacement transducer to sense sample changes by way of a probe and then convert them to electrical signals. The moveable LVDT core is supported on a shaft to which is coupled a probe inside a quartz sample tube. The core probe assembly is suspended from above on a float immersed in a high density liquid. The probe tip is maintained in contact with the sample, placed at the bottom of the quartz sample with the help of weights on a tray at the top of the float assembly. The furnace heating element serves as both a heater and resistance thermometer. The temperature was monitored by continuous output to a recorder pen from the sample tube chromel/alumel thermocouple. The program rate used was 0.316 °/minute and the program mode was for the recorder control accessory, in which the recorder chart drive was stopped at the upper temperature limit. The sensitivity is 0.5×10^{-4} mm/mm on a 10 mV recorder.

The original length of the sample was measured in mm to three decimal places and heated in the instrument from ambient temperature to 130 °C for PP and the in house prepared blends, to 135 °C for XLPP, to 175 °C for B5, to 165 °C for A23 and to 130 °C for R6000. The tests for each material were conducted in triplicate. A chart recorder was connected to the instrument controller output, with the x-axis representing

temperature change and the y-axis, representing the length change. This is a product of the sensitivity set on the instrument, multiplied by 10^{-3} mm/full scale, the fraction of full scale displacement. The slope of the tangent to this plot, over the temperature range of interest, is then divided by the sample length to give the linear thermal expansion coefficient.

3b.2.2 Temperature and Concentration effects on Water Vapour Permeability

The relationship between temperature and water vapour permeability was also investigated for selected systems since both the free volume and permeability are temperature dependant. The relationship is outlined in Section 2b.2, equ'n.[16] as the Arrhenius plot. Blends including both types of PA6 and microstructure have been tested at various temperatures. The results are shown in Figure 80 of Section 4.6.7.2. where they are also discussed.

The effect of molecular concentration on water vapour permeability was investigated using the same ampoules as the type used for the vapour determination, but on this occasion inverted so that the liquid was in contact with the polymer film. The materials tested were PP, XLPP, B5, A23, R6000, 70wt% PP/26wt% B5/4wt% PB3002, and 56wt% A23/36wt% PP/8wt% BMAcoMAgPP. The results of these tests are discussed in Section 4.6.7.3.

3b.3 Oxygen Permeability Determination

An attempt was made to monitor oxygen permeability colourimetrically using methods referenced as [58], [59], and [60] in Section 2b.6.2., with the indicator being liquid for the first two and solid for the last. The initial attraction of the first two methods was that several ampoules could be tested concurrently, each with the same or different polymers, and both a UV-Vis Spectrometer and light cell were available. The change in blueness of the liquid in the ampoules onto which the polymer films were mounted was monitored. In addition, OXTRAN equipment, see reference [54] of Section 2b.6.2, was not readily available or on site, although it is the standard method of measurement. Scatter of experimental data for methods [58] and [59] was experienced when monitoring the saturation level UV absorption of uncovered ampoules, and similarly when monitoring

tubes over the mouths of which were mounted hompolymer films of PA6(B5) and PP, due possibly to concentration changes in the reaction mixture caused by reverse permeation of water vapour. An exponential increase with time for blue UV absorption at ≈ 650 nm for the cupric ion ($Cu(NH_3)_4^{++}$) with method [58] was anticipated. Similarly, for method [59], at ≈ 700 nm for sodium sulphite ($Na^+SO_2^-$) oxidising the indigo-carmine was anticipated but the data in both cases unpredictably increased and decreased with time.

Hence a Light Cell method was evaluated. It is thought that a rate constant for ampoules containing no polymer membrane can be related to that obtained with membranes. The output of the Light Cell was connected to a chart recorder and an exponential curve obtained. However, the data obtained for both reactions again gave contradictory results in that once again the absorption for the amount of blueness using both reactions once again showed decreases with time after initial increases.

The third Manganese Dioxide method shows promise, on a qualitative basis, but was not evaluated in a system containing a sample, only one where the leakage rate was tested. Because the system needs evacuation prior to testing, a thin polymer film is likely to puncture during this process, if the upside of the film is left open to atmospheric oxygen. detector An alternative system would involve two chambers, one where the MnO indicator is placed and another through which atmospheric oxygen is passed at low pressure. Both chambers would be evacuated concurrently, with the polymer mounted between the chambers, and at time = 0, a low pressure purge of atmospheric O_2 would be admitted to the upside chamber.

The fourth method (OXTRAN 10/50A) tests were conducted by the CASE sponsors on PP, PA6(B5), PA6(A23), R6000, XLPP(2wt% A174 Silanes), and XLPP(10wt% Z6082 Silanes). The samples were of various thicknesses, measured using the method outlined in Section 3a.3. They were mounted on a brass tube of internal cross-sectional area 4.52 x 10^{-4} m^2 and measured at a specified temperature and humidity, using a carrier gas made moist by passing through a bubbler.

3b.4 Permeability and Uptake Measurements of Methane, Chlorinated Methanes, Methanol and Xylene

3b.4.1 Permeability Experiments

The polymers used for the gravimetric organic vapour permeability tests are as follows, PP co-polymer (DSM Stamylan 48M10), HDPE (BP Rigidex), LDPE (BP Novex), Lacquatene LLDPE, BASF Ultramid B5 PA6, EMS-Chemie Grilon A23 PA6, PTFE, silane cross-linked PP(XLPP)(2wt% A174 silanes), 90wt% PP/10wt% A174 silanes, 90wt% PP/10wt% Z6082 silanes, 97wt% PP/3wt% Z6082 silanes, and also Orgalloy R6000. The difference between the gravimetric organic vapour permeability method used and that used for water vapour permeability is that the vapour pressure term does not equate to unity in equ'n.[21] and therefore the saturated vapour pressure difference of each penetrant across the film has to be included, see Section 3b.1. The natural gas and DCM liquid permeabilities of PP, XLPP and B5 were also determined by the Differential Pressure Transducer Constant Volume Manometric (DPTCVM) technique[7]. See Figure 12. The results are tabulated in Section 4.8.1.

Films of PP co-polymer(DSM Stamylan 48M10), XLPP(2 wt% A174 Silanes), and PA6(BASF Ultramid B5), were prepared on a motorised, 12.7 cm platen, 80 ton Moore Press. For the PP and XLPP, the polymer was heated at 210 °C with 20 ton pressure(2.032×10^4 kg), between steel plates and aluminium foil, for 3 minutes, and cooled at ambient temperature for 10 minutes. The PA6 films were prepared in the same way but at 230 °C, and also using silicon free mold release between the polymer and foil. Average film thicknesses were measured in μm with a Mercer 122D pneumatic gauge fitted with a hemispherical non-invasive probe[8], by taking the arithmetic mean of sixteen measurements of the material where the permeability effective cross-sectional area diameter is taken.

The permeability cell is of mild steel construction and fitted with Viton "o" rings between the upper and lower chambers, between which the polymer film is sealed, by tightening six bolts, passing through the flanges of the cell. Supporting the film is a metal grid and filter paper, giving an effective cross-sectional surface area of 5.22×10^{-3} m^2 and downside volume of 8.50×10^{-3} m^3.

The reference transducer is fitted to the downside of the cell which is evacuated to low pressure, together with the upstream side, thus permitting high driving pressures, reducing experimental times for low permeability materials. The system is tested for leaks prior to permeability tests commencing, with a blank plate in place of the polymer film. An arithmetic mean of three tests gave an average leakage rate of 0.092 mbar/hour, within standard deviation limits of $\pm 1\%$, and is taken into consideration when calculating the pressure differentials.

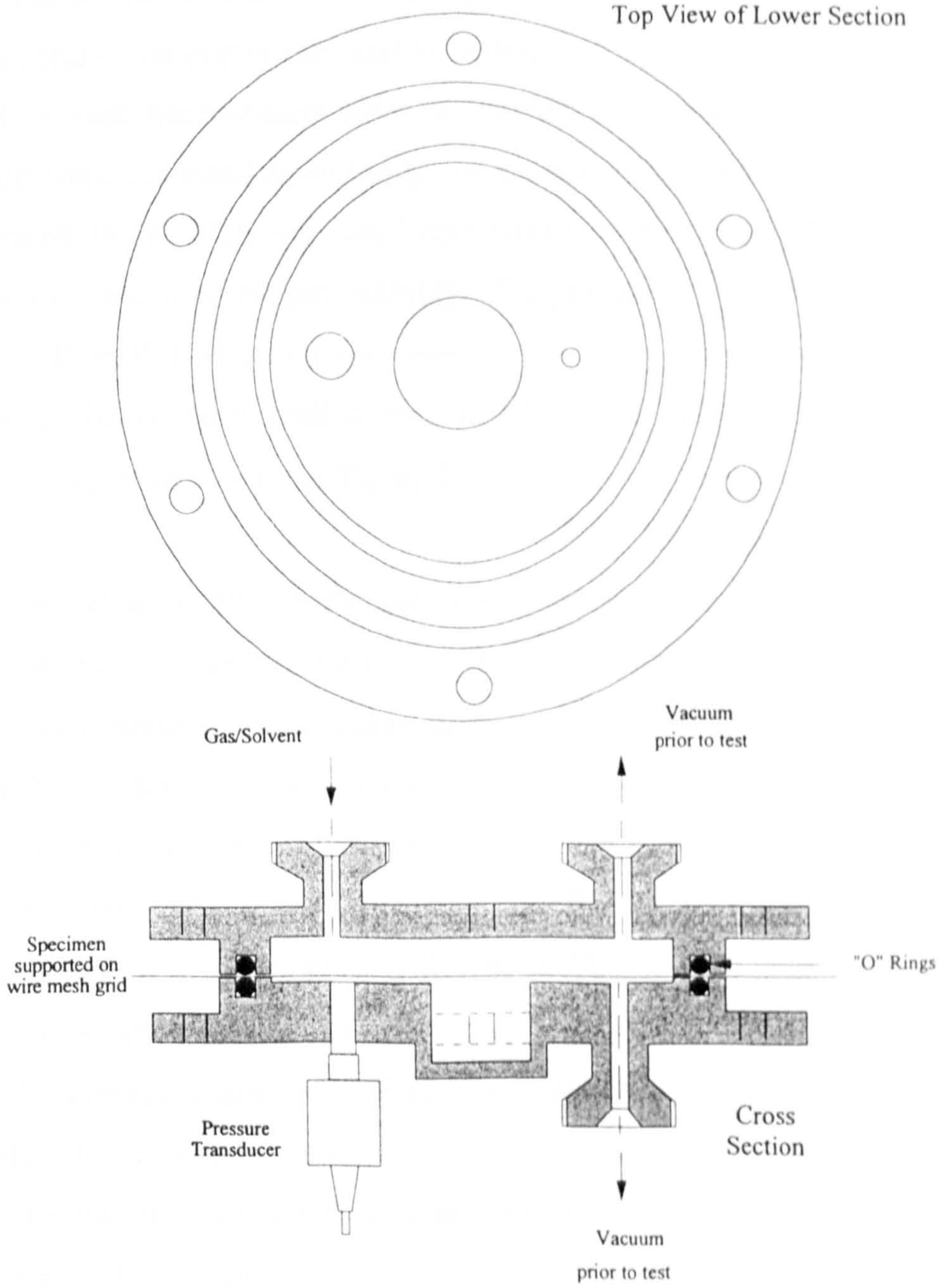

Figure 12 : Differential Pressure Transducer Constant Volume Manometric Cell

For natural gas determinations, the supply over-pressure (normally 25-30 mbar over that of atmospheric) is measured with the transducer/display unit system, before the test is commenced. After evacuation, the evacuated pressure is noted and the gas admitted from the supply.

Downside pressure readings are taken regularly during the test, until the final saturation plateau is reached, which is additionally monitored using a chart recorder. A similar procedure is followed for DCM, with the liquid being admitted through the same valve, until the upstream chamber is full, and is replenished as required. The test temperature is recorded for each measurement since the transducer is temperature sensitive, and the measured pressure corrected accordingly. In addition, the arithmetic mean taken as the test temperature in °K. Only the near linear (steady state) part of the pressure vs. time curve is used to calculate, the permeability. The permeability is calculated from :

$$P = V_s \, l / \blacktriangle t \; A \; \blacktriangle p \quad \text{---------- [53]}$$

The volume of the gas permeated is computed from the equation[9] :

$$V_s = (p_2 v_2 - p_1 v_1) \, T_0 / \, p_0 \, T \quad \text{---------- [54]}$$

where,

p_1 is the initial pressure of the gas on the low pressure side of the film in bar

p_2 is the final pressure of the gas on the low pressure side of the film in bar

$\blacktriangle p$ is the average partial pressure drop across the film during the test in bar

$\blacktriangle t$ is the test time elapsed in days

v_1 is the initial volume of test gas/liquid s on the low pressure side in cm^3

v_2 is the final total volume of gas/liquid on the low pressure side in cm^3

T_0 is the standard temperature in Kelvin of 273.16 °K

p_0 is the standard pressure of 1.015 bar

T is the average temperature of the low pressure gas during the test in Kelvin

l is the film thickness in mm

A is the effective film cross sectional area in m^2

Hence, equ'n.[54] becomes :

$$P = (p_2 v_2 - p_1 v_1) \, T_0 \, l \, / \, \blacktriangle t \; p_0 \; T \; A \; \blacktriangle p \quad \text{---------- [55]}$$

Since v_1 is equal to zero, equ'n.[55] reduces to :

$$P = (\text{slope } v_2) \, T_0 \, l \, / \, p_0 \, T \, A \, \blacktriangle p \quad \text{---------- [56]}$$

The slope is calculated from the steady state portion of a plot of p_2, corrected for the initial evacuated pressure, as a function of Δt. For natural gas, Δp is equal to the supply pressure minus the initial evacuated pressure, and for DCM, is equal to the DCM vapour pressure(P_{vp}) (converted from Torr) at the average test temperature in Kelvin, calculated from the following equ'n.[10], minus the initial evacuated pressure :

$$\mathbf{Log_{10}\, P_{vp} = (-0.2185\, M_{hv} / T) + B} \text{ ---------- [57]}$$

where, M_{hv} is the molar heat of vaporization obtained from tables, in calories per gram mole, T is the temperature in Kelvin, and B is a constant, also obtained from tables. P_{vp} is converted to mbar from the relationship that 1 mbar = 1.33322 Torr.

3b.4.3 Experimental Uptake Determinations

Gravimetric organic solvent uptake determinations were conducted using DCM, methanol, and xylene since these penetrants have also been used for permeability determination, and the latter two were used for surface tension determinations. The polymers used were, HDPE, LDPE, LLDPE, PP, PA6(B5), PA6(A23), PP silanated with A174 and Z6082 silanes, POM, PTFE, PVdF, PVdC(Saran), cured Epikote 828 epoxy resin, LCP Vectra A90, and LCP Vectra B900 polymers. Only the data for the polyolefins, both PA6's, R6000 and PTFE are reported in this work.

The tests were conducted on rectangular section thick films, all of which had similar thermal history. Samples were hot pressed to approximately 1mm thickness at 5 °C above their T_m, using the Specac 15.011 manual 15 ton press, followed by cutting to ≈ 7.5mm length and ≈ 6.5mm width. The samples were then weighed to four decimal places and were put in capped weighing bottles with the solvent. The mass change of the samples was monitored as a function of time in triplicate by weighing the samples intermittently to constant weight after drying. The results are plotted in Figures 84-88, Section 4.9.5. Each value is the arithmetic mean of four determinations for each system, within standard deviation limits of ± 10%.

CHAPTER 4 - RESULTS AND DISCUSSION

4.1 Introduction

The purpose of this work is to investigate the effect of PP/PA6 blend microstructure on water vapour permeability. Some oxygen permeability and organic solvent barrier measurements were also made for the homopolymers. Microstructure development will be discussed in terms of rheological properties, and the interaction with compatibilizers. The permeability results will be correlated with the observed microstructure. It will be shown that the presence of suitable functional groups is the decisive factor in determining the permeability properties of a given polymer blend.

4.2 Rheological studies

Most polymers are incompatible and their blending will produce large phases with weak interfacial bond and poor mechanical properties. For polymers which have similar melt viscosities a good dispersion can often result. Polymers with dissimilar viscosities are difficult to mix[1-3]. The reduction in interfacial tension will enhance the formation of elongated particles or strings. The interfacial interaction and the surface tension are interrelated, which means that increase in molecular interaction across the interface can result in phase coarsening. In view of these observations, the viscosity ratio of the blend components was firstly examined, since matched viscosities can produce an improved dispersion.

If the blend is well compatibilized and stable, with the dispersed phase size d $\leq$ 1 μm, the morphology may not be seriously affected by flow within the low range of shear stresses, when the rheological responses in dynamic and steady state shear are similar, as has been shown in other work[4] for Orgalloy R6000. Lower shear rate control is possible with the dynamic method without the artifacts of flow-induced morphology dominant in the steady state flow. The RDA II instrument used in this work operates under a blanket of N_2, takes a small sample size, is easy to clean, and has a short duplicate samples turnaround time.

4.2.1 Steady State Viscosity

Steady State Viscosity was measured with the simplest capillary rheometer, the Melt Flow Indexer (MFI). In this work the data gave a comparative viscosity value at 230 °C,

and the mass used for extruding the sample was 2.16kg. The MFI gives a single viscosity value at a single shear rate, by measuring the mass of polymer flowing through the capillary in a particular time, extrapolated to 10 minutes. MFI measurements were made according to ISO 1133:1981[5]/(ASTM D-1238) on all the homopolymers and PP/PA6 blends investigated, as described in Section 3a.12 and Figure 13 shows the concentration dependence of MFI for PP/B5 blends.

4.2.2 Dynamic Viscosity

Using the method outlined in Section 3a.12, complex viscosity determinations were conducted using a parallel plate rheometer[6] on all the PP/PA6 blends and homopolymers, in order to correlate these with MFI, dispersed phase size, and water vapour permeability. Derived data included the viscosity ratio, interfacial slip factor, β and the viscosity-concentration Z factor. The complex viscosity is quoted at the shear rate measured during the corresponding MFI determination and at 230 °C. The elastic and viscous moduli, G' and G", when divided by the angular velocity (ω), the strain rate, give the respective viscosity, ie, $\eta' = G''/\omega$ and $\eta'' = G'/\omega$. Usually however, the complex viscosity is quoted, as in this work, since it is the vector sum of the elastic (η') and viscous (η'') dynamic viscosities, where the latter is multiplied by i, the imaginary unit :

$$\eta^* = \eta' - i\eta'' \text{ ---------- [58]}$$

The complex viscosity is also a measure of the material overall resistance to flow as a function of shear rate and directly comparable with the steady state viscosity η through the Cox-Merz relationship[7].

4.2.3 Viscosity effects

PA6 (B5) of high melt viscosity was initially blended with PP, and a fine dispersion was only achieved near the phase inversion concentration or at low dispersed phase concentration, see Figure 15. To lower the B5 viscosity, plasticization was tried with acetic acid, MA and formic acid, as described in section 3a.2. Both MA liquid and vapour were found to dissolve the B5 rapidly at the 53.5 °C T_m of MA which was therefore unsuitable. Acetic acid was found to be a poor plasticizer for B5, so formic acid vapour was used, since the liquid will dissolve PA6 completely. The B5 granules were suspended above 25 wt% formic acid solution for 8 hours at 80 °C in a sealed

container. After plasticization, the B5 (Plast.B5) was dried similarly to the homopolymer, before chacterization and blending with PP. The PP (DSM 48M10) viscosity was increased by silanation (XLPP), and UV irradiation, but γ irradiation produced molecular weight decreases as evidenced by viscosity decreases. The microstructure of Plast.B5 and XLPP blends is shown in Figures 43 and 44.

4.2.4 Binary Blends

In common with 30% of immiscible polymer blends, the negative deviation from the Log Additivity Rule (NDB behaviour) was shown for the B5/PP binary blends (Figure 14). The curve fitted to Figure 14 shows non-linear relationship. The results of homopolymer, compatibilizer, and R6000 complex viscosity and MFI measurements are shown in Table 4 below.

The viscosity ratio λ of blend components was also correlated with the dispersed phase size, **d**, see Figure 17 for binary blends. The binary B5 systems show the smallest dispersed phase size near the phase inversion, for the low ratio blends, and also for a high ratio blend, at low concentration. It is significant that the ratio's for the finest dispersed blends are not close to unity for the B5 blends. Even for the A23 blends, where the ratio is closer to unity, the dispersed phase size is not significantly reduced for a 30wt% A23 blend, but inferior for the 60wt% blend. This could mean a different phase inversion concentration for this combination. For the plasticized B5 and XLPP blends, clear trends are difficult to observe, except that again the smallest dispersed phase size is obtained with a PA6 matrix, but on this occasion at a high ratio. The same material Correlations were sought between the complex viscosity of the blends. Firstly, the overall blend viscosity as a function of average dispersed phase size,d was correlated. For binary blends, some materials were found to lie near a straight line for **d** as a function of $1/\log_{10}$ η^*, as shown in Figure 16.provides the blends with ratio's closest to unity. Clearly, for low ratio blends, a PA6 matrix provides a better dispersion. For R6000, which provides a superior dispersion to the mechanical blends, the ratio is closer to unity.

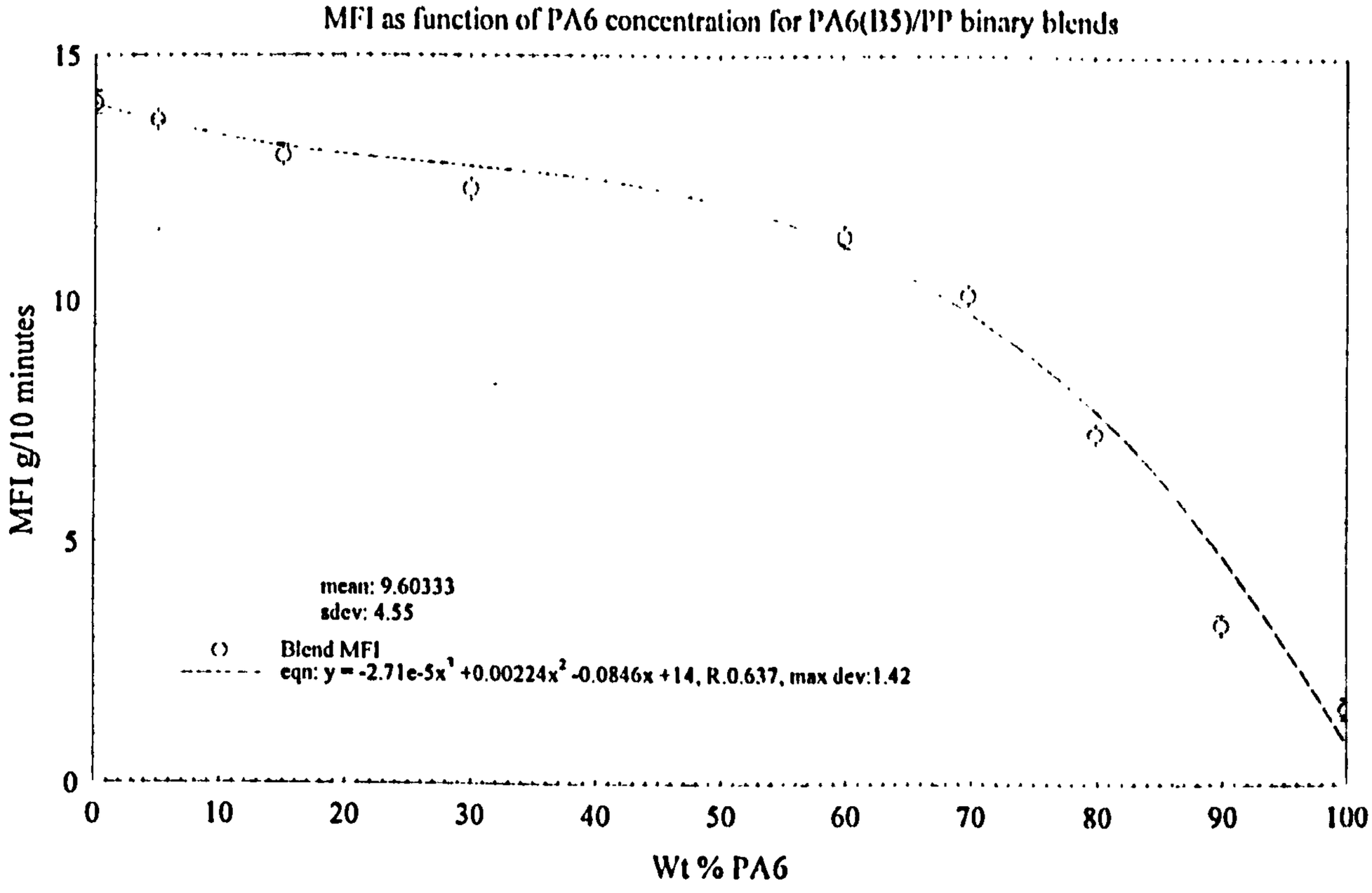

Figure 13 : Melt Flow Index of PA6(B5)/PP blends as a function of PA6 concentration

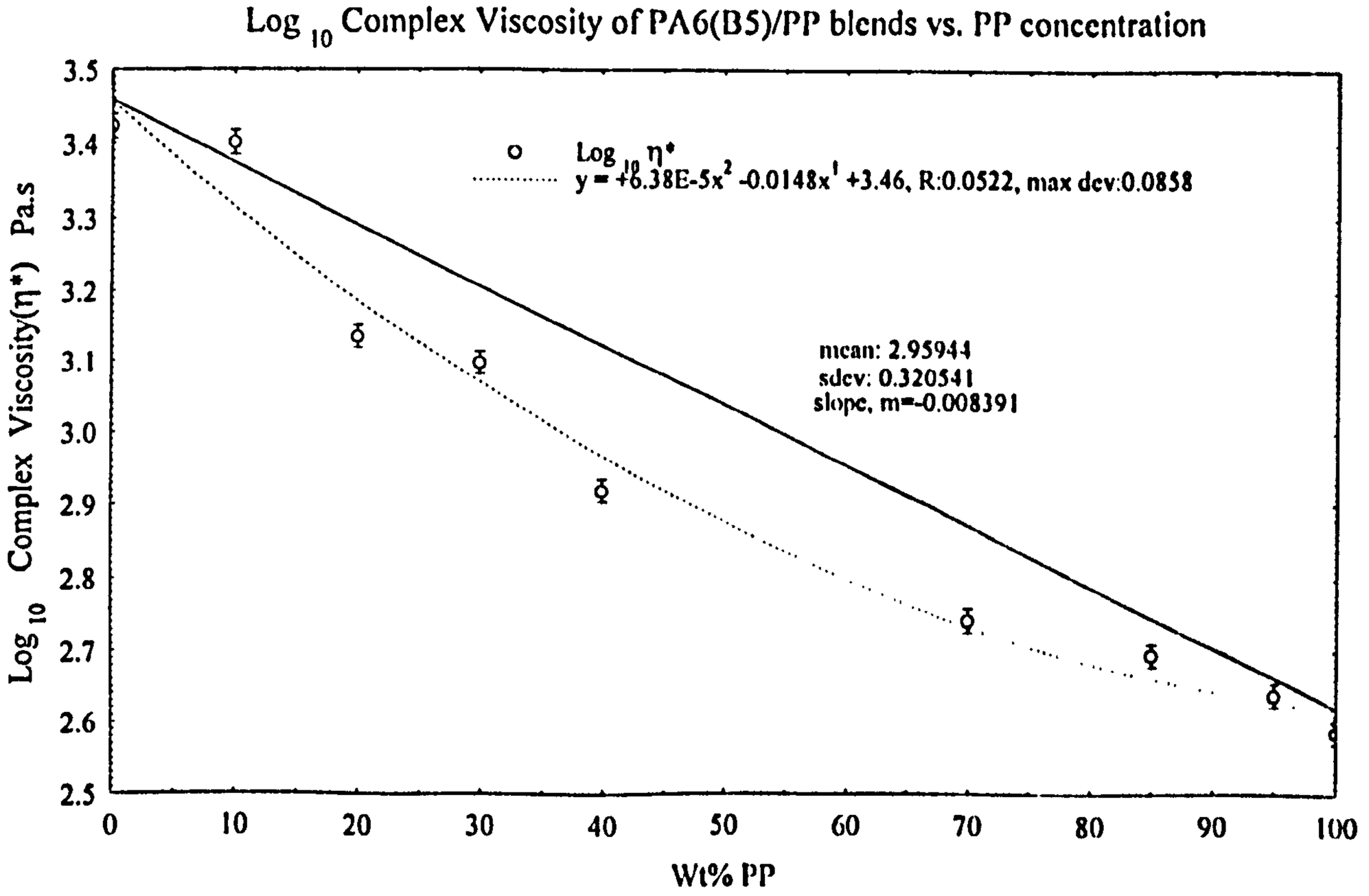

Figure 14 : Negative Deviation from the Log Additivity Rule behaviour for PA6(B5)/PP blends

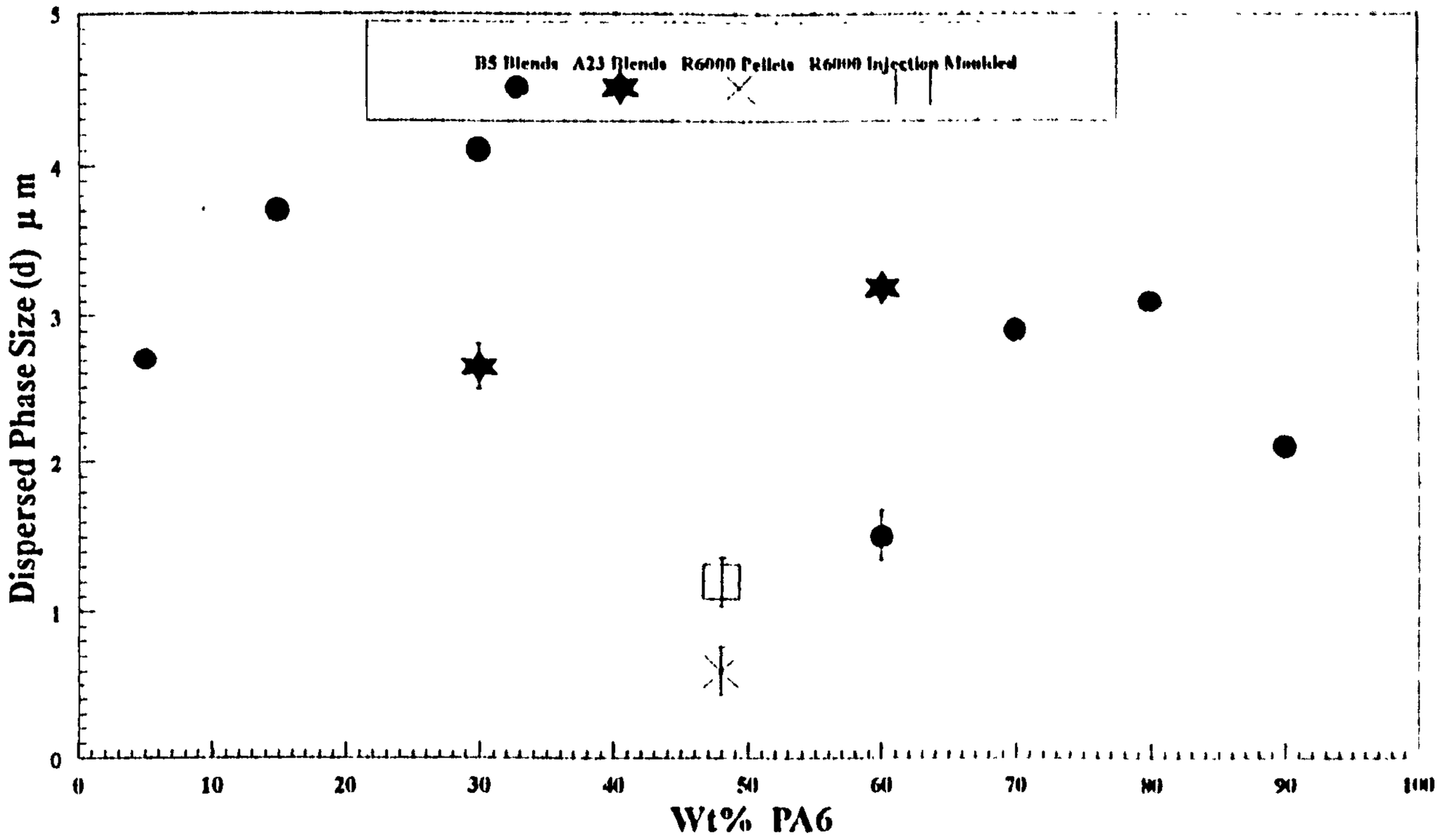

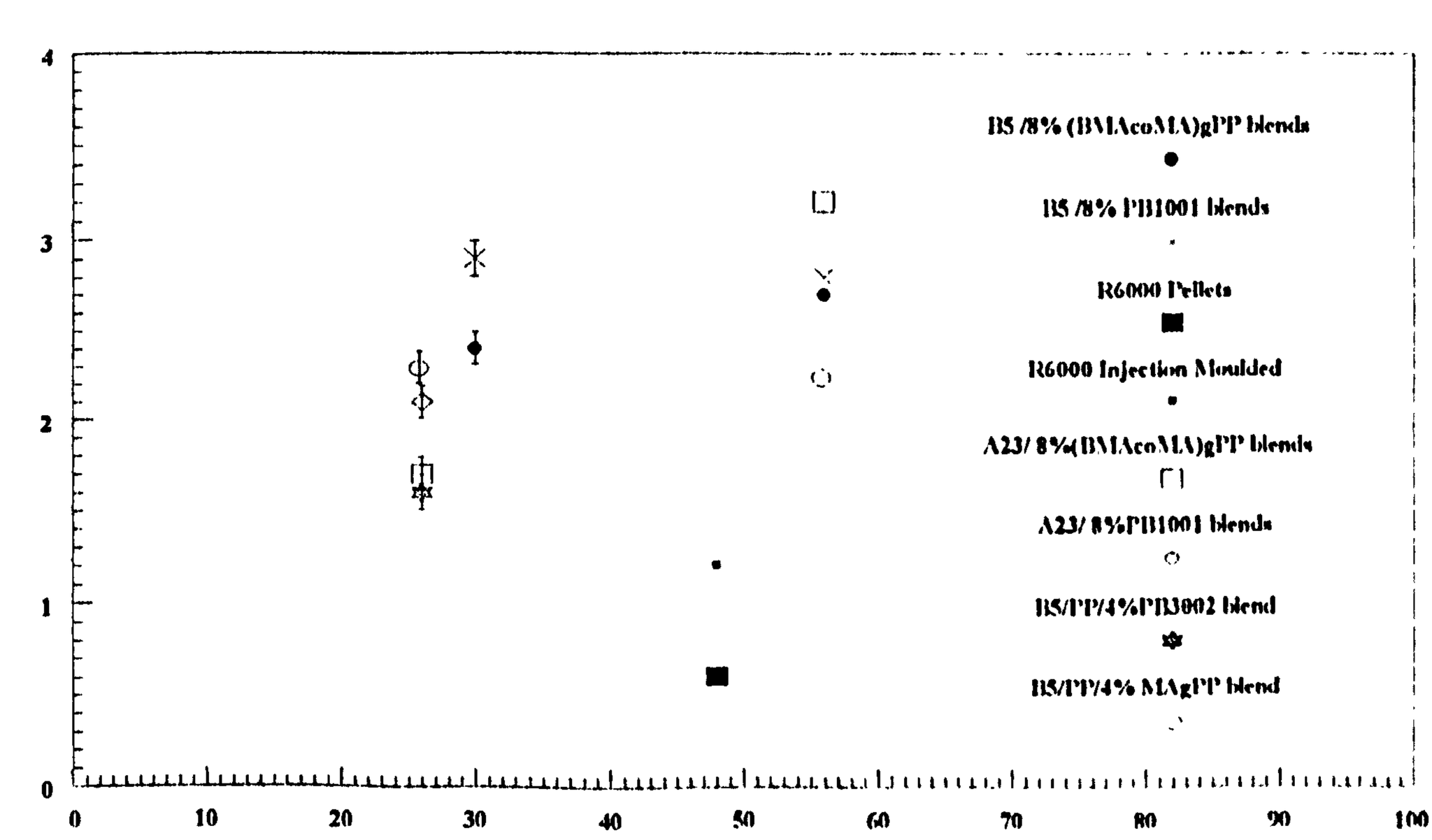

Figure 15 : Dispersed phase size d as a function of PA6 concentration for binary and ternary PA6/PP blends

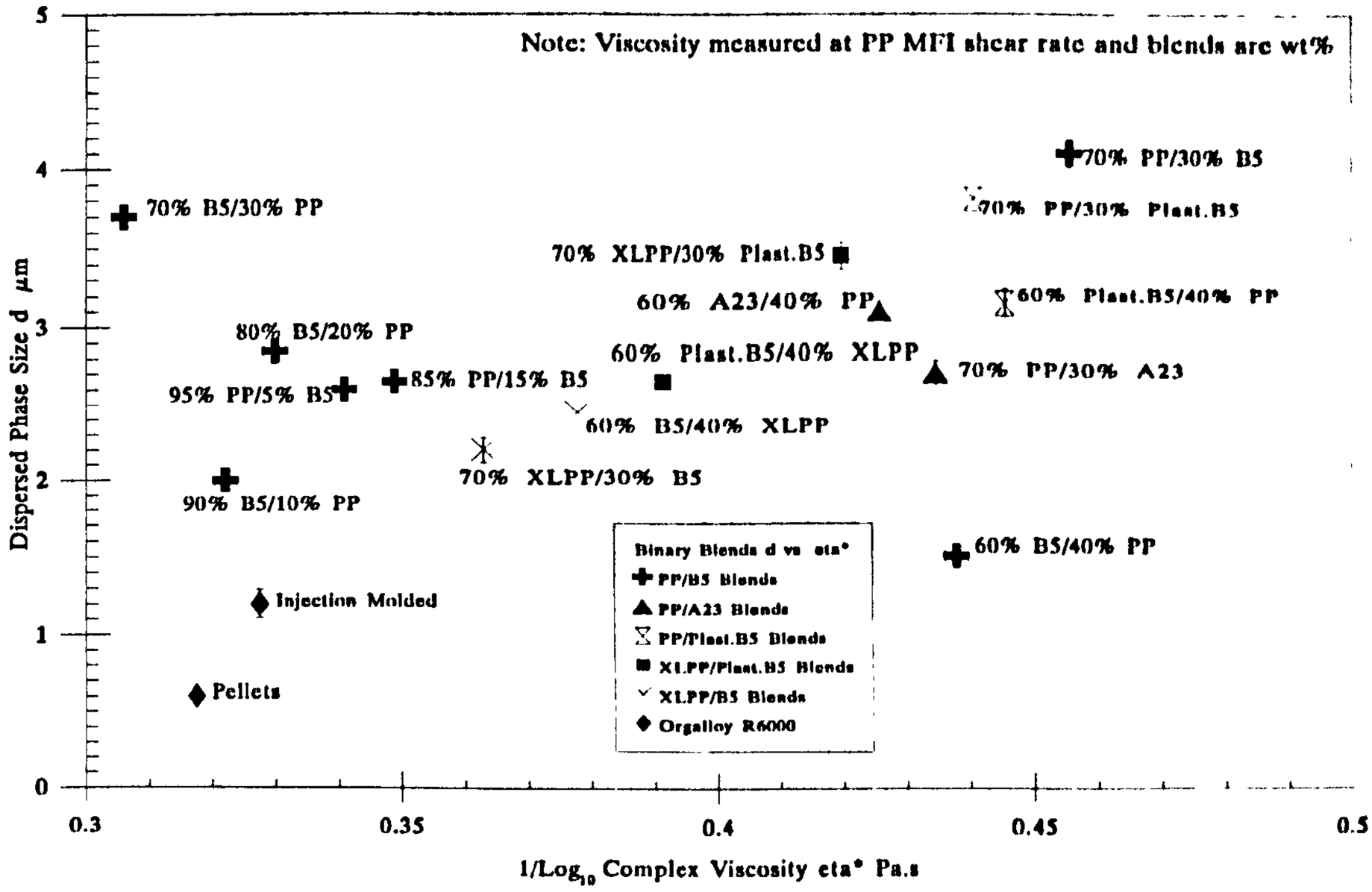

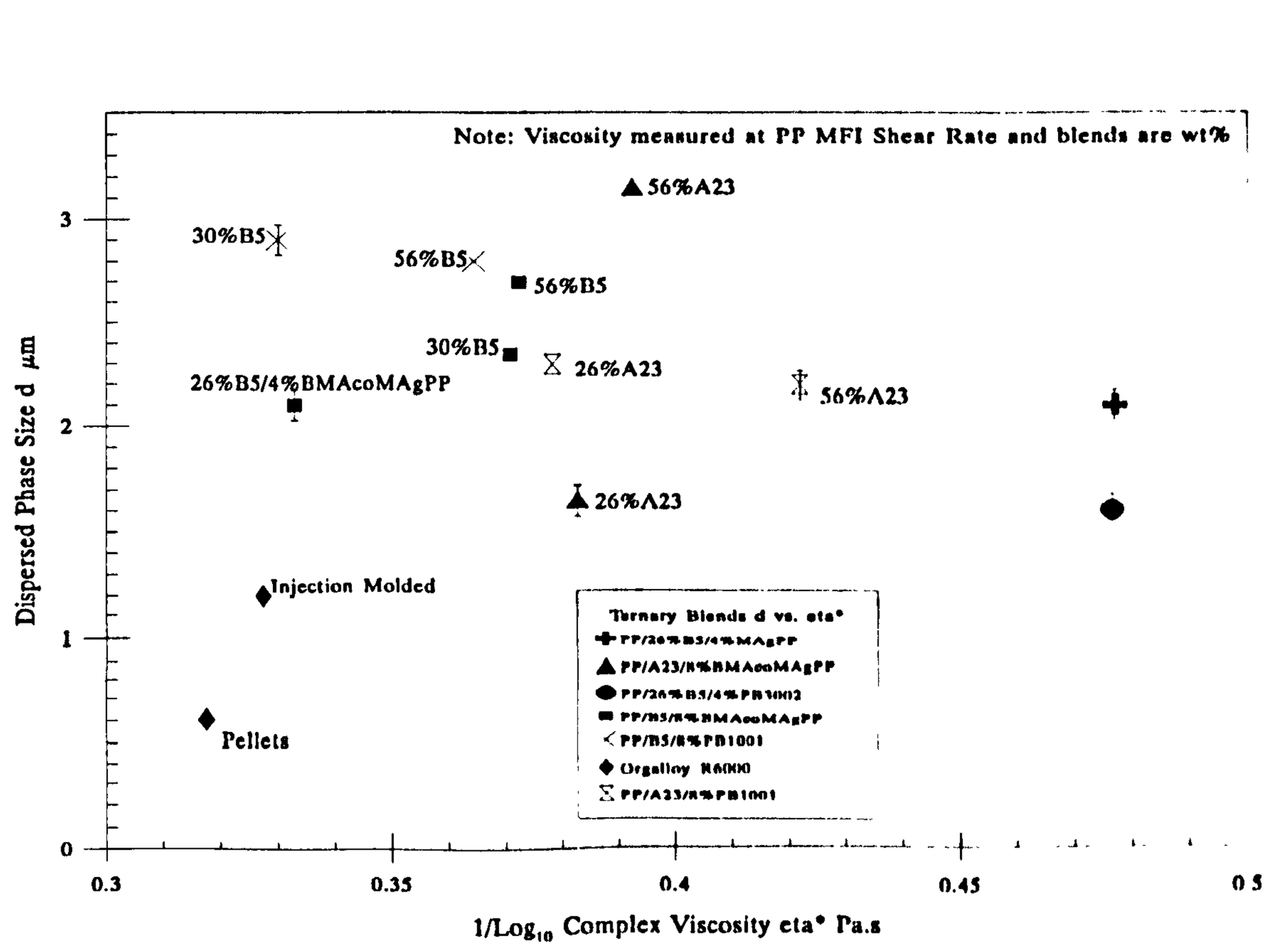

Figure 16 : Dispersed Phase size as a function of Complex Viscosity for binary and ternary PA6/PP blends

phase. Generally, the other trends are that for the higher viscosity PA6(B5) with BMAcoMAgPP, d decreases with λ, whereas for the lower viscosity PA6(A23), with the same compatibilizer, the d increases with increasing λ. For the PB1001 blends, their behaviour is similar to each other, ie. d increasing with increasing λ, although only marginally for the B5 blends. It is interesting to note that for the PB1001 blends, despite the viscosities of the two PA6's being so different, the value of d changes very little with concentration and likewise for the B5/BMAcoMAgPP material. Where the viscosities are similar, and phase inversion has occurred, ie. A23/BMAcoMAgPP blends, d increases dramatically with λ.

Figures 18 and 19 show the shear rate and concentration dependence of PP(DSM 48M10)/A23/PB1001 and PP/B5/BMAcoMAgPP blends at 230 °C and note the increase in viscosity of both PA6's and the PP when blended with 8wt% compatibilizer as a binary system. Note the shape of the ternary curves is similar to that of PP, suggesting a PP matrix, which is confirmed by fluorescence LM of these blends. The shape of the 8wt% PB1001 curve with A23 is also similar to the A23 curve and similarly for the PP curve when compared with PP plus 8wt% PB1001 curve. The 4wt% compatibilizer blend curve of the BMAcoMAgPP system suggests that the compatibilizer has lowered the B5 molecular weight by plasticization, resulting in a lower blend viscosity than that of PP. As will be shown later, the same compatibiliser when blended directly with both PA6's has increased the viscosity of the PA6's, whereas with 4wt% BMAcoMAgPP and 70wt% PP, lubricants in the PP have reduced the blend viscosity .

Since the compatibilizers are all functionalized PP, binary blends were prepared of 8wt% compatibilizers and the PA6 materials used in this work. Complex viscosity measurements were conducted on these materials. Except where free MA was present, the shear viscosity increased for each PA6 with each compatibilizer. The lowered viscosity of PA6/MA-g-PP binary blends is thought to be due to the presence of free MA.

4.2.6 Viscosity of Cross-linked PP

The PP which had been silanated with two different silanes, as described in Section 3a.8.1, showed complex viscosity,(η^*) and loss modulus (G") increases as a function of

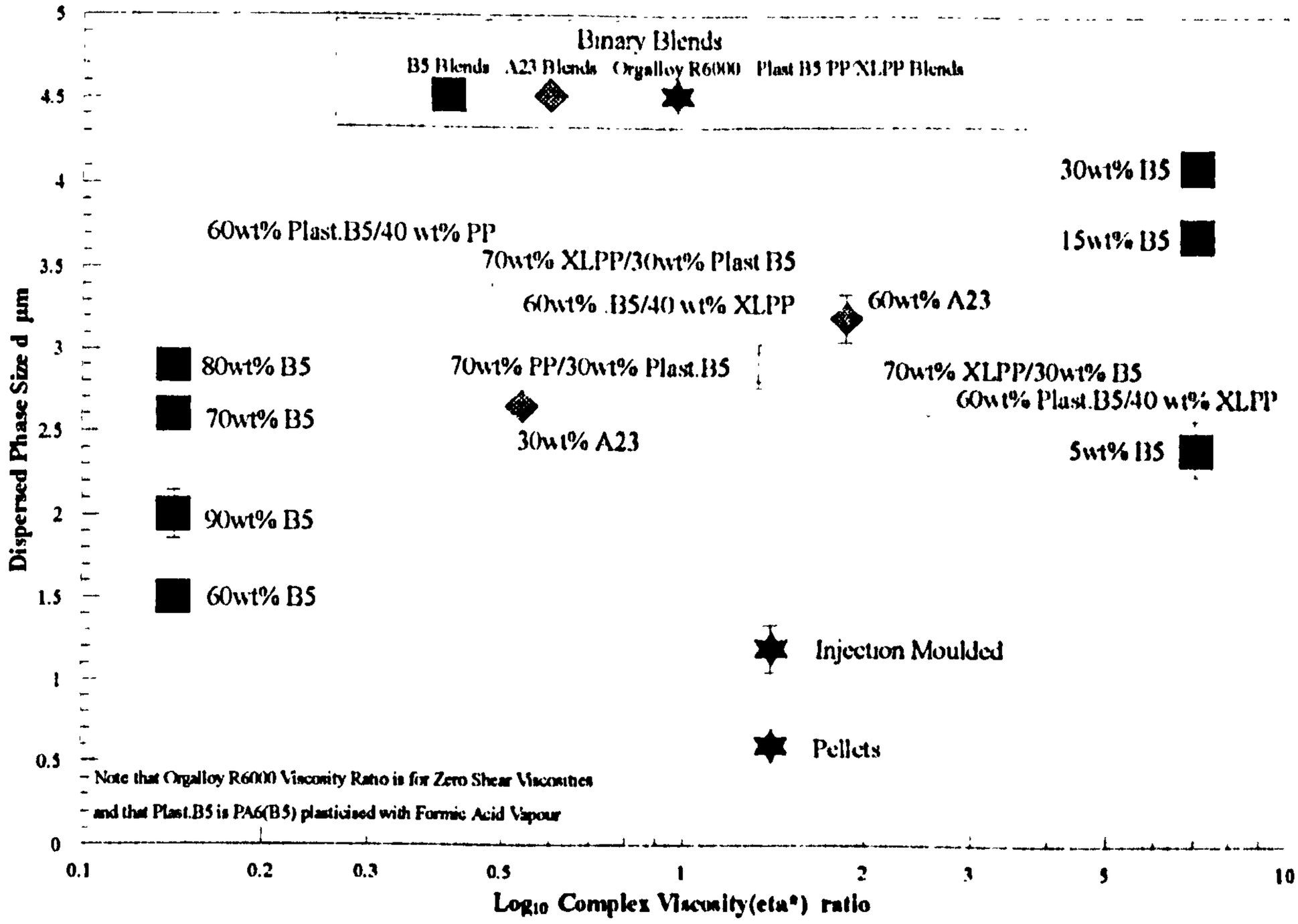

Figure 17 : Dispersed Phase Size as a function of Viscosity Ratio for binary and ternary PA6/PP blends

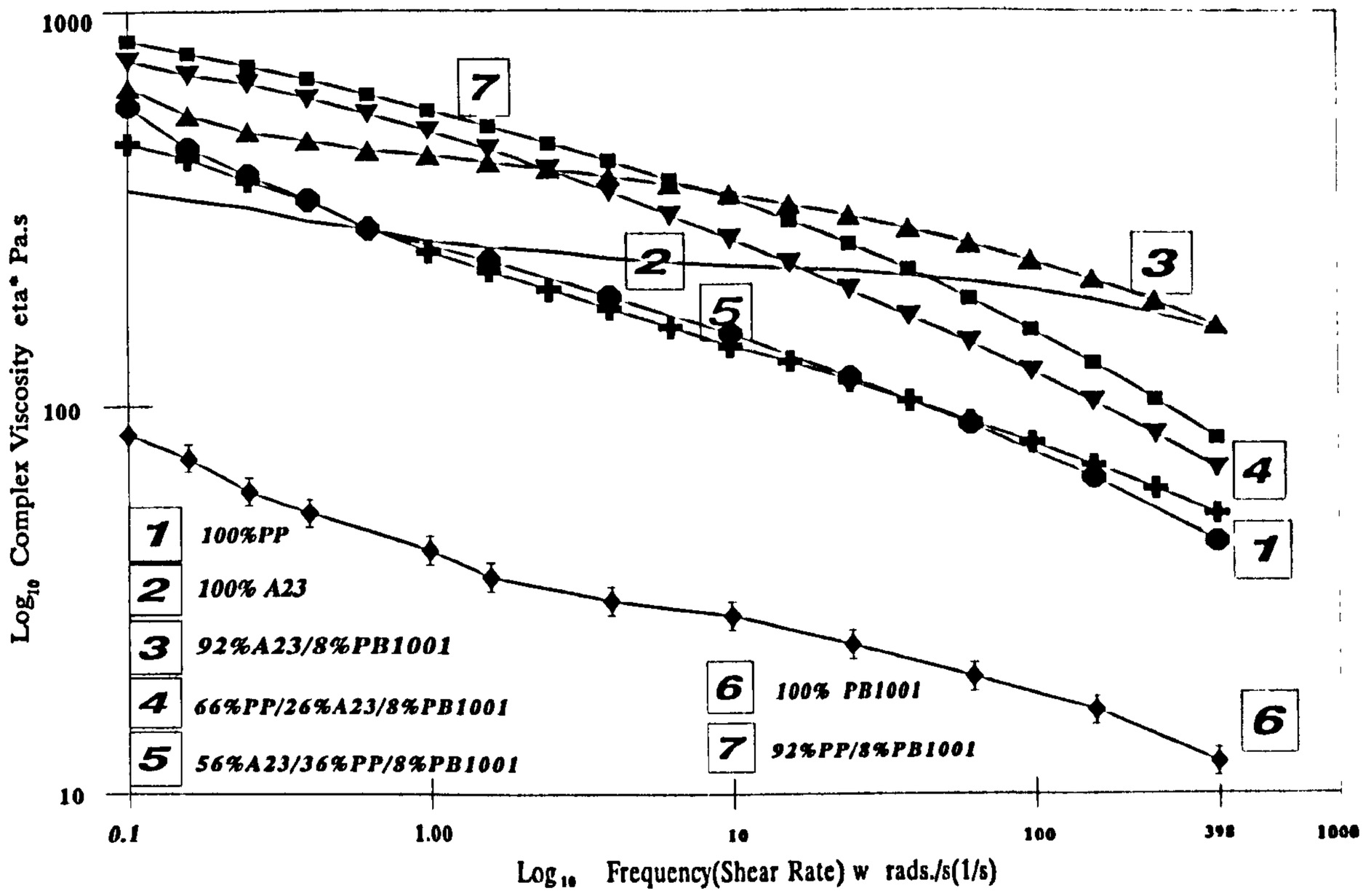

Figure 18 : Complex Viscosity as a function of Frequency at 230 °C for PA6(A23)/PP/PB1001 blends

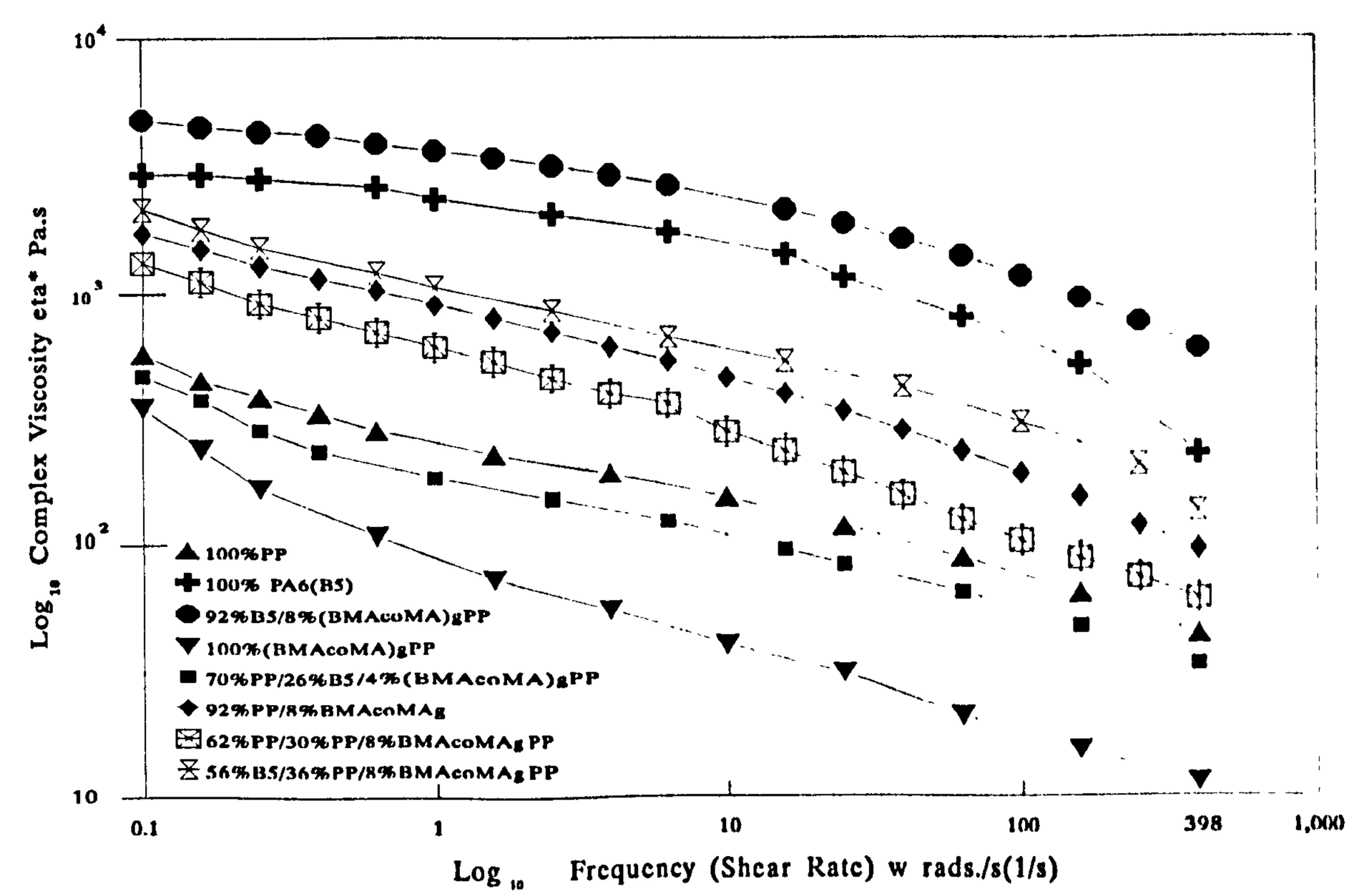

Figure 19 : Complex Viscosity as a function of Frequency at 230 °C for PA6(B5)/PP/BMAcoMagPP blends

Table 5 : Melt Viscosity data for XLPP measured at 230 °C

XLPP wt% composition, with PP	*MFI ,gms/10 x minutes*	*Complex Viscosity η*,Pa.s*	*1/ η** x10^{-3}
100wt% PP (DSM 48M10)	14	375	2.6666
1wt% A174	1.8	778	1.2853
2wt% " "	1.5	1268	0.7886
3wt% " "	1.0	1467	0.6816
5wt% " "	1.0	1674	0.5973
10wt% " "	0.5	1892	0.5286
1wt% Z6082	11.4	617	1.6207
3wt% " "	11.2	1084	0.9225
5wt% " "	8.7	1575	0.6349
10wt% " "	7.7	1766	0.5662
0.1wt% DCP	12.3	502	1.9920
0.5wt% DCP	16.1	370	2.7027
1.0wt% DCP	23.1	236	4.2372
2.5wt%DMF/0.5wt% DCP	18.9	379	2.6385
100wt% PP UV irradiated for 1 hour **	not known	524	1.9083
100wt% PP UV irradiated for 2 hours **	not known	576	1.7361

Note that the η* are measured at the respective MFI Shear Rates, except for **, which are measured at PP MFI Shear Rate

silane concentration consistent with the PP being cross-linked. It is clear from Table 5 that with 0.1wt% DCP, the viscosity has increased as compared to 100wt% PP. This behaviour is not shown by the MFI values, since some cross-linking may have occurred whilst the 0.5wt% DCP material has been residing on the parallel plates of the RDA II for some 10 minutes, whereas it is flowing through the MFI in a shorter period. From the proximity of the complex and dynamic viscosity plots in the experimental data, it also clear that the treated PP has lost some elasticity. Clearly, 0.5 and 1.0wt% DCP with PP

have reduced the PP molecular weight since the MFI is higher than that of PP. Even the addition of DMF to the PP with 0.5wt% DCP has shown only a marginal improvement on the PP complex viscosity, which is not reflected for the MFI measurements. However, with 0.1wt% DCP, a more significant improvement in both MFI and complex viscosity is observed.

4.2.7 Viscosity-Concentration Correlations

The microstructure of the PA6/PP blends was investigated in terms of the rheological "viscosity-concentration" equation, stated below[8]:

$Z = (\eta^*_1/\eta^*_2).(\phi_2/\phi_1)$ **> 1, PHASE 2 CONTINUOUS**

Z ——————— **< 1, PHASE 1 CONTINUOUS** ---------- **[59]**

Z ——————— **≈ 1, DUAL PHASE CONTINUITY**

where, dual phase continuity = co-continuity

Z = viscosity-concentration factor,

η^* = polymer melt complex viscosity,

ϕ = volume fraction of component phase,

phase 1 or 2 continuous = spherical phase dispersed in a matrix

and co-continuity = string like structures of each phase each containing deformed particles of the other phase. The above equ'n. has also been expressed as[9] :

$$\eta_{PA6(\gamma)}/\eta_{PP(\gamma)} = \phi_{PA6}/\phi_{PP} \quad \text{---------- [60]}$$

which equates to :

$$\eta_{PA6(\gamma)} \cdot \phi_{PP}/\eta_{PP(\gamma)} \cdot \phi_{PA6} = 1 \quad \text{---------- [61]}$$

when applied to PA6/PP binary and ternary blends, at a particular shear rate and temperature. When equ'n.[59] was applied to all the PP/PA6 blends for which rheological measurements were made, Table 19, Appendix I is produced.

The data from Table 19 is plotted in Figure 20, showing Z as a function of blend PA6 wt%. Clearly, for binary B5 blends, the Z factor approximates to the expected hyperbolic function with increasing PA6 concentration because the volume fraction term predominates by changing, whereas the viscosity term changes less frequently. The minimum, with the smallest Z value, is at the concentration for which the smallest dispersed phase size is found. This also indicates that the PP should be the continuous phase, which is not the case, as evidenced by fluorescence LM. Interestingly, the blend

which has Z closest to 1 is R6000, and on examination by fluorescence LM, a very homogenous structure is observed, of small dispersed phase size. Assumptions have nonetheless been made about the component viscosities for R6000, ie. the zero shear values have been used from literature, as stated in Appendix I. TEM unpublished micrographs also showed distinct two phase microstructure, with the PP particles overlapping, almost in a dual phase structure. For 70wt% PP/30wt% A23, 90wt% B5/10wt% PP, and 60wt% Plast. B5/40wt% PP blends from Figure 20, we find the result is $Z \approx 1$, implying dual phase continuity, which maintains some degree of continuity[10]. At this composition, phase inversion has possibly occurred and PA6 dispersed in PP is confirmed by fluorescence LM. The PA6 forming the majority portion of the honey-comb structure is also additional evidence for the presence of "amorphous" PA6 for these structures.

Interestingly, for the three finest dispersed blends, ie, 60wt% B5/40wt% PP, 70wt% PP/ 30wt% B5/4wt% PB3002, and 66wt% PP/26wt% A23 /8wt% BMAcoMAgPP, the equation predicts dual phase morphology since $Z \approx 1$, but the morphology only shows this phenomena in the latter case. Where the value of Z is $<< 1$, predicting phase 1 continuous, actually a dual phase morphology is observed. Similarly, the prediction proves to be correct for the low B5 concentration blends, but not for the higher concentration ones. For the two A23 binary blends, the prediction is correct for both, ie. $Z > 1$, so the majority phase 2 is continuous. The prediction is also correct for the 70wt% PP/30wt% Plast.B5 material and for the 70wt% XLPP/30wt% Plast.B5, since it is close to 1, where the dual phase structure observed is correctly predicted. The prediction is also correct for 70wt% XLPP/30wt% B5, and also for 60wt% Plast.B5/ 40wt% PP, since this is close to 1, with string like structures, approaching dual phase morphology being observed. Since for the 60wt% Plast.B5/40wt% XLPP material, the Z factor is > 1, then this means phase 2 should be continuous, which is the case. Despite the B5 being the majority phase for 60wt% B5/40wt% XLPP, the prediction that XLPP is the majority phase is correct, as shown by LM, where clear phase-in-phase behaviour is observed.

The compatibilized blends do not show the hyperbolic dependancy of Z on PA6 concentration, and tend to peak at 26wt% PA6 due the viscosity changes resulting from

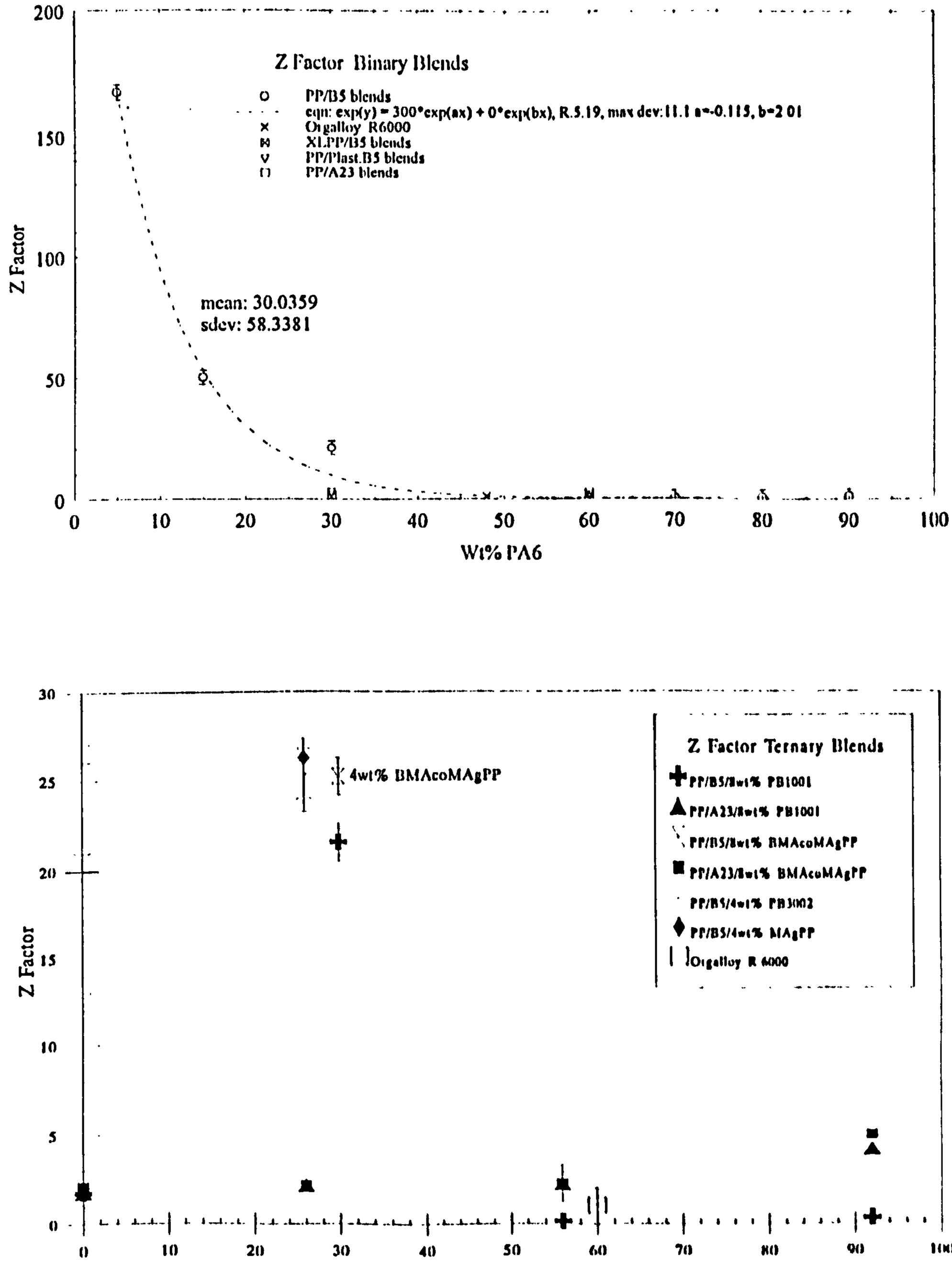

Figure 20 : Viscosity-Volume Fraction Z factor as a function of PA6 concentration for binary and ternary PA6/PP blends

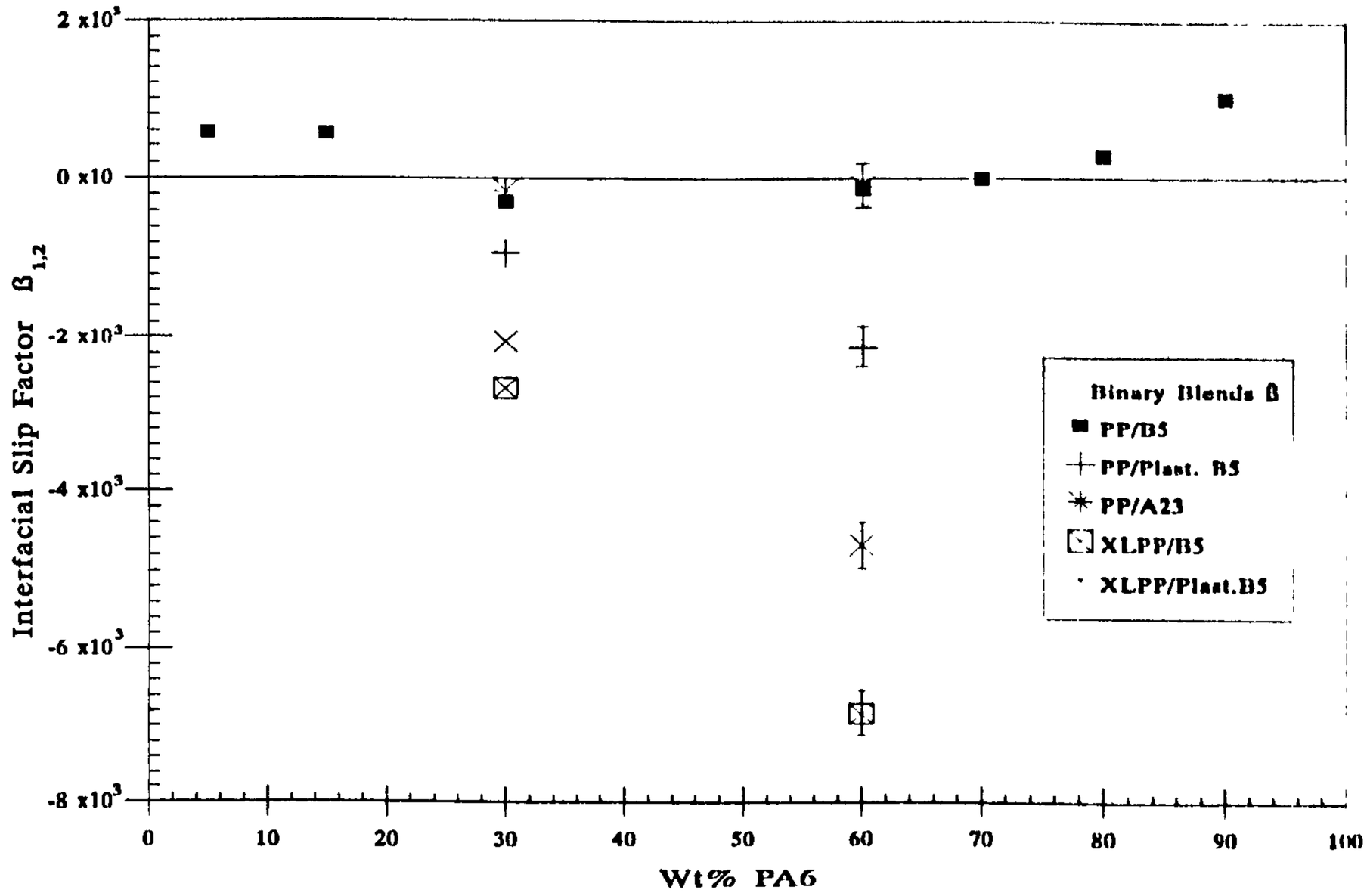

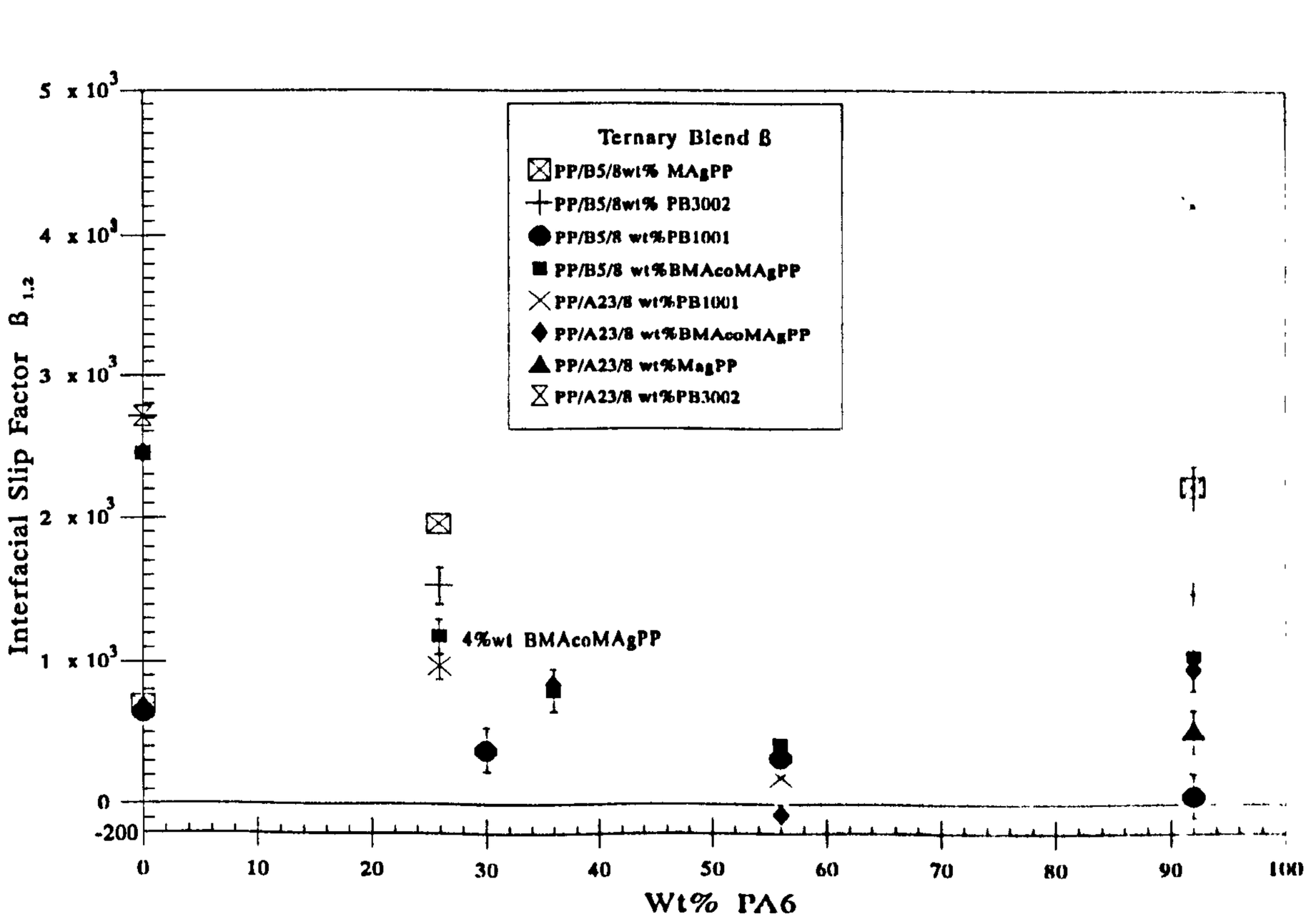

Figure 21 : Interfacial Slip Factor β as a function of PA6 concentration for binary and ternary PA6/PP blends

the compatibilizer. The prediction is correct for all but blend no's. 21, 23, 26, 27, see Table 19 of Appendix I, including the binary PA6/compatibilizer materials. The 8wt% PB1001 and 8wt% BMAcoMAgPP/A23 blends both appear to lie on a straight line, with an increasing value as PA6 concentration increases.This shows a greater probability of phase 2 continuity with increasing PA6 wt%, which reinforces that the lower viscosity material (A23) tends to encapsulate the higher viscosity material, when compatibilized. The same compatibilizers with B5 show a increasing Z value at low concentrations, showing a PP matrix and decreasing towards the phase inversion concentration, but increasing afterwards.

4.2.8 Interfacial Slip Factor

The interfacial tension is difficult to measure without sophisticated high pressure, high temperature equipment. Hence another parameter was investigated, the slip factor, β[11], which formally allows prediction of NDB behaviour, if $\beta_{1,2} \leq 0$. It is defined by equn's. [7] and [8] in Section 2a.4 as the interlayer slip factor β_1 :

$$\beta_1 = 1/\eta^*[w_1/\eta^*_1 + w_2/\eta^*_2] \text{ ---------- [7]}$$

and the characteristic slip factor $\beta_{1,2}$:

$$\beta_{1,2} = (1-\beta_1)(G'')/(w_1w_2)^{0.5} \text{ ---------- [8]}$$

where w_1 and w_2 are the weight fractions of each component in the blend. G", the Shear Loss Modulus of the blend, represents the constant stress level, used instead of $\sigma_{1,2}$, the shear stress on the wall[12], and can be taken as constant in equ'n. [7]. For a ternary blend, extra w and η terms are included, with the mass fraction product term raised to power 0.33, instead of 0.50. The results for the systems investigated are shown in Table 19, Appendix II, and are plotted in Figure 21. For binary blends, it is clear that for the B5/PP blends close to the phase inversion concentration, the slip factor is approaching zero or below it, suggesting NDB behaviour. For the lower concentration blends the slip factor becomes more positive, indicating possibly limited miscibility and these blends also have a smaller dispersed phase, with the exception of the 60wt%B5 blend, indicating less miscibility. Not surprisingly, the deviation is less for the Plast. B5/PP blends, and intermediate for the XLPP/Plast.B5 blends.

Considering the ternary systems, we find that for the PB1001 blends the slip factor is only of the same order for concentrations close to the phase inversion, diverging

considerably at 92wt% PA6, in line with the differing viscosities of the PA6's, ie. for A23 the slip factor is higher, indicating less immiscibility, due to the similarity of the viscosities. The converse is true for the B5.

4.2.9 Rheology Summary

No correlation was found for the MFI and complex viscosity of the blends and homopolymers tested. It is clear from both the MFI and complex viscosity measurements that the viscosity obtained for the blends is lower than would be expected from an additivity rule. The viscosity of the PA6, does not effect the degree of dispersion markedly, with the blends having a lower viscosity than would be expected from the ratio of the blend components.

The viscosity ratio and the interfacial tension of the phases was adjusted by plasticization, cross-linking, and compatibilization, to optimise the phase dispersion in line with that of Orgalloy R6000. The resulting microstructure was compared to that originally found, using light microscopy.

4.3 Blend Microstructure

4.3.1 Micrographs

The micrographs shown in Figures 22-51 show typical microstructures for the blends investigated. Orgalloy R6000, Figures 30 and 31, shows for the finest phase dispersion and superior blend permeability properties. The binary blend of 60wt% PA6(B5)/40wt% PP, Figure 25, shows a coarser dispersion, but similar to the injection moulded R6000. PA6(B5) has a much higher melt viscosity than 48M10 (PP), so the first attempt at reducing the average dispersed phase size, (d), was by making the component melt shear viscosities similar, based on the conclusions drawn from the rheological data.

PE/PA6 blends have been made by others, resulting in the ternary compatibilized blends of HDPE and LDPE being made, as shown in Figures 22 and 23. The PA6 phase in polyolefin/PA6 blends is shown here as the lighter majority phase, showing clear co-continuity, with the dark areas being the PE. The phase dispersion is coarse, probably because the compatibilizer is immiscible with the PE phases. Therefore, PA6/PP blends were concentrated on, for compatibility and cost reasons.

For the B5/PP blends, the phase size for the inverted composition, where PA6 (BASF Ultramid B5) is the major phase, has a finer phase dispersion even without a compatibilizer because the phase with the higher viscosity (B5) can transfer the shear forces more easily onto the softer phase. Examples of this behaviour are shown in Figures 24 and 25. Where PA6 (EMS-Chemie Grilon A23) is the major phase, with a melt viscosity lower than the PP, this phenomena is not observed, as shown in Figures 26, 27, 28, and 29. When compared to R6000, Figures 30 and 31, the binary blends with a low viscosity PP matrix have a coarser structure.

With the PP matrix binary B5 blends, the best dispersion is found with only 10wt% B5, with **d** gradually increasing with increasing B5 percentage, see Figure 15. For the B5 matrix binary blends, the best dispersion was obtained with 60wt% B5, indicating that the phase inversion concentration is close to 50wt%. For the two A23 binary blends, the PP viscosity is higher than that of the A23, and the 30wt% A23 material has a smaller **d** than the 60wt% material.

The commercial R6000 has a superior phase dispersion to all the other binary and ternary blends, measured by other researchers as 1.11 $\pm$ 0.63 μm,[4] but cited as containing 40wt% PP and 12 $\pm$ 2wt% compatibilizer[13]. It does however, show phase coarsening after processing. A similar **d** reduction was obtained by compatibilization of 70wt% PP blends with 4wt% of both the MA-g-PP (Maleic Anhydride grafted on PP) materials, see Figure 33 (PB3002 compatibilizer). Less significant reductions were seen with PB1001 (AA-g-PP) and also with the bi-functional (BMAcoMA)gPP (Butyl Methacrylate co MA grafted on PP). The 66wt% PP/26wt% PA6(A23)/8wt% BMAcoMAgPP blend, Figure 47, also showed similar phase dispersion to injection molded R6000. With BMA-g-LDPE and PB3009 (MA-g-HDPE) increases in **d** were found, as compared to the binary blend, probably due to the immiscibility of LDPE and HDPE with PP. Experiments conducted by adding free MA, with and without BPO initiator, to some B5/PP blends were inconclusive and only had marginal effect on the microstructure, ie, 4.1 μm for 70wt% PP/30wt%B5 (Figure 24) reduced to 3.5μm for 65wt% PP/30wt% B5/5wt% MA (Figure 32). In addition, a brown material was produced, indicating PA6 degradation and molecular weight lowering.

For the 56wt% A23/36wt% PP/8wt% PB1001 blend, Figures 34 and 35, PP forms the matrix due to a reduction in the effective volumes of the blend components caused by the interphase. This is despite A23 being the major phase with a lower viscosity than the matrix, at the same shear rate and temperature. When **d** for this blend is compared to that of the uncompatibilized version, 60wt%A23/40wt%PP, Figures 28/29, there is a reduction in **d**, which could account for the chemical reaction product of the matrix, dispersed and compatibilizer components. Certainly, the amine end groups of the PA6 will contribute to the formation of the interfacial amide groups. It is interesting to compare this material with the microstructure of the 56wt% A23/36wt% PP/8wt% BMAcoMAgPP blend, Figure 45, which has a much coarser structure, in fact a **d** which is hardly reduced. Light microscopy clearly shows a fluorescing PA6 matrix.

The morphology of several blends, ie. 66wt% PP/26wt% PA6(A23)/8wt% PB1001, 70wt% XLPP/30wt% B5, and 56wt% A23/36wt% PP/8wt% BMAcoMAgPP see Figures 39, 40, and 37, is similar to the composite droplet morphology reported by Lavallee et al[14], Sorenson[15] and Utracki[16], the latter applying to Orgalloy R6000. This is defined as a two or three component system where some of the dispersed phase can contain small inclusions of the matrix component, also known as phase-in-phase behaviour. These researchers concluded that similar blend morphology can only be obtained through phase inversions of blend components at particular viscosity and compositional ratios stated in the viscosity ratio-concentration equ'n.[59], in Section 4.2.7[10].

Other blends, ie. 60wt%PA6(B5)/40wt% XLPP, 60wt% Plast.PA6(B5)/40wt% PP and 60wt% Plast.(plasticized with formic acid vapour) PA6(B5)/40wt% XLPP show co-continuous structures (Figures 41, 43, and 44). This could be attributed to a concentration effect of the phase inversion particularly for the XLPP/B5 materials, where the 30wt% B5 material, Figure 40, has lower dispersed phase size than the 60wt% material. This is also the trend for the PP/Plast.B5 blends, whereas where the blend is Plast.B5/XLPP, a smaller dispersion is obtained with the 60wt% Plast.B5 material, if the co-continuous structures are ignored. The co-continuity of the 60wt%Plast.B5/40wt% XLPP blend, probably makes it a less useable material. However, the 70wt% XLPP/30wt% Plast.B5 blend (Figure 44) shows clear phase separation. In addition, the viscosity ratio effect on the morphology, Figure 17, shows that where the ratio is larger

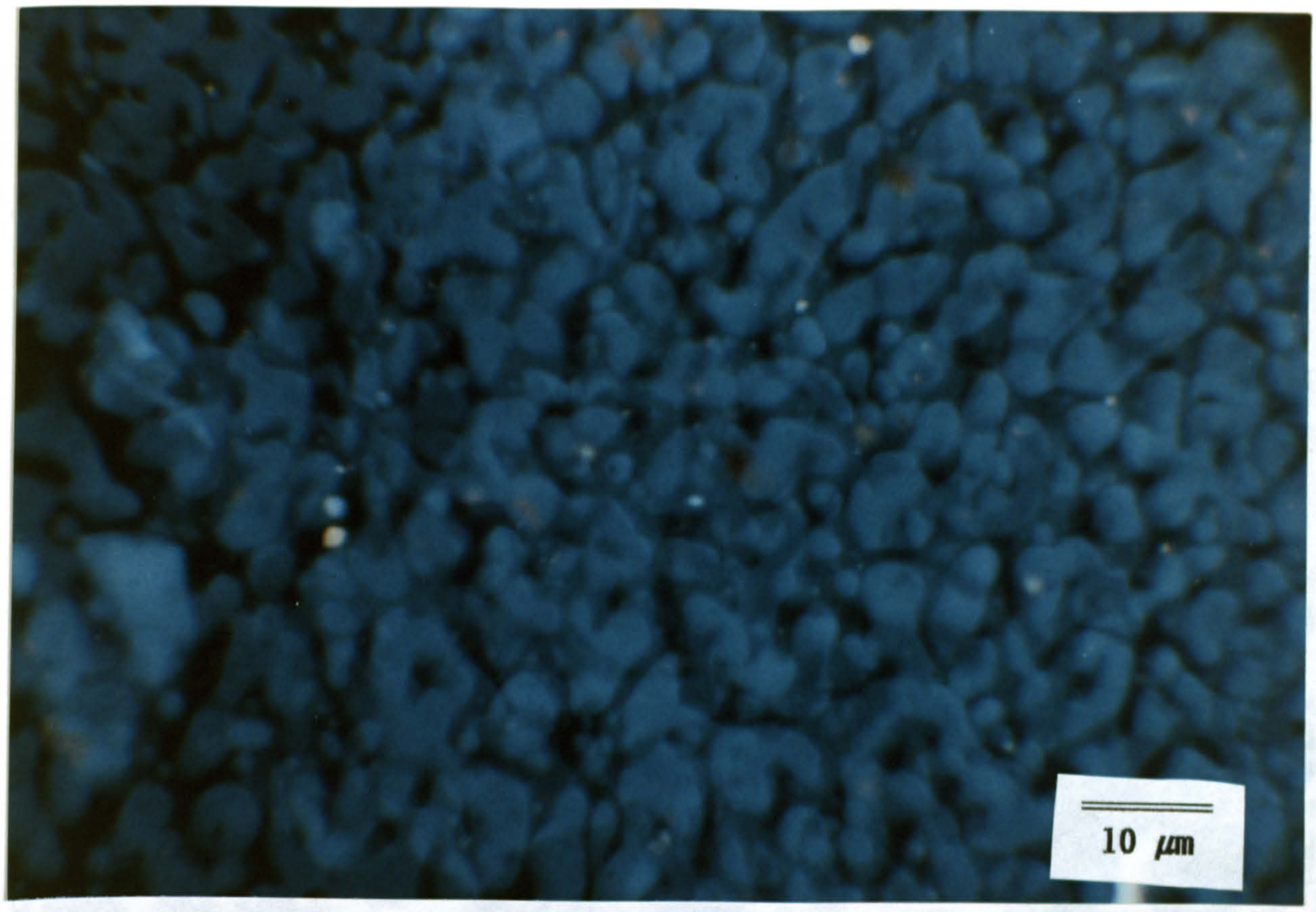

Figure 22 : 71wt% PA6(B5)/24wt% LDPE/5wt% MAgPP Fluorescence

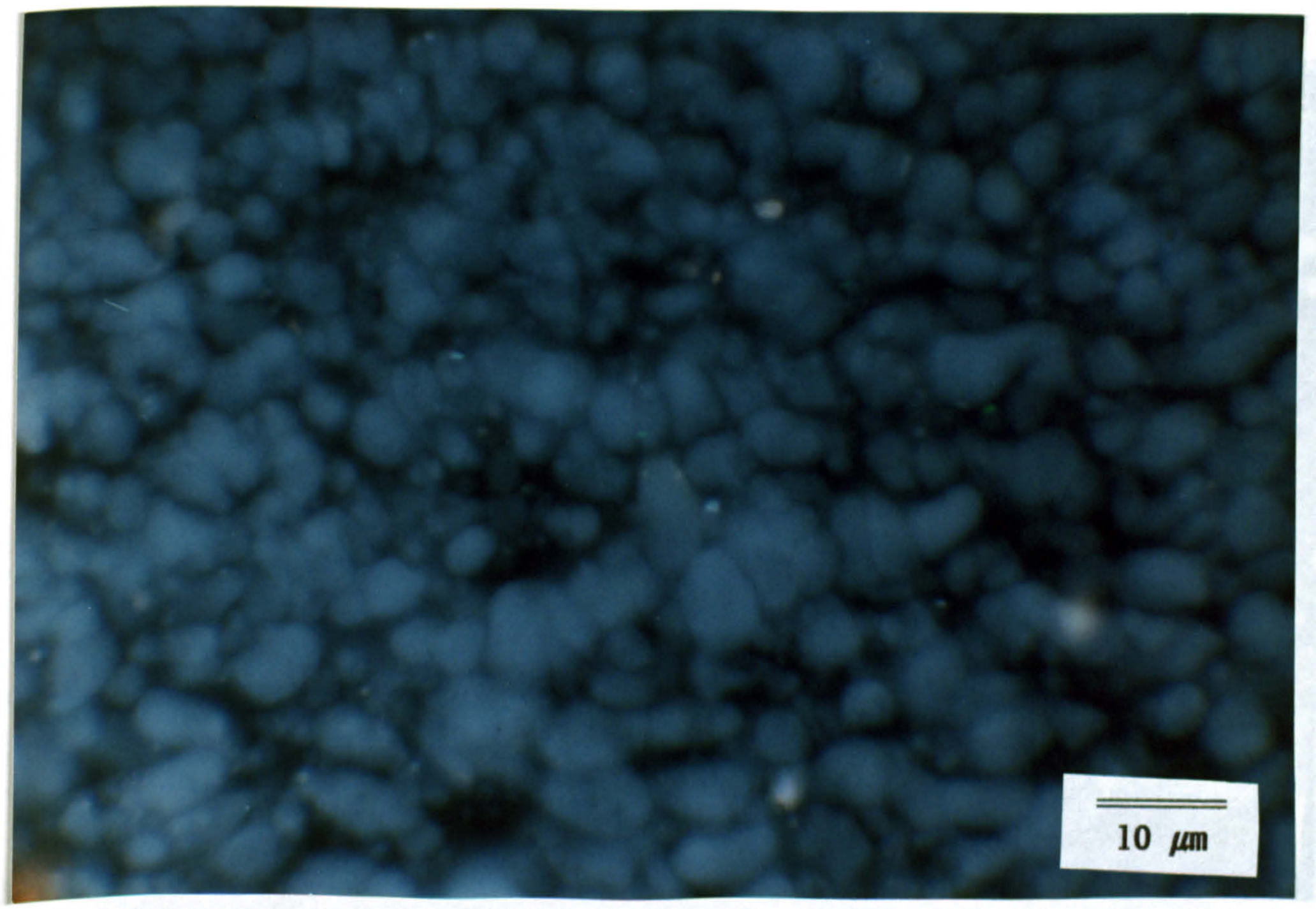

Figure 23 : 71wt% PA6(B5)/24wt% HDPE/5wt% MAgPP Fluorescence

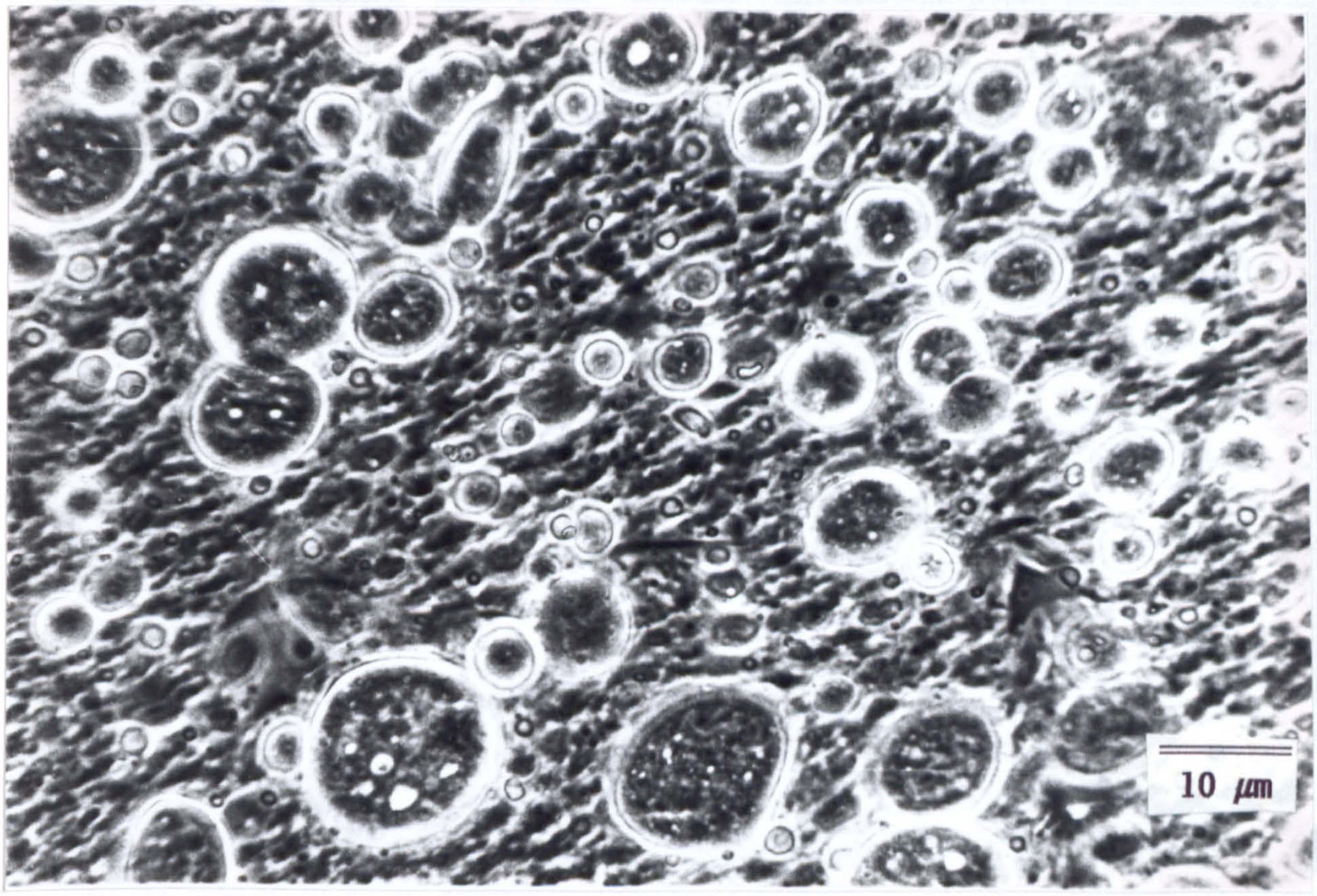

Figure 24 : 70wt% PP/30wt% PA6(B5) **Phase Contrast**

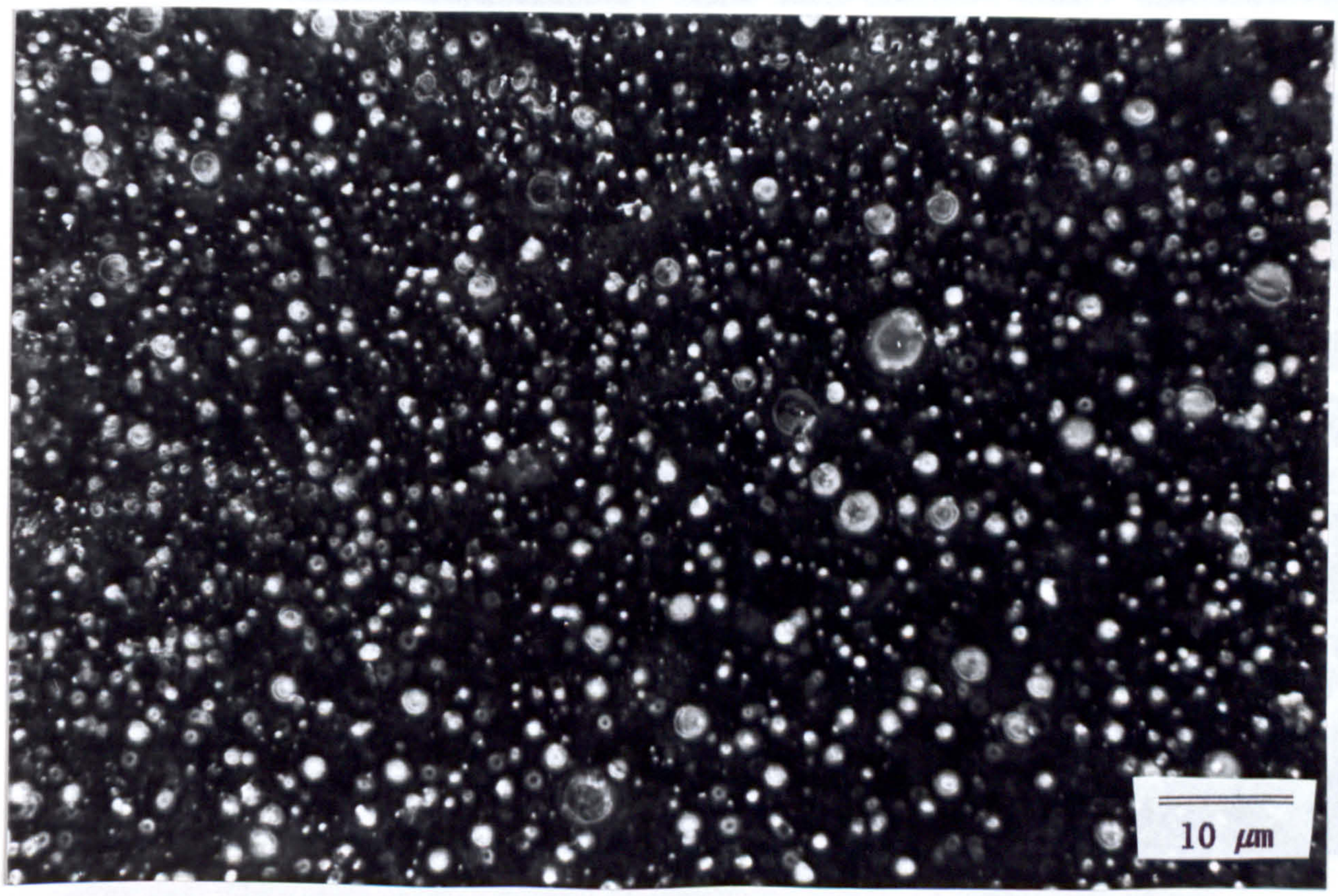

Figure 25 : 60wt% PA6(B5)/40wt% PP **Phase Contrast**

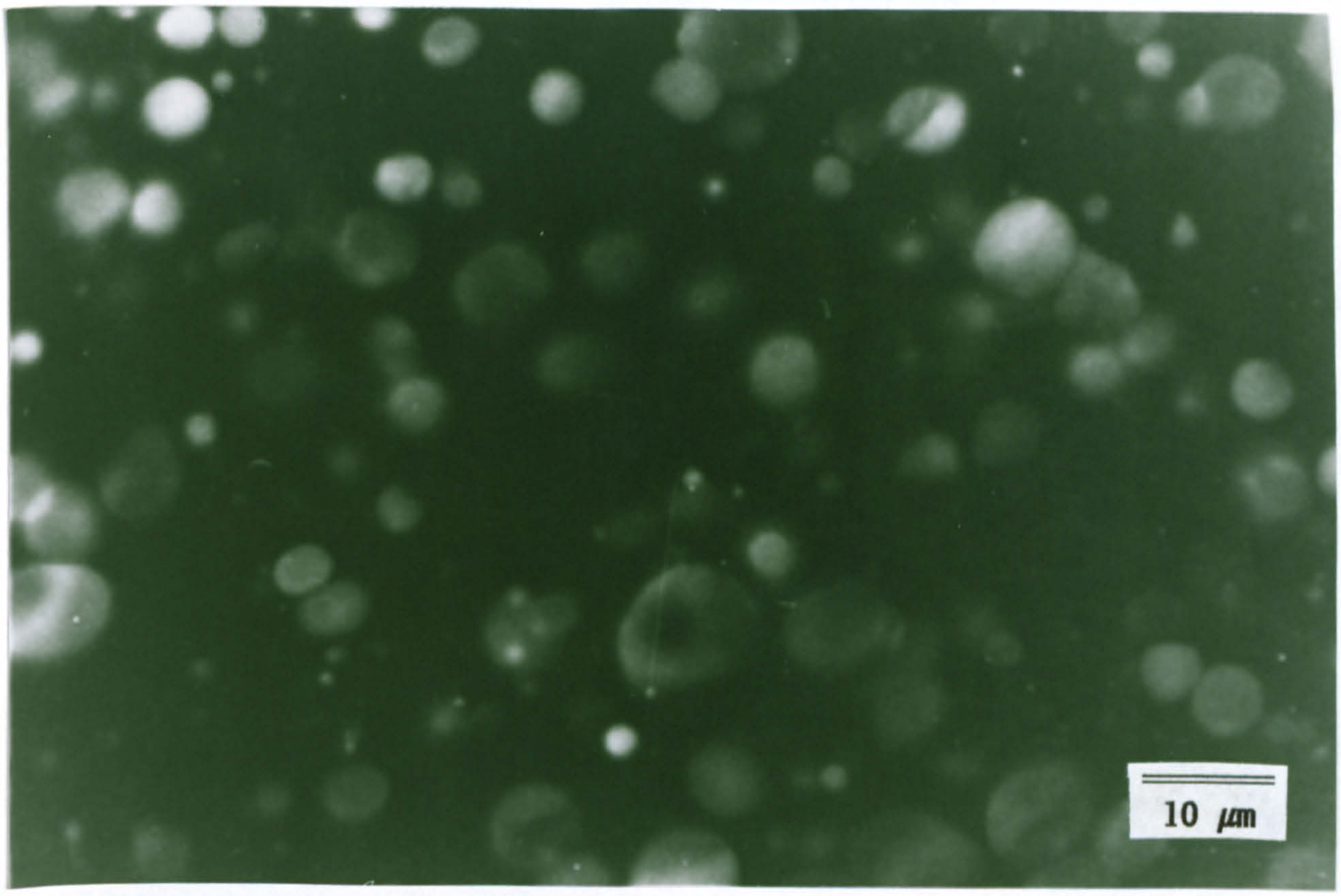

Figure 26 : 70wt% PP/30wt% PA6(A23) Fluorescence

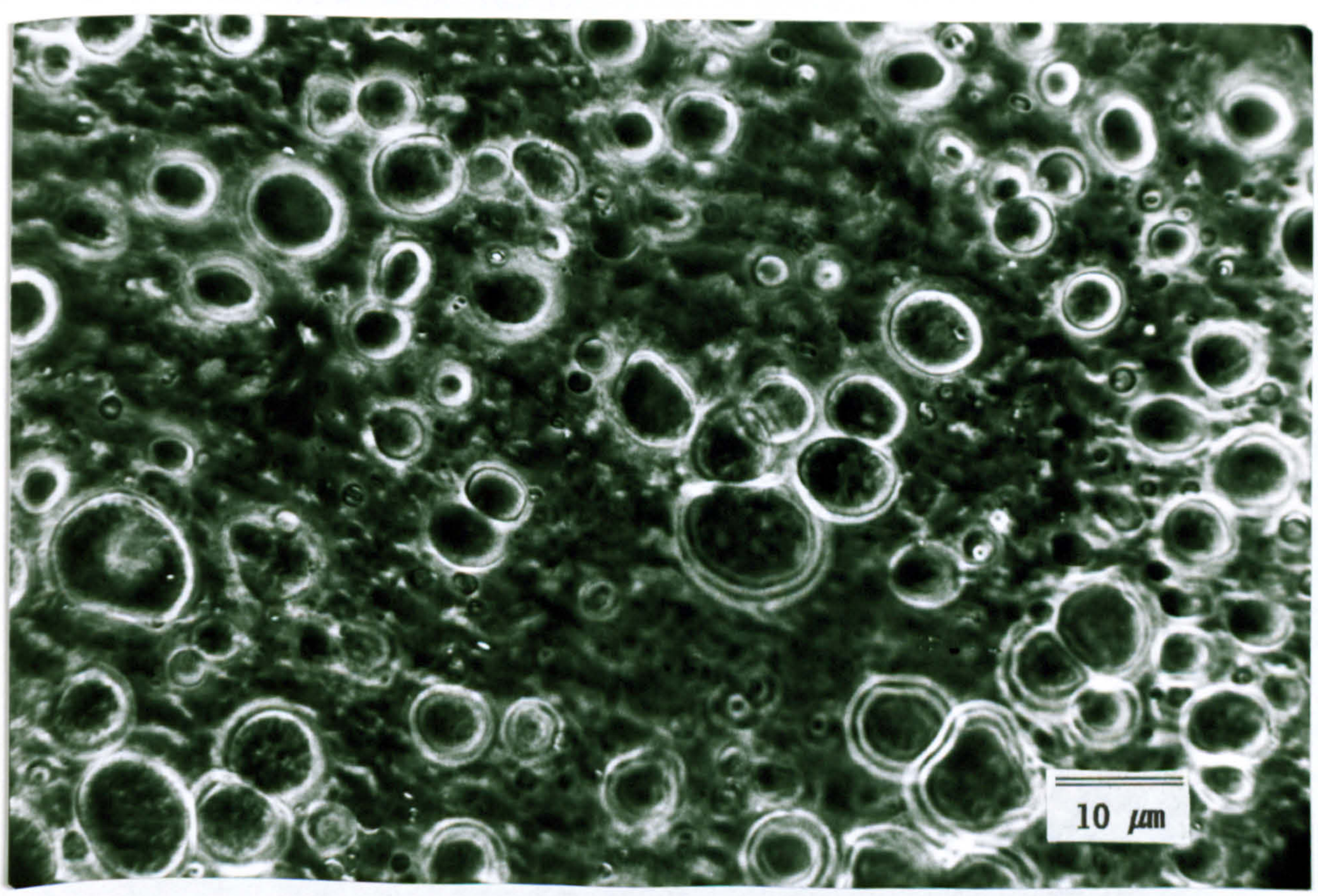

Figure 27 : 70wt% PP/30wt% PA6(A23) Phase Contrast

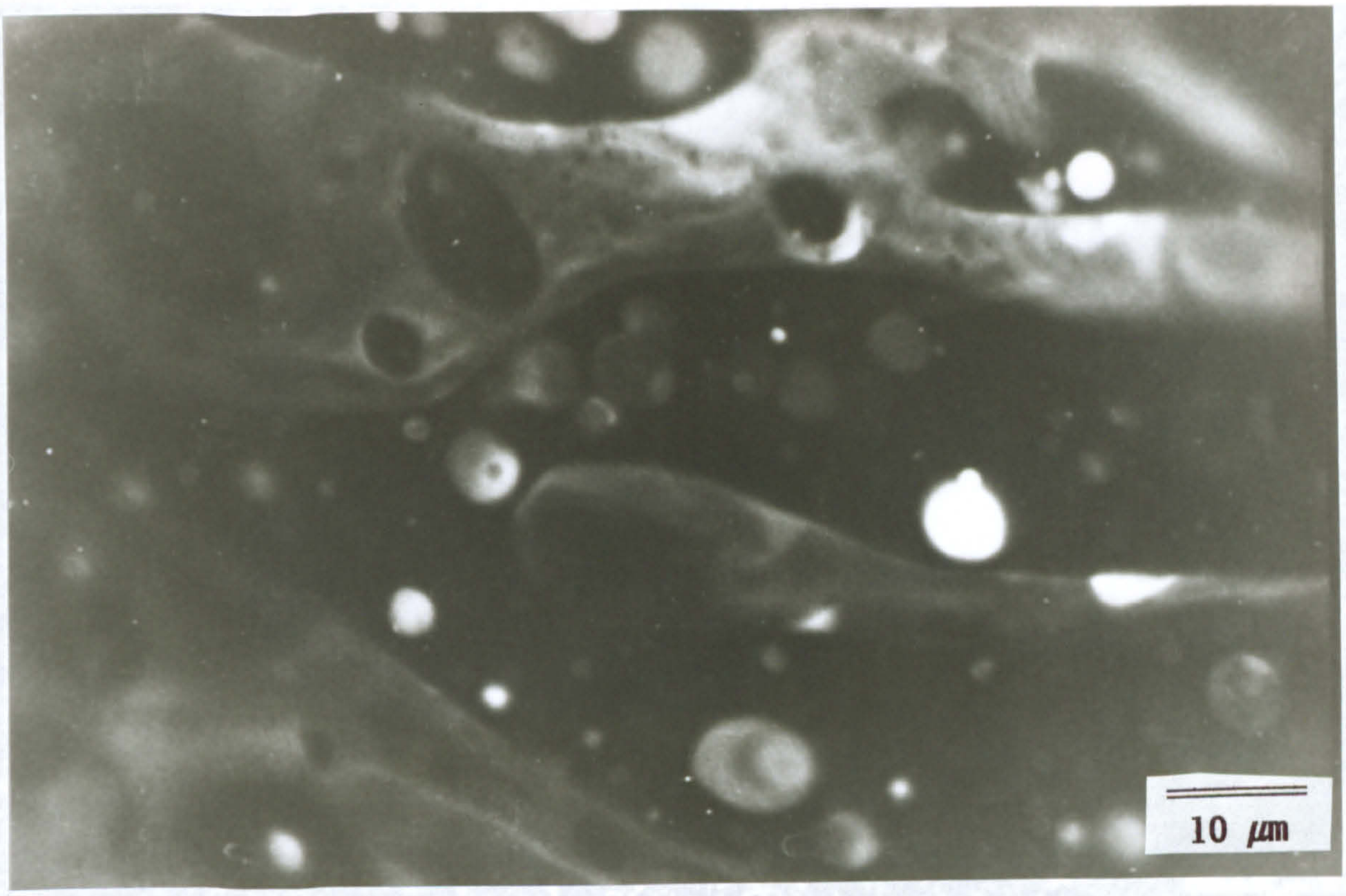

Figure 28 : 60wt% PA6(A23)/40wt% PP **Fluorescence**

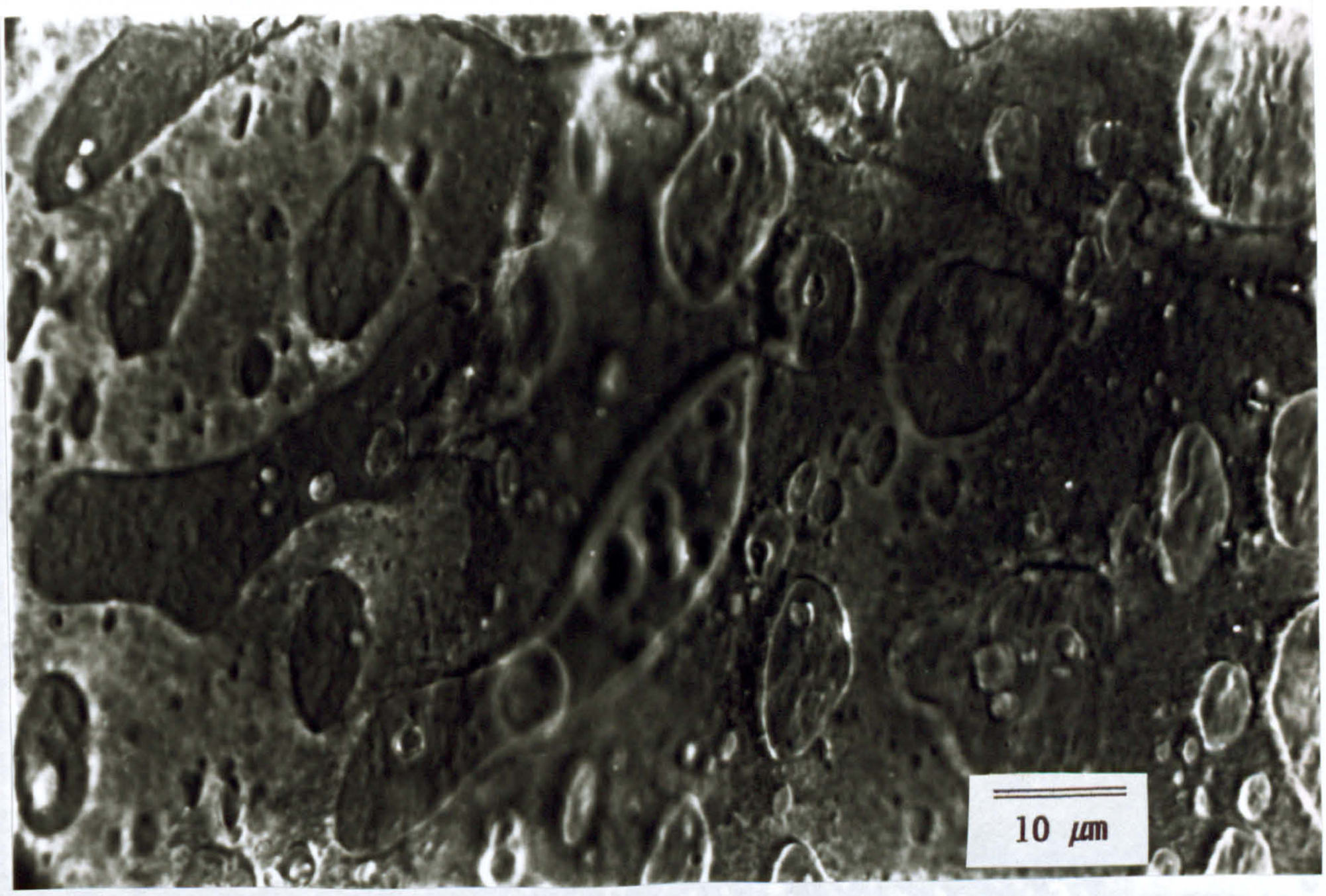

Figure 29 : 60wt% PA6(A23)/40wt% PP **DIC**

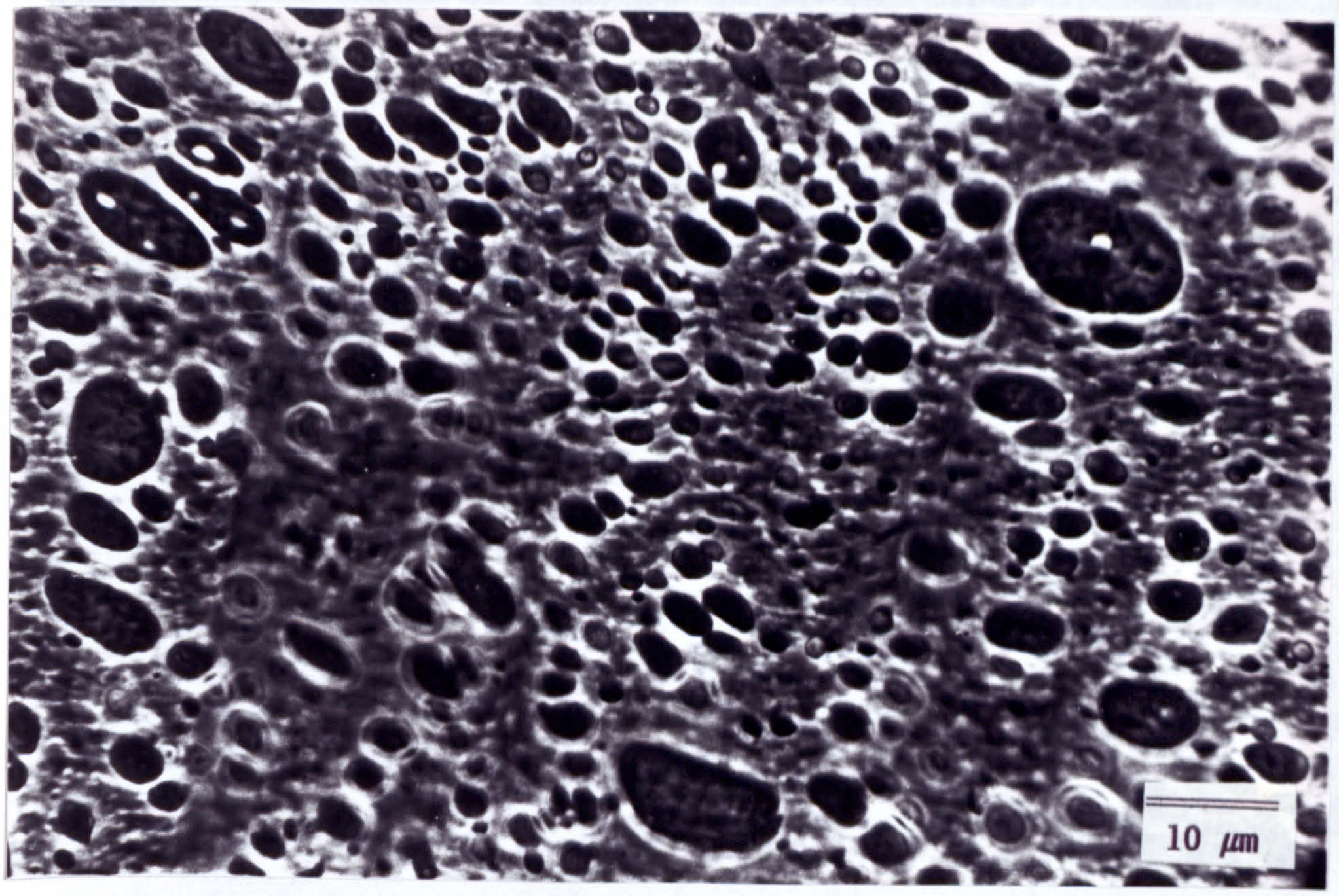

Figure 32 : 65wt% PP/30wt% PA6(B5)/5wt% MA Phase Contrast

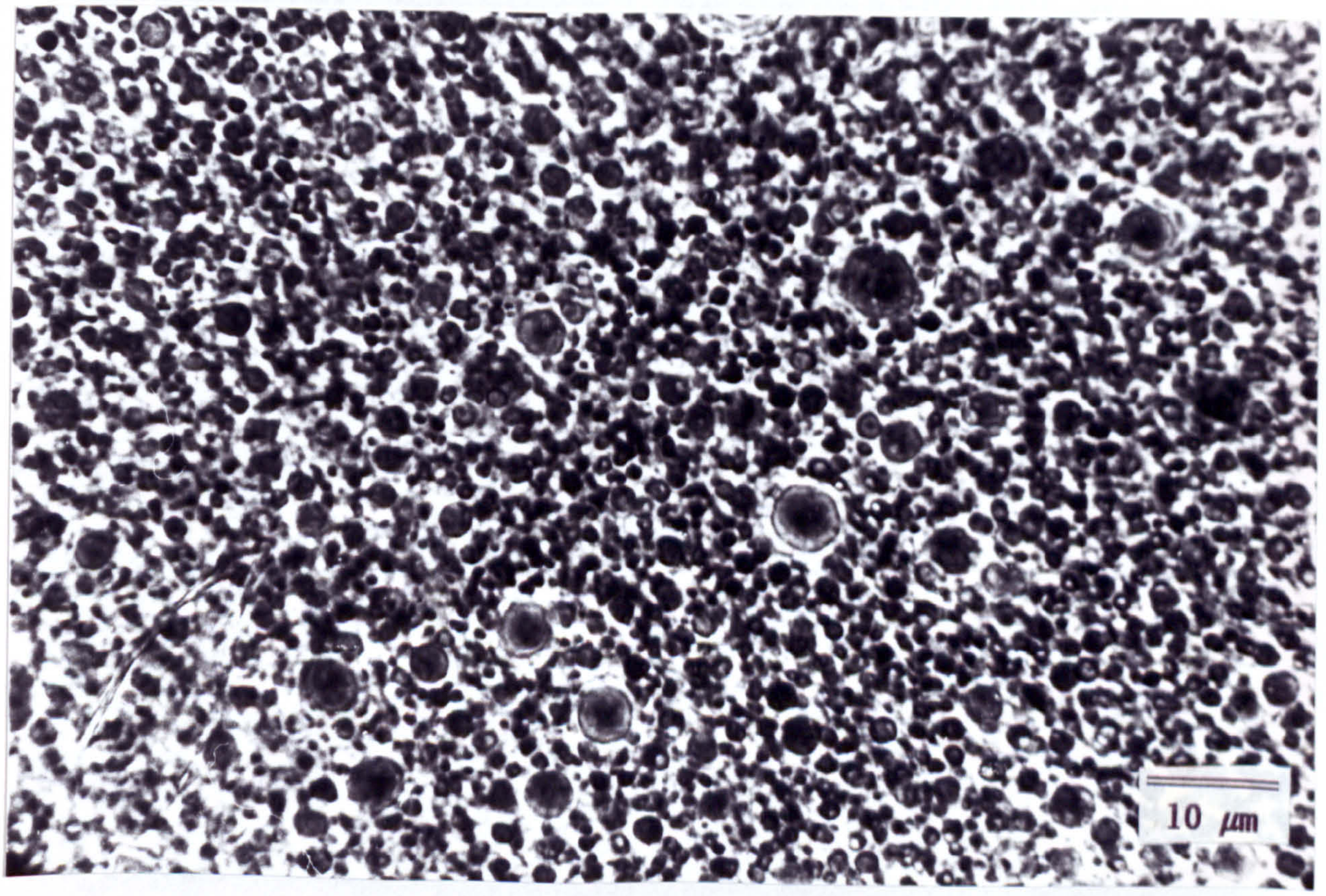

Figure 33 : 70wt% PP/26wt% PA6(B5)/4wt% PB3002 Phase Contrast

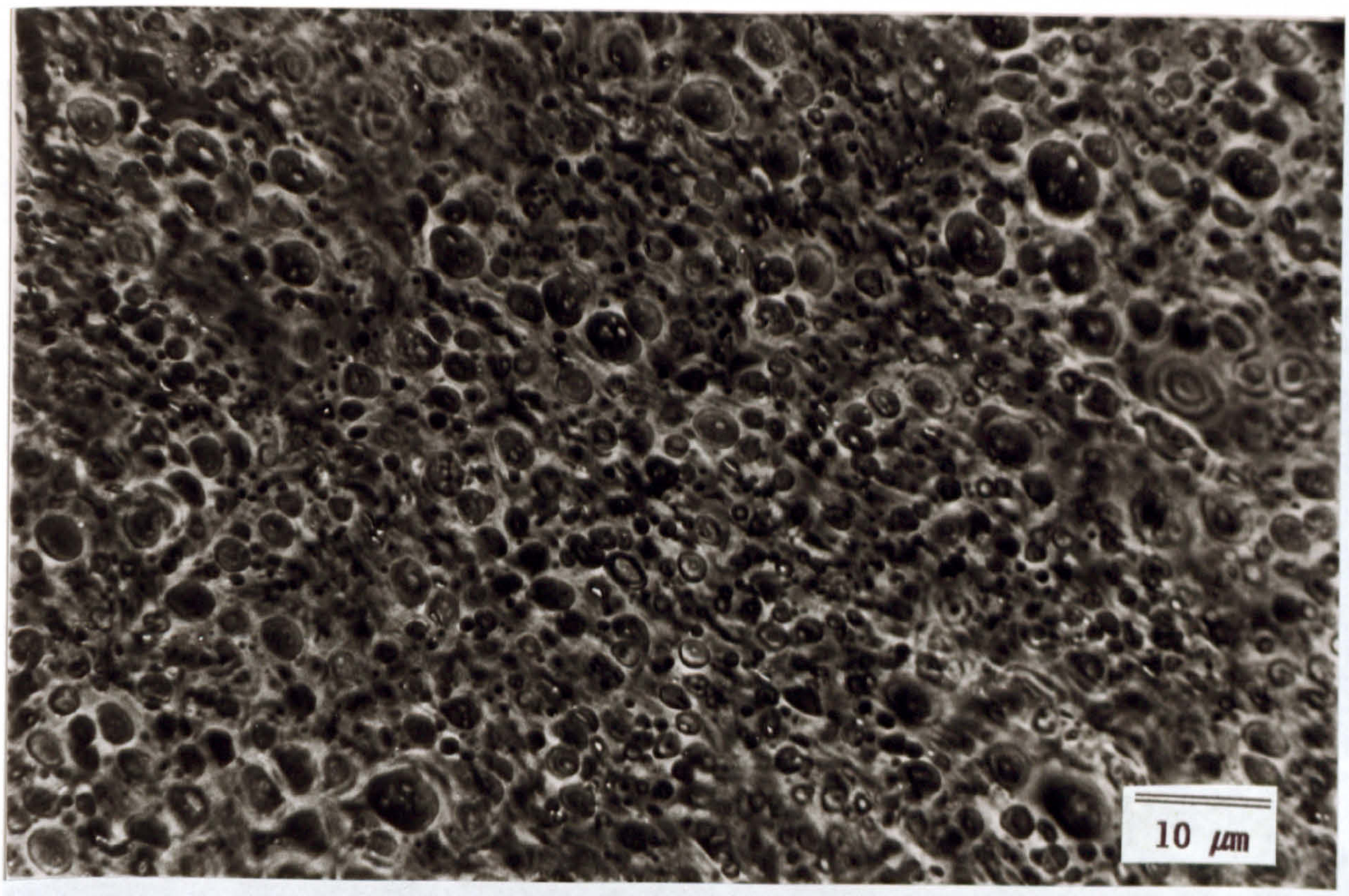

Figure 34 : 56wt% PA6(A23)/36wt% PP/8wt% PB1001 Phase Contrast

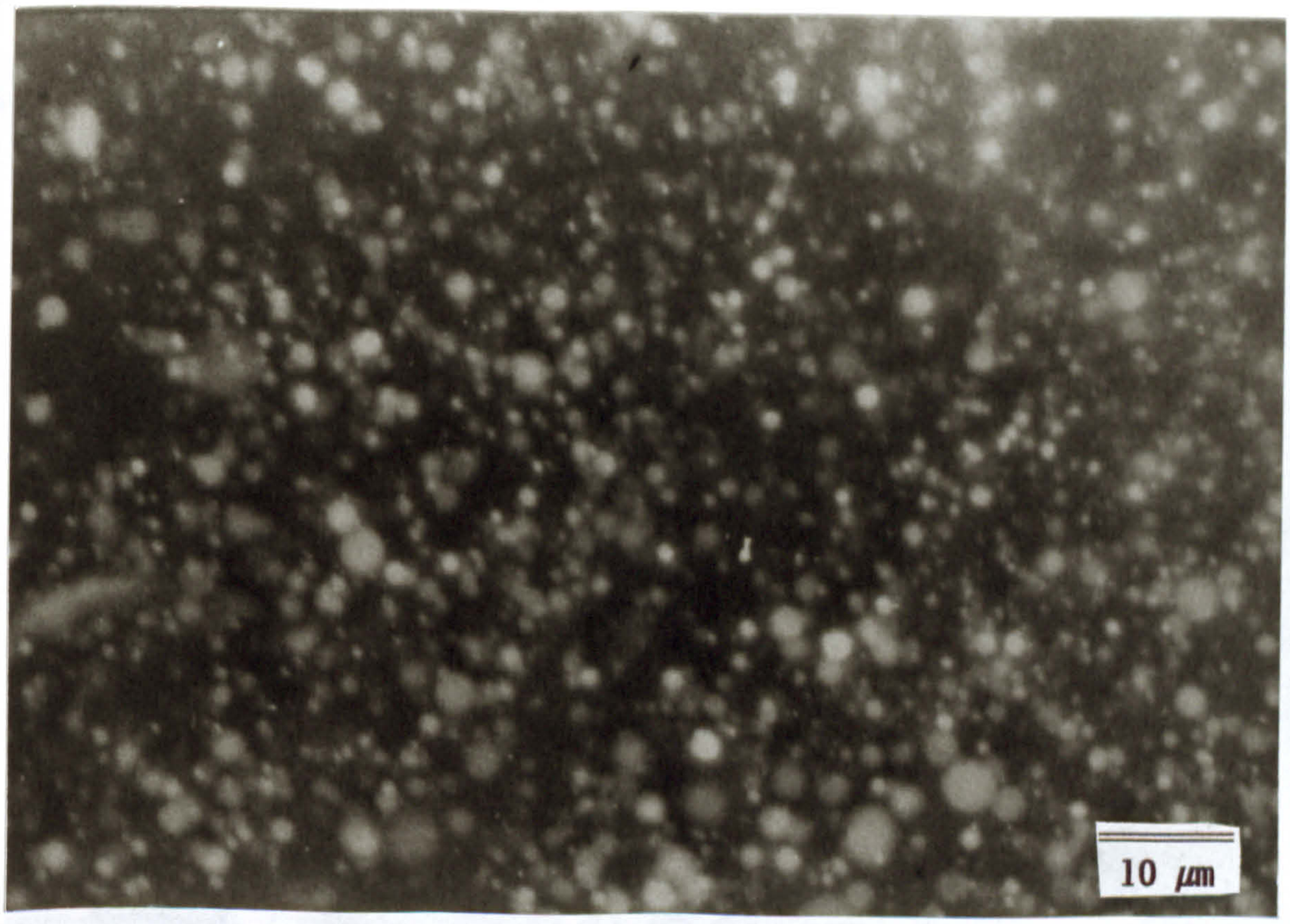

Figure 35 : 56wt% PA6(A23)/36wt% PP/8wt% PB1001 Fluorescence

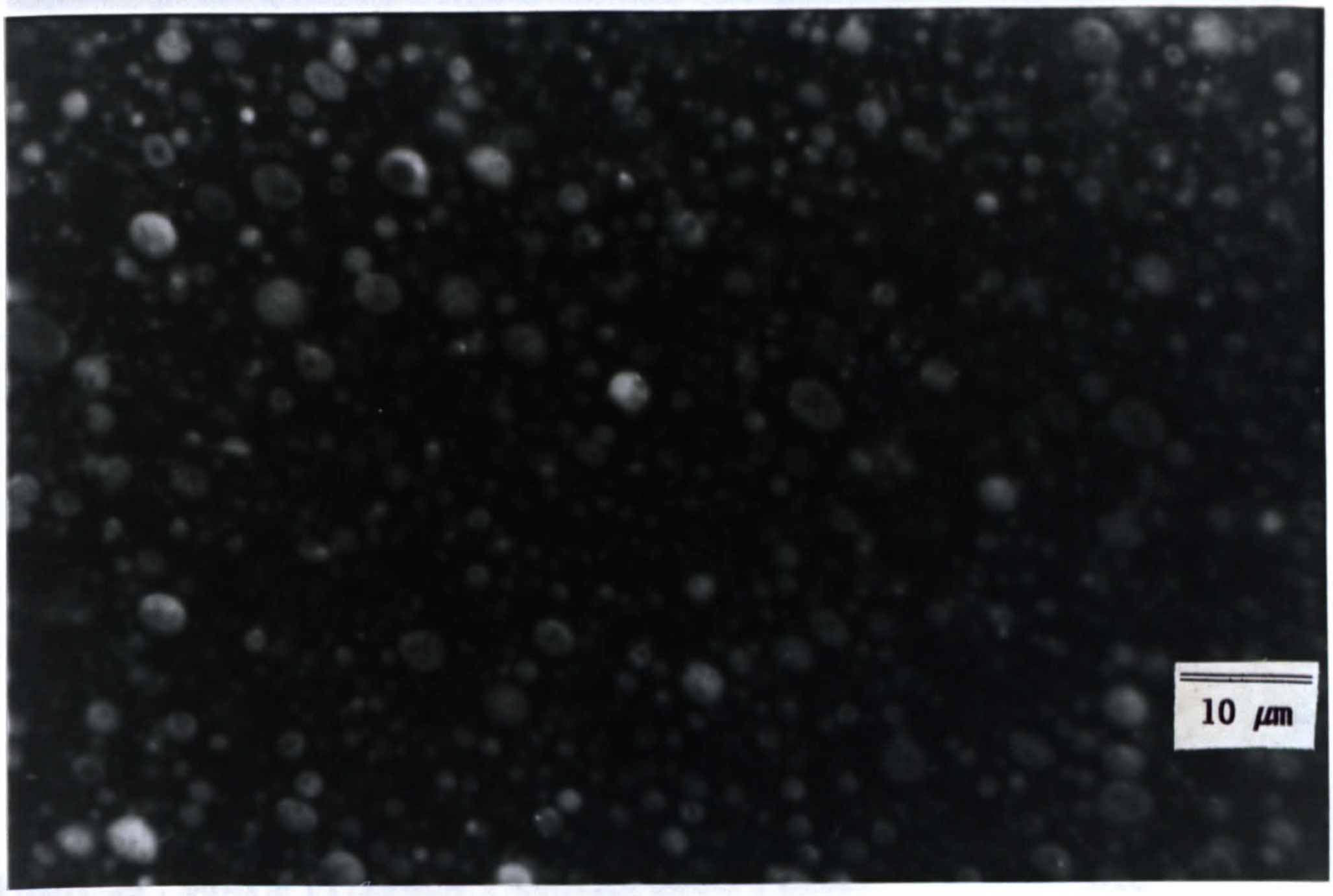

Figure 36 : 66wt% PP/26wt% PA6(A23)/8wt% BMAcoMAgPP Fluorescence

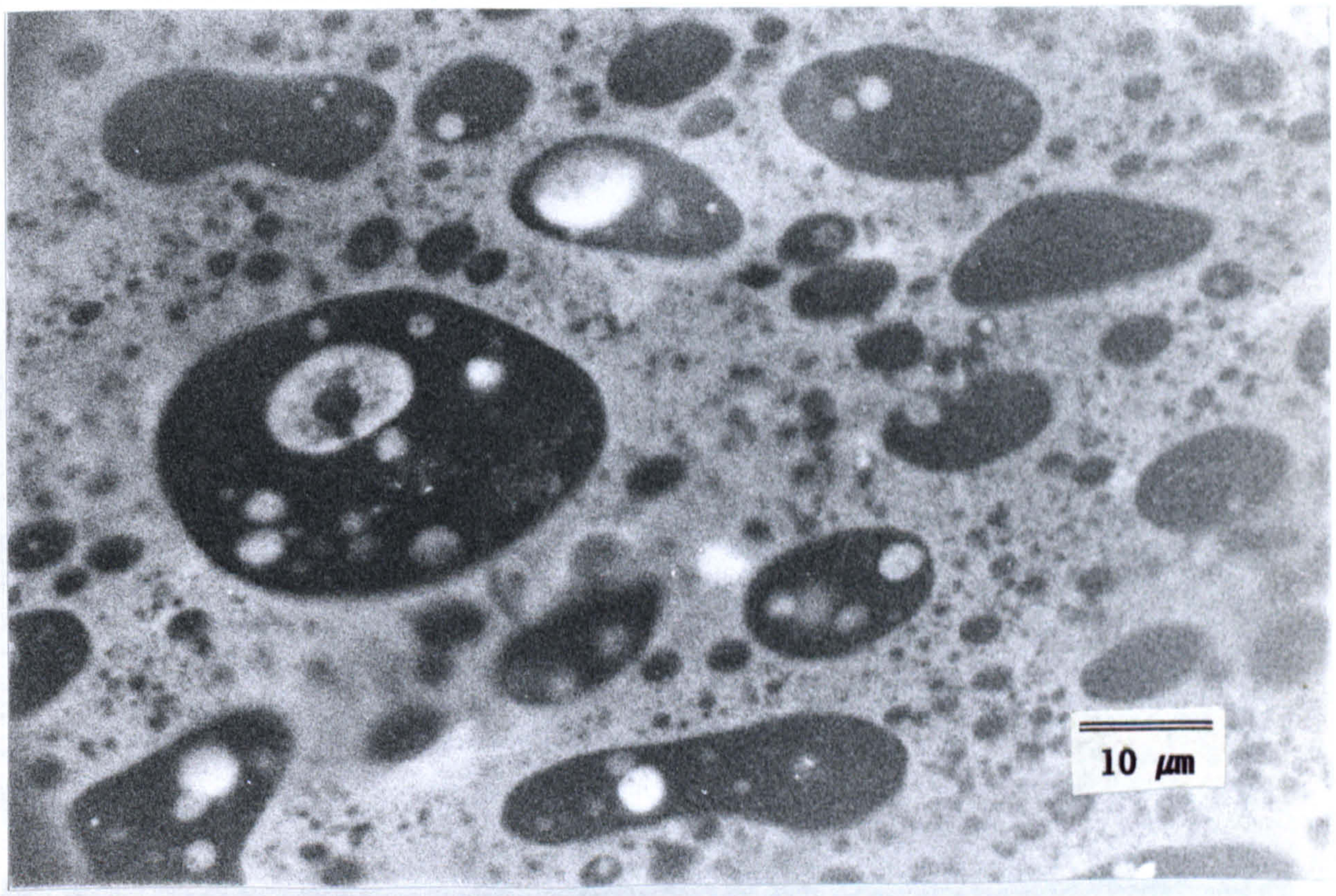

Figure 37 : 56wt% PA6(A23)/36wt% PP/8wt% (BMAcoMA)gPP Fluorescence

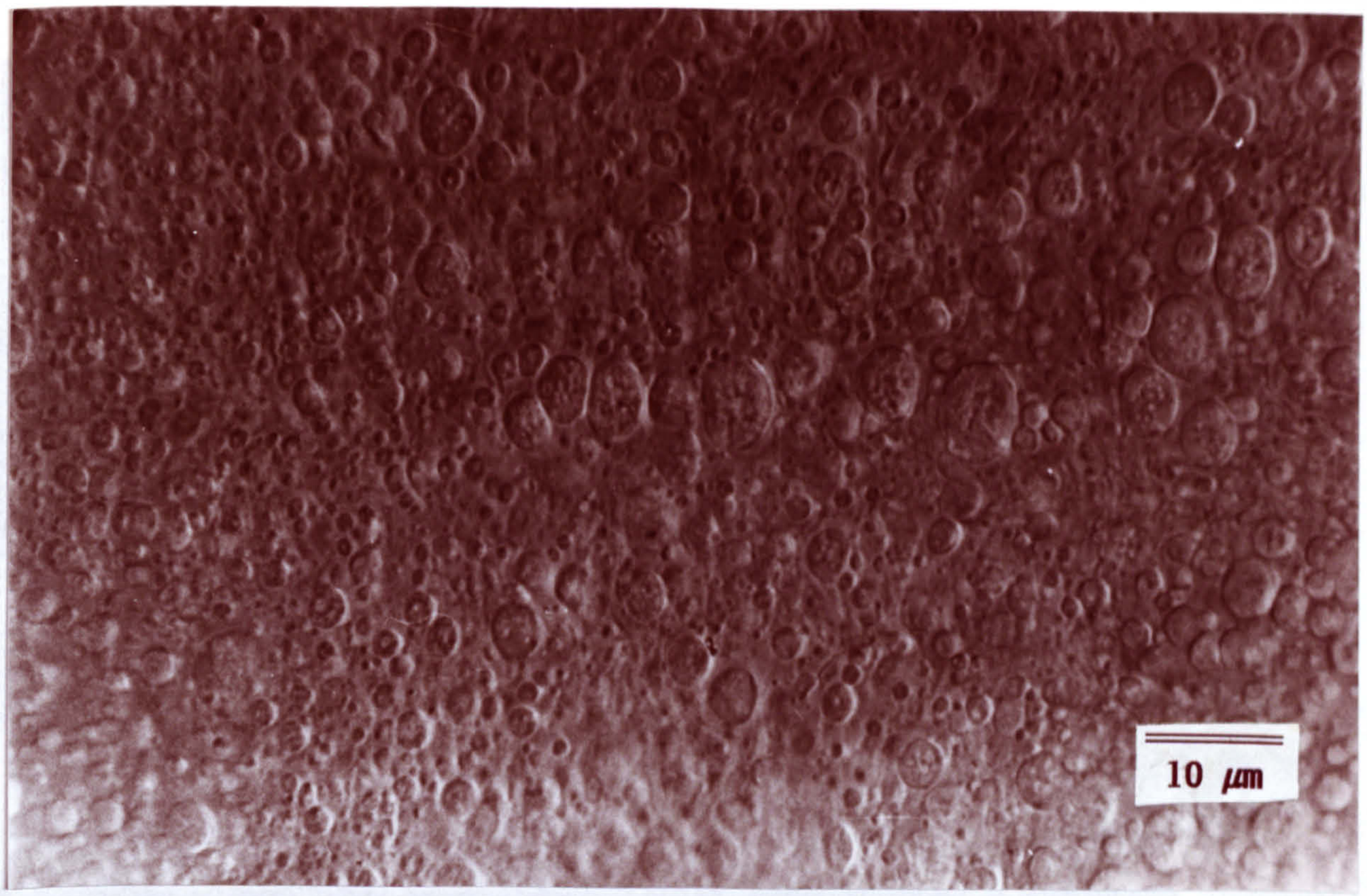

Figure 38 : 66wt% PP/26wt% PA6(A23)/8wt% PB1001 DIC

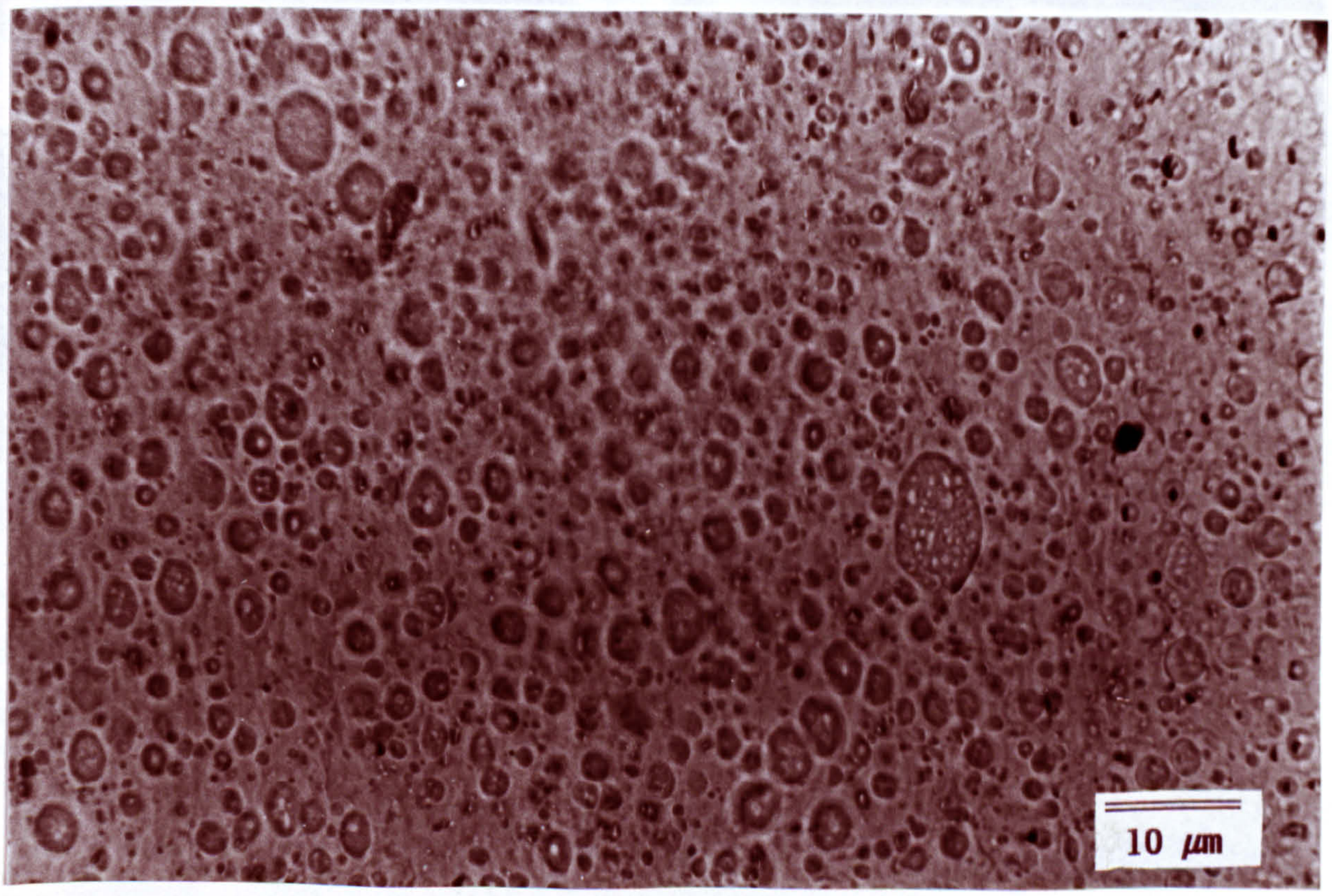

Figure 39 : 66wt% PP/26wt% A23/8wt% PB1001 Transmitted Light

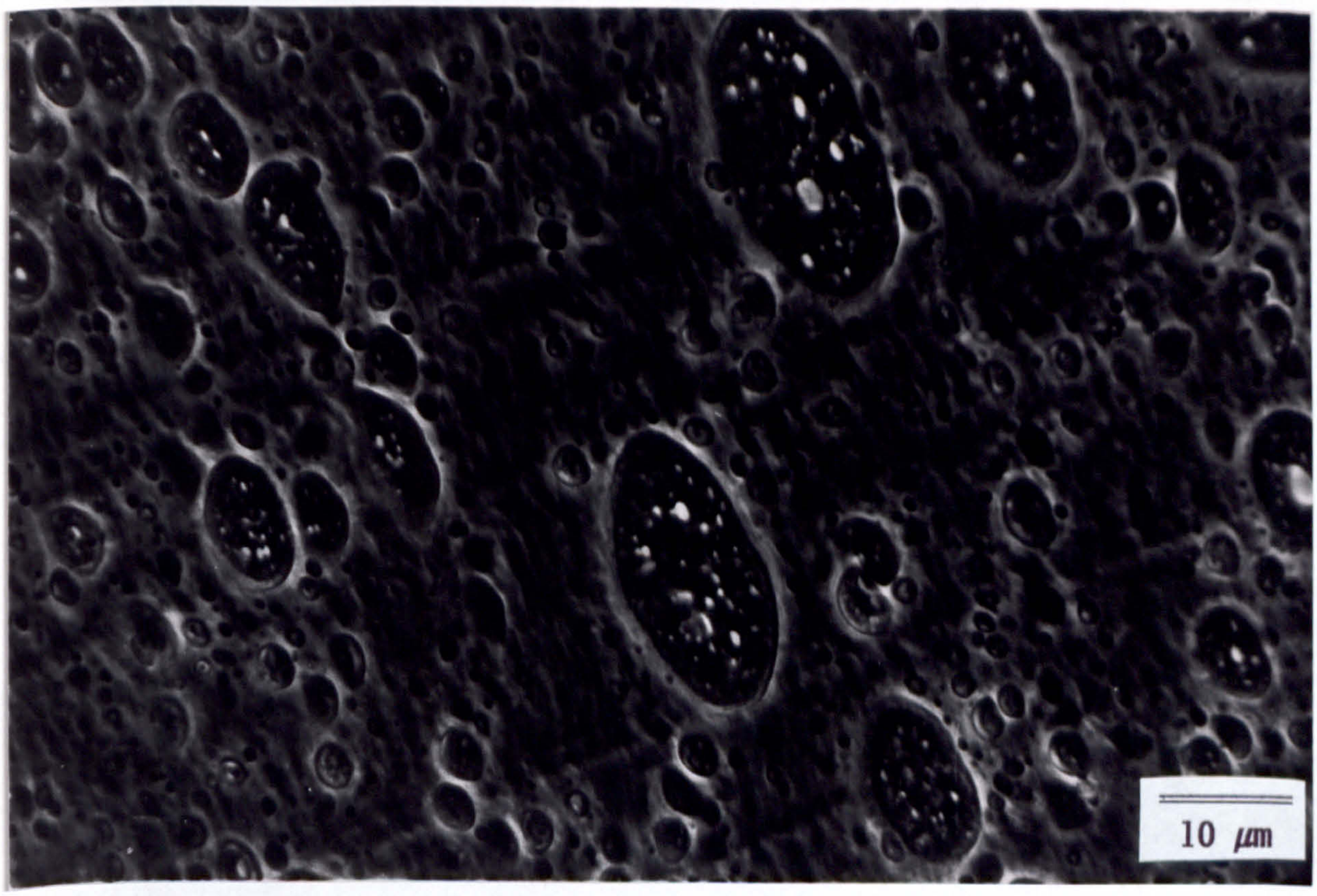

Figure 40 : 70wt% XLPP/30wt% PA6(B5) **Phase Contrast**

Figure 41 : 60wt% PA6(B5)/40wt% XLPP **DIC**

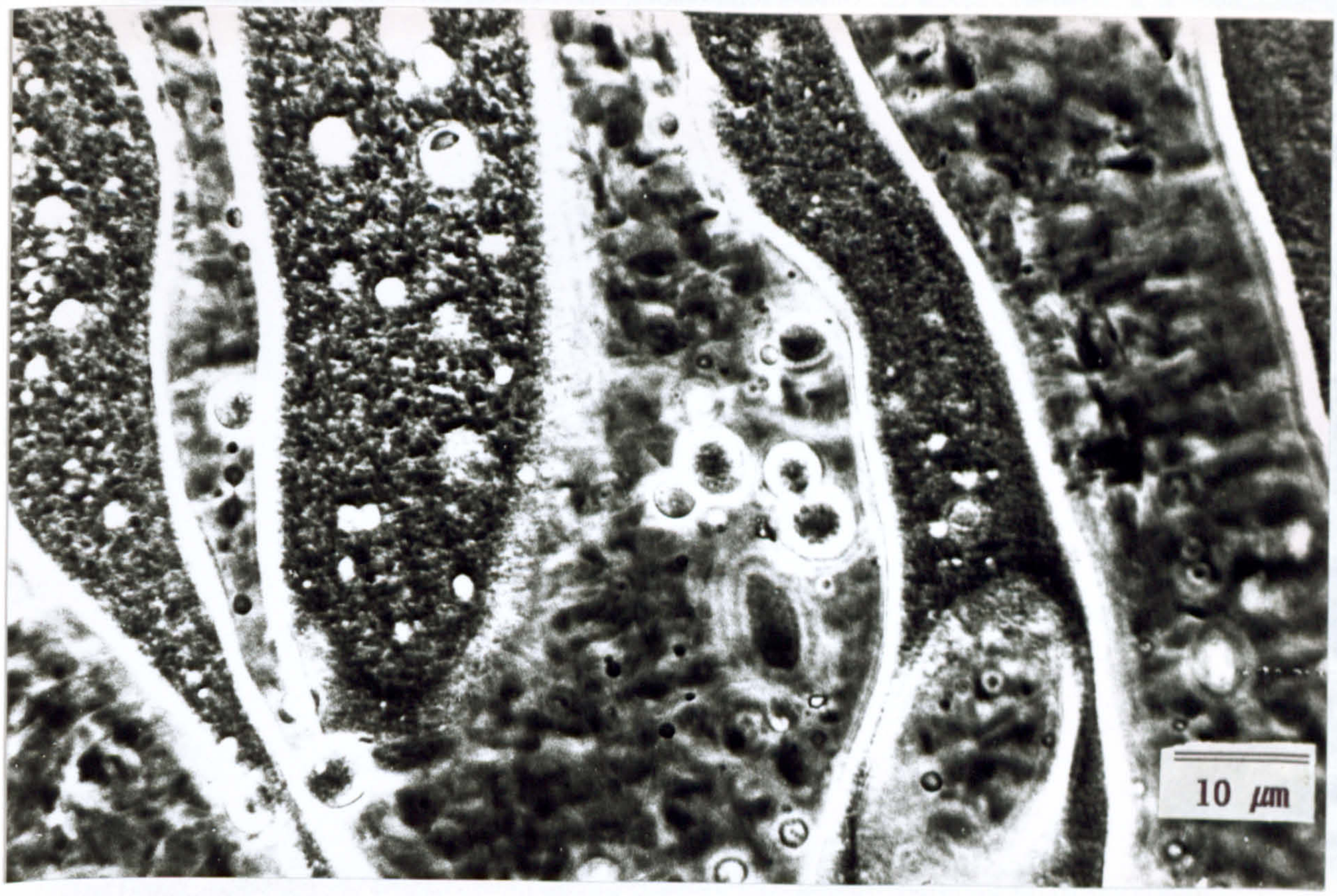

Figure 42 : 60wt% Plast.PA6(B5)/ 40wt% PP Phase Contrast

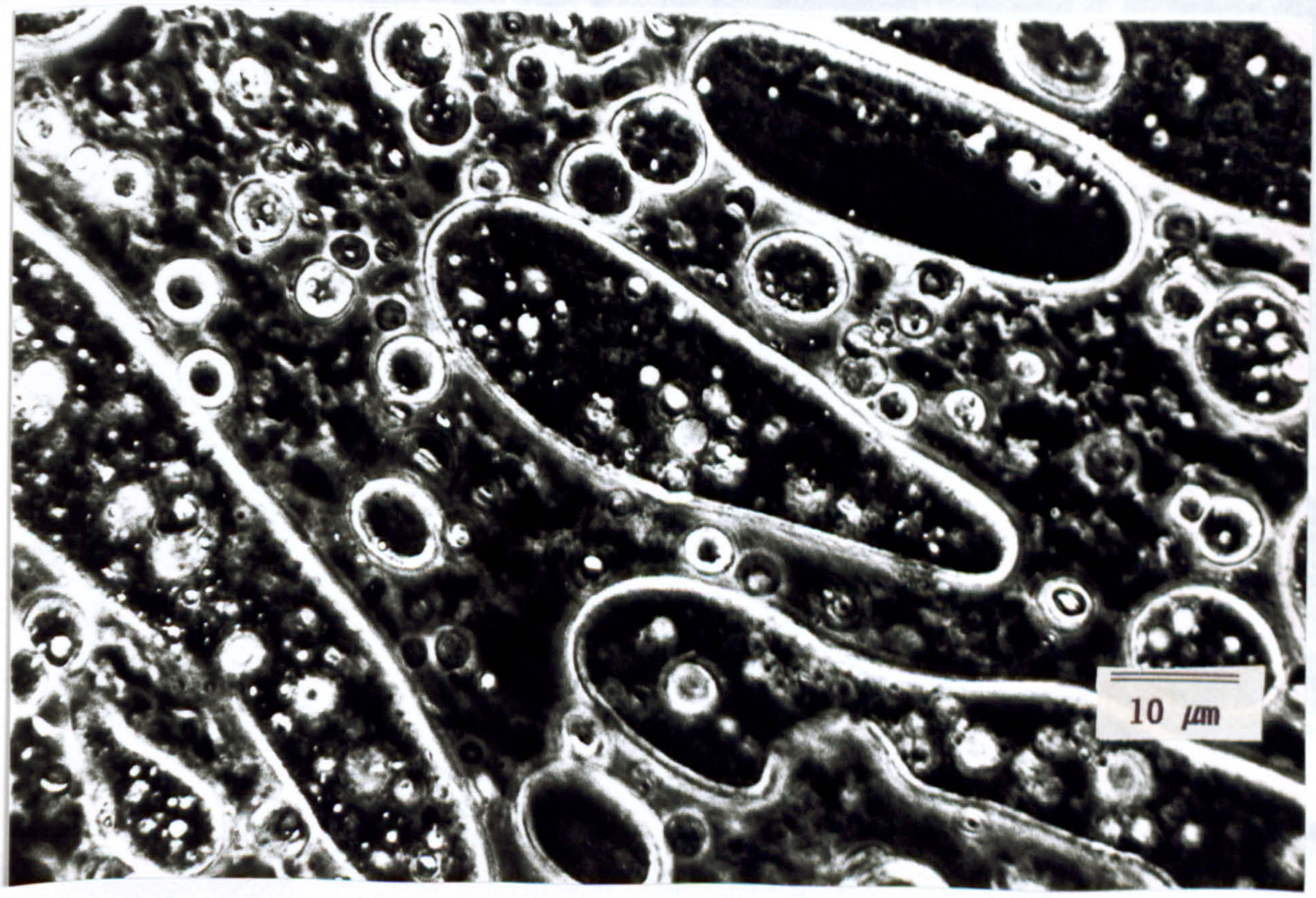

Figure 43 : 60wt% Plast.PA6(B5)/ 40wt% XLPP Phase Contrast

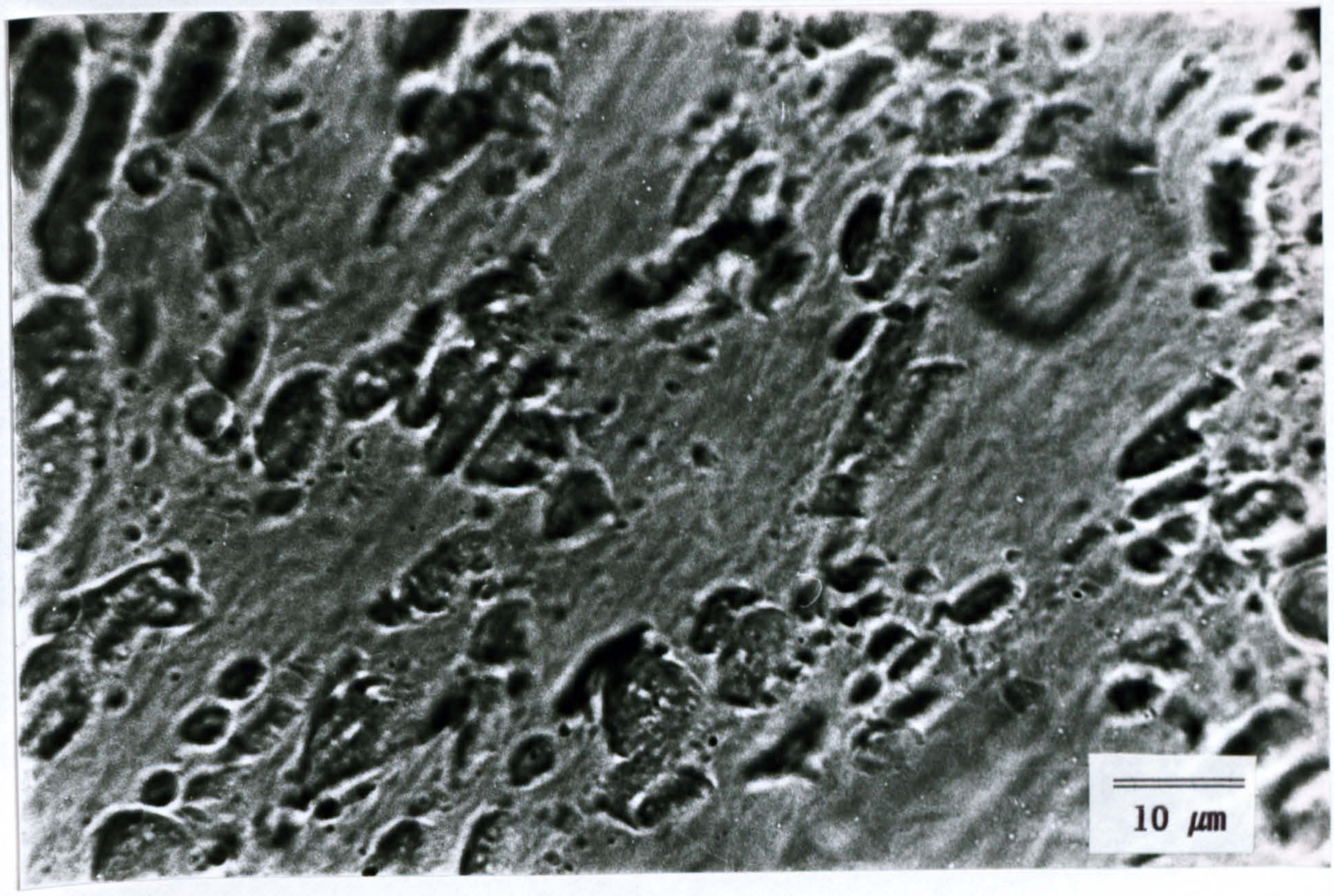

Figure 44 : 70wt% XLPP/30wt% Plast.PA6(B5) Phase Contrast

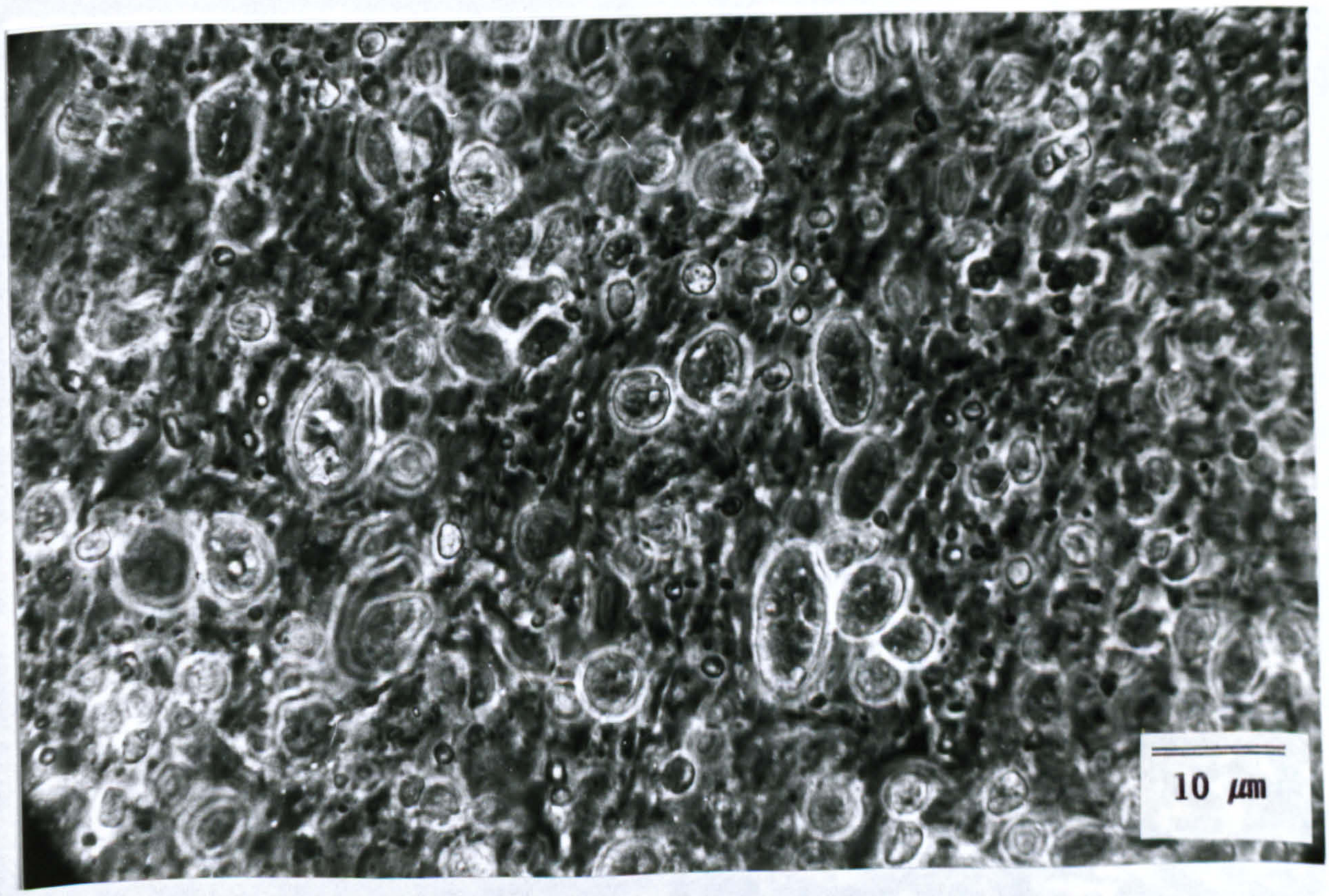

Figure 45 : 70wt% PP/30wt% Plast. PA6(B5) Phase Contrast

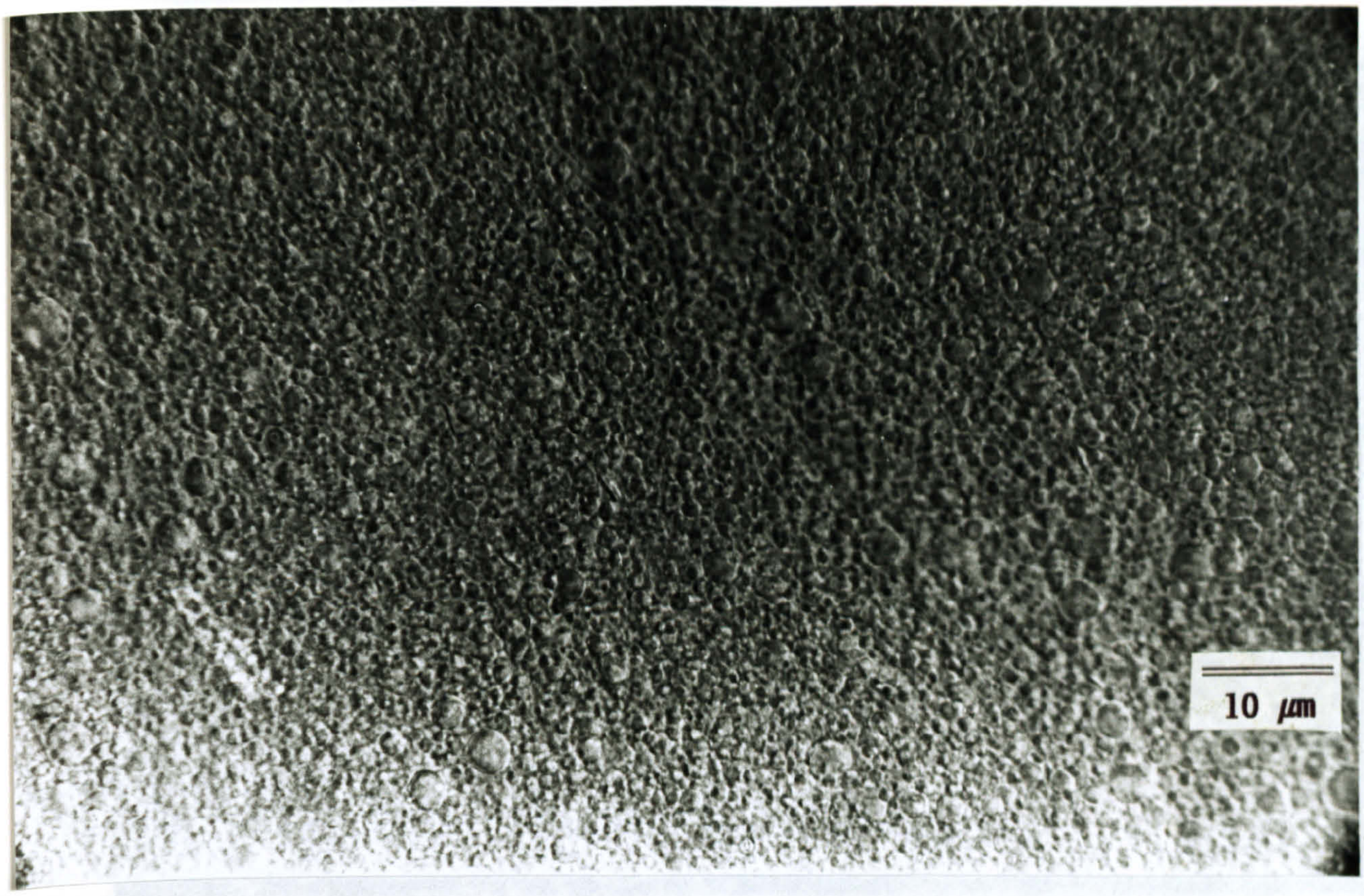

Figure 46 : 66wt%PP/26wt% PA6(A23)/8wt% (BMAcoMA)gPP DIC

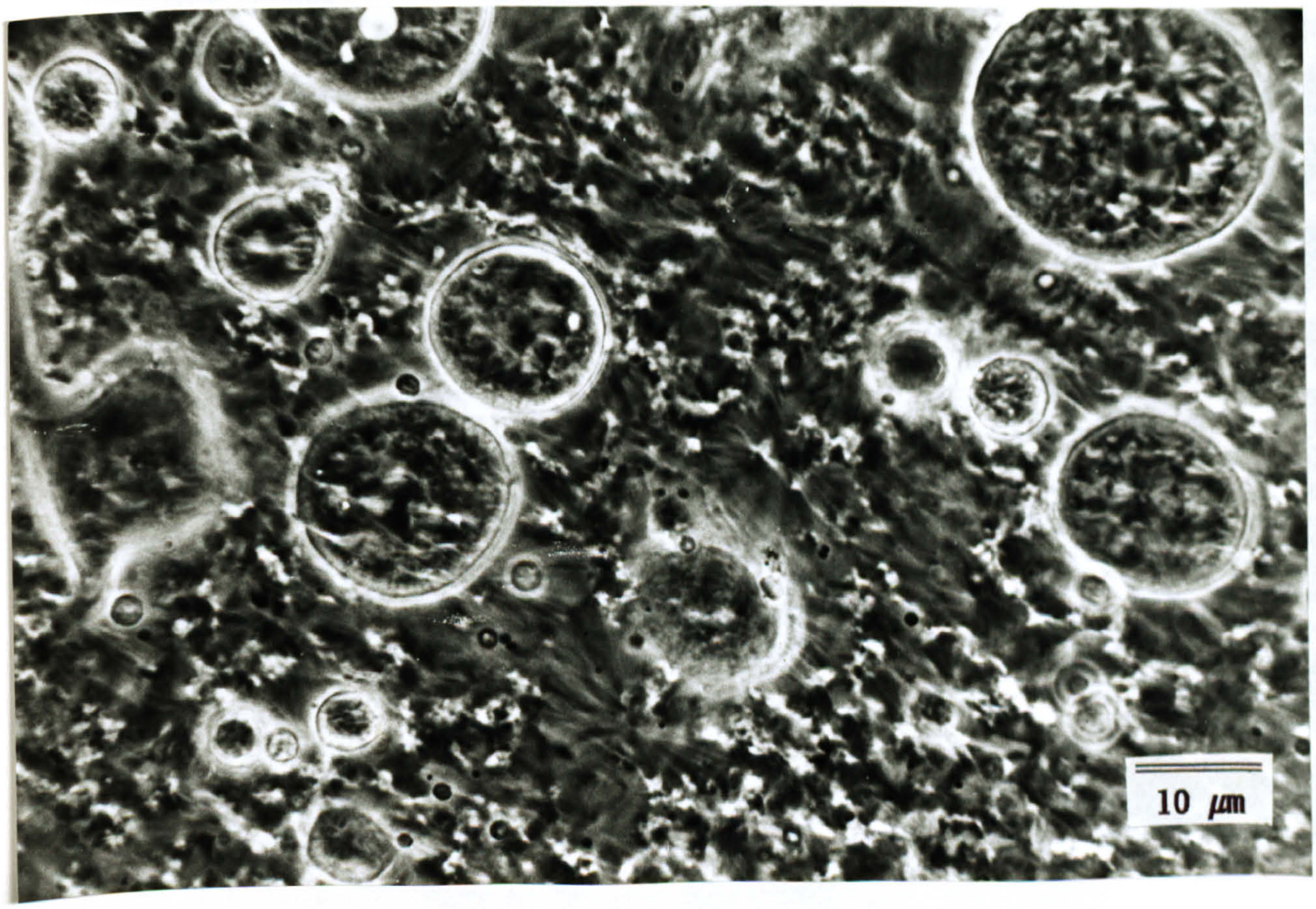

Figure 47 : 70wt% PP/26wt% PA6(B5)/4wt% BMAcoMAgPP Phase Contrast

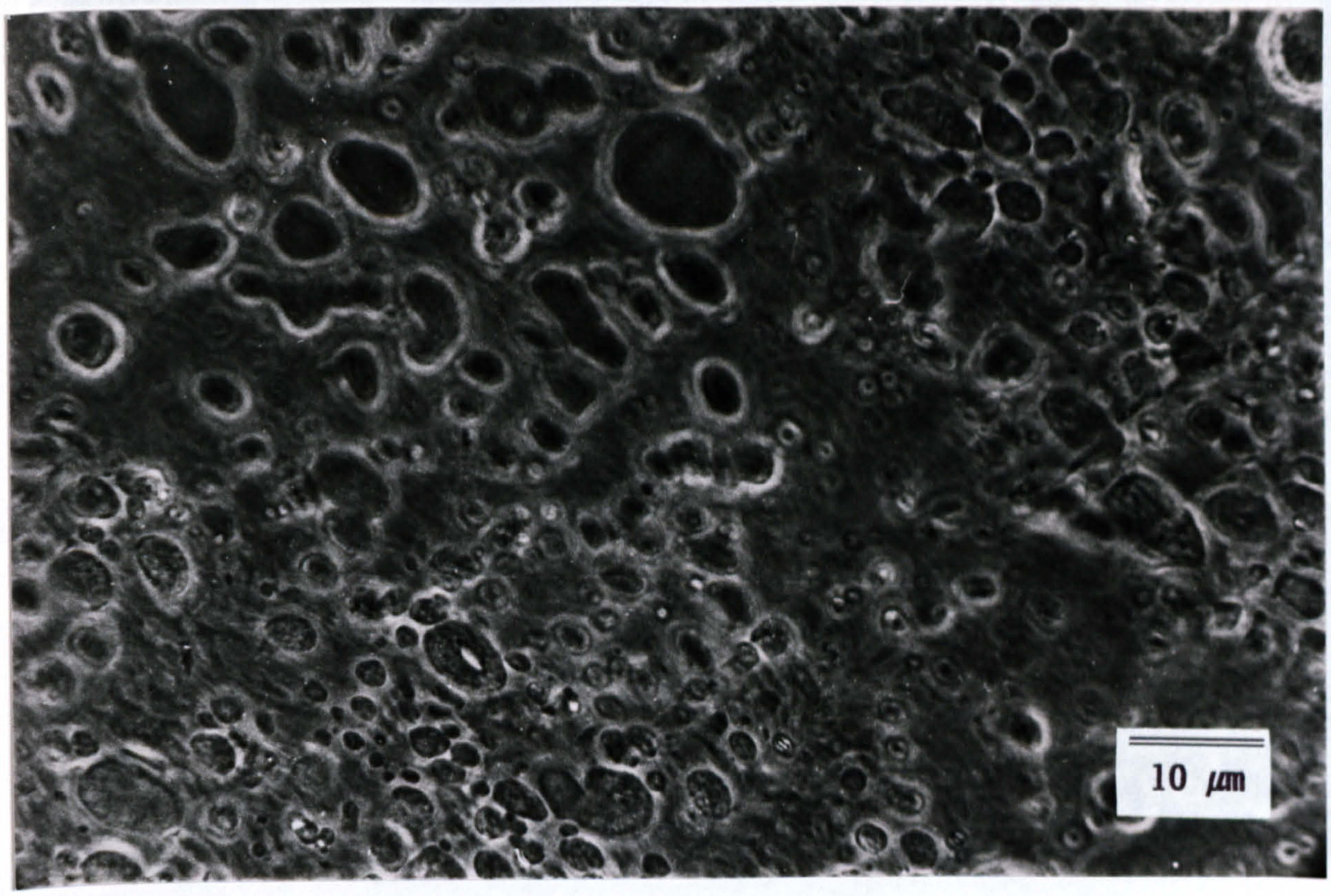

Figure 48 : 62wt% PP/30wt% PA6(B5)/8wt% BMAcoMAgPP Transmitted Light

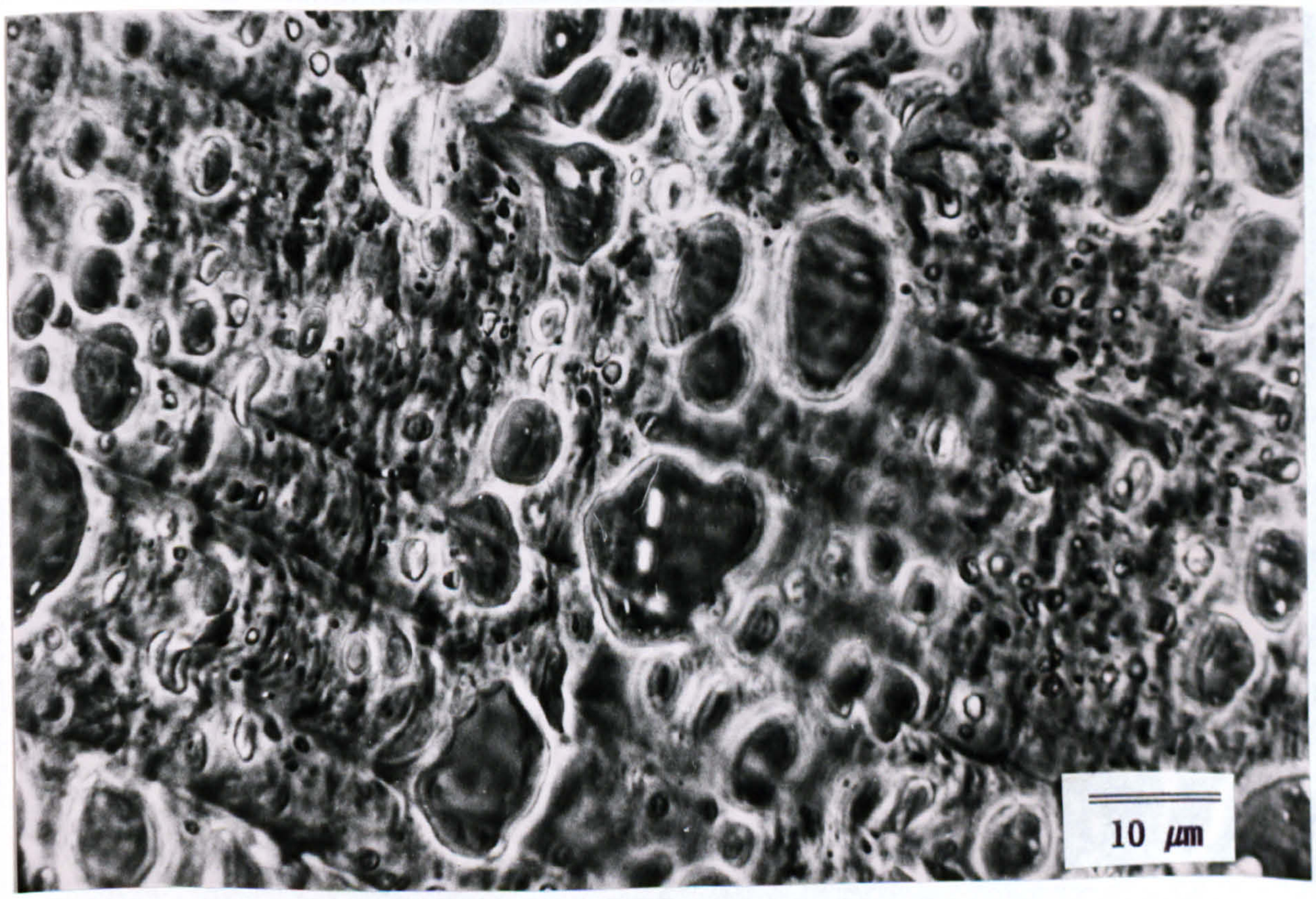

Figure 49 : 56wt% PA6(B5)/36wt% PP/8wt% BMAcoMAgPP Transmitted Light

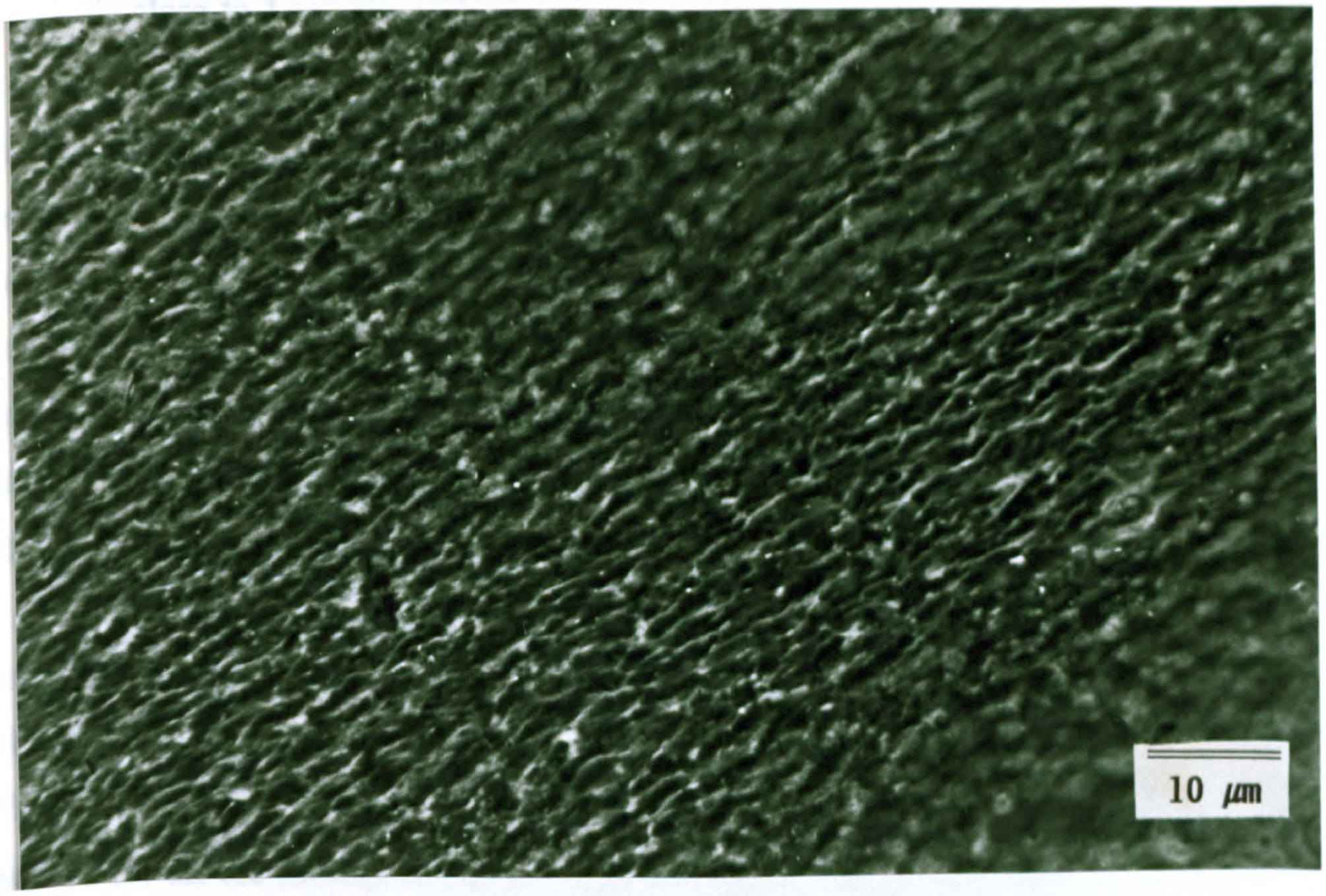

Figure 50 : 92wt% PP/8wt% MA-g-PP Phase Contrast

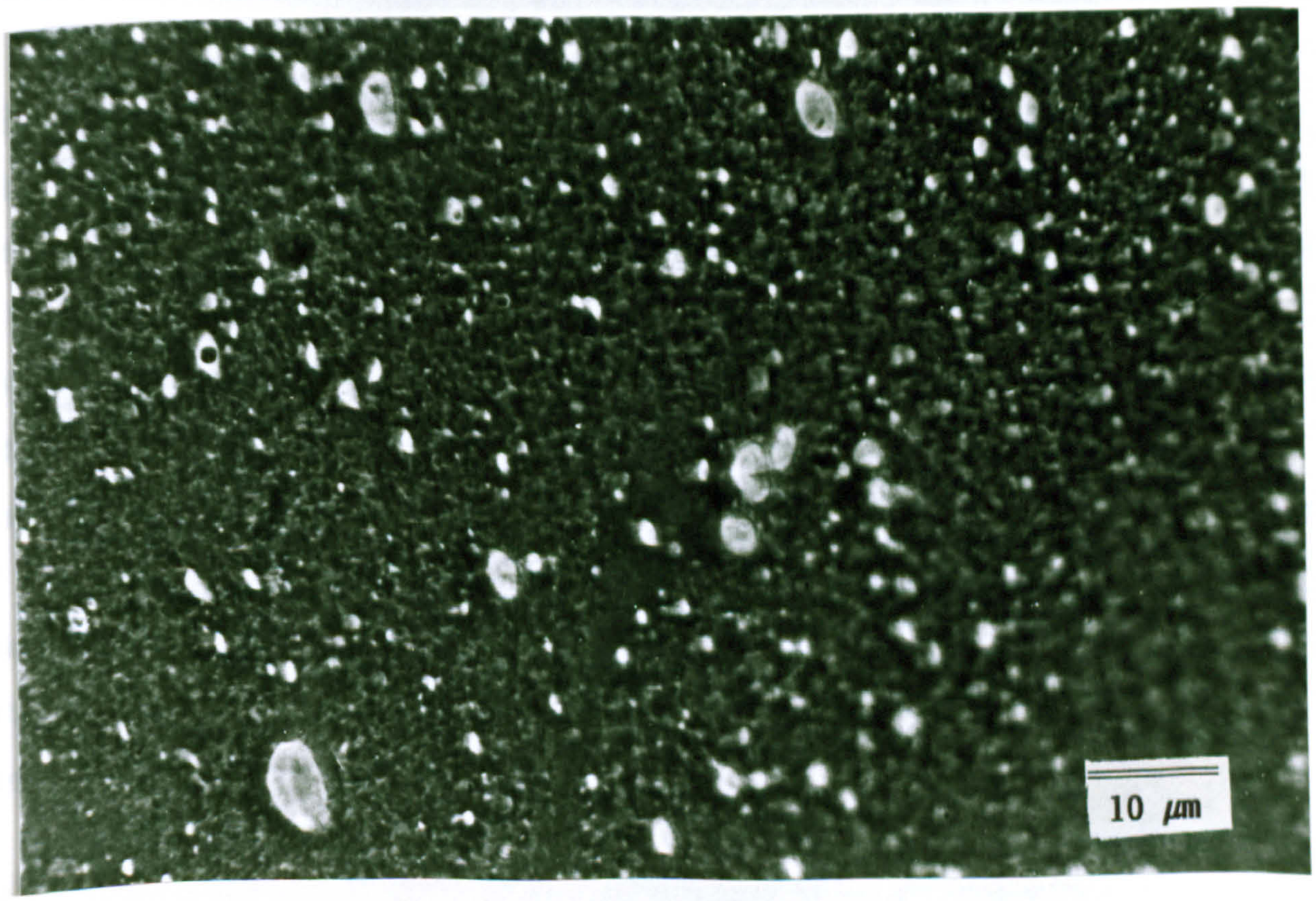

Figure 51 : 92wt% PA6(B5)/8wt% BMAcoMAgPP Phase Contrast

or smaller than 1, a smaller d results. For R6000, however, with the finest dispersion the ratio is close to 1.

The effect of reducing the dispersed phase size by increasing the compatibilizer concentration can be seen in Figures 47 and 48, where the microstructure of the 4wt% material has a coarser dispersed phase size than the binary 70wt% PP/30wt% PA6(B5) material. However, upon increasing the compatibilizer concentration from 4-8wt% the dispersed phase size has reduced from 3.4 μm to 2.3 μm. With the same compatibilizer concentration, but with an increase of B5 concentration to 56wt%, Figure 49, the dispersed phase size has increased to 2.8 μm.

For binary blends of homopolymers and compatibilizers, (Figures 50 and 51) show typically that phase separation occurs for the PA6/compatibilizer systems but not for the PP/compatibilizer blends, where a homogenous structure results. This behaviour has been observed for all the homopolymer/8wt% compatibilizer systems prepared.

The calculation of **d** for the phase-in-phase behaviour blends, is based only on the smaller particle diameters, not showing co-continuity, as described in Section 2a.

4.3.2 Phase-in-phase behaviour

Another commonly observed feature of this work was the phase-in-phase behaviour observed in both the binary and ternary PP/PA6 systems, and is a difficult phenomenon to explain but has been reported elsewhere[16]. It occurs in materials where the dispersed phase contains inclusions of the matrix and is a statistical result of during the initial blending period, minority dispersed phase A being dispersed in majority matrix phase B. Then as further blending takes place, particles of B are broken off at the interface, some of which will rejoin the matrix whilst a minority will be encapsulated in the still relatively large particles of A. Within a short time, equilibrium is attained and the relatively large A particle size will be reduced. If however, the mixing is poor, due to immiscibility, then the phase-in-phase structures will remain.

4.3.3 Binary Blend Microstructure Summary

The phase dispersion has been improved for the PP matrix blends and for the 60wt% B5 binary blends, a similar phase dispersion to that of injection molded R6000 was achieved, which has been shown by fluorescence LM to have a B5 matrix. R6000 is coarsened by injection molding since the phases are not in equilibrium. The adjustment of the component viscosities has therefore not affected the phase dispersion significantly.

4.4 Interfacial Modification

4.4.1 Compatibilizer effects

The effect of each compatibilizer on the phase dispersion is discussed in Section 4.3.1. To summarize, the most successful compatibilizer for reducing the dispersed phase size of B5 blends was found to be PB3002, due to having a viscosity closer to that of B5, despite having a low level of MA grafting, as published by BP (3wt%), and from FTIR spectroscopy. MA-g-PP was little inferior for the same blends and was shown to contain greater MA functionality, 1.5wt% compared to < 1 wt%, which was probably due to a mixture of grafted and unreacted MA. This conclusion was made because MA-g-PP when blended with both PA6's reduced both their complex viscosities, whereas the other compatibilizers increased the complex viscosities. For the A23 blends, BMAcoMAgPP was found to be the most successful compatibilizer for reducing the dispersed phase, due not only to having a similar viscosity to A23 but having double the functionality of PB1001, but a lower level of grafting, 3wt% as compared to 5wt%. It is likely that the compatibilizer affinity for and solubility in PP, as shown from LM, puts the compatibilizer at the interface, instead of the bulk, where the reactivity is more useful, due to low concentration. It is however difficult to separate the effect of the compatibilizer on the phase dispersion from that of the interfacial tension. Compatibilization has therefore been successful in reducing the dispersed phase size close to that of processed R6000, even though R6000 contains more compatibilizer. The material is probably compounded by reactive extrusion, in which ϵ-caprolactam monomer is polymerised with PP and the compatibilizer in a twin screw extruder.

4.4.2 Surface Tension and Contact Angle measurements

In the absence of high pressure and temperature equipment for measuring melt interfacial tension, surface tension determinations were conducted, using the method described in Section 3a.7. The values obtained are close to those quoted literature values. The published value of τ (surface tension) for PP is 29.4 mN/m[17] and for PA6 is 43[18], both at 20 °C. By using different solvents, which incidentally were also used for measuring barrier properties, it was thought that the surface energy could be calculated and related to the interfacial tension. The standard methods for estimating the interfacial tension between molten polymers are, the sessile drop, the pendant drop, and the spinning drop methods. The last shows the most applicability to polymers, since the time to reach equilibrium is reached more quickly this way[19]. However, even for this latter method, high temperature/high pressure equipment is required.

Table 6 : Surface Tension Determinations

Polymer	*Surface Tension, τ mN/m*			*Contact Angle °*		
	with H_2O	with Methanol	with Xylene	with H_2O	with Methanol	with Xylene
PP	37.89	21.17	26.72	55.93	38.29	22.70
XLPP(2 wt% A174 Silanes)	34.52	24.14	22.85	59.33	39.26	28.50
PA6(B5)	44.87	23.46	26.99	49.81	30.27	16.87
PA6(A23)	48.23	23.51	25.87	46.26	34.16	22.49
Orgalloy R6000	32.64	23.26	26.11	61.63	43.67	21.81

Theoretical approaches such as that of Rotenbureg, Borukva, and Neumann[20], use the sessile and pendant drop models. Because the extrapolation of surface tensions of melts to room temperature leads to reliable values for solid polymers, the surface tension of solid polymers may be calculated from the parachor per structural unit, by applying the equation :

$$\tau = (P_s / Vg)^4 \text{ ---------- [62]}$$

The parachor, P_s is calculated from tables of group contributions for each of the atoms, bonds (double, single, triple, rings, etc.), and methylene groups[21]. The group molar

volume V_g is calculated from the density, ϱ_g and single unit molar mass, M, and only the amorphous state has to be used, since semi-crystalline polymers usually have amorphous surfaces, when prepared by cooling from the melt. The average value for PP from the above table, from the three solvents, is 28.6 and that calculated from equ'n.[62] is 32.5. The average value for PA6(B5) from the above table is 31.8 and that from equ'n.[62] for PA6 is 47, whilst the average value from the above table for PA6(A23) is 32.5.

To summarise, the contact angle and surface tension data produced could not be correlated with the melt interfacial tension of the blend components or the observed phase dispersions, although as discussed in section 4.8.1, the surface tension can be related to the thermal expansion coefficient of polymers through equ'n.[70].

4.5 FTIR Spectroscopy

4.5.1 Homopolymer FTIR Spectroscopy peak assignment

The infrared (IR) spectra is often used[22]for comparison of characteristic absorption bands in the IR spectrum, which can lead to identification of the bonds and functional groups present in the polymer. Poly(amides) are usually characterised by the 3302 cm^{-1} band, due to the NH stretching vibration of the secondary amide[23]: the 1642 cm^{-1} band due to the carbonyl stretching frequency; and the 1545 cm^{-1} band[24], due to the NH deformation vibration[25]. IR band assignment for PA6, not covered[23-25] in Table 7, includes the broad shoulder observed in some PA6 samples in the region 3440-3560 cm^{-1}, attributed to bound amorphous phase water OH. The amide II band, which involves coupling of NH deformation with CN stretching, occurs at $\approx$ 1545 cm^{-1} is sometimes known as the CNH waveband, involving the N and H moving in opposite directions to the C.

Grilon A23 has a relatively lower molecular mass than B5 (Section 3a.2), hence, not surprisingly, by similar arguments, the NH stretch H-bonded band occurs at a higher frequency of 3299 cm^{-1}, as compared to that of B5 at 3302 cm^{-1}. Similar shift in the same band was also observed by Ismat[23], between PA6 and PA6/iodine complex samples. The CH_2 asymmetric and symmetric stretch bands also occur at higher waveband for B5 as compared to A23, again indicating increasing molecular mass. Also included in Table 7 are characteristic wavebands for PP.

The CH_2 deformation bands produce two B5 and three A23 absorptions but the CH_2 scissoring absorptions are absent from both materials. It is likely that the higher molecular weight and melt viscosity of B5 results from molecules having to assume a more "zig-zag" type chain contraction conformation, which would result in "bridges" being made between the carbonyl group and the amide group, in the neighbouring distort sheet. These bridges have a tendency to disrupt hydrogen bonding and possibly account for the deformation bands. Matsubara et al[26] also made similar assumptions for the zig-zag type chain contraction of molecules in order to accommodate the large I_3 ion present in the PA6/iodine complex.

4.5.2 Blend FTIR Spectroscopy

4.5.2.1 Introduction

The application of IR spectroscopy in characterisation of immiscible polymer blends is extensive. FTIR spectroscopy is used not only to study hydrogen bonding but also identification of the specific interaction mechanism in polymer blends. Generally, these interactions can affect the -OH absorption region (3500-3600 cm^{-1}) and the C=O stretching (1737 cm^{-1}), the CH_2 symmetric stretching (2886 cm^{-1}) as well as the finger-printing frequency region (1300-650 cm^{-1}), and others[27]. For example, shifts to a lower wave number (higher frequency) of the hydrogen bonded NH stretch band in the blends could indicate a lowering of molecular mass, as compared to the PA6 materials.

4.5.2.2 Binary Blends

The FTIR spectra of the homopolymers used in this work are shown in Figure 52, and the FTIR spectra of Orgalloy R6000, 60wt%B5/ 40wt%PP, and 70wt% PP/30wt% B5 blends are shown in Figure 53. Figure 54 shows binary blend FTIR spectra of 60wt% A23/40wt% PP and 70wt% PP/30wt% A23. Spectra of the following materials were also obtained, Orgalloy R6000 after exposure to Acetic Acid for 6.5 hours, BMAcoMAgPP, Poly(ButylMethacrylate), MAgPP, PB3002, PB1001, in addition to spectra of all the blends and cross-linked material produced during this research. As discussed in Section 3a.9, the R6000 was exposed to glacial (saturated aqueous) acetic acid for 6.5 hours to establish whether or not the PA6 phase could be dissolved by the acid, in a similar fashion to the homologous series formic acid. The results were inconclusive.

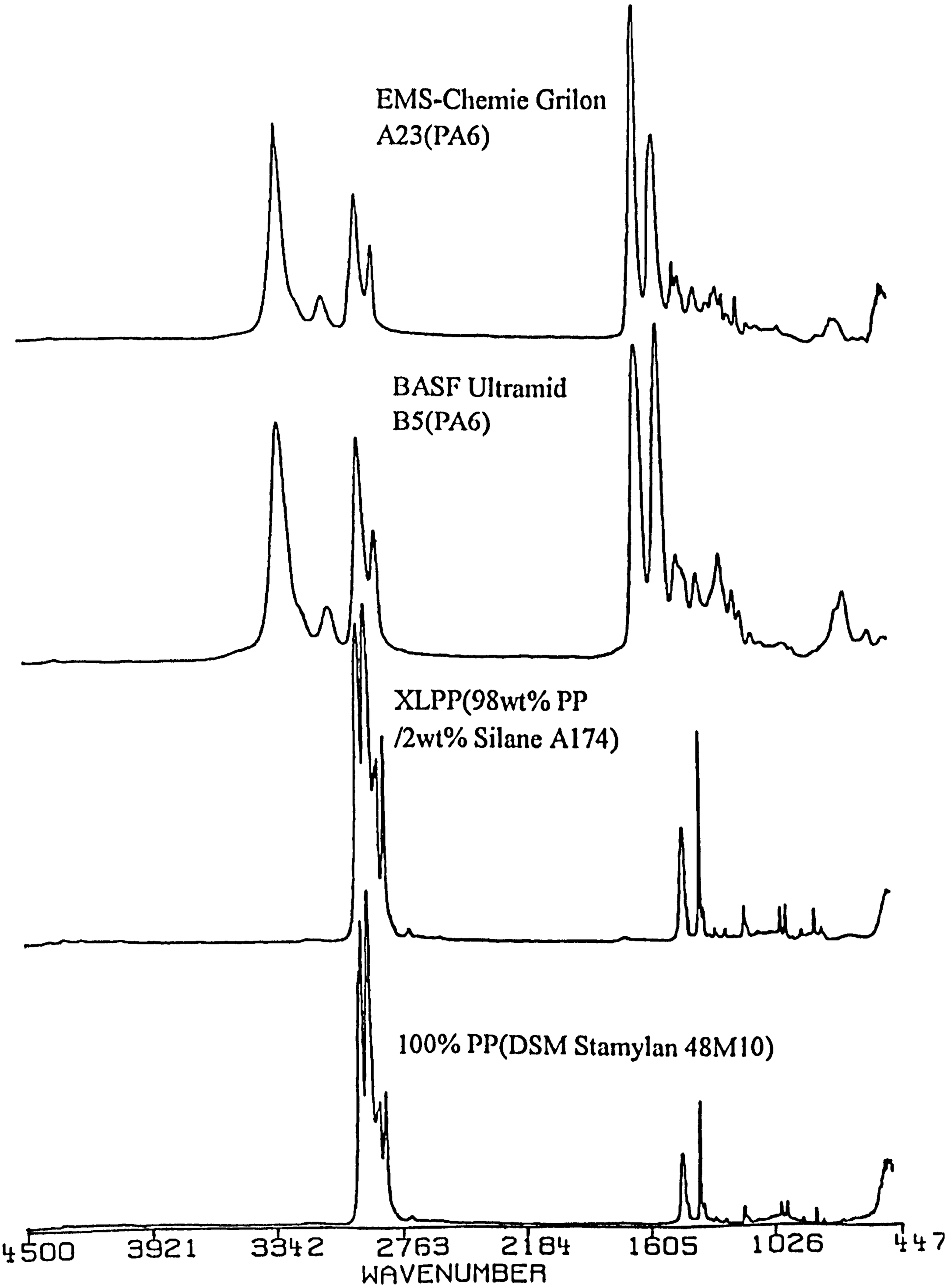

Figure 52 : FTIR spectra of blend homopolymers

Table 7 : FTIR waveband assignment for homopolymers

Band Assignment cm^{-1}	*Ultramid B5*	*Plast. B5*	*Grilon A23*	*PP Stamylan 48M10*	*XLPP(2 wt% A174 Silane)*	*Literature Reference*
NH str. H-bonded	3302	3298	3299	———	———	3302[23]
-CONH- trans.mono subst.amide (shoulder of above)	3188	3207	3204	———	———	3220[26]
NH str.non H-bonded o/t amide II	3079	3077	3092	———	———	3080[28]
CH_3 symm. str.	———	———	———	2840	2839	2873[29]
CH_3 asym. str.	———	———	———	2960/ 2951	2954	2965[25]
CH_2 asym.str. (aliphatic)	2936	2937	2933	2919	2919	2940[24]
CH_2 symm.str. (aliphatic)	2864	2866	2857	2867	2867	2865[23]
amide I C=O	1649	1637	1641/ 1646	———	1721 α,ß-unsat. aliph. esters	1642[23] 1730-1705 [30]
CNH def.(N/H move opp. rel. to C)	1546	1541	1552	———	———	1545[23]
CH_2 scissor.	absent	absent	absent	1481	1478	1480[23]
CH_2 def. " " " " " "	1462 1441 1421 1372	1462 1439 1419 1370	1463 1437 1416 1368	1329[29] (range 1160-1390) 1304 1296 1256 1220	1457 1437 1429	1465[23] 1438 1417 1390[32]
CNH def.(N/H atoms move same rel. to C)	1237 (shoulder)	1238	1235	———	———	≈ 1250 (w) [27]

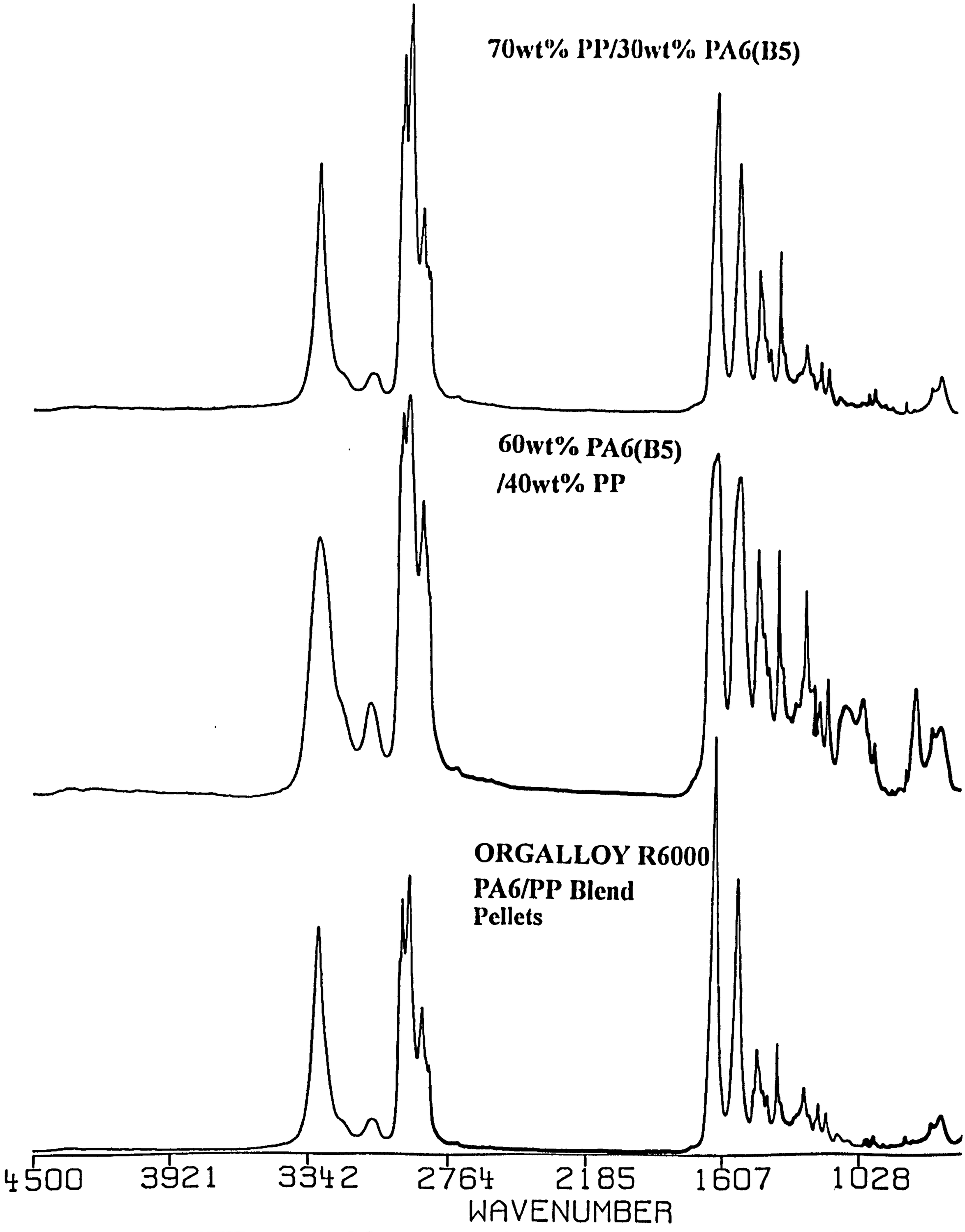

Figure 53 : FTIR spectra of Orgalloy R6000, 60wt% PA6(B5)/40wt% PP, and 70wt%PP/30wt% PA6(B5) blends

Table 8 : Peak Assignments for binary PP/PA6 blends and Orgalloy R6000

Band Assignments cm^{-1}	Orgalloy R6000 Pellets	Orgalloy R6000 Injection Molded	90wt% B5/ 10wt% PP	80wt% B5/ 20wt% PP	70wt% B5/ 30wt% PP	60wt% B5/ 40wt% PP	30wt% B5/70wt% PP	15wt% B5/85wt% PP	5wt% B5/ 95wt% PP	60wt% Plast. B5/ 40wt% PP	30wt% Plast.B5/ 70wt% PP	60wt% Plast. B5/ 40wt% XLPP	30wt% Plast. B5/ 70wt% XLPP	60 wt% B5/ 40wt% XLPP	30wt% B5/ 70wt% XLPP	60wt% A23/ 40wt% PP	30wt% A23/ 70wt% PP
NH str. H-bonded	3300	3300	3300	3298	3300	3298	3298	3296	3295	3302	3295	3297	3296	3298	3295	3304	3294
CH_3 symm. str.	2841	2839	——— ———	2841	2939	2935	2926	2840	2839	2946	2843	2848	2841	2850	2845	2836	2840
CH_3 asym. str.	2954	2949	2958	2955	2954	2959	2955	2954	2955	2959	2958	2949	2954	2953	2953	2945	2953
CH_2 asym. str.	2920	2921	2930	2922	2923	2935	2920	2919	2919	2930	2918	2926	2921	2922	2917	2931	2925
CH_2 symm. str.	2867	2866	2860	2865	2865	2868	2863	2868	2867	2866	2868	2868	2868	2868	2866	2865	2867
CH_2 def.	1462 1437 1416	1462 1437 1421	1462 1437 1418	1462 1437 1419	1462 1437 1416	1462 1437 1419	1462 1437 1419	1460 1434 1416	1457 1434 1419	1462 1434 1419	1462 1432 1416	1462 1434 1416	1462 1437 1416	1462 1442 1419	1462 1437 1419	1462 1437 1416	1462 1437 1416
Olefinic CH_2 str.	2876	2876	——— ———	——— ———	2876	2963	2867	2878	2878	2876	2875	2874	2876	2874	2877	—— —	2876
C=O str. amide I	1638	1642 and 1718 (C=O str. from α,ß-unsat. aliph. esters)	1642	1633	1636	1638	1638	1638	1644	1638	1637	1639	1638	1641	1638	1642	1636
CNH(N/H move opposite rel. to C)amide II	1545	1542	1548	1541	1547	1547	1545	1543	1539	1546	1540	1544	1544	1544	1546	1545	1539
CNH(N/H move same rel.to C)amide II	1240	1239	1237	1237	1237	1241	1240	1239	1233	1240	1239	1265	1240	1242	1239	1240	1238

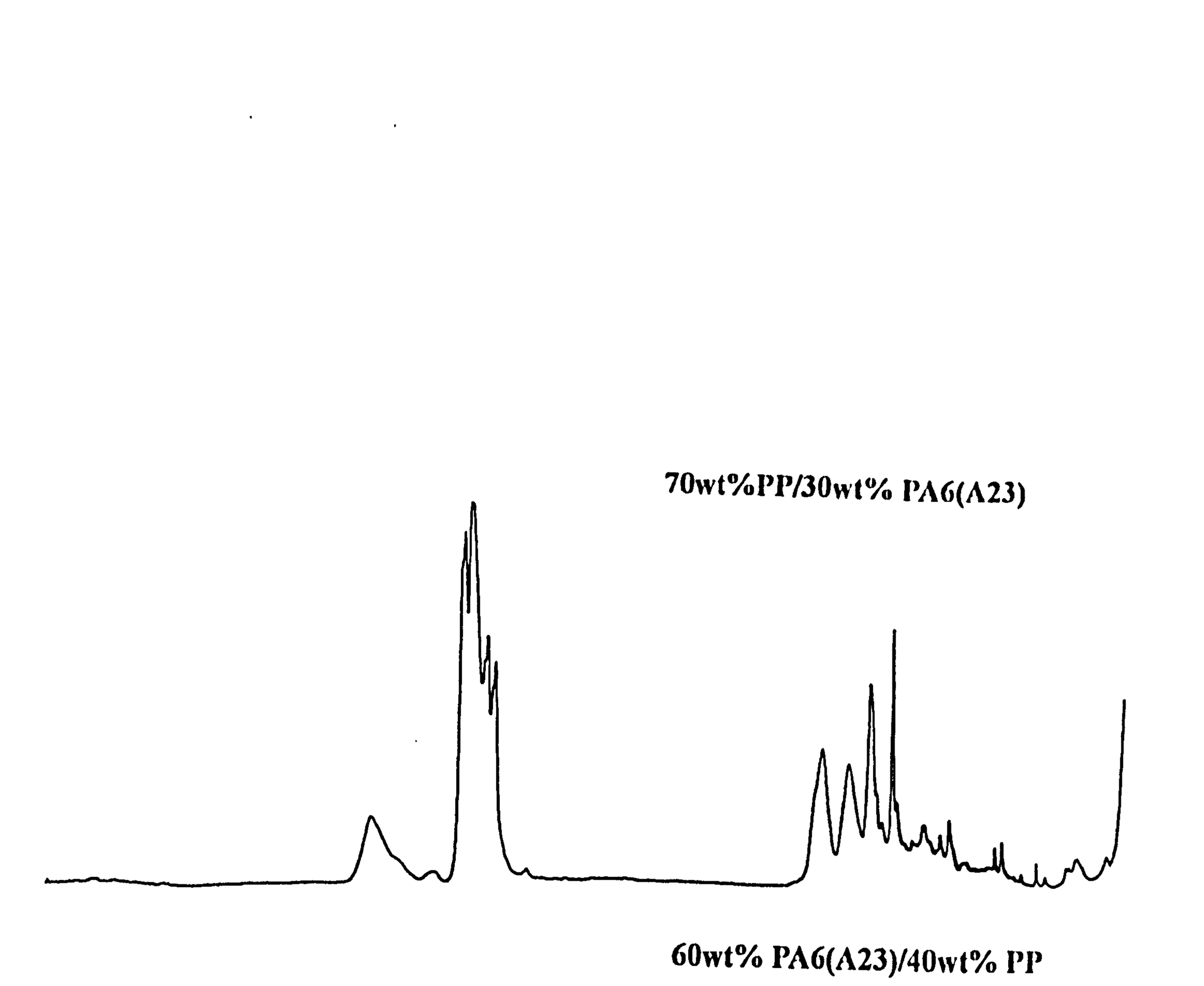

Figure 54 : FTIR spectra of binary PA6(A23)/PP blends

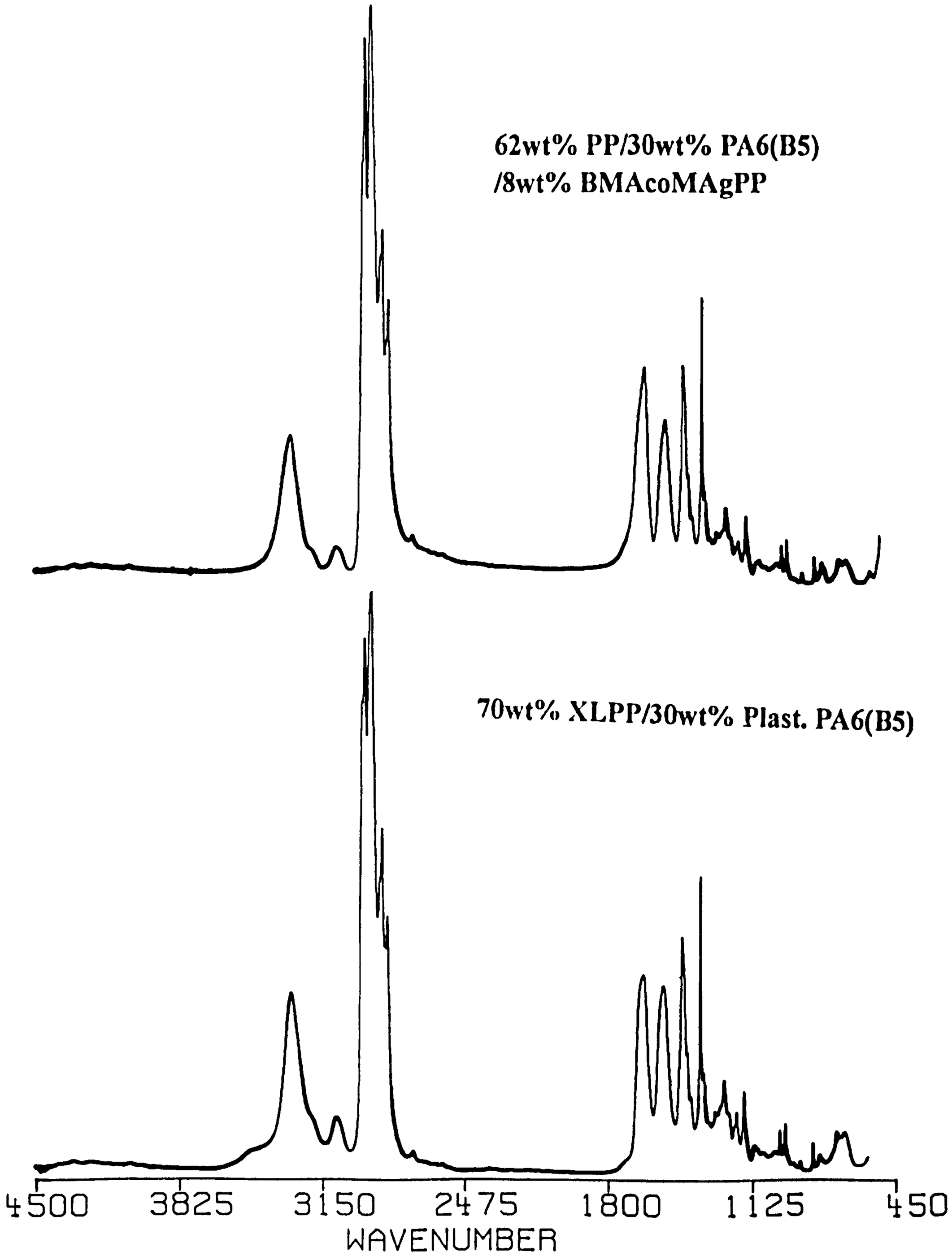

Figure 55 : FTIR spectra of 70wt% XLPP/30wt% Plast.PA6(B5) and 62wt%PP/30wt% PA6(B5)/8wt% BMAcoMAgPP blends

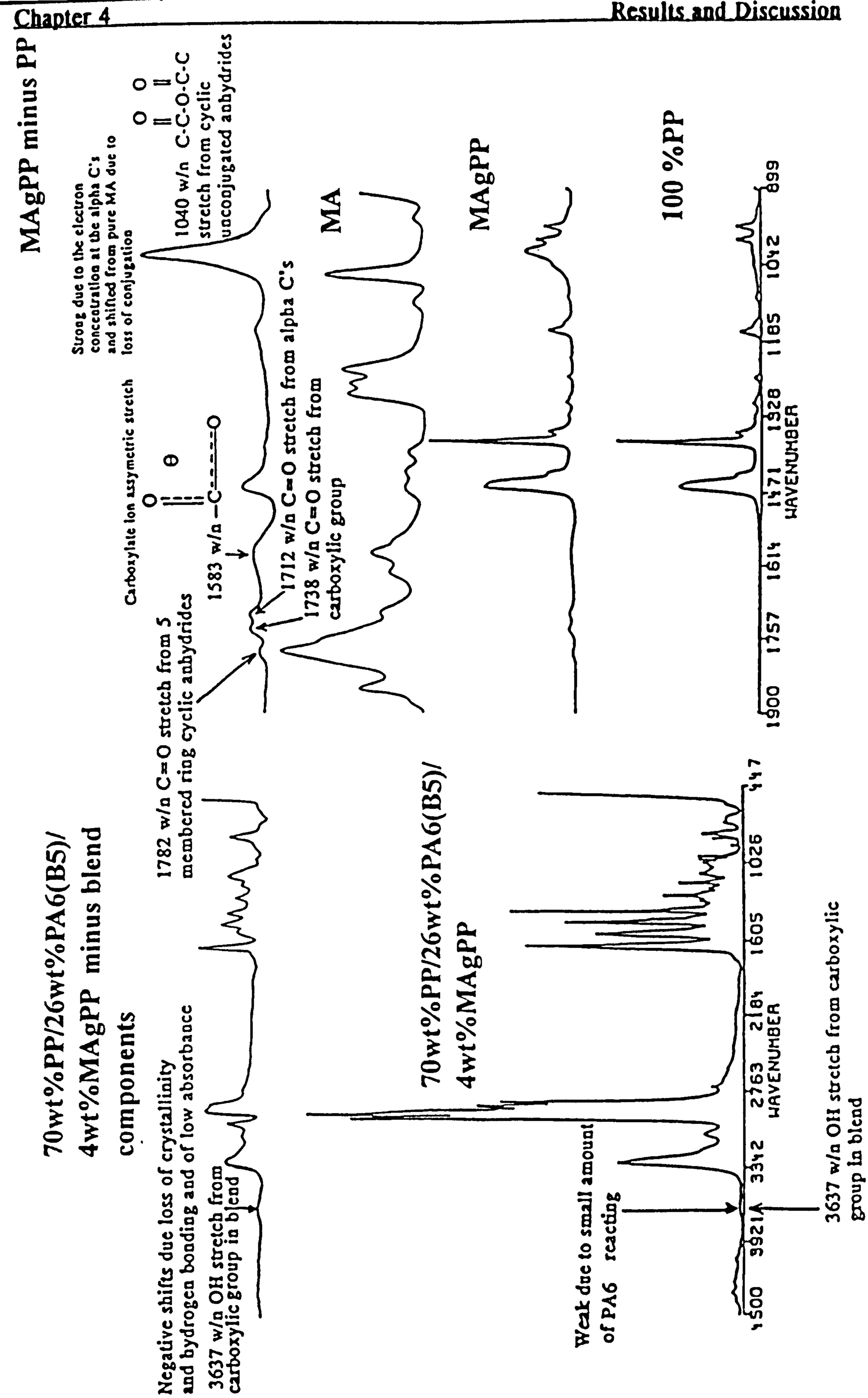

Figure 56 : FTIR Spectra of 70wt% PP/26wt% PA6(B5)/4wt% MAgPP,subtraction spectra, and partial spectra of PP, MA, MAgPP, and MAgPP minus PP

Since we are interested in examining any possible interaction between PA6 and PP, as well as understand the reaction mechanism involved, it is therefore important to consider both the aliphatic -CH_2- stretching mode at 2860-2880 cm^{-1} and the olefinic -CH_2- stretching band at 2900-3100 cm^{-1}. Table 8 summarises these characteristic bands associated with uncompatibilized PA6/PP blends, including R6000. All PP/PA6 binary and ternary blend FTIR spectra, were compared with the spectra of PA6, for evidence of interaction. The N-H associated (hydrogen bonded) trans primary amide asymmetric/symmetric stretch, medium to strong vibration, at 3180-3360 cm^{-1} (two overlapping peaks) and also, the C=O stretch amide I carbonyl band, at 1650 cm^{-1} were examined. With the exception of the 60wt% A23/40wt% PP, these peaks had shifted to a lower waveband (higher frequency), showing no interaction, but evidence of a loss of crystallinity, probably due to the interfacial co-polymer of PP/PA6. The FTIR spectra of 70wt% XLPP/30wt% Plast.PA6(B5) is shown in Figure 55 as a typical binary XLPP blend.

Another blending implication is that the resulting decrease in the PA6 concentration of the blends has apparently influenced the NH stretching deformation. Shifts to lower waveband of the band at 1641/1646 for A23 and 1649 cm^{-1} for B5 are observed for all the blends with respect to the PA6 homopolymers, suggesting that changes in blend composition have significant effect on the C=O amide I stretch deformation, due possibly to the disruption of the hydrogen bonding, as a result of less C=O groups being present in the blends of lower PA6 content. Refering to Figure 54, it can be seen that the 70wt% PP/30wt% A23 material shows low absorption for the A23 wavebands due to the low molecular weight A23 being encapsulated by the higher viscosity PP.

Note that extra carbonyl peaks at 1720-1770 cm^{-1} has appeared in low concentration systems, ie. 5wt% B5 with PP, and some of the binary compatibilizer/PA6 systems, which can be assigned to amides containing a -CO-NH-CO- group , which can be a doublet, with small separation. This would normally be strong, but the absorption is small, due to the small amount reacting. No branched PP is presumed to have formed in the binary samples since no characteristic C=O deformation band for aldehyde at 1730 cm^{-1} is detected, which would be an indication of this type of structure. The exception are, blends of 95wt% PP/5wt% B5 90wt% B5/10wt% PP, and 85wt% PP/15wt% B5.

The former has three extra peaks at 1718, 1740, and 1772 cm^{-1}, as listed in Table 8. These are due to, C=O stretch from formates, C=O stretch from saturated aliphatic esters, and C=O stretch from γlactones, respectively. The other two only have the weak absorptions at 1740 cm^{-1}.

4.5.2.3 FTIR spectra of the compatibilizers

Differences in the spectra of MA-g-PP, were identified by subtraction, which supports the reaction scheme proposed for the grafting and subsequent reaction with PA6. The

Table 9 : FTIR spectra peak assignment of MA-g-PP

Wavenumber	Functional Group	Strength
1015 (peak 1)	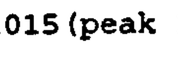 Stretch from cyclic anhydrides.	Usually medium but strong, due to the electron concentration at the α C.
1400	Carboxylate ion symmetric stretch	Usually weak but absent due to the overlaying medium C-CH, asymmetric deformation waveband.
1583	 Carboxylate ion asymmetric stretch.	weak
1712	C=O stretch due to saturated aliphatic ketones, from the C=O attached to the α C.	medium
1738	C=O stretch due to saturated aliphatic esters, from the carboxylic group.	medium
1782	C=O stretch from 5 membered ring cyclic anhydrides.	weak

shift in peak at 1015 cm^{-1} due to the stretch of the cyclic anhydrides group, from MA to the MA-g-PP is due to loss of conjugation on grafting, reinforcing that the MA ring opens only after reaction with PA6. In addition, the CH_3 asym. str. waveband at 1457 cm^{-1} of PP has shifted to 1460 cm^{-1} in MA-g-PP indicating an increasing methyl group population. The differences have been highlighted by subtracting the spectra of PP from that of MA-g-PP, and also including that of MA. The comparison of the PP IR spectra with that of MA-g-PP is shown in Table 9 above.

The shift in peak 1 (Figure 56) from that of pure MA to the MA-g-PP is due to loss in conjugation on grafting, which reinforces:

i) That grafting takes place.

ii) The MA ring does not open.

iii) The MA peaks are weak on the blend spectra due to low concentration and the fact that only a small amount of PA6 reacts.

iv) There is also a new peak appearing in the blend at 3637 cm^{-1}, due to the carboxylic OH group produced during the mechanism proposed in Figure 4. Note that this peak does

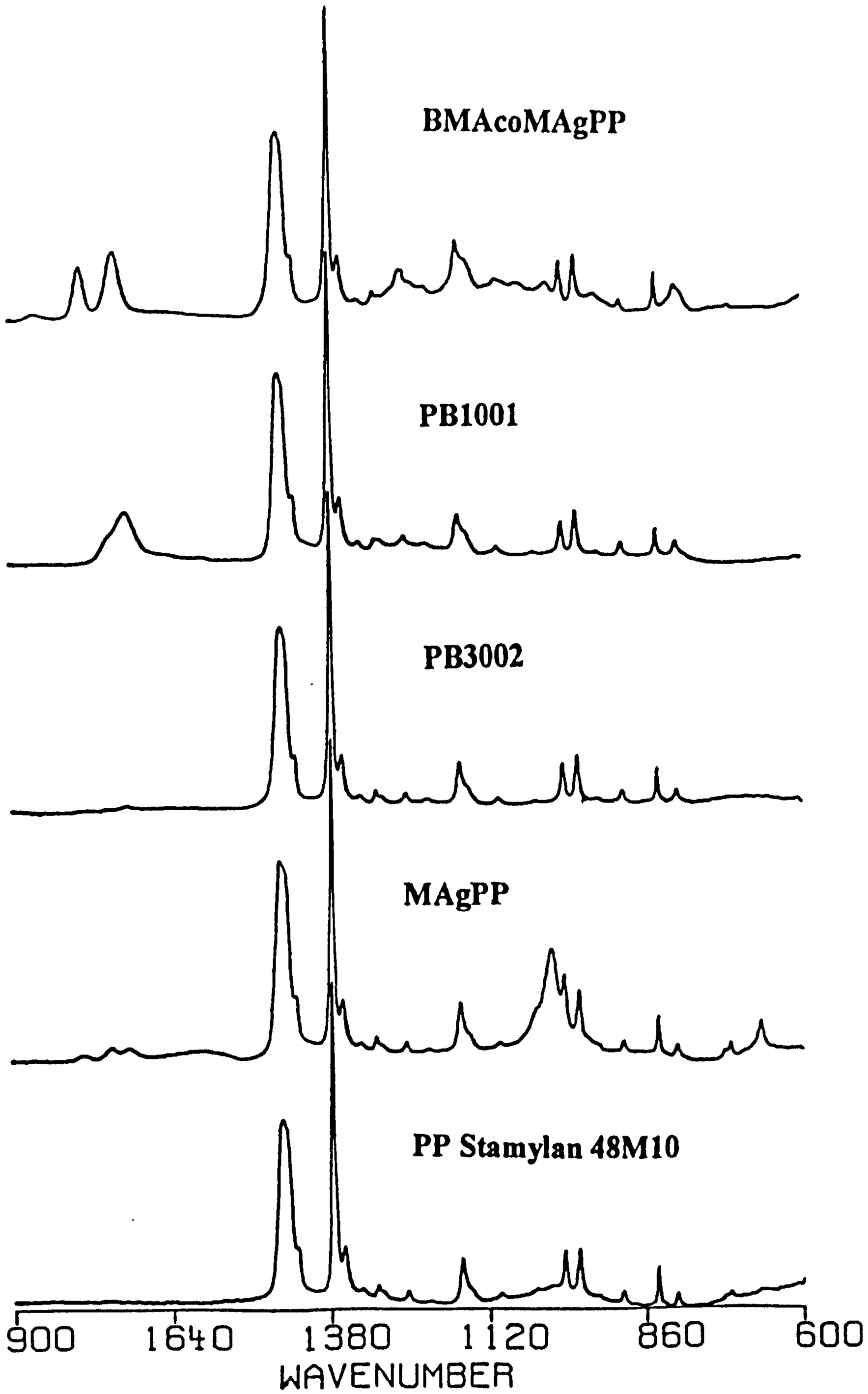

Figure 57 : Partial FTIR spectra of compatibilizers(lower wavenumbers)

not appear in the MA-g-PP spectra, prior to the ring opening.

v) The waveband at 1458 cm^{-1} in PP, due to CH_3 asymmetric stretch has shifted to 1461 in the MA-g-PP, showing that the tertiary C attached to the methyl has taken part in the grafting.

The FTIR spectra of the (BMAcoMA)gPP, see Figure 57, shows sharp medium bands at 1850, 1790, 920 cm^{-1} (C=O str. and C-O-C str.), and 750/1120 cm^{-1}, characteristic of the cyclic anhydride and ester groups, respectively. The spectra of PB1001 shows at 3197 cm^{-1} a C-O-H acrylate absorption as bonded OH...O and symmetric/asymmetric stretch CH_2 absorptions at 2951 and 2877/2868 cm^{-1}, in addition to the 1710 cm^{-1} carboxylic acid dimer -C-COOH absorption (with a shoulder at 1736 cm^{-1} for saturated aliphatic esters), and at 1305 cm^{-1} an -O-CH_3 absorption. The -CH_3 asym. deformation waveband at 1460 cm^{-1}, is shifted from the PP absorption at 1457 cm^{-1}. The FTIR spectra of PB3002 shows low absorption C=O stretch at 1738 cm^{-1}, due to saturated aliphatic esters.

4.5.2.4 PA6/Compatibilizer Blends

Since examination of the ternary PP/PA6/compatibilizer blend FTIR spectra were difficult to interpret in terms of new functional group appearance, binary PA6/compatibilizer blends were prepared and examined for new functional group appearance. For the MA-g-PP/B5 system, an NH_2 waveband from a -CH_2NH_2 has appeared at 798 cm^{-1}, indicating more terminal amine groups, and hence more molecules of lower molecular weight. At 813 cm^{-1} a CH_2 wag absorption is observed from a $(CH_2)_{n>4}$-O-CH=CH_2 grouping and at 972 cm^{-1} this is reinforced by a $(CH_2)_{n>4}$-O- grouping. The out of plane NH wag doublet at 699 cm^{-1} and 722 cm^{-1} have shifted to 704cm^{-1} and 730 cm^{-1} respectively, the former of diminished absorbance, hence producing a negative peak upon subtraction.

Similar bands to those discussed above are observed at 1729 cm^{-1} for 92wt% B5/8wt% BMAcoMAgPP (Figures 65/66), at 1721 cm^{-1} for 92wt% B5/8wt% PB1001, at 1719 cm^{-1} for 92wt% A23/8wt% MAgPP, and at 1726 cm^{-1} for 92wt% A23/8wt% BMAcoMAgPP. It is noticeable that the lower waveband occurs for an MAgPP material, where free MA reduces the melt viscosity.

FTIR spectroscopy and the gross discoloration shows that B5 is decomposed, when mixed with MA, by the loss of terminal amine groups, rather than forming amide groups, and the formation of conjugated bonds, most likely as a result of chain scission. From comparing the FTIR spectra of the 95wt% B5/5wt% MA with that of B5, it was found that various methylene wavebands had disappeared and also hydrogen bonding amide wavebands. Shifts indicating chemical reaction were observed for methylene rocking at 454 cm^{-1}.

The higher waveband part of the 92wt%A23/8wt%PB1001 material spectra, see Figure 64, exhibits negative and positive shifts as compared to 100% A23, ie. the CONH trans stretch shoulder at 3204 cm^{-1} has been shifted to 3192 cm^{-1} because of interaction with C-O-H peak of the compatibilizer, at 3197 cm^{-1}. This is in contrast ot the B5/PB1001 material, where the interaction has increased the waveband from 3188 cm^{-1} in the homopolymer to 3192 cm^{-1} in the mixture. The explanation is an increase in hydrogen bonding potential in the latter and not the former. Likewise for the NH str. absorption at 3092 cm^{-1} for the A23/PB1001, caused by the overtone of the amide II band, which has shifted in the mixture to 3077 cm^{-1}. However, the CH_2 asym. stretch at 2933 cm^{-1} has been shifted to 2936 cm^{-1} in the mixture, the symm. CH_2 stretch at 2857 cm^{-1} has shifted to 2865 cm^{-1} and the NH stretch absorption, caused as a combination of C=O str. and NH bending, at 3299 cm^{-1}, has shifted slightly to 3300 cm^{-1}. The subtraction spectra notably exhibits a broad peak at 3640 cm^{-1}, which is due a terminal primary amine NH_2 grouping, suggesting a decrease in molecular weight due to an increased number of these groups.

Examination of the lower waveband portion of the same spectrum (Figure 58) reveals that the -C-COOH carboxylic acid dimer peak (1710 cm^{-1}) is responsible for the 1717 cm^{-1} low absorption peak, which in the subtraction spectra has shifted to 1721 cm^{-1}. Negative shifts appear for the 1641 cm^{-1} C=O group and the CNH group at 1551 cm^{-1}. They are shifted to 1639 and 1545 cm^{-1} respectively, which is not surprising, but not reinforced by the increase in shear viscosity for this mixture. Absorptions indicating some interaction occur in the mixture spectrum at 1475 cm^{-1}, from the methylene absorptions of the compatibilizer, to form a CH_2-N- grouping vibration. This is also present in the B5/PB1001 mixture spectra. The peak at 1368 cm^{-1} in the homopolymer has shifted to

1376 cm^{-1} due to the $N(CH_3)_2$- absorption for tertiary amine groups. Also appearing, shifted from 712 cm^{-1} to 714 cm^{-1}, is the NH deformation peak from secondary trans amides CONH grouping.

Where the PB1001 has been mixed with 92wt% B5, more evidence of interaction is present in the upper part of the FTIR spectrum, since the 3300 and 3079 cm^{-1} peaks have shifted in the mixture to 3302 cm^{-1} and 3084 cm^{-1} respectively. The OH stretch shoulder at 3188 cm^{-1} has shifted to 3192 cm^{-1} in the mixture, under the influence again of the OH stretch broad low absorption peak at 3197 cm^{-1} in the compatibilizer. For the methylene portion of the spectrum, negative shifts are observed, due to the relevant absorptions being lower for the compatibilizer. There is also no evidence in the mixture spectra of the methyl absorptions of the compatibilizer, but the CH_3 asym. str. absorption at 2966 cm^{-1} was resolved by subtraction. More evidence of terminal amine group increase is the revealing from the subtraction spectra of a peak at 1610 cm-^{1} vibration, due to the (R-CO-NH_2)NH_2 grouping from the doublet at 722/691 cm^{-1}, due to the NH deformation grouping from the secondary trans amide CONH bend.

The 92wt% A23/8wt% BMAcoMAgPP mixture, exhibits this waveband at 1727 cm^{-1}, resulting from a shift of the compatibilizer absorption at 1712 cm^{-1}, due to OH....O hydrogen bonding. However, when 8wt% of the same compatibilizer is mixed with B5, Figures 60-61, the same behaviour is observed, with the new peak appearing at 1728 cm^{-1}, and at 1731 cm^{-1} in the subtracted spectrum. This is due to amides containing -CO-NH-CO-, which can be a doublet with small separation. Different changes observed included the partial resolution of the peak overlain by the amide I C=O absorption. The mixture shows a double peak, 1649 and 1639 cm^{-1}, the latter remaining after subtraction of the B5 spectra. This is due to the second primary amide I band, or less likely, due to the rarity of this being resolved, a C=C alkene or *cis* -CH=CH- stretch. A weak peak due to $(CH_2)_5$ and $(CH_2)_7$ rocking, in the mixture, has shifted to 1548 from 1546 cm^{-1}, indicating interaction. But the amide II CNH peak at 1263 cm^{-1} in B5 has shifted negatively to 1261 cm^{-1} for the mixture. The propyl group in the compatibilizer is present at 719 cm^{-1} whereas the mixture also shows at 798 cm^{-1} a peak for NH_2, reinforcing the increasing influence of -CH_2-NH-CH_2-, since the doublet at 722 and 691 cm^{-1} has shifted to 730 and 709 cm^{-1}. The latter is due to out of plane NH wag from CO/NH interaction.

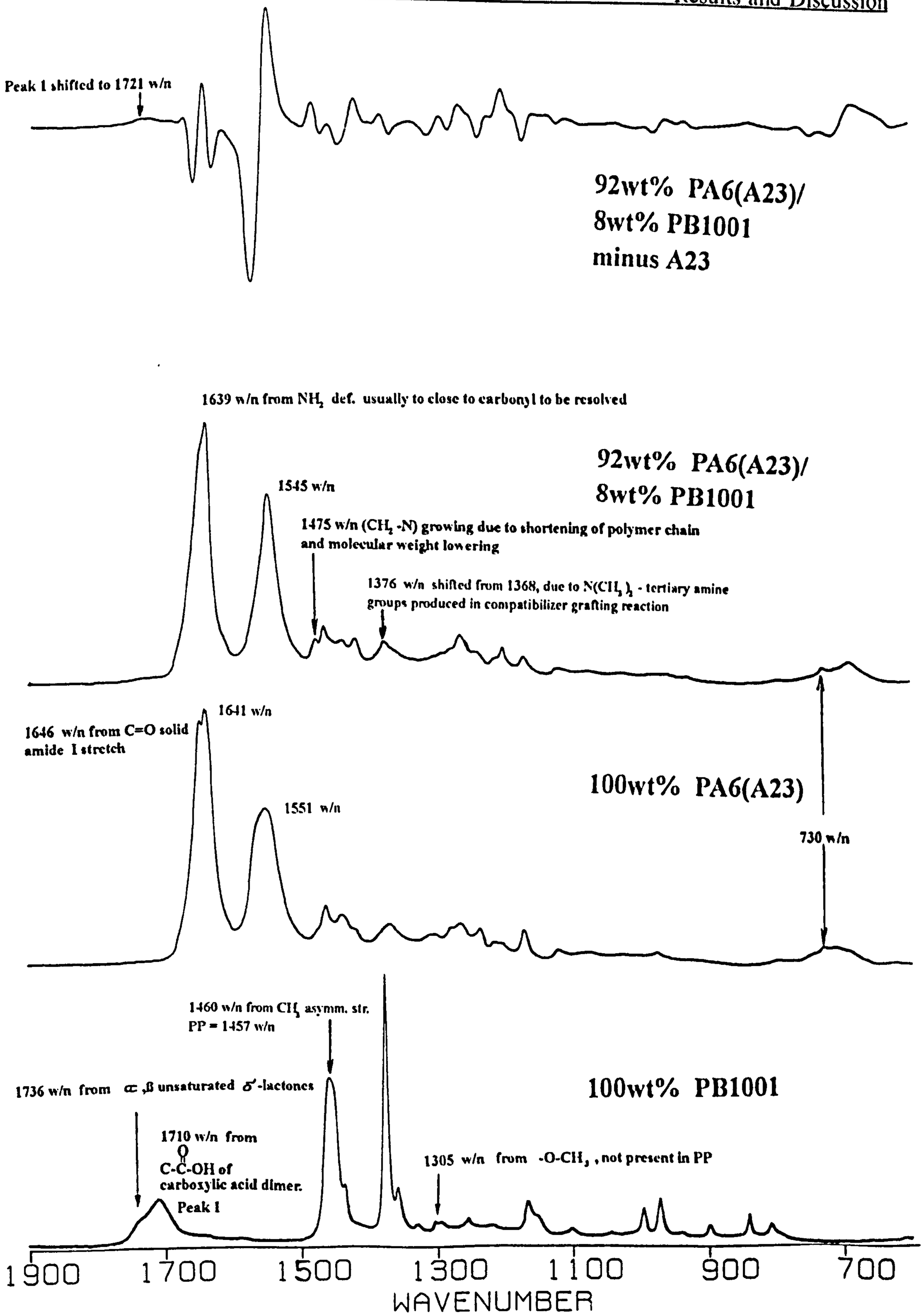

Figure 58 : Partial FTIR spectra(low wavenumbers) of 92wt% PA6(A23)/8wt% PB1001 blend

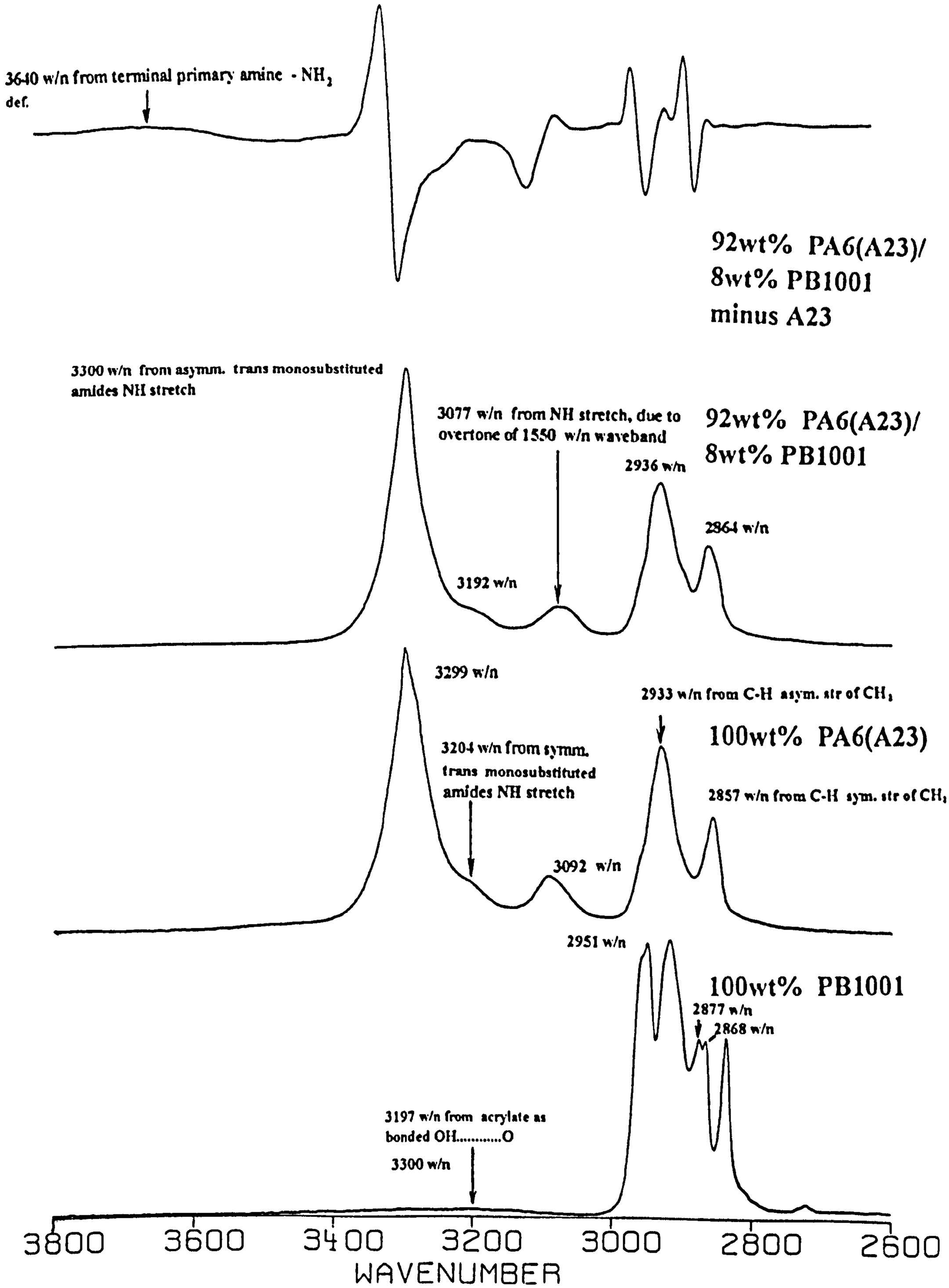

Figure 59 : Partial FTIR spectra(upper wavenumbers) of 92wt% PA6(A23)/8wt% PB1001 blend

The so-called amide III band from C-N str. at 1461 cm^{-1} for the homopolymer has shifted to 1463 cm^{-1} in the mixture, indicating interaction. From the compatibilizer spectrum, the peak at 1843 cm^{-1} is from C=O of an OC-O-CO grouping, which reinforces the appearance of C-O peaks at 1020 and 941 cm^{-1}.

For the lower frequencies, the CONH trans mono subst. stretch absorption at 3184 cm^{-1} of the B5 has shifted in the mixture to 3189 cm^{-1}. Likewise for the NH stretch absorption at 3079 cm^{-1} , due to the o/t of the amide II 1550 cm^{-1} waveband, shifting to 3088 cm^{-1} in the mixture. In the subtraction spectra, these peaks were resolved to 3209 and 3097 cm^{-1}. The hydrogen bonded NH str. absorption at 3300 cm^{-1} has not shifted, but negative shifts were observed for the CH_2 asym. and symm. stretch absorptions at 2937 and 2864 cm^{-1} , to 2931 and 2858 cm^{-1} respectively because the absorptions in the compatibilizer appear at 2919 and 2840 cm^{-1}, respectively.

4.5.2.5 Macroradical formation in the blends

Large elongational or shear forces are well known to produce chain radicals[33]. The subsequent reaction then propagates through hydrogen extraction on a nearby polymer chain and terminates when two radicals react between themselves, possibly forming branched molecules. Two component systems, like blends of PA6 and PP create a more complex situation, where two types of macroradicals can be formed. They in turn can react with themselves or with radicals of different chemical nature forming, respectively, branched molecules and various types of graft co-polymers[34]. It has been reported that PA6 tends to form radicals more easily than polyolefins[34] in a homolytic chain scission process. The C-N bond in PA6 is known to be weaker than the C-C bond in polyolefins, ie. 66 vs. 85 kcal mol^{-1}. The homolytic scission of the peptide (C-N) link depends largely on the structure in which it is located. The C-N bond which is in the alpha position to the carbonyl is stronger than the C-N bond which is beta to the carbonyl group[35]. As expected, the radical density of the polymers depends very much on the shearing forces imposed.

PP degrades predominately by chain scission to form -$CH(CH_3)$-$CH^{\cdot}$- and $(CH_3)CH_2^{\cdot}$- radicals[36,37]. The first can easily react with oxygen to from a peroxy radical, whereas the second is less likely to react due to the -CH_3 steric hinderance. From information

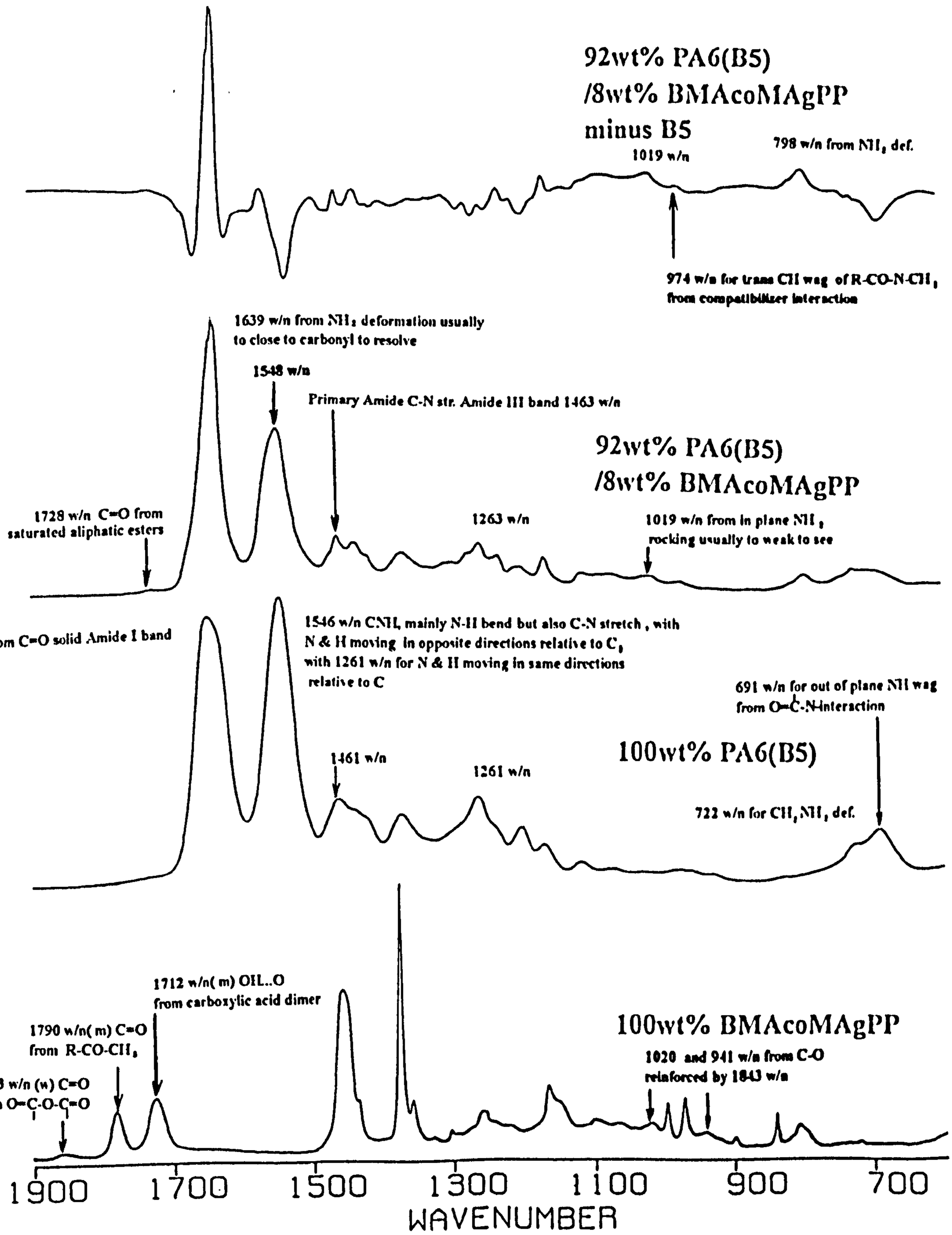

Figure 60 : Partial FTIR spectra(lower wavenumbers) of 92wt% PA6(B5)/8wt%BMAcoMAgPP blend

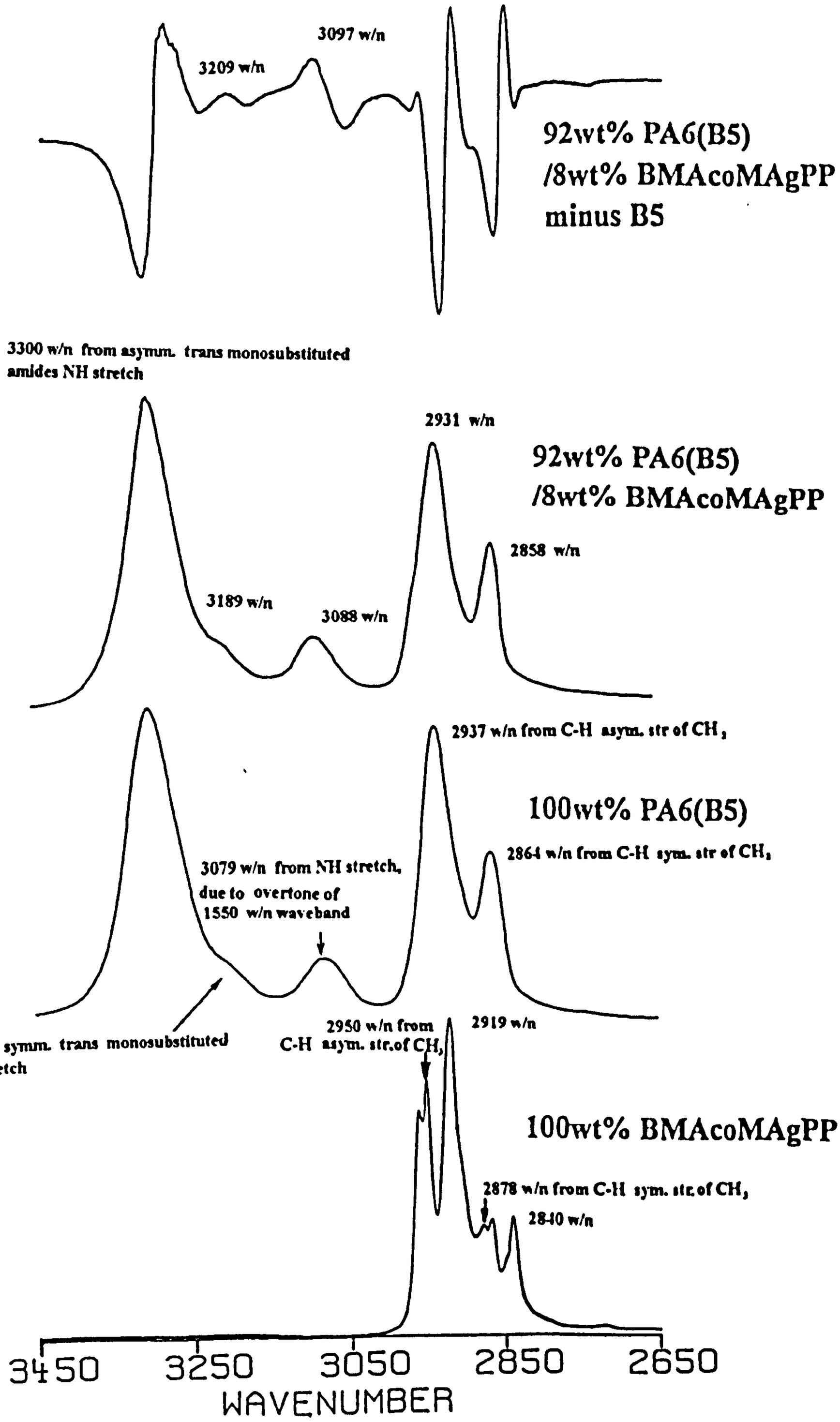

Figure 61 : Partial FTIR spectra(upper wavenumbers) of 92wt% PA6(B5)/8wt% BMAcoMAgPP blend

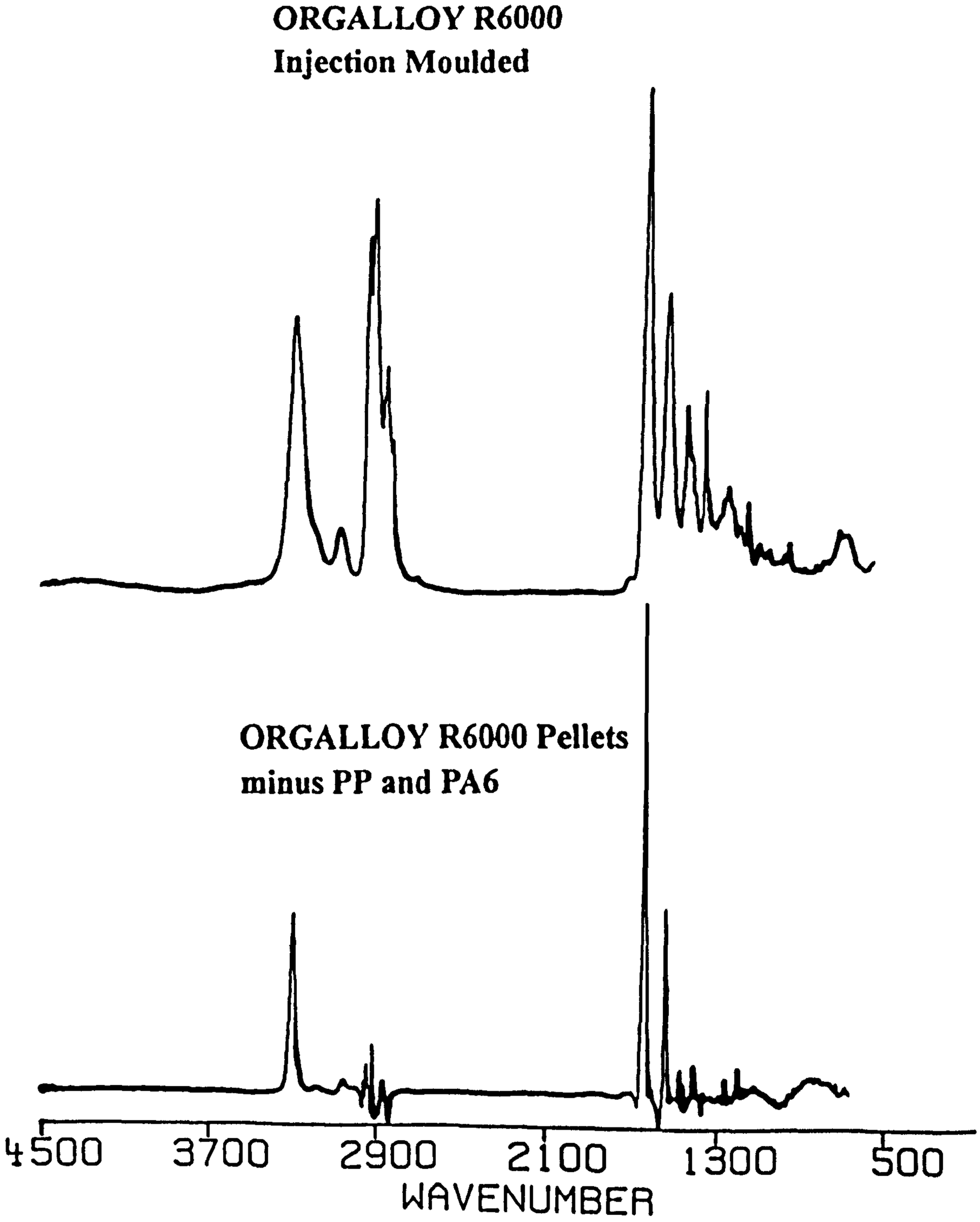

Figure 62 : FTIR spectra of Orgalloy R6000 blend Injection Molded and R6000 pellets from which PP and PA6 are subtracted

supplied by the PP co-polymer manufacturer[38], it is known that the mole ratio of the PE monomer units to those of PP is 8:100. It is also known that 9.9 x 10^{18} bonds/cm^3 are broken during rupture of a PE chain as compared to 2.5 x 10^{18} bonds/cm^3 in the case of PP[33], indicating that interaction between the PP and PA6 is more likely to happen between the NH group and the PE Sections of the co-polymer, hence to a limited extent only. It is likely that the breakage of the C-N bond beta to the carbonyl will occur preferentially to that alpha to the carbonyl, in the main PA6 chain. This is a possible explanation for the shift of the amide II CN absorption band from 1542 cm^{-1} for B5 to 1548 and 1547 cm^{-1} respectively in the 10wt% PP and 30wt% PP binary blends. This has the effect of lessening the hydrogen bonding effect on the overall crystalline structure of PA6.

For the formation of PP branched structures from macroradicals, it is well known that in the presence oxygen, the double bonds formed by the reaction sequence above can react to form aldehyde end groups and the carbonyl stretching vibration will exhibit an amide I absorption band at 1720 cm^{-1}. From examination of the blend spectra the R6000 injection molded material exhibit a weak band shoulder at 1719 cm^{-1}, indicating the likely formation of a highly branched PP.

It is unlikely that B5 will form macroradicals since it is made by hydrolytic polymerisation, and hence will not form branched structure. However, A23 is made by anionic polymerisation and therefore ISO 372[39] does not recommend the Molau Test[40] standard for this type of material, primarily due the problem of its insolubility in formic acid solution, presumably as a result of branching. The Molau test has been used with PE/PA6 blends free of graft co-polymers which were placed in pure formic acid. The PA6 dissolves completely, leaving the PE component to precipitate as coarse white flakes. If the same test is performed with a PA6/PE blend containing graft co-polymer, the a colloidal suspension is observed, without any insoluble precipitation. The ultimate fate of macroradicals and their ability to co-react is not necessarily predictable. Braun et al[32] found no evidence of graft co-polymers in a PA6/HDPE blend prepared in an extruder, concluding therefore that the macroradicals formed during the mixing process react only with themselves.

4.5.2.6 FTIR spectra of compatibilized ternary blends

The FTIR spectra of the 62wt% PP/30wt% PA6(B5)/8wt% BMAcoMAgPP blend is included in Figure 55 as a typical ternary spectra. Only negative waveband shifts are observed for the compatibilized blend NH and amide I C=O stretching deformations. However, for the 62wt% PP/30wt% B5/8wt% PB1001 (micrograph Figure 70) and 56wt% A23/36wt% PP/8wt% PB1001 (Figures 34/35) blends, substantial shifts of absorption bands to lower frequencies are recorded for both the aliphatic CH_2 symmetric (2860 cm^{-1}) and asymmetric (2936 cm^{-1}) stretching deformation of B5 and 2933 and 2857 of A23, indicating some loss of crystallinity/hydrogen bonding. Similar trends were observed for the olefinic CH_2 stretching deformation region. The phase dispersion of these blends represent d values of 2.9 and 2.3 respectively, indicating some stability of spherical phase in matrix, the former showing some phase-in-phase behaviour and the latter a PP matrix, despite a PA6 majority phase.

It is significant to observe the presence of a C-N stretching deformation band at 1240 cm^{-1} for all the functionalized PA6/PP blends, except 56wt% PA6(A23)/36wt% PP/8wt% BMAcoMAgPP. Earlier a unique C-N stretching deformation band at 1239 cm^{-1} was recorded for the non-compatibilized 60wt% A23/40wt% PP blend. However, the slightly lower waveband suggests that a different C-N bond may be present in the compatibilized and non-compatibilized samples. In view of these findings, it is suggested that the compatibilizer forms a PA6/PP co-polymer, resulting from amidation between the PA6 amide group and carbonyl groups of BMAcoMAgPP.

By spectral subtraction of PP, the FTIR spectra of these compatibilized blends suggest that a number of PA6 chains are bonded to the PP polymer chain to form possibly a PA6/PP co-polymer, notably through the detection of shifts in the CN band at the 1213-1239 cm^{-1} region for some blends, only present as shoulders in the PA6 homopolymers.

The FTIR spectra of R6000 from which the blend components have been subtracted is shown in Figure 62. Note that the CONH trans.mono subst. stretch absorption at 3196 cm^{-1} is unchanged compared to R6000, whereas the NH stretch non H-bonded o/t of the amide II band at 3057 cm^{-1} is at a higher frequency than the blend, where it is present at 3070 cm^{-1}, showing that hydrogen bonding is a significant factor, particularly since the

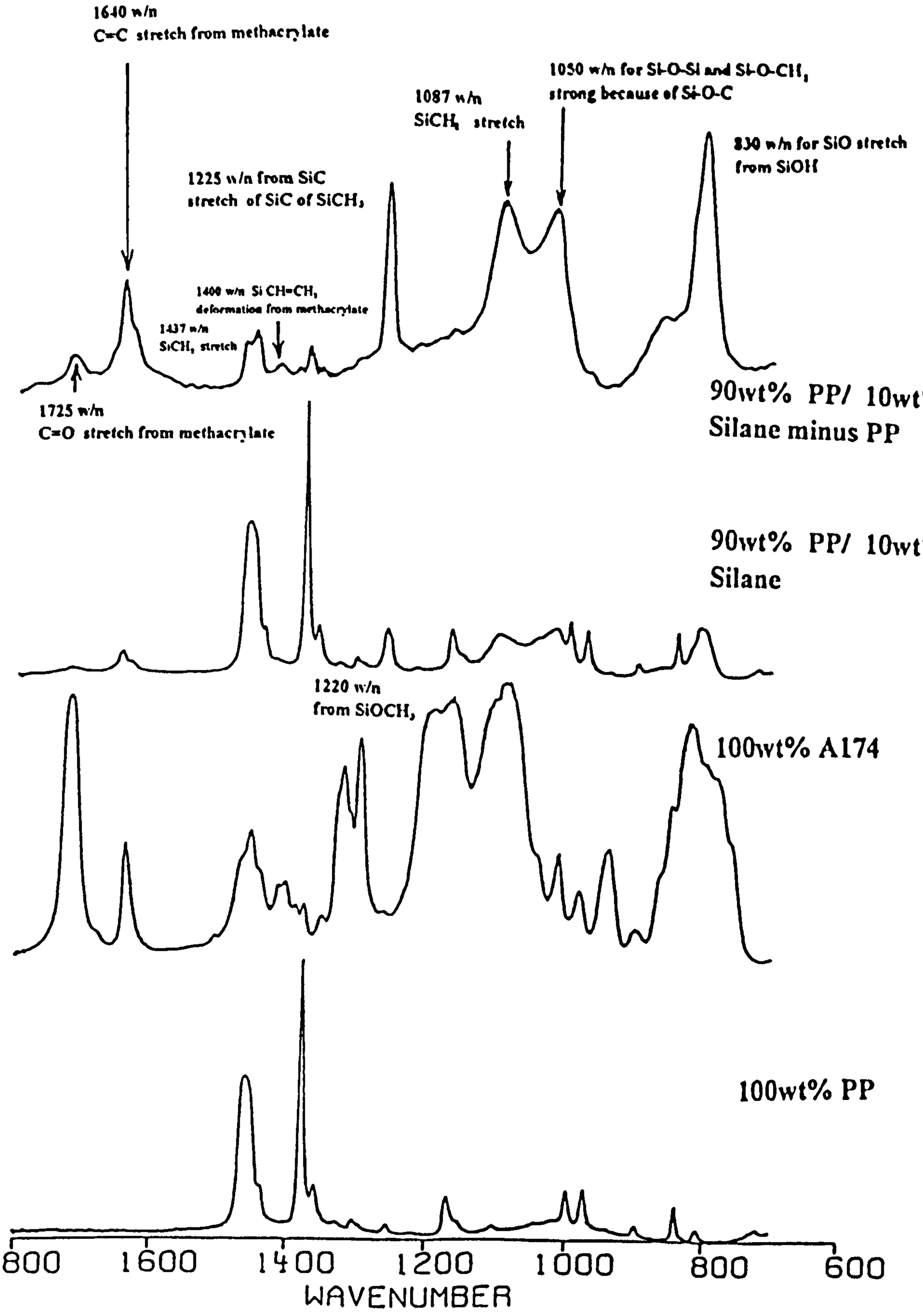

Figure 63 : FTIR spectra of XLPP(2wt% A174 Silanes), A174, PP, and a subtraction spectra

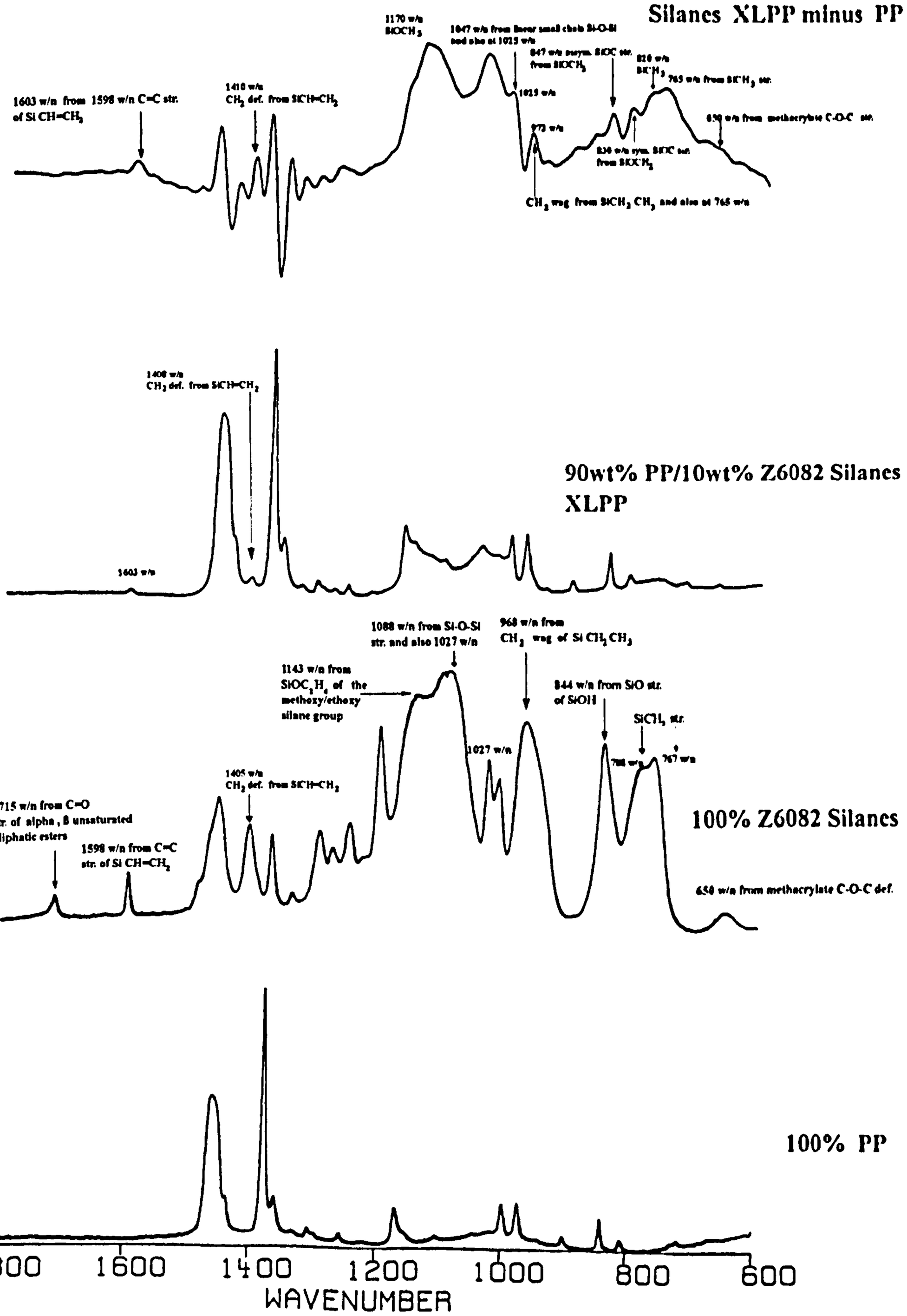

Figure 64 : FTIR spectra of 90wt% Z6082 Silane/10wt% PP, PP, Z6082, and subtraction spectra

NH stretch hydrogen bonded absorption at 3300 cm^{-1} has not changed as compared to the blend. Also unchanged are the amide II CNH waveband at 1545 cm^{-1}, where the N and H move in opposite directions to C, and the C=O stretch amide I band at 1638 cm^{-1}. The new C=O band, resolved by subtraction at 1710 cm^{-1}, is due to α,β-unsaturated acid anhydrides, possibly indicating a compatibilizer.

For the aliphatic -CH_2- stretch band region, shifts to lower frequencies(higher wave number) at around 2934-2865 cm^{-1} is observed for most binary blends with the greatest shifts being notably shown for both the 60wt% PA6 blends, for B5, 16 cm^{-1} and for A23, 12 cm^{-1}. This suggests some interaction effect on the CH_2 stretching deformation. For the characteristic absorption band at 2878/2867 cm^{-1}, due to olefinic -CH_2- symm. stretch, reverse shifts of bands to higher frequencies are observed for all the blend samples with respect to the pure PP spectra. This latter observation suggests no appreciable interaction exists between the blend components in the olefinic -CH_2- region. A distinct absorption band is observed at 1265 cm^{-1} with a medium intensity, corresponding to a CN stretching deformation for the PA6/PP blend of composition 60wt% Plast.B5/40wt% XLPP, which is similar to the band observed in the PA6/compatibilizer blends (Section 4.5.2.4). The 100% PA6 samples exhibit this particular absorption band at a lower waveband, ie. 1237 and 1235 cm^{-1} for B5 and A23 respectively. It is likely that this unique band can possibly provide some experimental evidence on the likely formation of a PA6/PP co-polymer between the amide group of PA6 and the functionalized PP chain.

The most effective compatibilizer for reducing phase size was the commercial PB3002 material, based on MA-g-PP, but with a reduced grafting ratio of 0.5wt%, as advertised by the manufacturer. Despite the MA-g-PP compatibilizer reducing the viscosity of the PA6, with evidence from the FTIR spectra of free MA, it was found to be the joint second most effective compatibilizer for reducing the dispersed phase size. The MA present is approximately 3wt%, computed from FTIR extinction factors for the five membered ring anhydride C=O peak at 1782 cm^{-1}, from the following relationship :

$$W = \frac{A \times 100}{e \times t \times \rho} \quad \text{---------- [63]}$$

where W = wt% of MA,

A = absorbance of 1782 cm^{-1} C=O peak,

e = extinction coefficient = 8150,

t = thickness of sample, and ρ = density of sample.

Macroradical formation is unlikely for MA-g-PP blends, due to the plasticization of the excess unreacted MA. However, for the other compatibilizers, it has been shown by rheological measurements that PA6 viscosity is increased, resulting from macroradicals causing branching. No branched PP is presumed to have formed in the functionalized samples since no characteristic IR deformation band for aldehyde at 1730 cm^{-1} is detected. For blends 62wt% PP/30wt% B5/8wt% BMAcoMAgPP and 70wt% PP/26wt% B5/4wt% MAgPP blends, co-polymers of PA6/MA-g-PP, PA6/BMAcoMA-g-PP are likely to have formed, ascribed to their dispersive actions[40].

4.5.3 FTIR Spectra of Silanated PP

The spectra of 90wt% PP/ 10wt% A174 silanes and 90wt% PP/ 10wt% Z6082 silanes are presented in Figures 63 and 64 respectively and the wavebands due to PP silanation are identified. Initially, FTIR spectra of 99wt% PP/1wt% A174 solution were obtained, both in bulk/film, before and after water exposure for ≈ 20 hours and also after refluxing in water for the same time. The film spectra were found to show greater functionality and this conditioning was then also applied to the following wt% silane blends, 97wt% PP/3wt% A174 solution, 95wt% PP/5wt% A174 solution, 90wt% PP/10wt% A174 solution., 95wt% PP/5wt% Z6082/ DBTDL/DCP solution, and the 98wt% PP/2wt% A174 material.

Silane wave bands have been identified in the silanated A174 PP spectra, together with additional ones, possibly due to cross-linking, notably Si-O stretch from SiOH, Si-O-C from Si-O-CH_2, and Si-O-Si. Figure 63 shows the silanation of the 90wt%PP with 10wt% A174 Silane, by spectral subtraction. The silanated PP spectra wavebands were assigned to the various functional groups present and the spectra were examined for evidence of cross-linking/interaction, before and after hydrolysation. Significantly, in the 5 and 10 wt% A174 spectra, for the films exposed to water overnight, wavebands were observed for, silanols Si-OH vibrations (900, 1030, 3375 cm^{-1}) and also those for cis

C=C bending for conjugated vinyl esters (1650 cm^{-1})/Si-CH_3 (780 cm^{-1}) and that for the ketones C=O stretch peak (1720 cm^{-1}). For the 3wt% blend of the same silane, the film treated similarly exhibited the latter three peaks, but not the former three, with a proportionate diminishing of intensity, for similarly thick films.

Further materials were compounded in the laboratory blender with the Z6082 silane as 1wt%, 3wt%, and 10wt% mixtures with PP. A 5wt% Z6082 film exposed to water overnight showed a medium peak at 1120 cm^{-1} which would normally be very strong in the pure silane solution, representing Si-O-alkane group, where in this case the alkane is C_4H_9. Also in evidence are peaks for the CH_3 rocking of $SiOCH_3$ (1190 cm^{-1}) and the Si-O-C (1070 cm^{-1}) asymmetric stretch of the same group. Further functional group wavebands were identified in the subtraction spectra, as shown in Figure 64. In this example, the 90wt% PP/10wt% Z6082 material is examined, for new functional groups.

4.5.4 FTIR Spectra of UV Irradiated PP

An FTIR spectra of a 205 μm PP film swollen in acetophenone for 24 hours and UV irradiated for 10 hours, showed minimal evidence of C=O carbonyl peak development, at 1712 cm^{-1}, due to α,ß unsaturated aliphatic esters. The 192 μm film similarly in acetophenone for 60 hours has a C=O absorption at 1742 cm^{-1} due to saturated aliphatic esters. These results suggest that for similarly thick films, the oxidation species induced by the radiation depends upon the length of exposure time, since the acetophenone decomposes to DCP, which forms free radicals with the PP. The other UV irradiated PP IR spectra showed no evidence of specific reactions.

4.5.5 FTIR Spectra of γ Irradiated PP

Very little evidence of degradation/cross-linking was observed from the FTIR spectra of the material irradiated with the 3.6 Ci source, since this dose rate, at 3 cm is equivalent to only 0.468 Gy/h. The exception was a 6.2 μm film, irradiated for 24 hours at 30 cm from the source, which showed two C=O peaks at 1740 and 1712 cm^{-1}, due to α,ß unsaturated aliphatic esters and saturated aliphatic esters. Both 64.5 μm and 416 μm films were also irradiated for 96 hours at 32mm by the 400 Ci source. Not surprisingly, the former was brittle and yellow coloured, but the FTIR spectra showed no evidence of

oxidation. The γ irradiated films used as a control experiment, in which PP films which had been swollen in acetophenone and dicumyl peroxide solution, for 12 hours, giving a total dose of 3.36 Mrads, were exposed for 24 hours. Evidence was then sought of oxidation by observation of the carbonyl vibration at 1690 cm^{-1}, but none was observed. The PA6(A23) was exposed for 96 hours with the 400 Ci source, without any noticeable changes in the IR spectrum, but the material produced was very brittle.

4.5.6 Summary of FTIR Spectroscopy results

The FTIR spectra for all the binary and ternary PP/PA6 blends showed negative wavenumber shifts for the PA6 amide I carbonyl peak at 1650 cm^{-1}, and the NH asym. stretch H-bonded peak at 3300 cm^{-1}, with the exception of the 60wt% PA6(A23)/ 40wt% PP blend, which showed positive shifts for both absorptions. Therefore, interaction has been minimal for all but one blend and hydrogen bonding of the PA6 will have been reduced due to the concentration effect of the PP. When compatibilizers were blended directly with PA6, spectral shifts and specific reactions have been recognized from the resulting IR spectra. The reactions proposed between two different silanes and PP have been reinforced by FTIR spectral subtraction.

4.6 Water Vapour Permeability

4.6.1 Multiphase Water Vapour Permeability

4.6.1.1 Theoretical Approaches

Three theoretical approaches were applied to the experimental data for predicting the water vapour permeability, as follows, the Maxwell Equation, the Higuchi Equation, and the Robeson Equation, each of which was described in Section 2b.5., as refs.[121], [122], [123], and [124]. All have been used to describe the effect of a second phase on

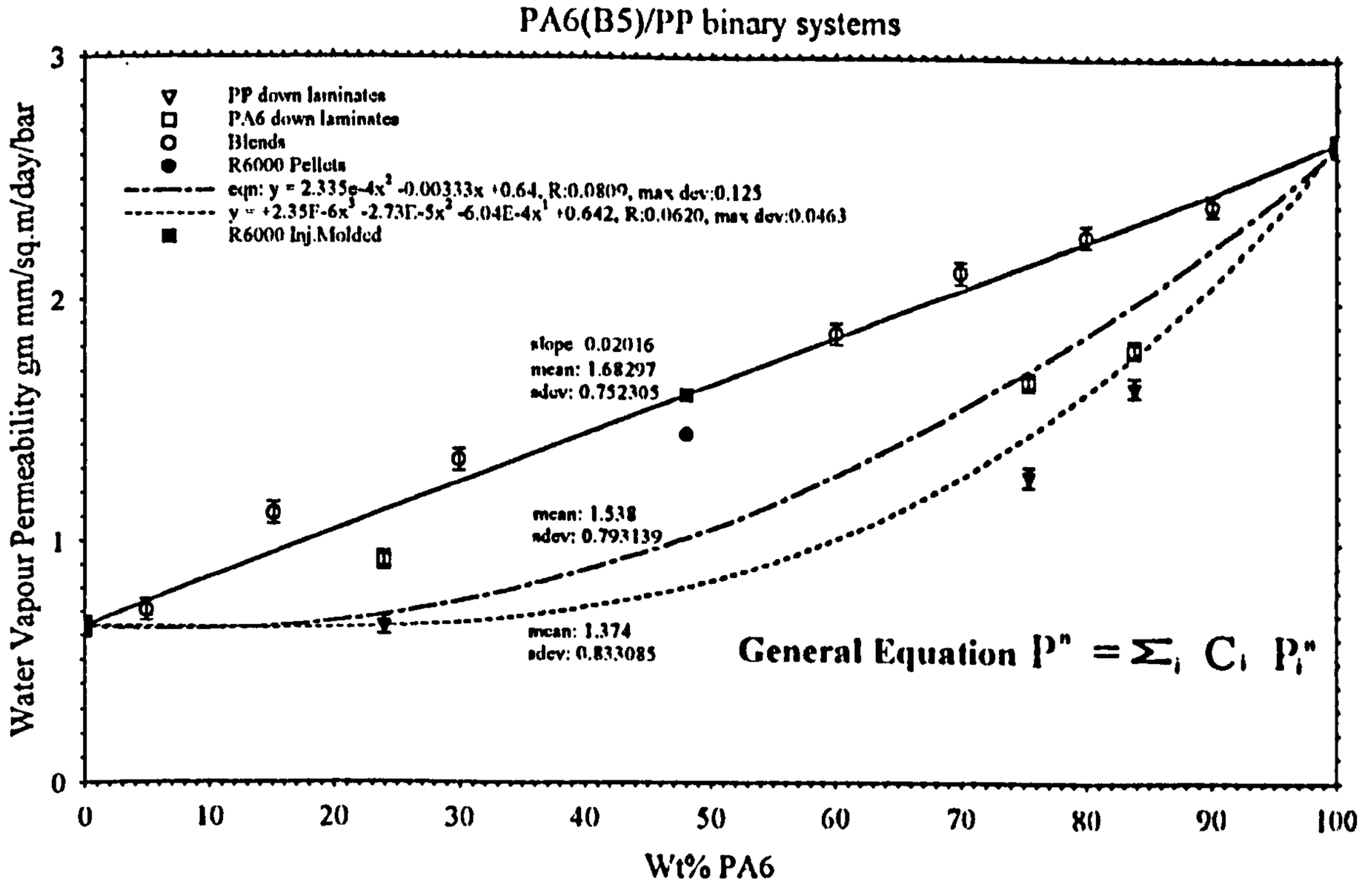

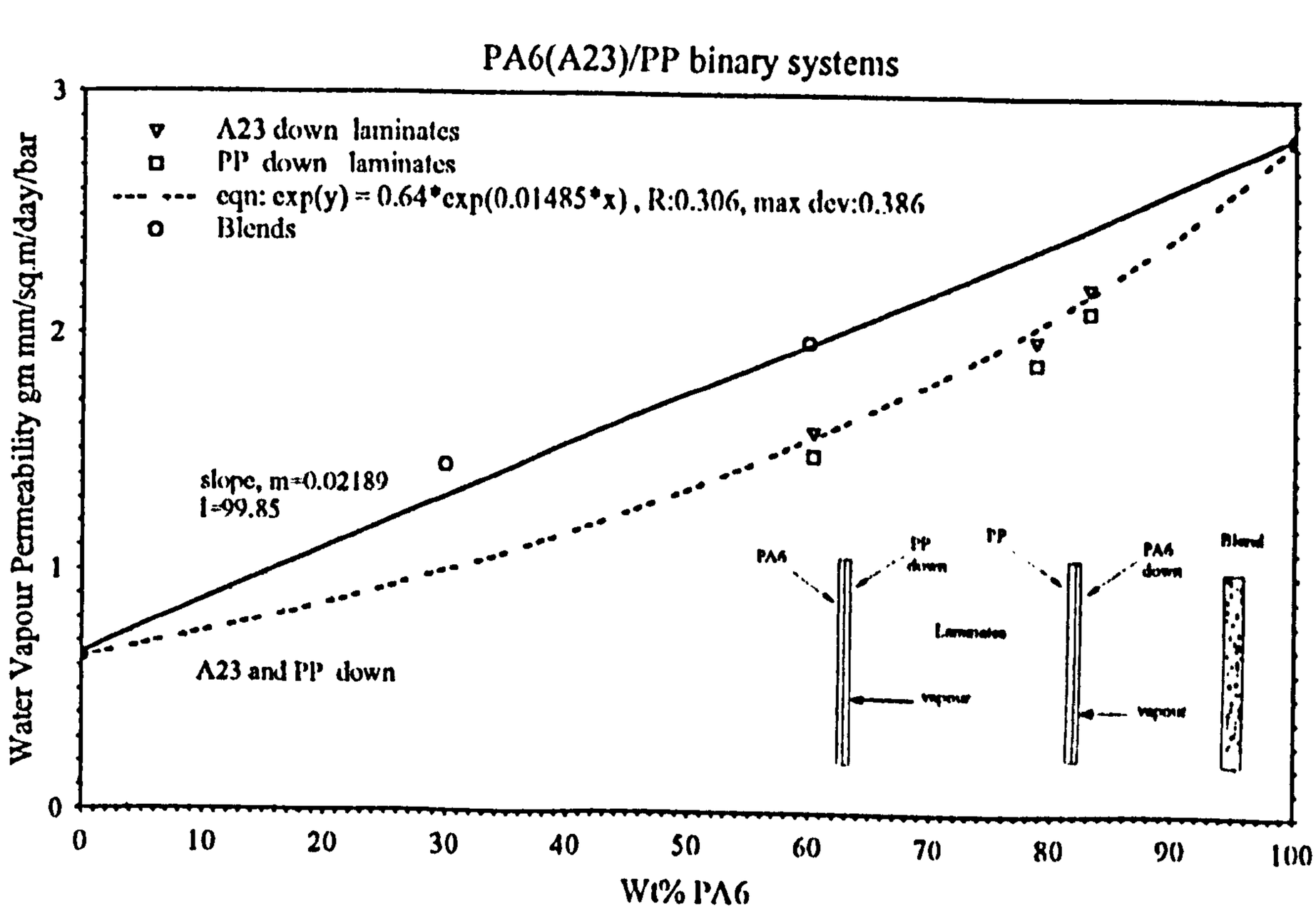

Figure 65a : Binary PP/PA6 systems water vapour permeability

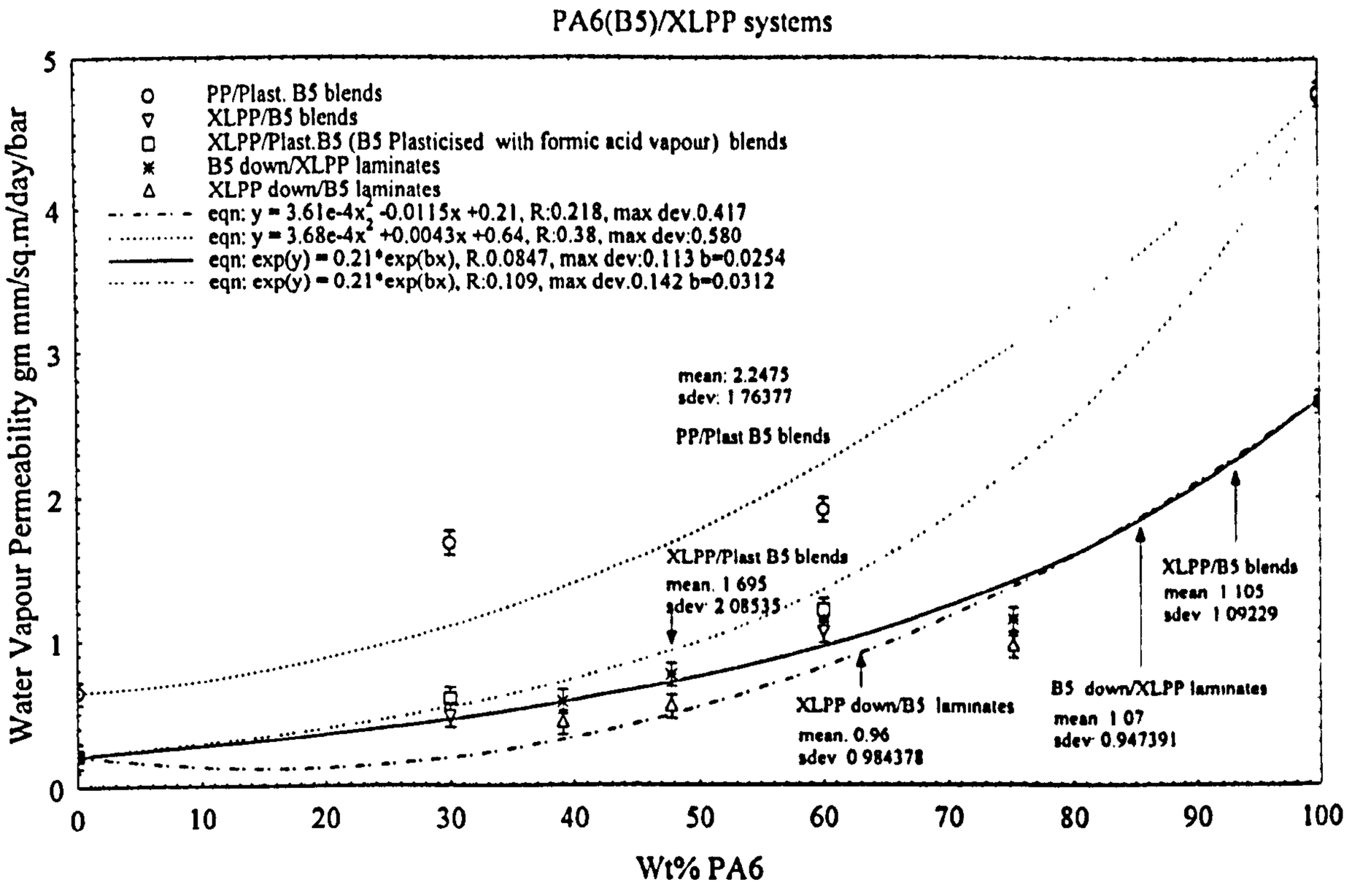

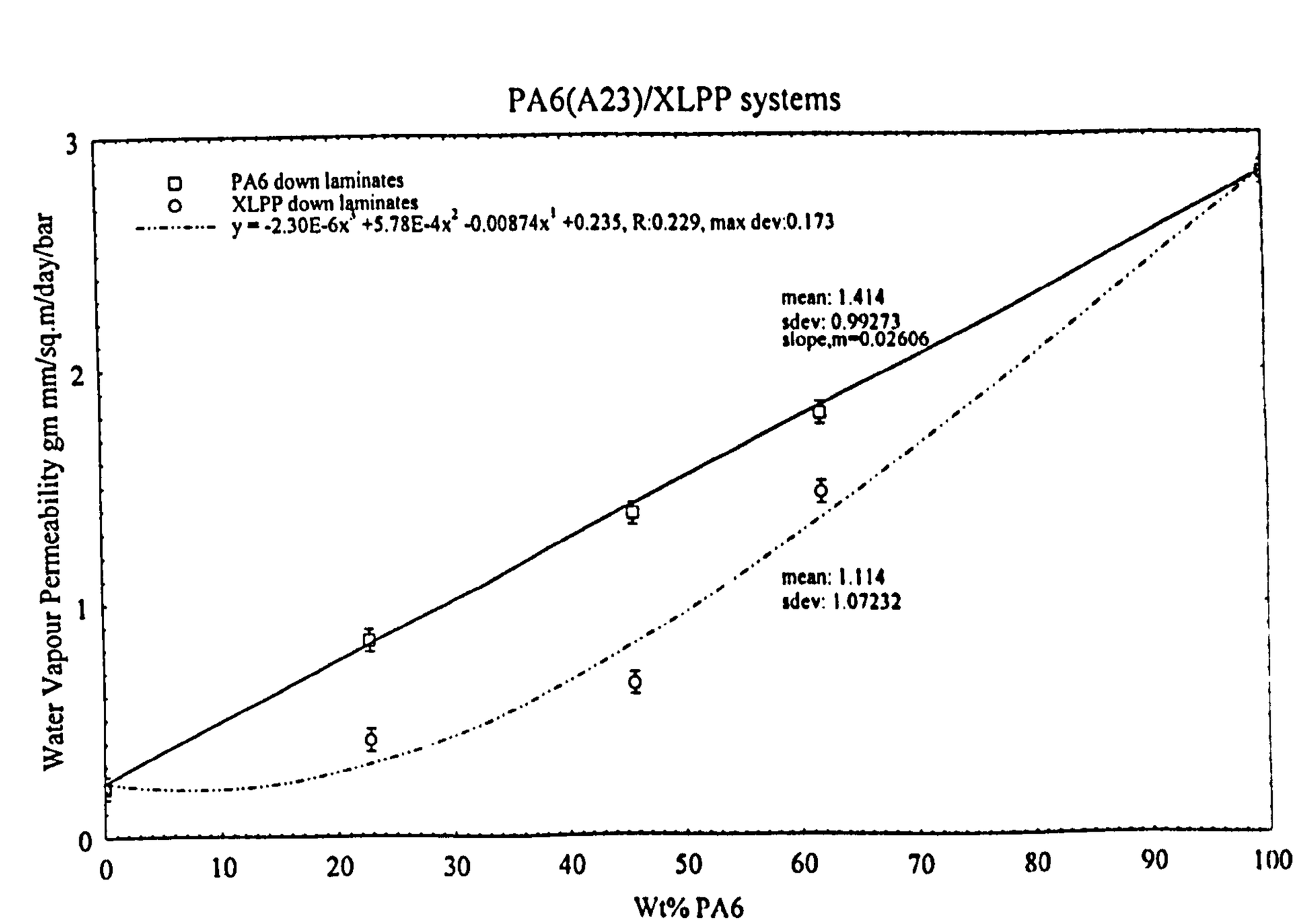

Figure 65b : Binary XLPP/PA6 systems water vapour permeability

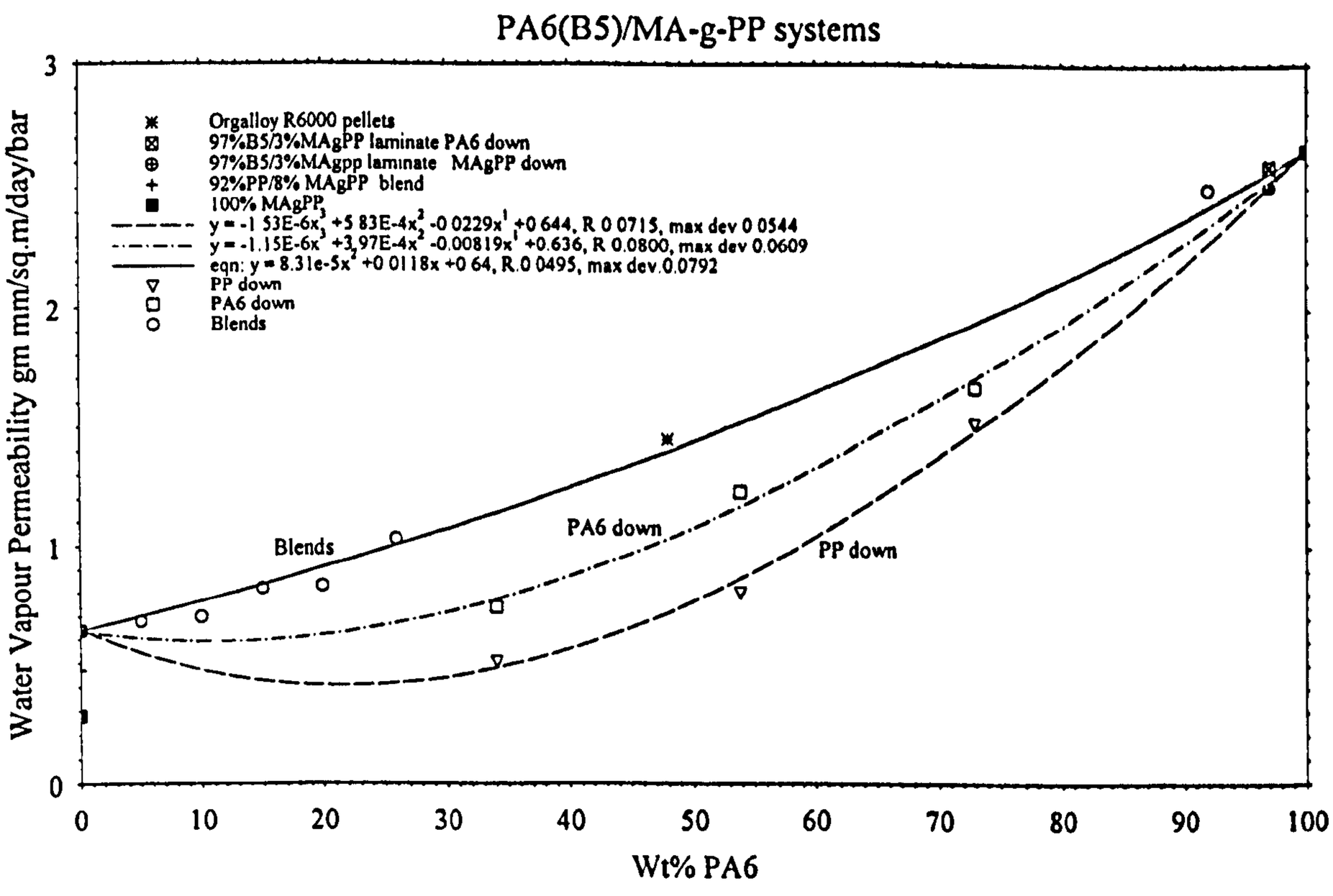

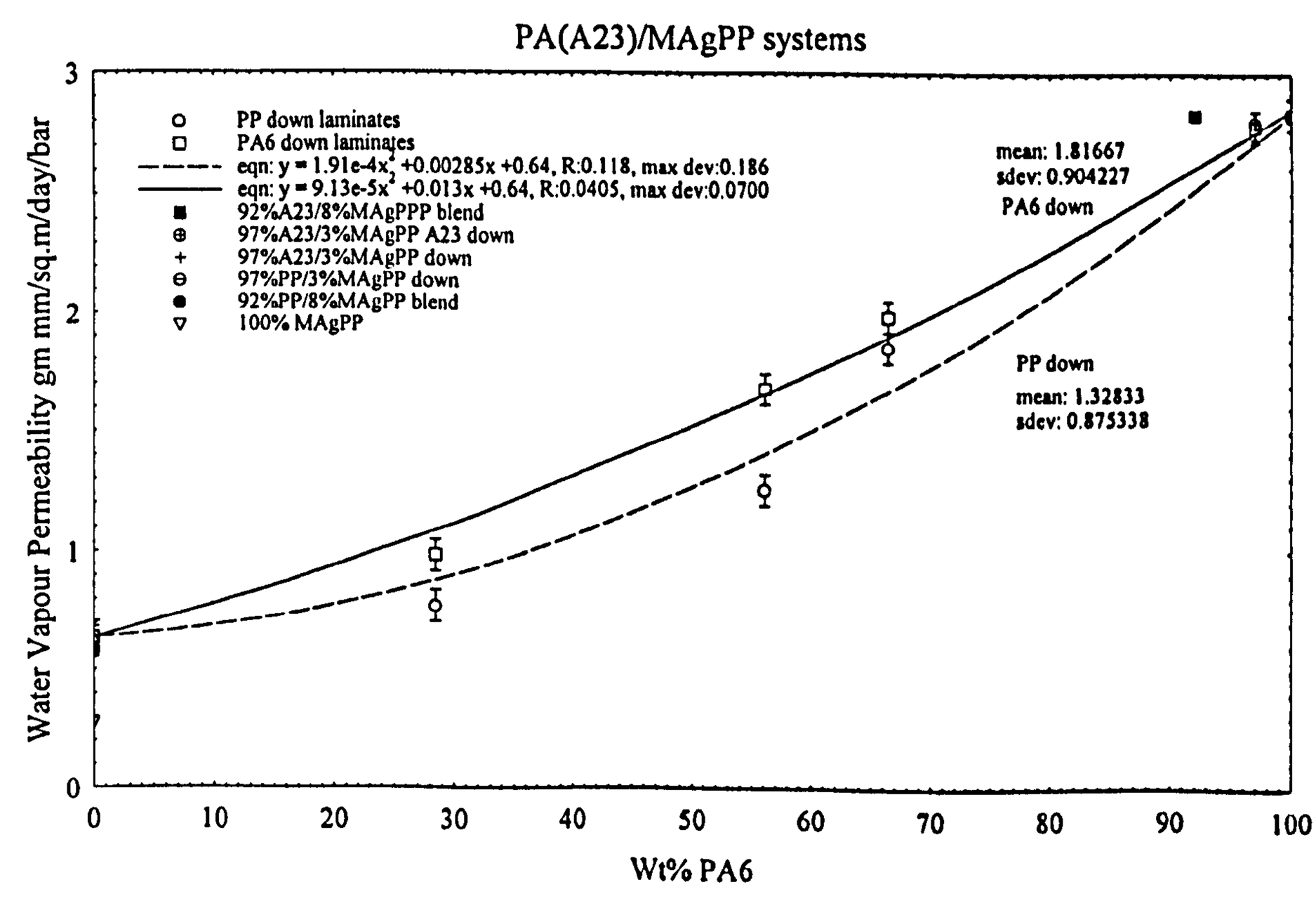

Figure 66 : MA-g-PP compatibilized systems water vapour permeability

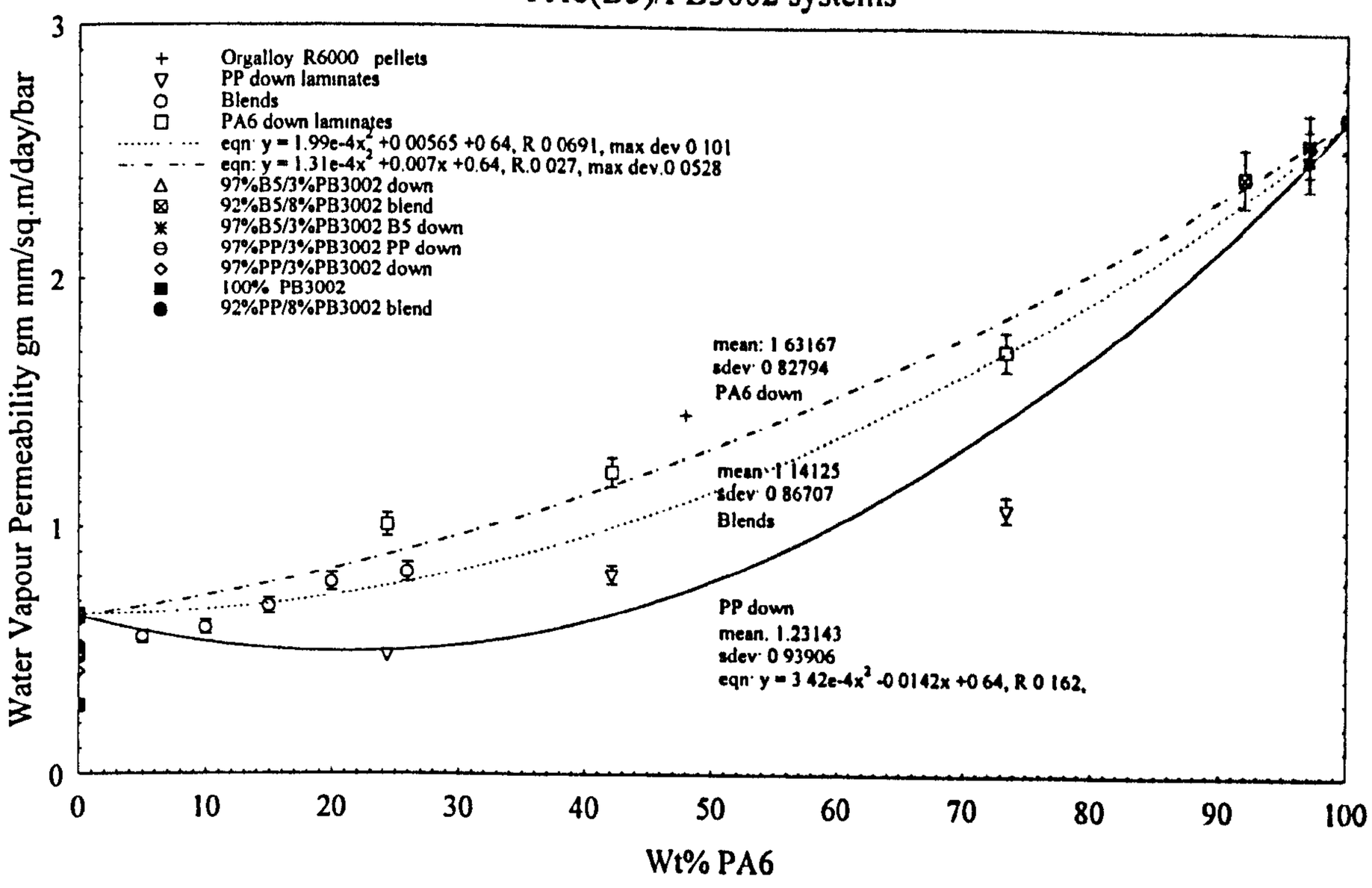

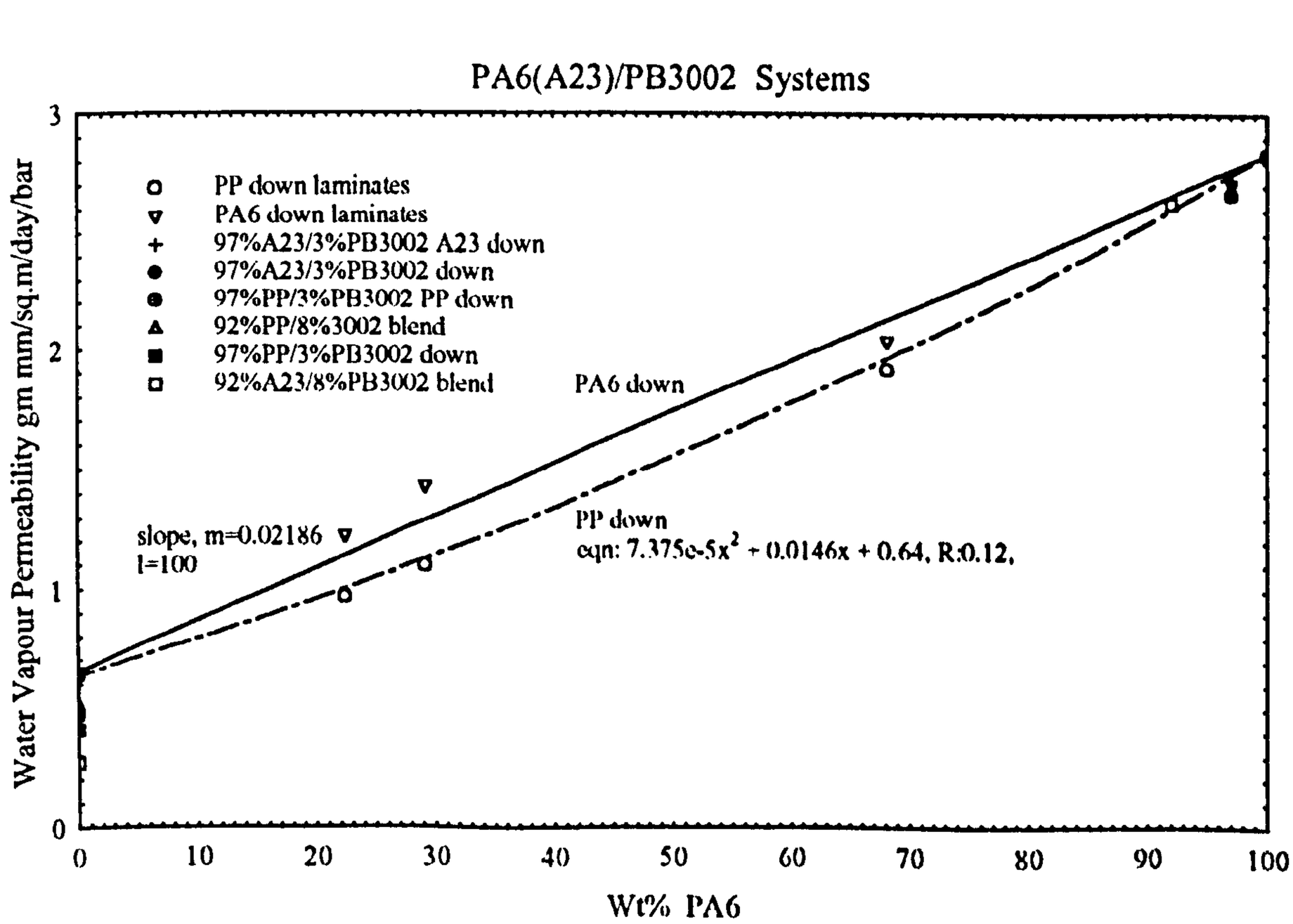

Figure 67 : PB3002 compatibilized systems water vapour permeability

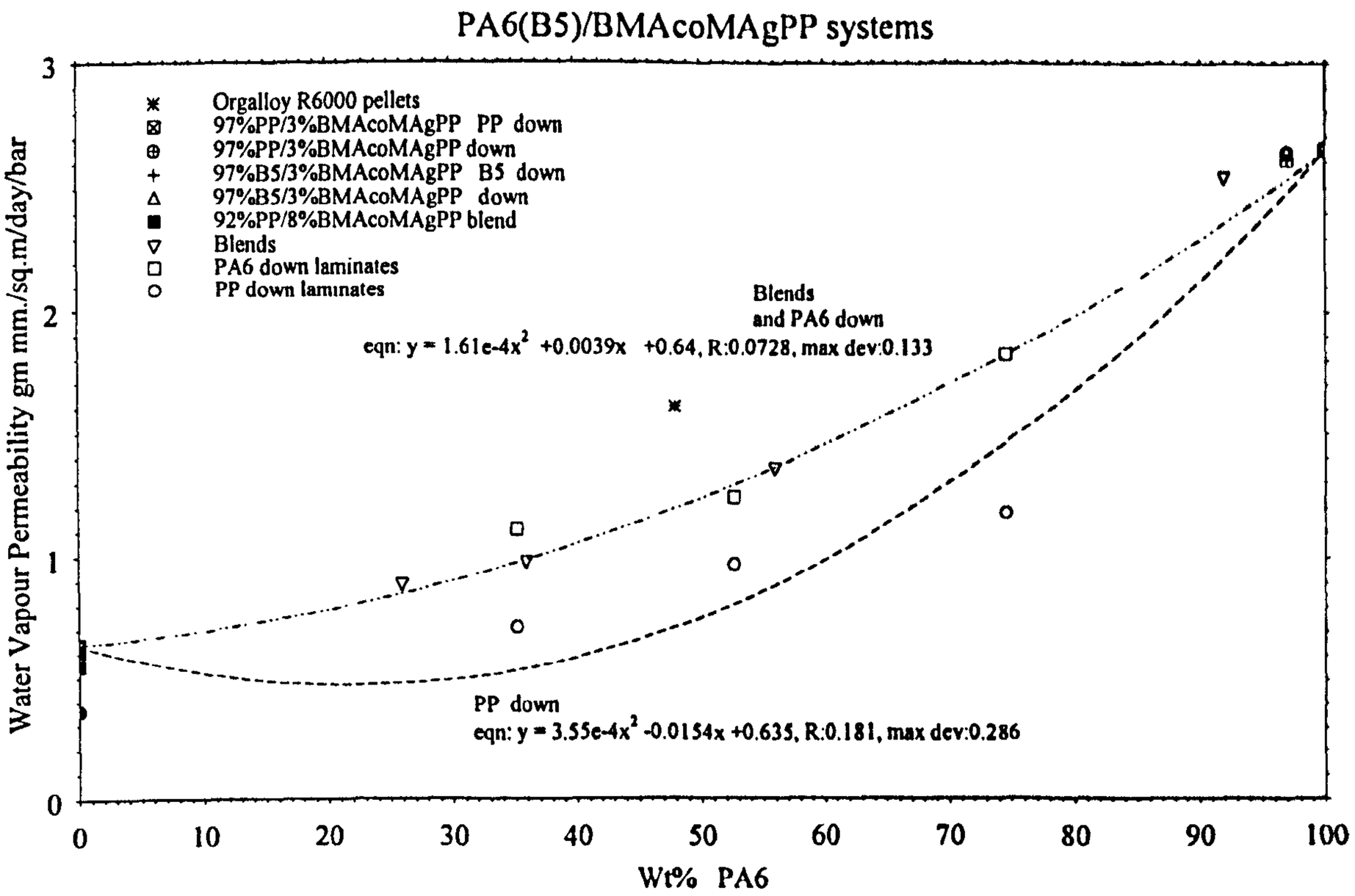

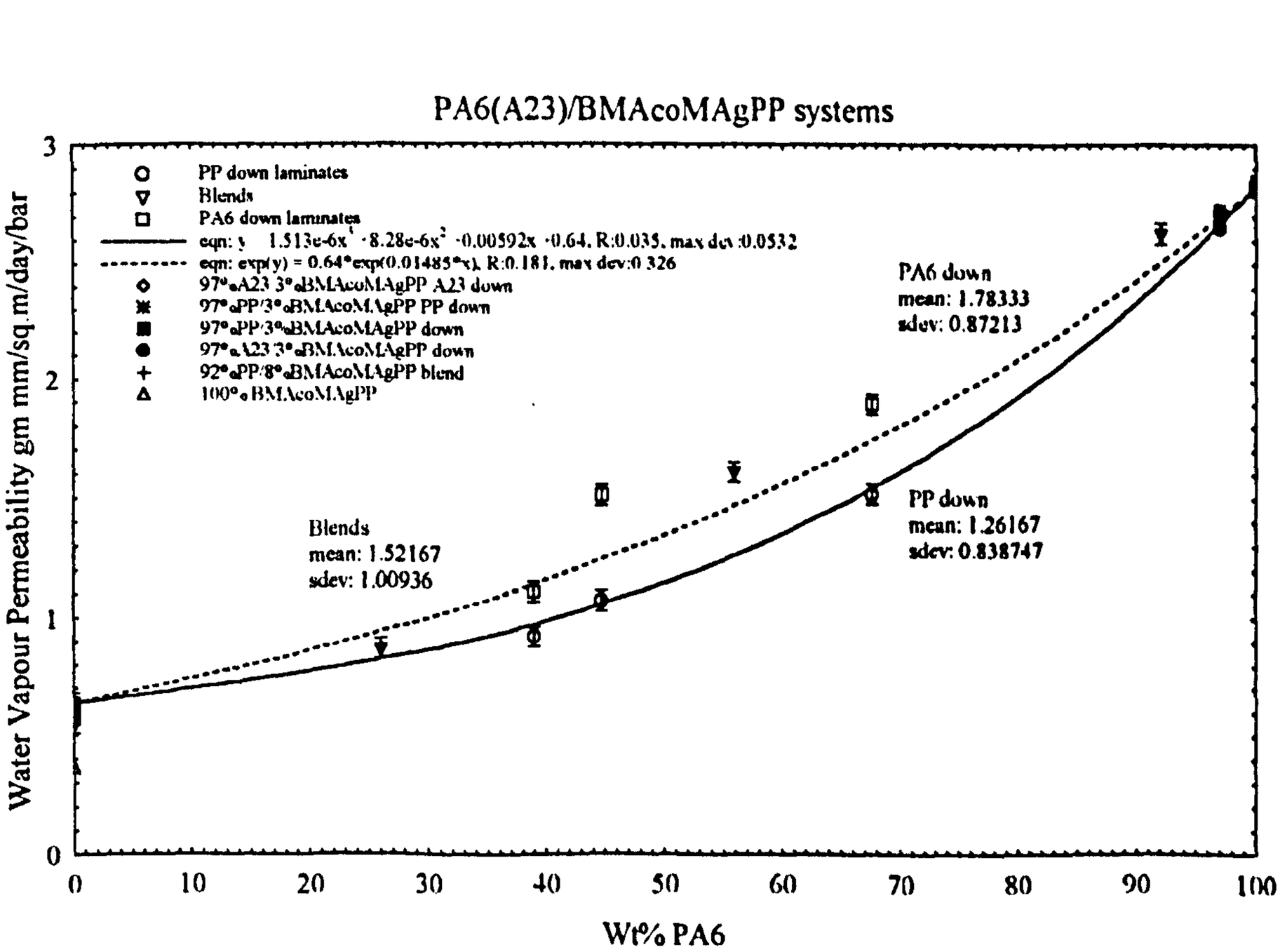

Figure 68 : BMAcoMAgPP compatibilized systems water vapour permeability

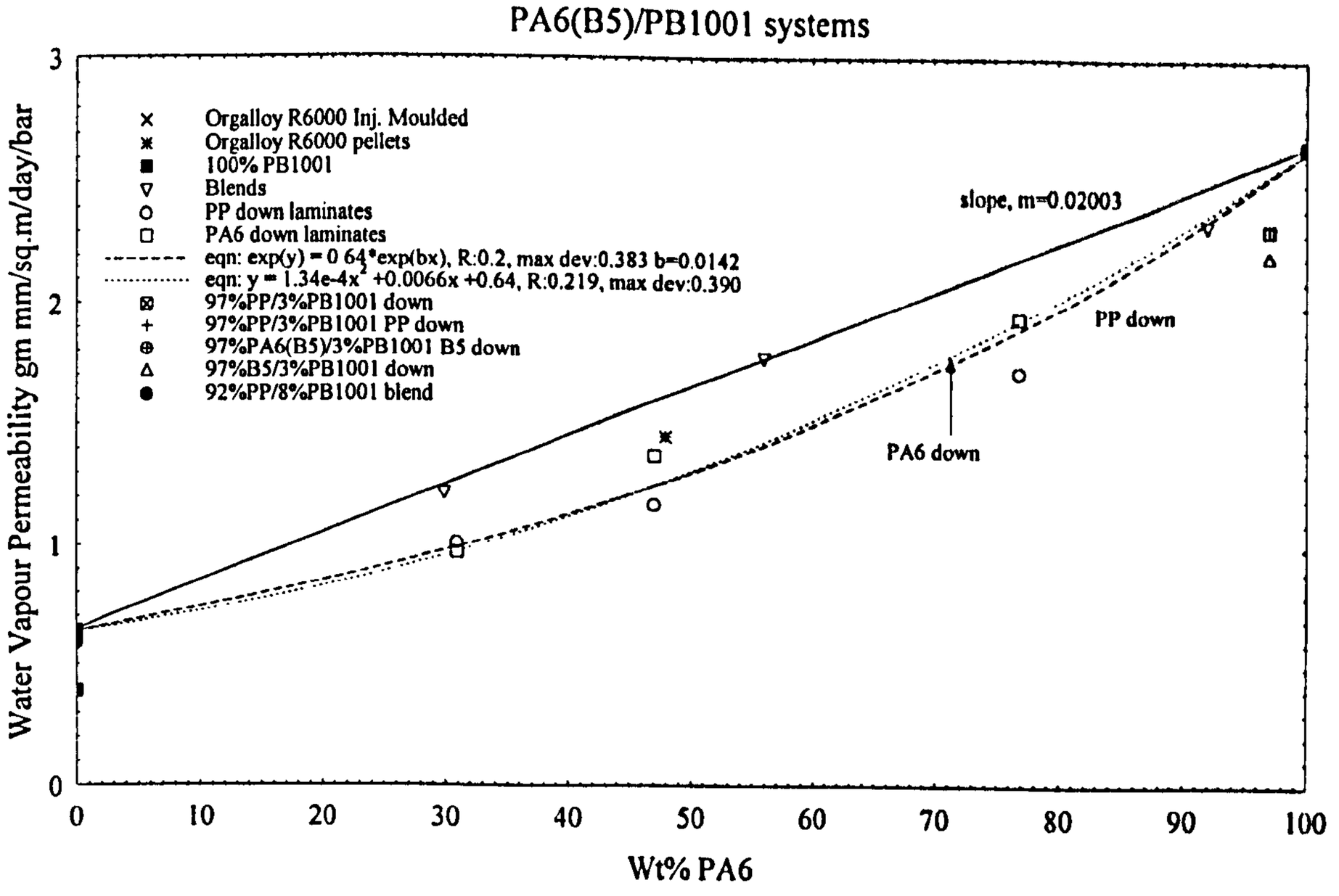

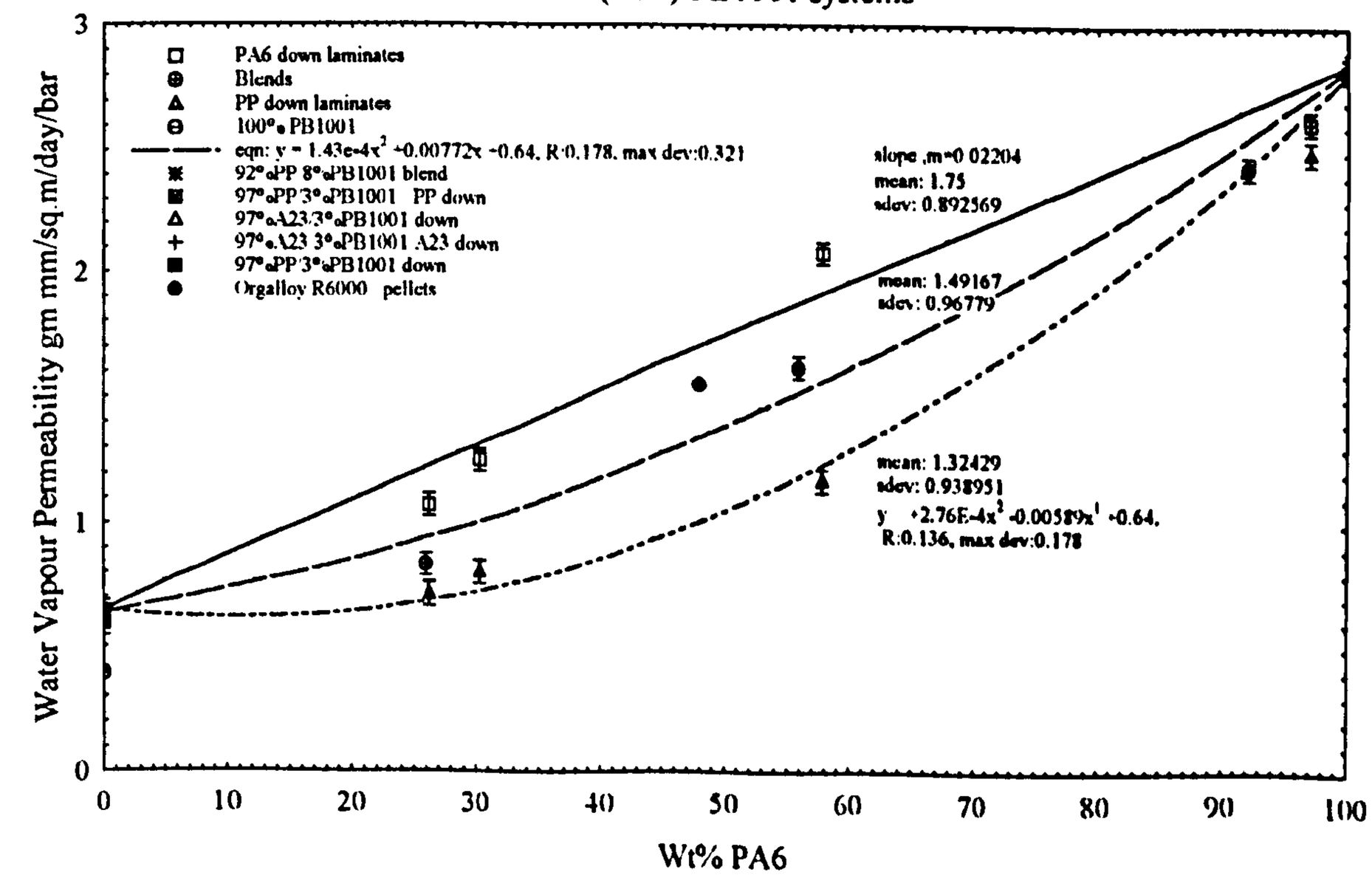

Figure 69 : PB1001 compatibilized systems water vapour permeability

the overall composite/blend/laminate permeability. However, in this work another empirical model was found to match the majority of experimental results. The general equation to describe this relationship is :

$$P^n = \Sigma_i P^n_i C_i \text{ ---------- [64]}$$

where, the multiphase permeability, raised to constant power n, is the sum of each component permeability raised to power n, multiplied by the component concentration. In this work, the latter term is the mass fraction, and for two component systems, the mass fraction subtracted from unity. For a three component system, the sum of the mass fractions of the other two components would be subtracted from unity. The nonemclature used from now on in this work for the laminate systems water vapour permeability is that "PP down" and "PA6 down" refer to the PP being nearest the water or the PA6 being nearest the water, respectively.

4.6.1.2 Binary PP/PA6 systems water vapour permeability

The water vapour permeability for both the binary PP/PA6 blends and laminates is shown in Figure 65a. Promising results have been obtained with the PP/PA6(B5) laminate combination, since little difference is observed between the PP or the PA6 layer being nearest the permeant. The scatter is smoother for PA6 nearest the penetrant, unlike that for the converse. Non-linear behaviour is observed in both cases. Generally speaking, for the lower barrier PA6(A23) both nearest the penetrant and the converse, an exponential relationship can be observed, see equ'n.[69]. For both the binary PP/B5 and PP/A23 blend systems, a similar linear additivity rule exists between the water vapour permeability and PA6 concentration.

Water vapour permeability results for some laminates and blends fitted the logarithmic relationship :

$$\ln P = \phi_1 \ln P_1 + \phi_2 \ln P_2 \text{ ---------- [65]}$$

where ϕ_n is the component volume fraction, and P_n is a component permeability. From the linear parallel equation at 60wt% B5 :

$$P = \phi_1 P_1 + \phi_2 P_2 \text{ ---------- [66]}$$

the water vapour permeability value obtained is 1.84 gm mm/m^2/day/bar, and from the blend linear relationship straight line, the value obtained is 1.85. For the PP down laminates the value obtained at 60wt% B5 from the inverse parallel equation :

$$1/P = \phi_1/P_1 + \phi_2/P_2 \text{ ---------- [67]}$$

is 1.09 gm mm/m^2/day/bar.

The A23/PP blends experimental values coincide with linear concentration dependence, equ'n.[66], while for laminates, an exponential dependence, equ'n.[65], has been observed, see Figure 65a. Both the laminate data sets for the A23 are close together, possibly due to the similar melt viscosities of the homopolymers providing improved adhesion and homogeneity of the laminates.

The blends with both PA6's show a linear additivity dependence of the water vapour permeability with PA6 concentration. However, for the binary laminates, an improvement in permeability was obtained due to non-linear behaviour.

4.6.1.3 Binary XLPP/PA6 systems water vapour permeability

Exponential behaviour, equ'n.[65], describes the XLPP/B5 blends, B5 down/XLPP laminates (which share the same curve of Figure 65b), and XLPP/Plast.PA6(B5) blends. For the XLPP/PA6(A23) laminates the relationship is non-linear for the XLPP down systems and linear for the PA6 down systems. The XLPP down/B5 laminates and PP/Plast.B5 blends also exhibit non-linear behaviour, although the data are scattered for the latter. Note that the XLPP low water vapour permeability has counteracted the high permeability to some extent for these systems. Plasticized B5 laminates were not prepared, for comparison with the plasticized B5 blends.

4.6.1.4 Ternary compatibilized systems water vapour permeability

For compatibilized ternary systems, both laminates and blends, a similar additivity function relating the water vapour permeability to the PA6 concentration as that found for binary systems, has been found. The additivity function is shifted in the direction of better barrier, towards that of a commercial PP/PA6 blend, Orgalloy R6000.

Data for binary laminates consisting of the homopolymers and each of $\approx$ 3wt% of the compatibilizers, without any PP, is included in Figures 65a-69. In addition, data for

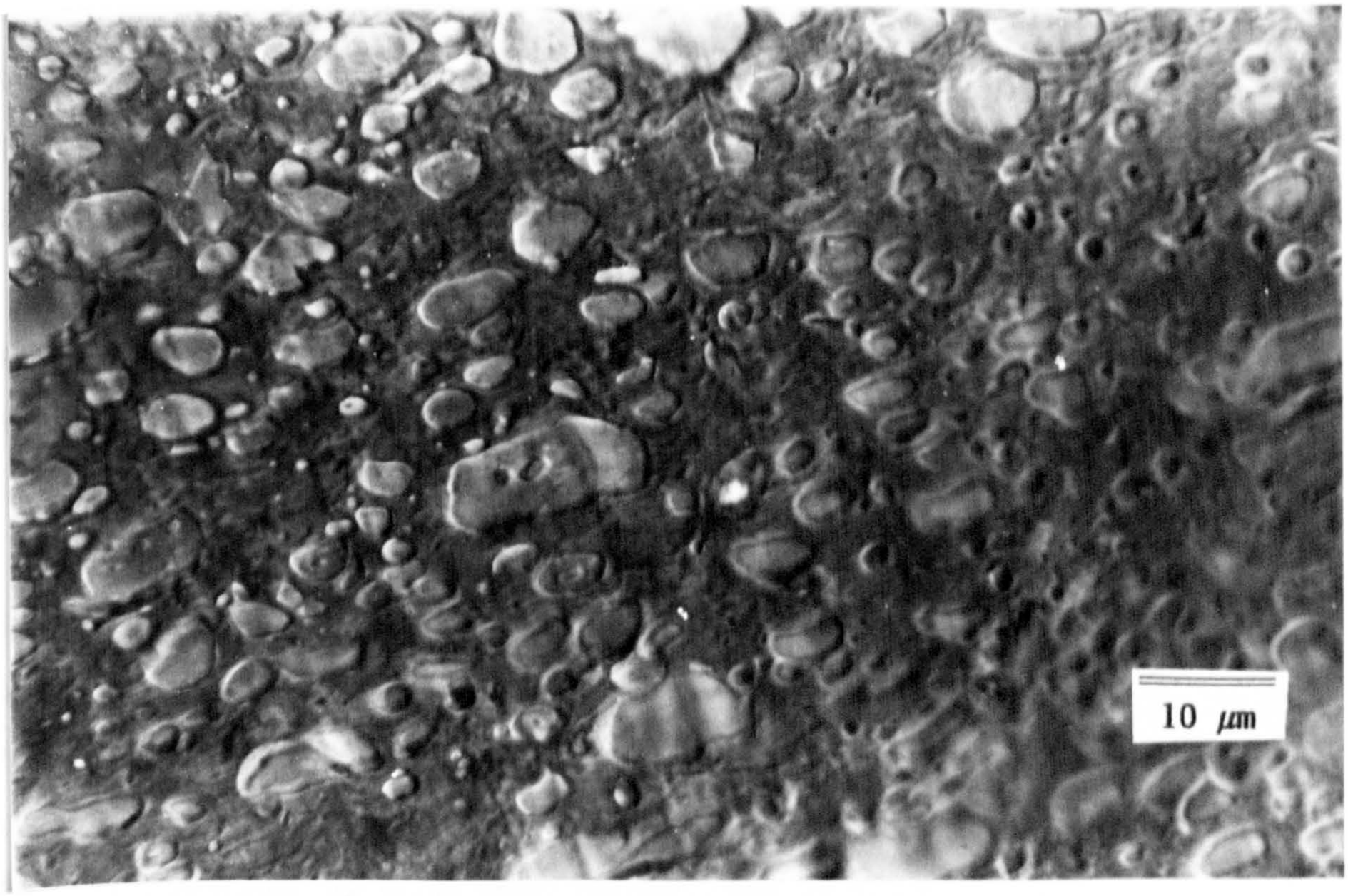

Figure 70 : Light Micrograph of 62wt% PP/30wt% PA6(B5)/8wt% PB1001 blend (DIC)

binary blends consisting of 8wt% of the compatibilizers with the homopolymers is included in the same figures.

For the MAgPP compatibilized B5 systems (Figure 66) slight reductions in water vapour permeability are seen for the PP down laminates as compared to both the blends and the PA6 down laminates. So, the blends are inferior to both of the laminated systems and the relationship is non-linear for polynomial for the B5/MAgPP PA6 and PP down laminated systems. From the MAgPP/A23 compatibilized laminate data the conclusion to be drawn is that the PP down system is slightly less permeable than the PA6 down system, as compared to the a similar relationship for the PP down system.

The effect of the PB3002 compatibilizer on the blends water vapour permeability is shown in Figure 67. For 0% PA6, the value for PP is higher than for the blend of PP with PB3002. The lowest value shown is that for the pure compatibilizer permeability, showing that the compatibilizer has very different water vapour barrier properties. It is again the most efficient barrier in the form of laminates, where it is only included as

3wt%, as compared to blends. The good performance of Orgalloy R6000 can therefore be explained by the prescence of a suitable compatibilizer.

The ternary BMAcoMAgPP/B5 laminates, see Figure 68, where the PP is down are slightly superior to both the blends and the B5 down laminates. The relationship is the same non-linear curve for the blends and PA6 down systems, although the PP down system data is scattered, with a different non-linearality. Again for A23 systems, the PA6 down and blend data are very similar and the PP down data are also scattered for the A23 systems.

The PB1001 ternary systems blends/laminates, Figure 69, for B5 blends, follow a linear relationship, whereas for the PP down laminate systems, the relationship is non-linear for the PA6 down systems. For A23 systems, the PP down laminates and blends follow a non-linear relationship, whereas for the PP down laminates, the relationship is linear. At low PA6 concentrations, the water vapour permeability is similar for all three B5 systems and the microstructure of the 30wt% B5 blend certainly supports this (Figure 70), since elongated particles are observed, but for the 56wt% material, a finer dispersion, exhibiting phase-in-phase behaviour, is observed, which supports the water permeability value lying on the exponential curve. For the A23 systems, the trend is similar, with some particle elongation/phase-in-phase behaviour at 26wt% PA6 concentration (Figure 38), with a finer dispersion being seen for the 56wt% A23 blend, (Figures 34/35). For both PP and PA6 down B5 system laminates, the exponential relationship of equ'n.[65] approximates to the data well.

4.6.1.5 Compatibilizer and Tie Layer Adhesive water vapour permeability

In order to establish more precisely the mechanism by which the compatibilizer can effect the water vapour permeability, tests were conducted on 100% compatibilizers and tie layer adhesives, as shown in Table 10. The properties of the tie-layer adhesives is described elsewhere in section 3.3.

4.6.1.6 Tied Laminate water vapour permeability

The binary laminate water vapour permeabilities are compared with those of the tie layered materials in Figures 71 and 72. For PP/B5 systems with PP being closer to the permeant, the results show that despite Scotchgrip having an inferior water vapour

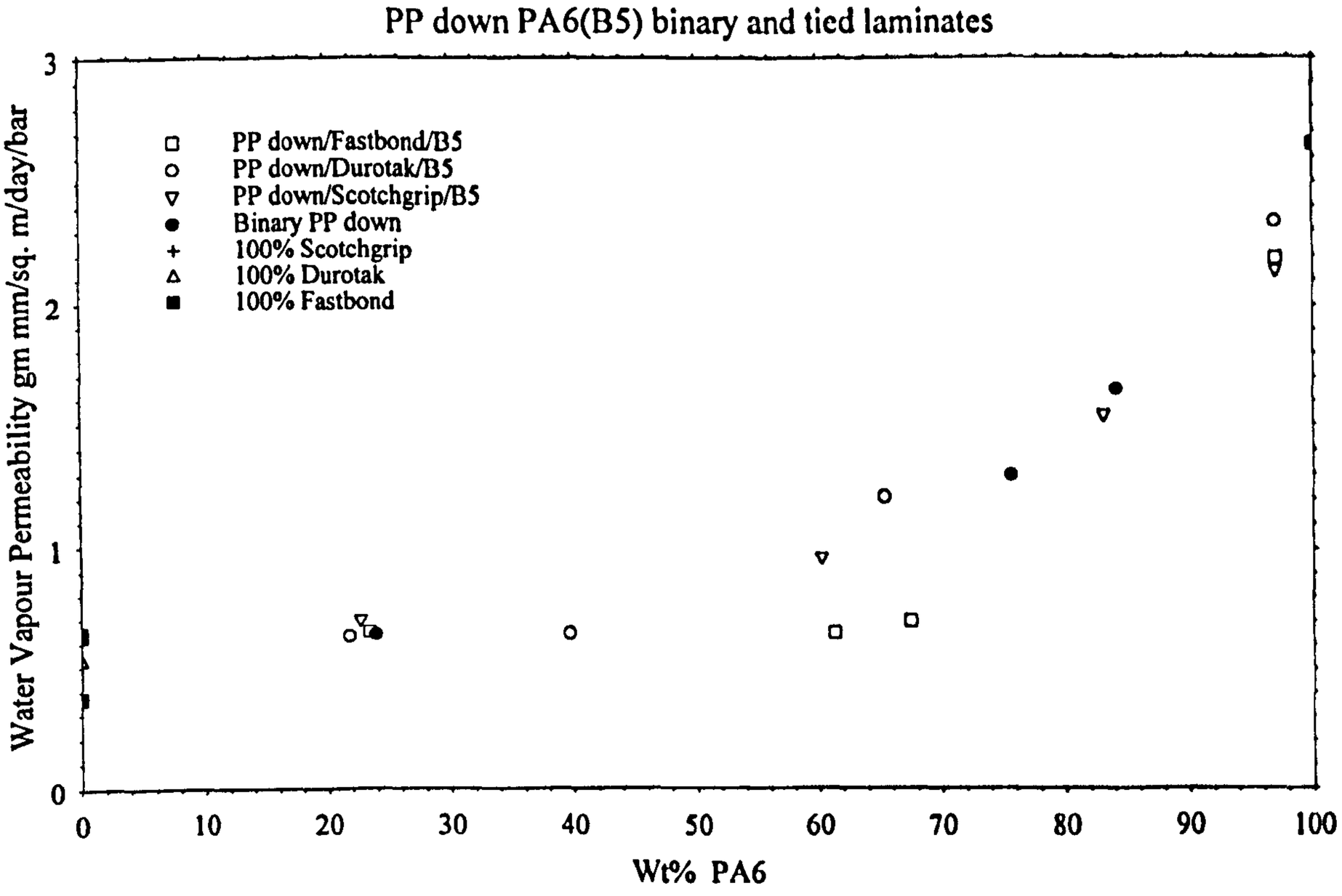

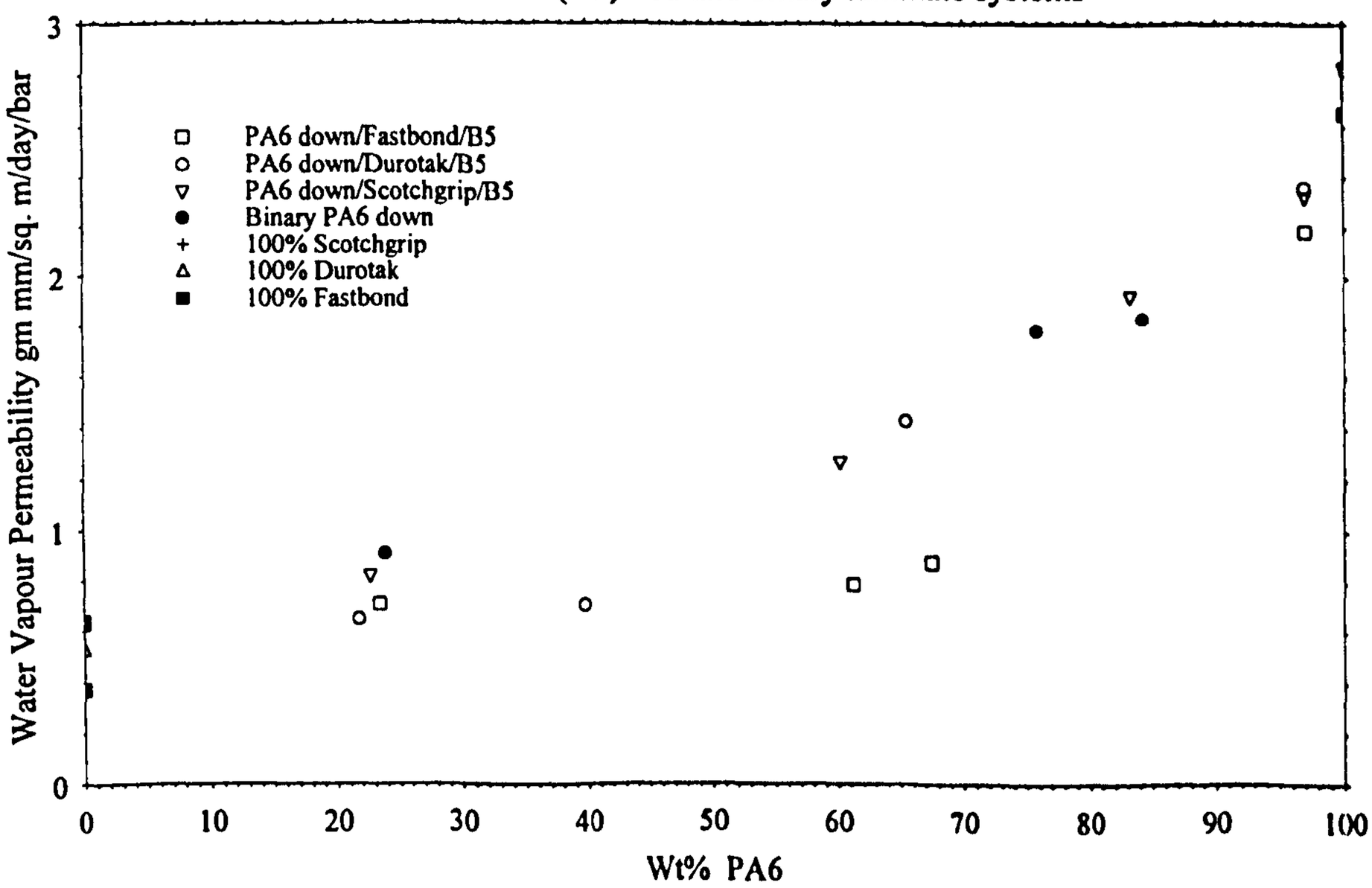

Figure 71 : Water Vapour Permeability of PA6(B5) tied laminates

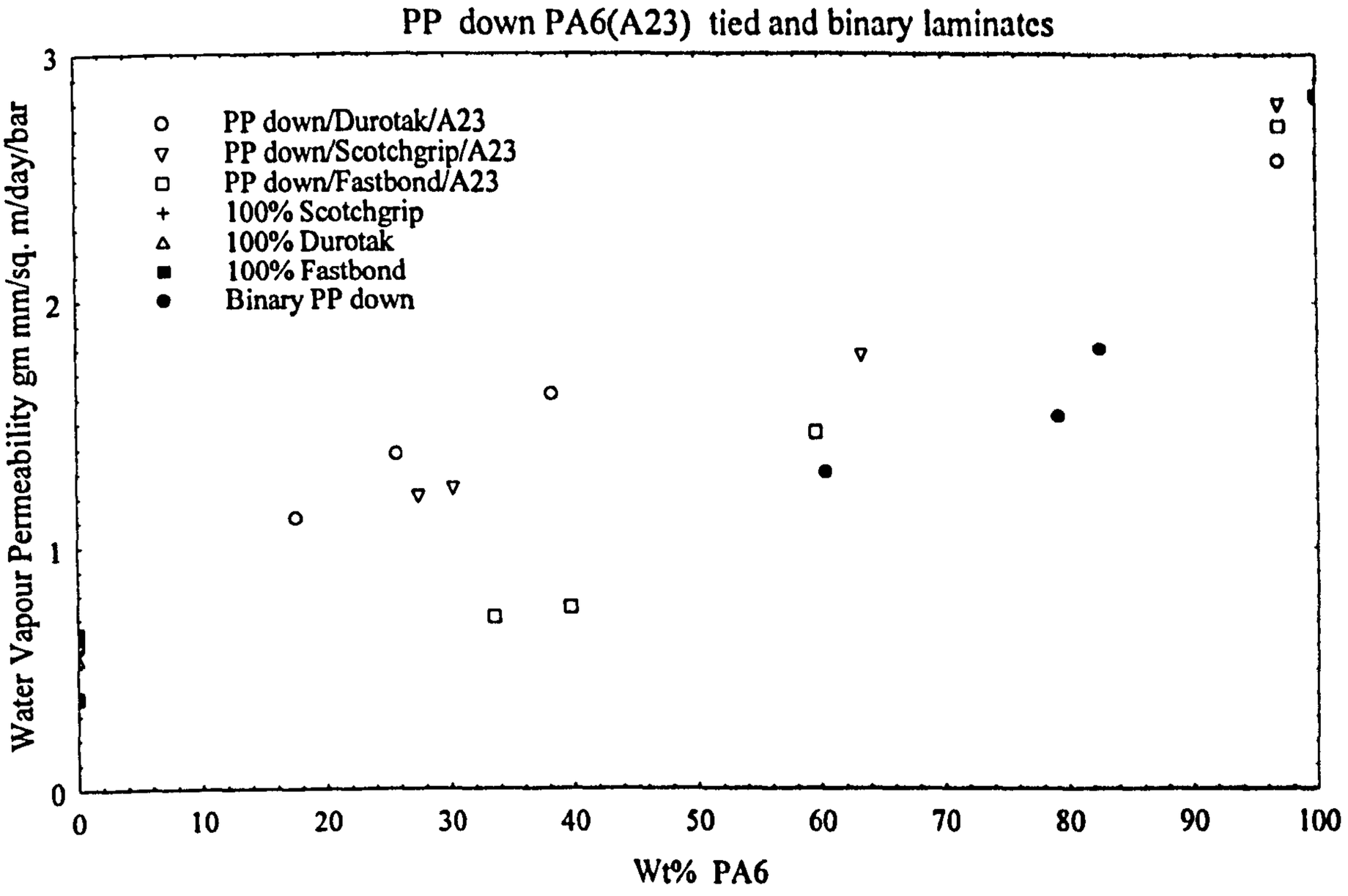

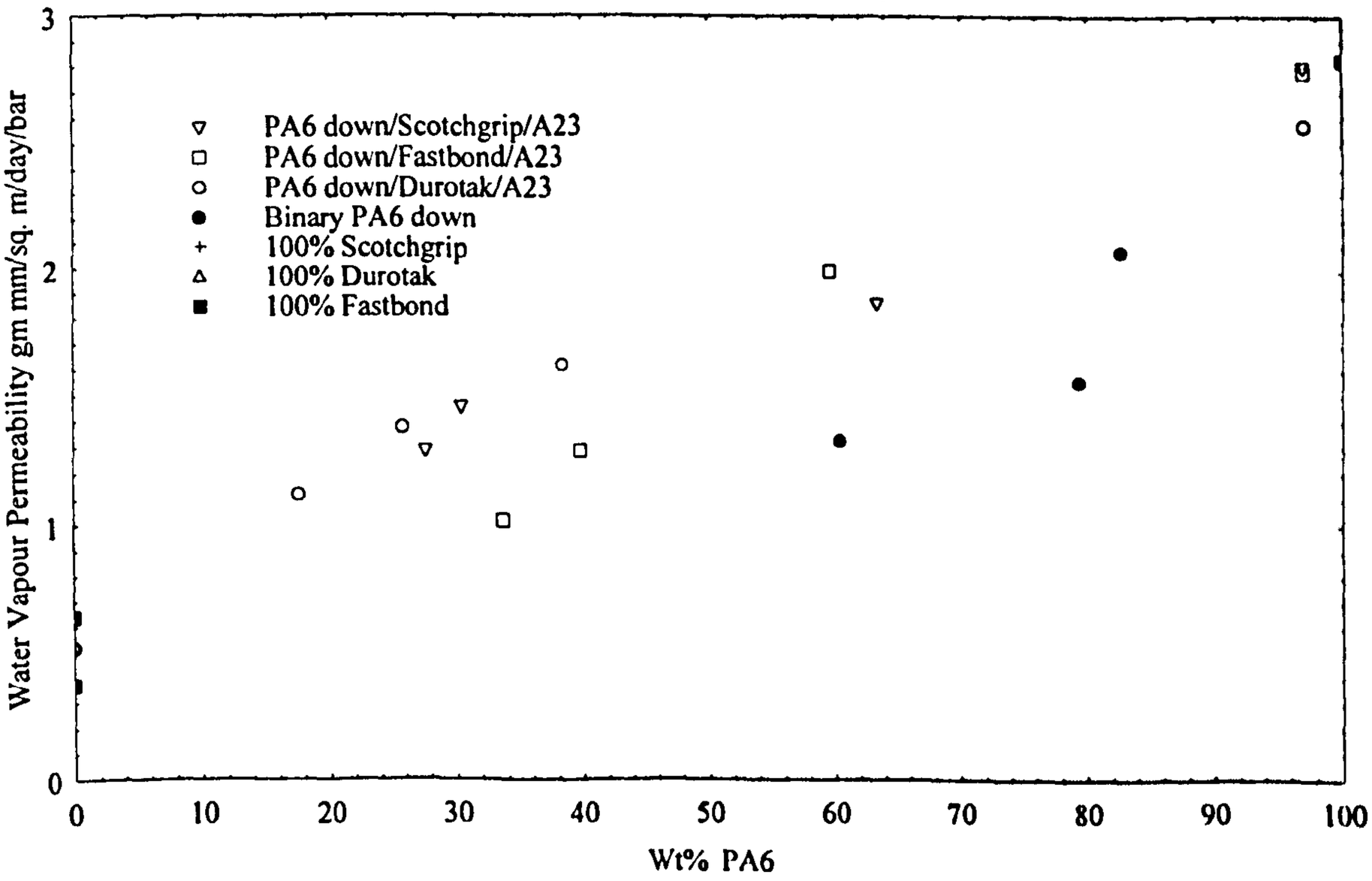

Figure 72 : Water vapour permeability of PA6(A23) tied laminates

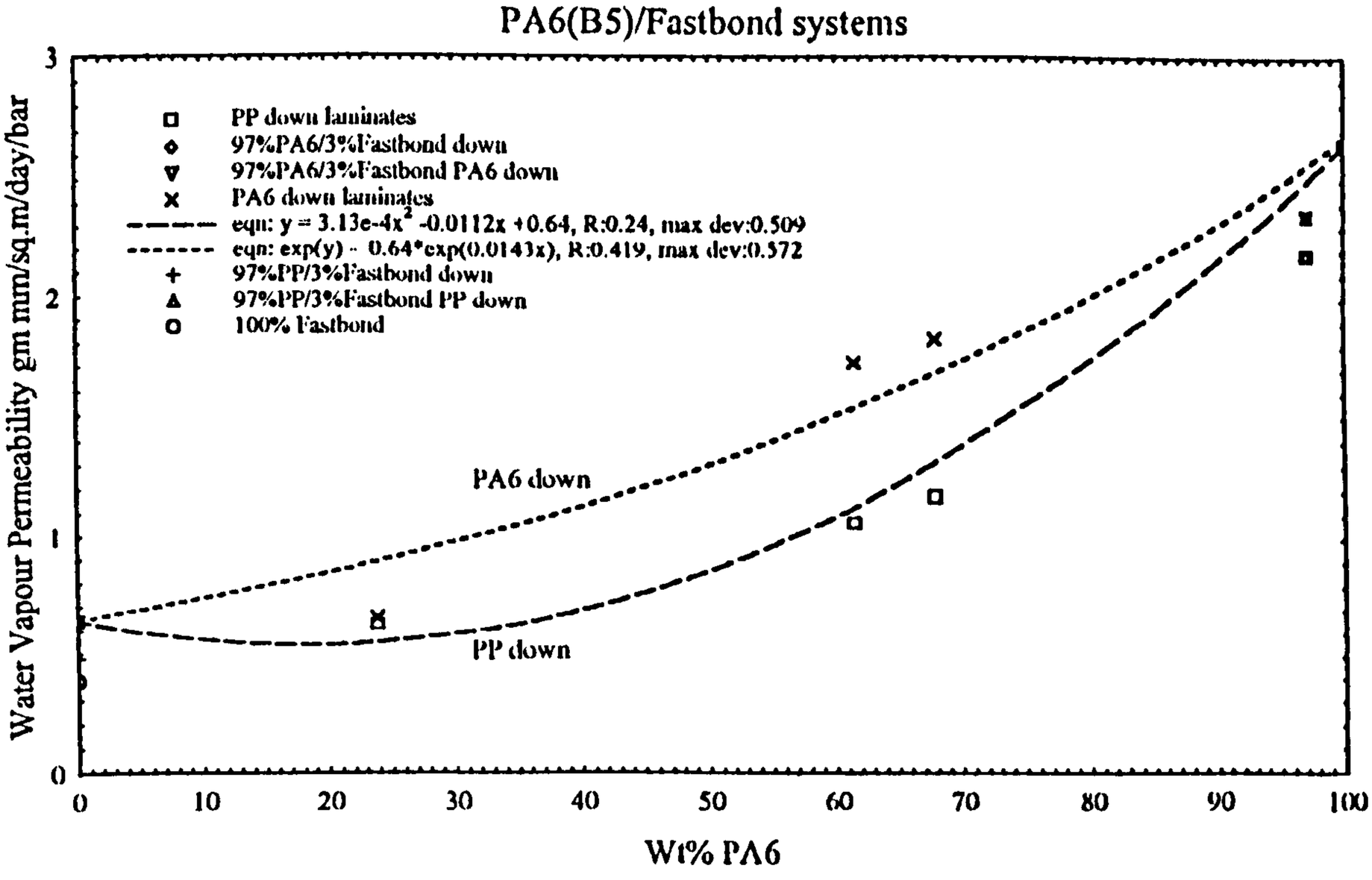

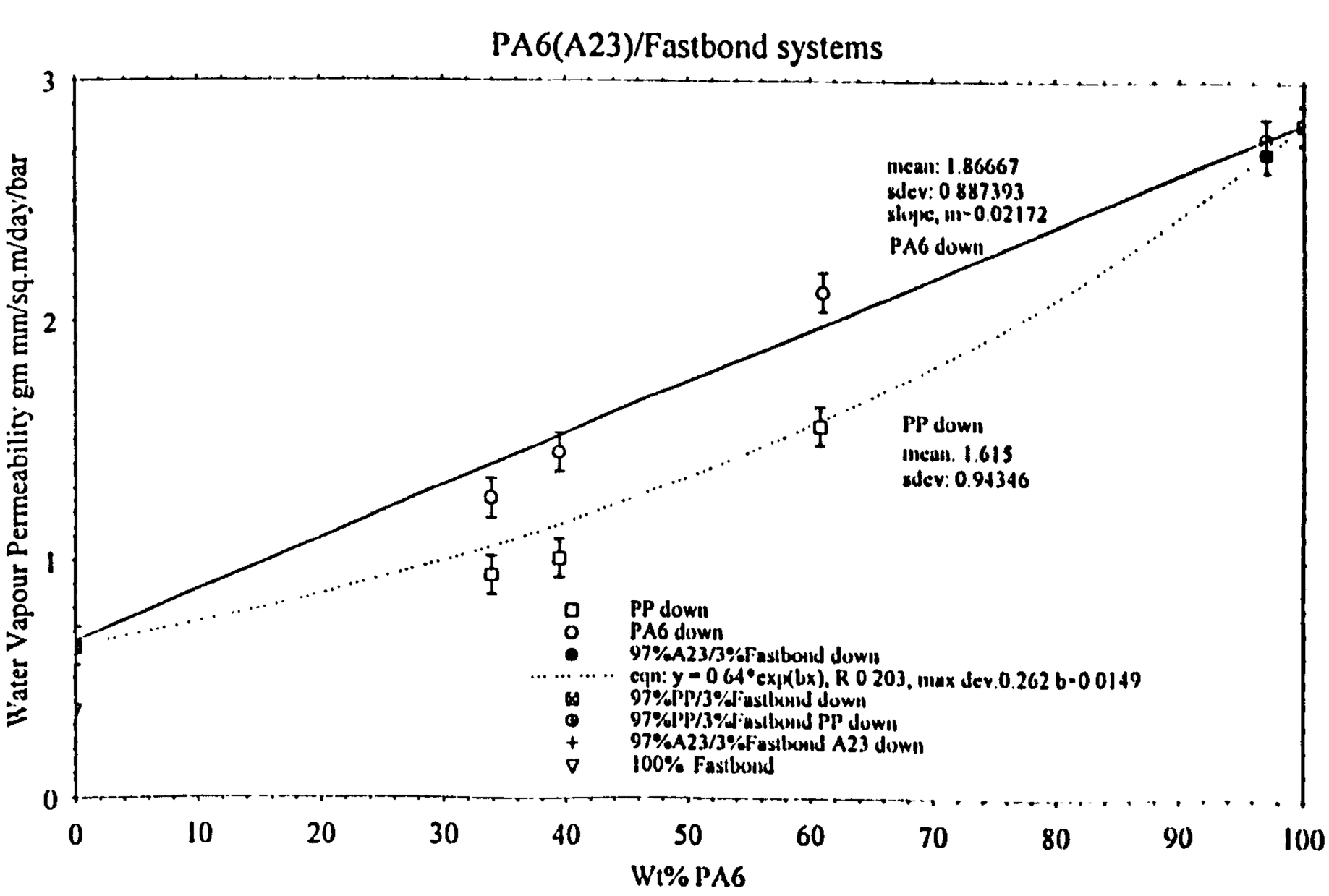

Figure 73 : Water vapour permeability of Fastbond tied laminates

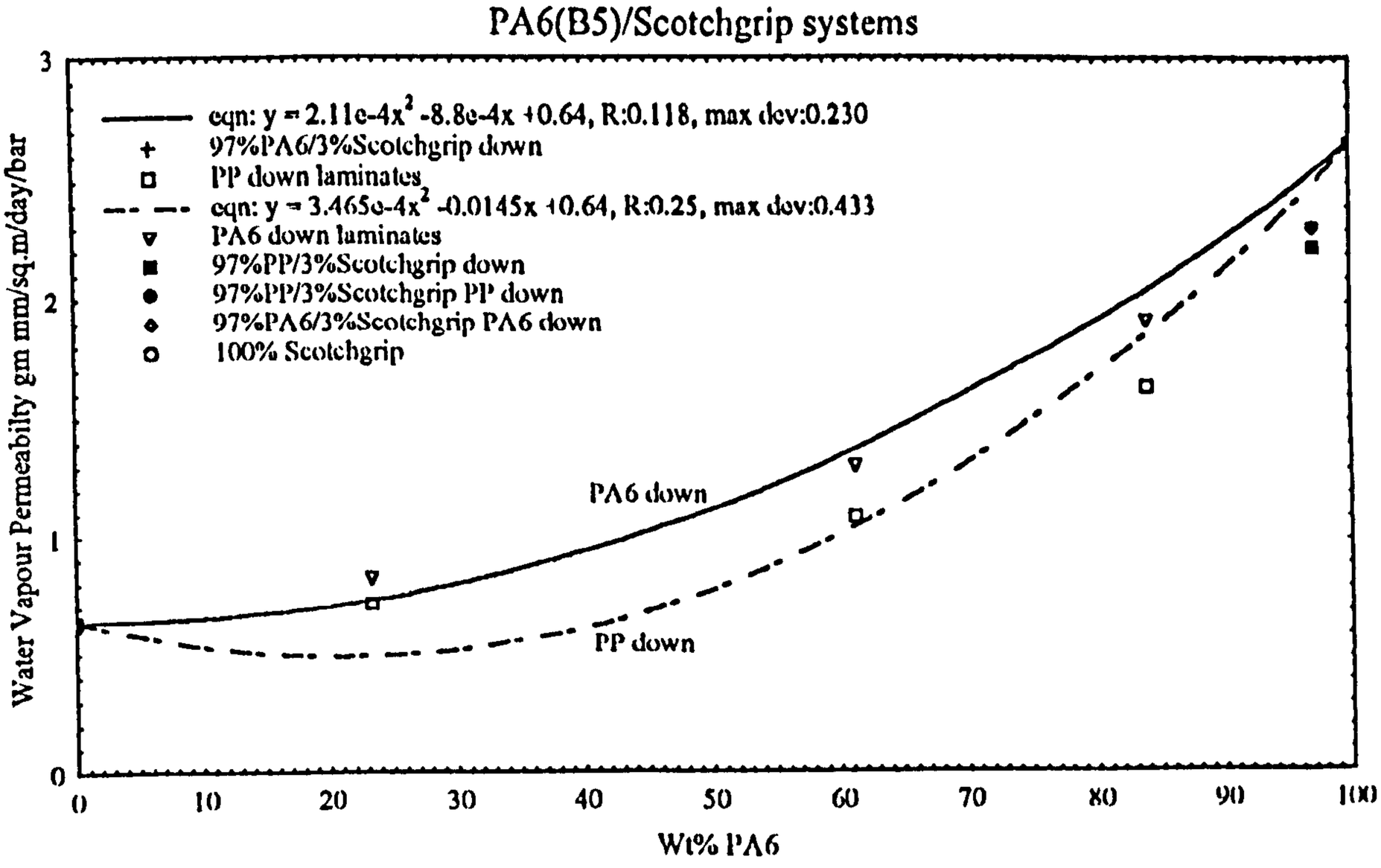

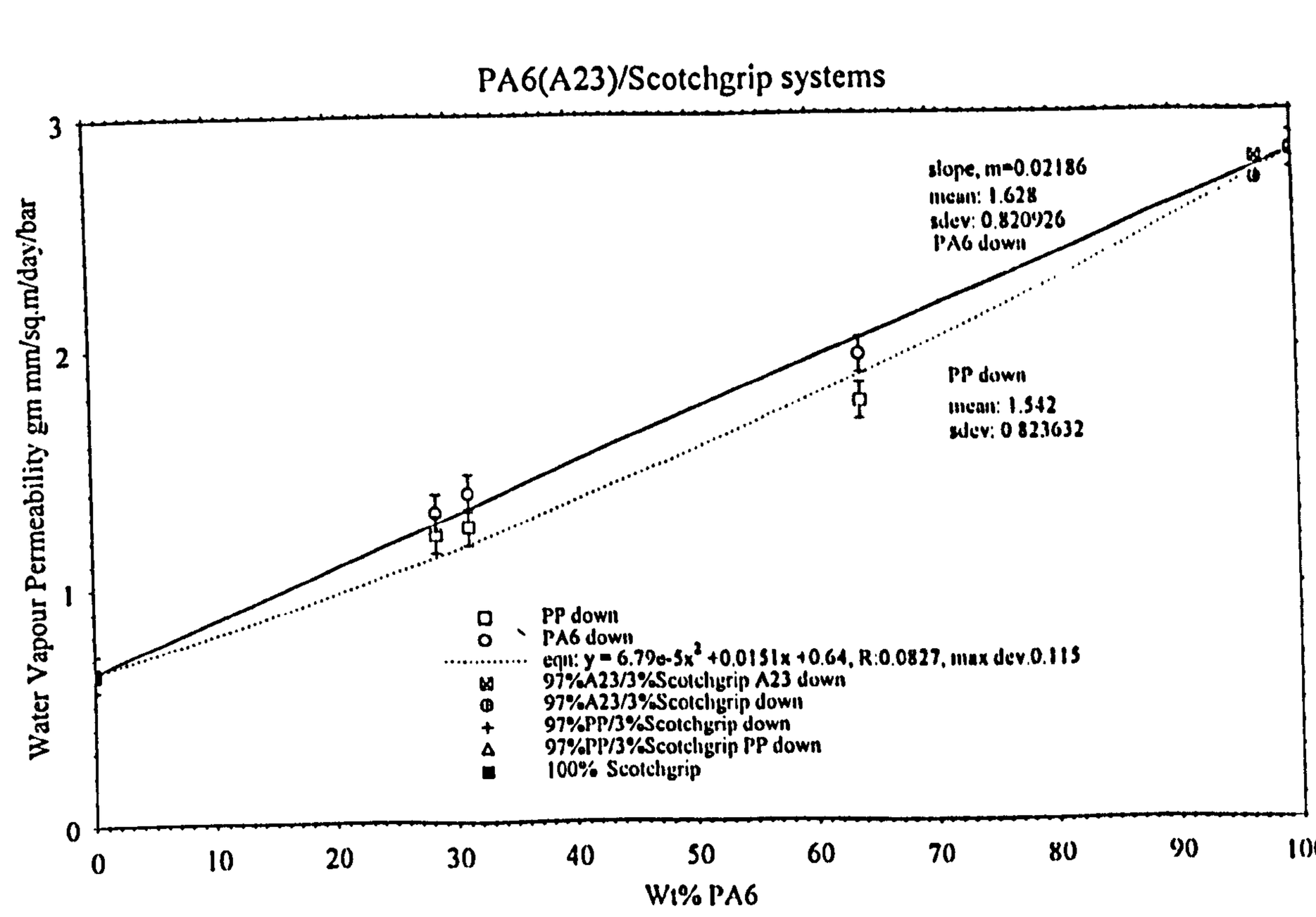

Figure 74 : Water vapour permeability of Scotchgrip tied laminates

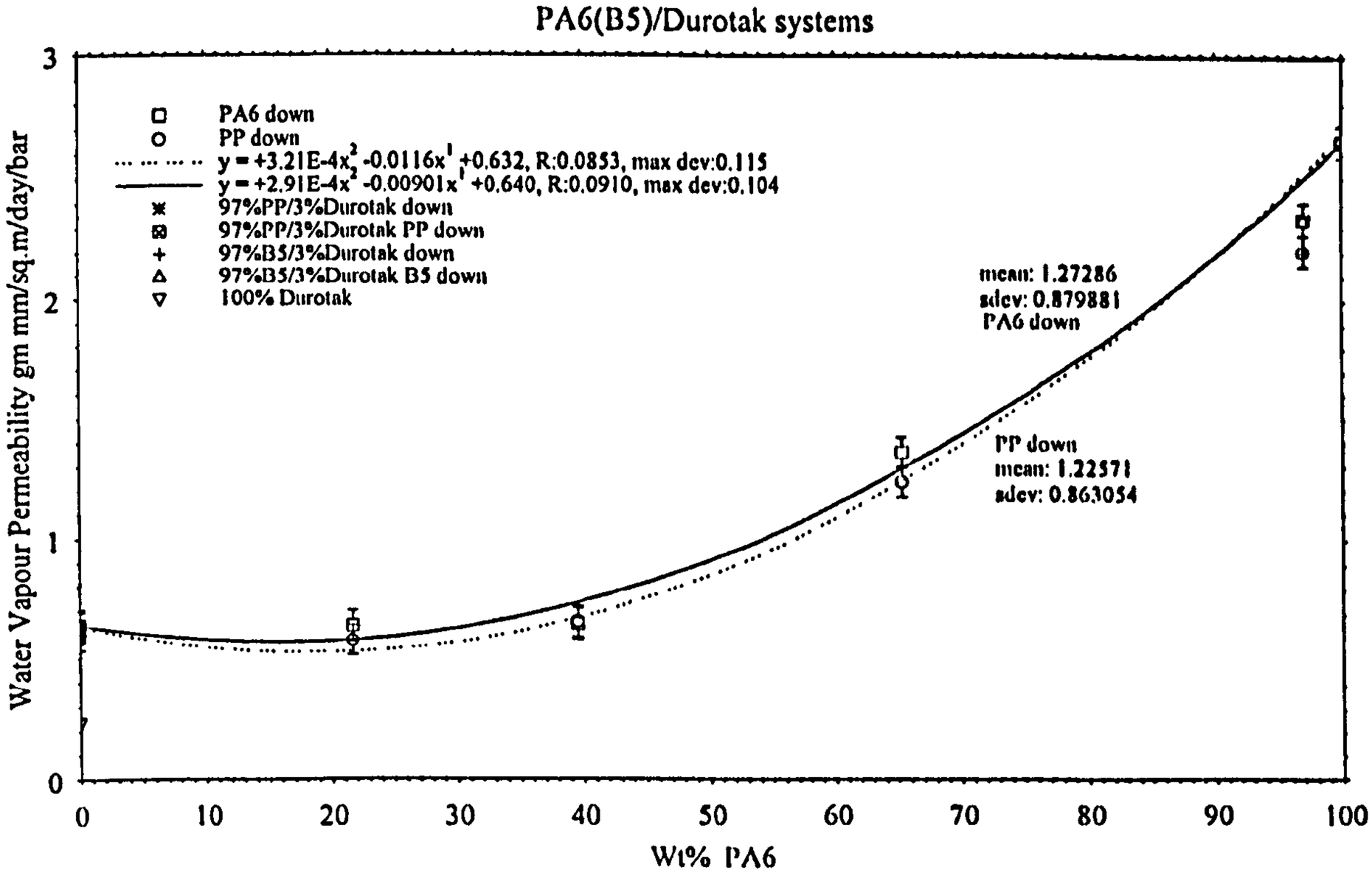

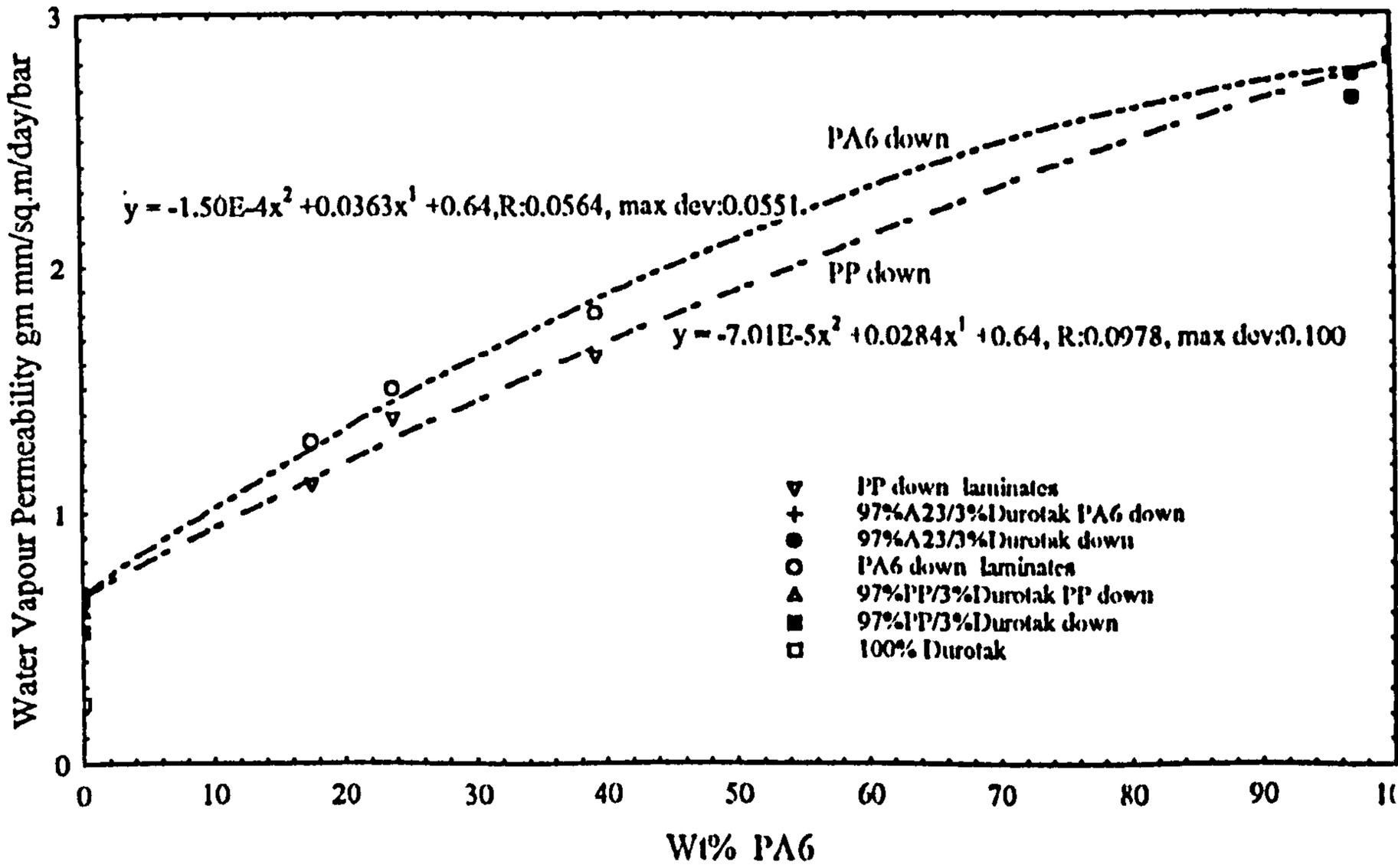

Figure 75 : Water vapour permeability of Durotak tied laminates

permeability for Durotak or Fastbond, at higher PA6 concentration, the system shows surprisingly very similar permeability to the other tied systems. At high PA6 concentration, Durotak is marginally the superior system. However, when the PA6 is nearest to the penetrant, the Durotak system shows lower permeabilities at all PA6 concentrations. At higher PA6 concentration, the Fastbond/Scotchgrip tied systems showing higher permeability than the binary systems. The explanation for this is that the hydrophillicity of the toluene based Durotak displays a synergism with the water vapour plasticized B5, which is not possible when the PP is nearer to the penetrant.

Table 10 : Compatibilizer and tie layer adhesive water vapour permeabilities

Material	*Water Vapour Permeability, g mm/m²/day/bar*
100wt% BP Polybond PB3002	0.27
MA-g-PP	0.28
100wt% BP Polybond PB1001	0.39
(BMA-co-MA)-g-PP	0.36
3M Fastbond 30	0.37
3M Scotchgrip 4235	0.63
Durotak 380-1846	0.53
Tufloc TLC06	not known

Note that data for binary laminates containing ≈ 3wt% of the adhesive and each of the PP or PA6 are also included in Figures 71-75. The water vapour permeability is measured, both with the homopolymer or adhesive closer to the permeant.

For the A23 systems, although the results are more scattered, with the PP nearer the penetrant, a trend for Durotak systems being inferior to the other systems, including binary systems exists. At low PA6 concentrations the Fastbond systems are superior and the Durotak data appear to lie on a straight line.

Where the PA6 is closest to the penetrant, the binary systems are of lower permeability, with Scotchgrip showing the better tied barrier at mid PA6 concentration, Durotak at high PA6 concentration, and Fastbond again performing better at lower concentration. More surprising is the apparent synergism of the 33.5wt% PA6 PP down material, since

the structure permeability is almost the same as the 40wt% PA6 down material. Even when the PA6 is nearest the penetrant, the permeability is lowest of the tied laminates at 40wt% PA6. Remarkably, a similar phenomena is observed for the slightly more hydrophillic Fastbond adhesive with B5 systems. Up to a PA6 concentration of ≈ 70wt% the water vapour permeability of the PP down systems only increases by ≈ 90% as compared to 100% PP. The PA6 down system shows at the same PA6 concentration, an increase of ≈ 260%.

100% Scotchgrip is more permeable to water vapour than the other adhesives (Figure 74), and the experimental values with A23 indicate that the synergism which exists for the B5/Durotak systems is absent in this case. The PA6 down systems show a linear relationship of permeability with PA6 concentration, and the PP down systems a non-linear relationship. For A23/Durotak systems, the difference between the two data sets is in the range 11-25%. Surprisingly, both the PP and PA6 down systems show similar positive non-linear deviations from the additivity rule. For the A23/Fastbond systems, the only trend being that the PP down data follow an exponential relationship. The deviation between the PP or the PA6 being nearest the penetrant is in the range 12-51%, whereas for the A23/Scotchgrip system the range is only 4.7-11.6%, indicating that this is possibly a suitable adhesive for this system. Notably, for the B5/Scotchgrip systems, the deviation between the two data sets remains almost constant, with increasing PA6 percentage.

The B5/Fastbond systems again show a clear divergence of the two experimental data sets with PA6 concentration above 24%. The relationship between water vapour permeability and PA6 concentration is non-linear for the PA6 down B5/Fastbond systems and the PP down systems. For the PP down A23 systems, the relationship is exponential and linear for PA6 down, although the data are scattered.

For the B5/Durotak systems, the water vapour permeabilities deviate in the range of 2.23-19%. The data sets difference envelope diverges slightly and then converges again. Both data sets follow closely similar non-linear behaviour. PA6(A23)/Durotak tied laminates also exhibit the same behaviour, but with positive deviation from the additivity rule, indicating that Durotak is possibly not a suitable adhesive for this system.

Figure 73 represents the Fastbond systems, and an exponential relationship approximates for the B5 down laminates, and the inverse equation approximates for the PP down systems, showing non-linearity. Likewise for the A23/Fastbond systems, the linear equ'n. approximates for the PA6 down laminates, and exponentiality applies to the PP down laminates.

4.6.1.7 Summary of Multiphase System Water Vapour Permeabilities

It is clear from the above water vapour permeability results that with the exception of R6000, the blend dispersed phase size shows no correlation with water vapour permeability. In fact, laminated structures with the PP nearest the penetrant showed superior barrier to the blends and also some with the PA6 nearest the penetrant. This included coarse structures showing gross phase-in-phase and/or co-continuous morphology of plasticized B5 and silanated PP. The superior barrier water vapour materials therefore benefit from more hydrophobic functional groups, some of which will be shown later to promote oxygen barrier. This result was also confirmed by measuring the water vapour barrier of binary compatibilizer/PA6 blends. Those not plasticized by the compatibilizer showed better water vapour barrier than 100% PA6, due to an increase in end group hydrogen bonding. The water vapour permeability of PP is also enhanced when binary blends are made with low water vapour permeability compatibilizers. The water vapour permeability as a function of dispersed phase size showed no correlation, for both compatibilized and uncompatibilized systems.

4.6.2 Silanated PP Water vapour permeability

It was thought that PP which had been silanated to increase the PP viscosity would produce a fine spherical phase dispersion when blended with B5. This was not the case, but the blends showed better water vapour barrier than the corresponding B5/PP blends. When blended with plasticized B5 the silanated material also partially counteracted the inferior water vapour barrier of plasticized B5. The water vapour permeability of the silanated PP was thus measured at different silane concentrations, without PA6.

The results of tests conducted on the silanated PP, normalised against that of 100% PP are shown in Table 11. Since a dramatic three fold reduction in the water vapour permeability, as compared to PP, was achieved with only 2wt% of A174 Silane, Table

11 shows that to obtain a further 50% reduction, 10wt% silane has to be used.

By including in a PP matrix a material which would not migrate upon moisture cross-linking, it was found possible to improve the water vapour and also the oxygen barrier properties of PP threefold, see Section 4.8, using only 2wt% of A174 Silane. Similar improvements resulted from using Z6082 Silane. The relationship between the mass percentage added to PP and the water vapour permeability of these materials normalized against that of 100% PP is plotted in Figure 76. The reason for the exponential relationships between the normalized water vapour permeability and silane concentration converge at ≈ 5wt% is due to minimal effect on the water vapour permeability of increased silane concentration. At the ≈ 5wt% silane point, either the cross-link density of the amorphous part of the PP has reached an optimum value or the reaction of the PP and silane to form the new functional groups, evidenced by FTIR spectroscopy, has also reached an equilibrium, due to the reaction

Table 11 : Water Vapour Permeability of Silane cross-linked PP

Weight percentage of Silane in Xlinked PP	*Water Vapour Permeability, normalized against that of PP*	
	A174	Z6082
0.0	1.00	1.00
1.0	0.52	0.68
2.0	0.31	———
3.0	0.21	0.43
5.0	0.18	0.24
10.0	0.16	0.17

occurring at the surface of the polymer. This occurs upon hydrolysation, after compounding in an extruder/blender. Encapsulated in the polymer particles would be silane attached to the methyl side groups and methylene chain, but unable to react with the water during hydrolysation. FTIR spectra of this material, prior to hydrolysation has been shown to contain the pre-hydrolysation functionalization. Furthermore, the shape of the normalized water vapour permeability plots is similar to those in Figure 77,

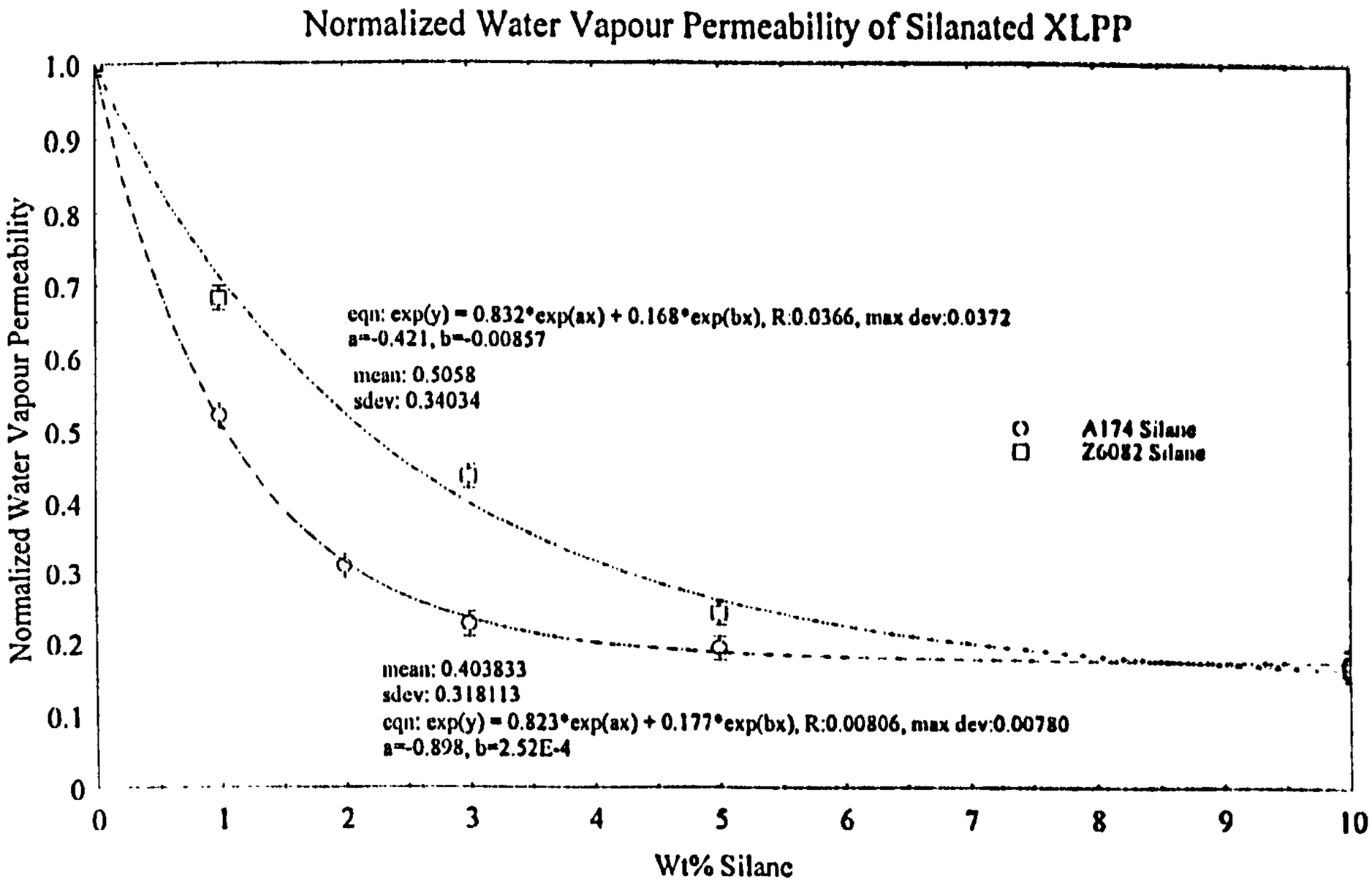

Figure 76 : Normalized Water Vapour Permeability for Silanated PP(XLPP)

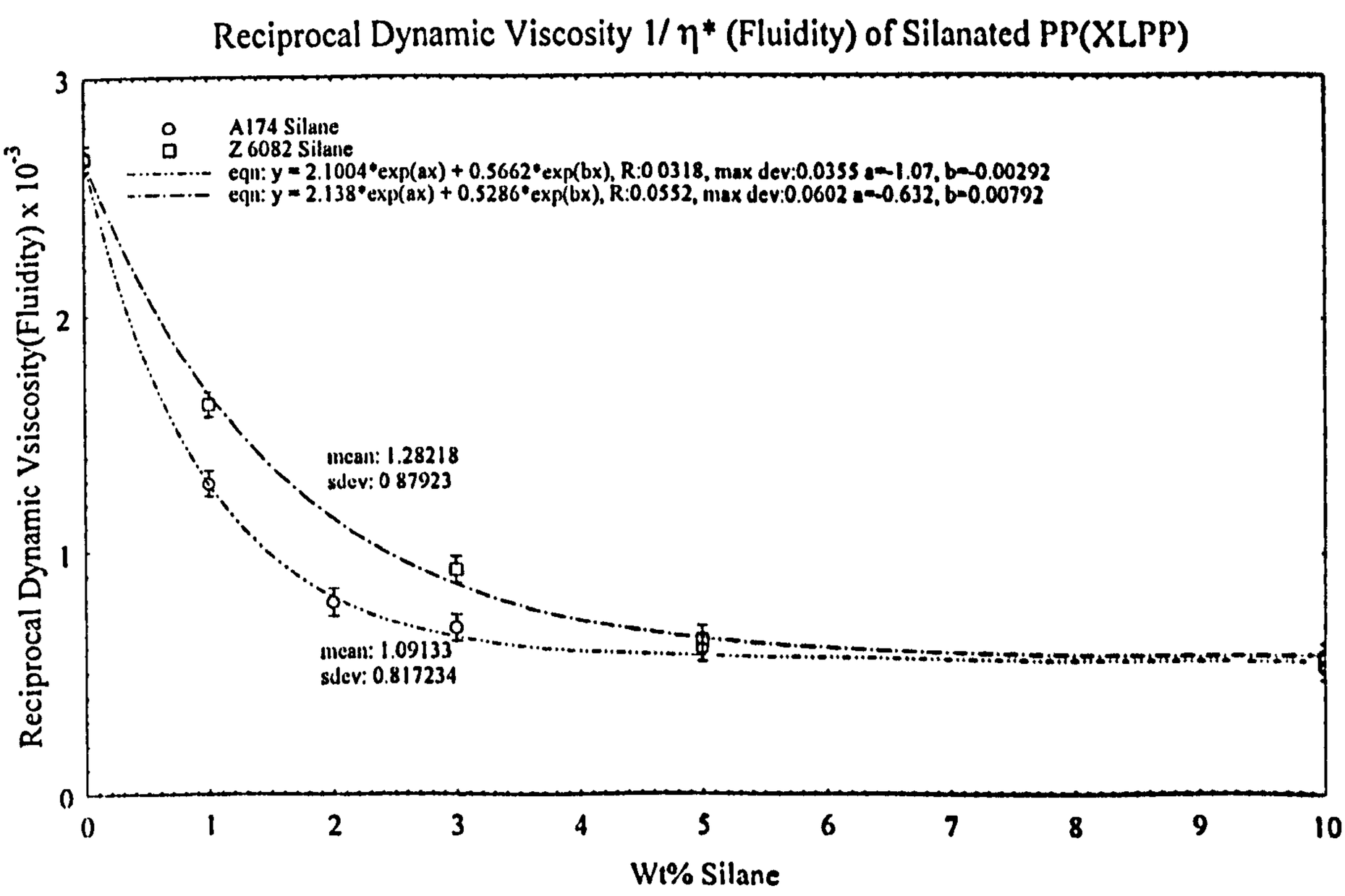

Figure 77: Reciprocal Complex Viscosity of silanated XLPP as a function of silane concentration

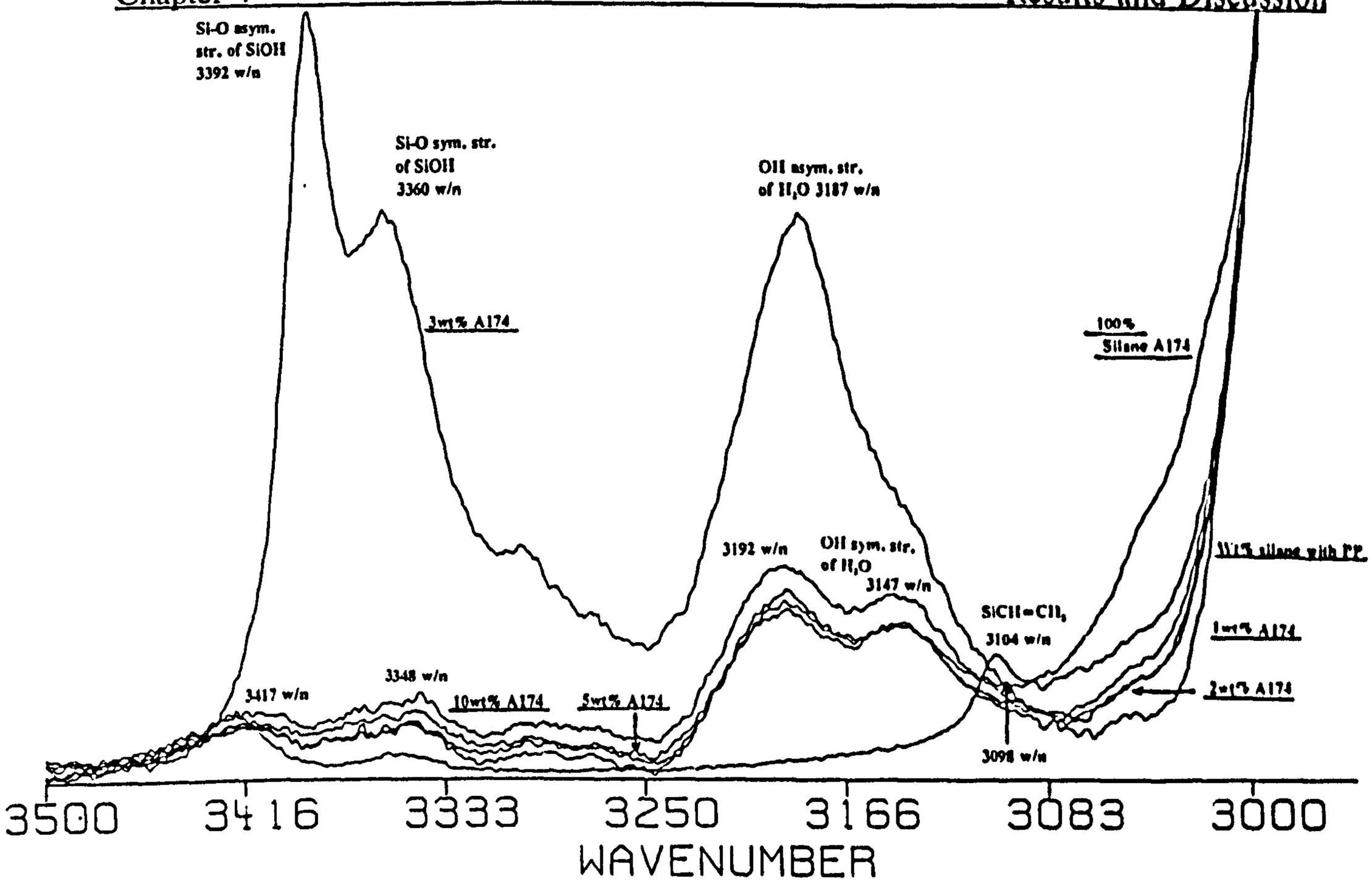

Figure 78 : Partial FTIR spectra of A174 Silanated PP(XLPP) (High wavenumbers)

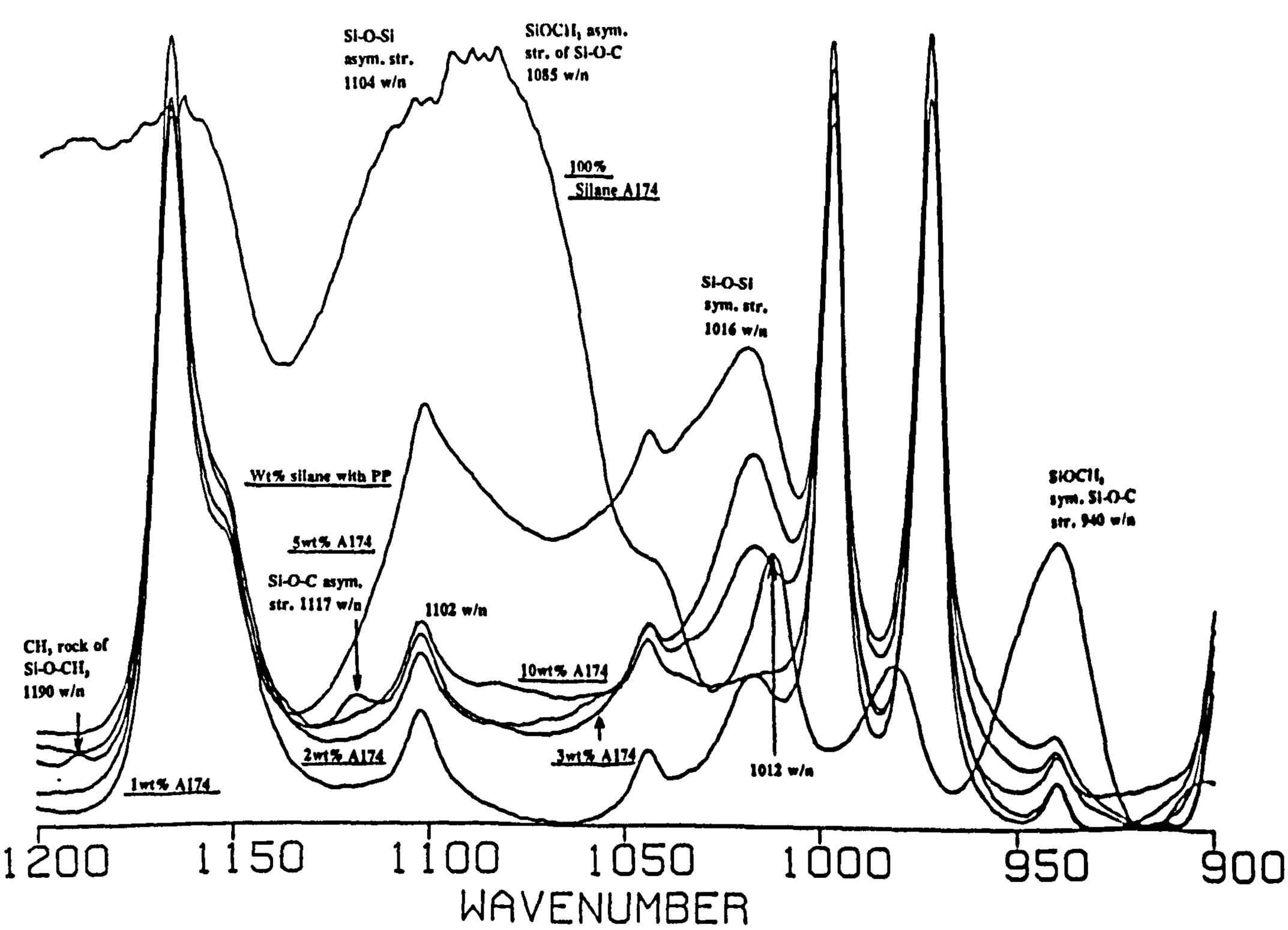

Figure 79 : Partial FTIR spectra of A174 silanated XLPP (Lower wavenumbers)

showing the fluidity/silane concentration dependence, for the same materials, confirming the conclusion that the reaction is both cross-link density and saturation level dependant.

Confirmation was also sought for the apparent optimum amount of silane required during the cross-linking, using FTIR spectroscopy. This was by examining the growth and/or diminishing of functional group peaks, for the A174 systems, with silane concentration, notably bonded Si-OH(OH str.), at 3400-3200 cm^{-1}(wavenumbers) (m)/955-835 cm^{-1}(s) (Si-O str.), Si-CH_2-Si, at 1080-1040 cm^{-1}(s), $SiOCH_3$ at 850-840 cm^{-1}(s)(Si-C str.) and Si-O-Si str. at 1130-1000 cm^{-1}(s)/625-480 cm^{-1} sym. str.(w,br). The results of this investigation is shown in Figures 78 and 79 above. Clearly, the SiOH peaks at 3392 and 3361 cm^{-1}, due to Si-O- asym. and sym. stretch, increase in absorption up to 3wt%, followed by a diminishing to 10wt%. Similar behaviour is shown by the asym. and sym. stretch OH peaks from water at 3187 and 3126 cm^{-1} respectively. Both the 5 and 10wt% A174 materials show peak shifts from 3 to 5wt% materials for these peaks, indicating that the water hydrolysation reaction is enhanced by the greater silane concentration. This behaviour confirms the hydrolysation reaction occurring at the surface only. The Si-O-Si asym. stretch peak at 1104 cm^{-1} increases in absorption gradually up to 10wt% silane, showing a slight negative shift as compared to the 100% silane. However, the sym. Si-O-Si stretch peak at 1012 cm^{-1} of the silane is shifted more considerably positively, and also shows a gradual increase in absorption with silane concentration. Si-CH_2-Si absorptions are less significant, since not surprisingly, the absorption for this waveband at 1043 cm^{-1} is present in the silane weakly and as a shoulder. The $SiOCH_3$ absorption at 850 cm^{-1} of the 100% silane is absent from the silanated PP spectra, since these functional groups have been converted to silanol functionality.

The thicknesses of the polymer films was normalized against that of 100% PP, 12 μm, and therefore semi-quantitative studies of absorption vs. silane concentration were correlated in Table 12 and plotted in Figure 80, using the following equation derived from Beer's Law[41] :

$$c_1 = 100/[1 + (a_1/a_2)\,(A_2/A_1)] \text{ ---------- [68]}$$

where, Beer's Law is A = a x b x c

A is the absorbance, $\log_{10}(I_0/I)$

where, I_0 is the intensity of monochromatic radiation entering a sample

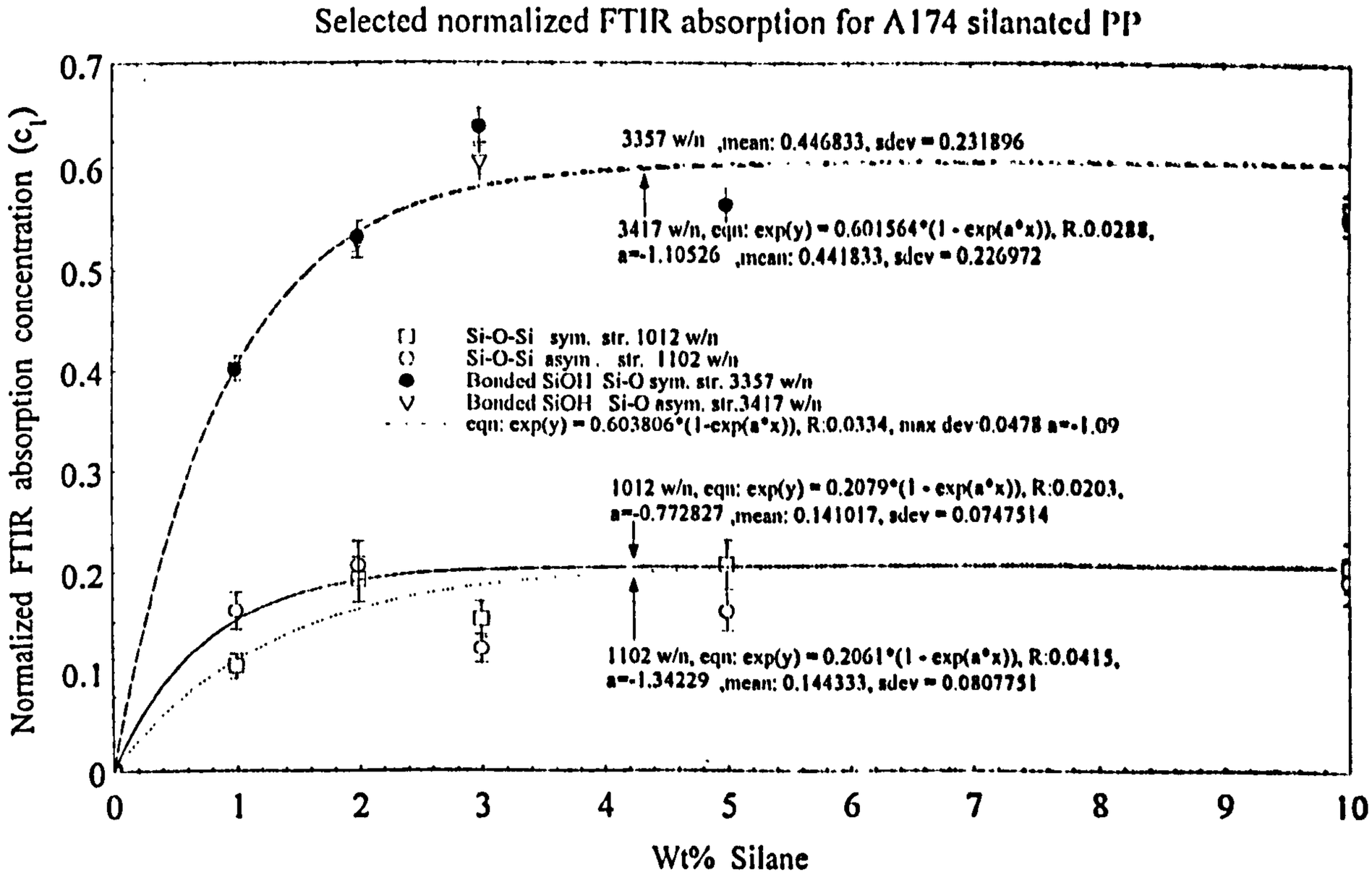

Figure 80 : FTIR normalized peak absorptions as a function of silane concentration for PP/A174 systems

I is the intensity transmitted by the sample

a is the absorptivity, a constant specific for the substance at a particular wavelength and also varies with the units used for b and c

b is the sample thickness in μm

c_1 is the calculated mass fraction concentration of the band to be analyzed, in a standard for equ'n.[69], and sample for equ'n.[68]

A_2/A_1 is the ratio of absorptions of two components each of which has no interference from the other component

A_2 is band for which the concentration c_2 is known, whereas A_1 is of unknown concentration

(a_1/a_2) is a constant determined by running the spectrum of one standard where c_1 is known and A_2/A_1 is measured.

(a_1/a_2) is calculated by transposing equ'n.[68] to give :

$$a_1/a_2 = [(100/c_1) - 1]/(A_2/A_1) \text{ ---------- [69]}$$

Once (a_1/a_2) is known, then c_1 for a sample can be determined from equ'n.[68], by the measurement of (A_2/A_1). In this work, the analytical band used as A_2 is the weak to medium isopropyl C-C stretch band at 842 cm^{-1} of PP. From Figure 80, at 3-5wt% of

silane, the above results show clearly for the bonded SiOH Si-O str. wavebands, an increase in Si-OH concentration, confirming the reaction scheme proposed for PP silanation with silane A174, Figure 7 of Section 2a.. The fitted exponential curve then shows the expected asymptotic behaviour dependence on concentration, showing only a slow depletion of these functionalities during the hydrolysation reaction.

However, for the Si-O-Si str. absorptions, which would be generated during the proposed reaction scheme, the trend from Figure 80 is the converse, above 2wt% silane, where the maximum c_1 occurs at 5-10wt%. The apparent reduction in this functionality at 3wt% silane is due to the excess SiOH functionalities concentration being depleted rapidly by precipitation, before the exponential fitted dependancy levels off at 5-10wt% as an overshoot. A similar trend to Figures 76 and 77 exhibited in Figure 80 is the minimal change in c_1 from 5 to 10wt% silane. After the 5wt% silane point, the increasing silane

Table 12 : Normalized peak absorptions for PP/A174 Silanated materials

Material	*Film thicknesses normalized against 100% PP*	*(a_i/a_r)*	*Assigned band absorptions(A_i) and c_i*							
			SiOH sym. Si-O str. 3357 cm^{-1}		*SiOH asym. Si-O str. 3417 cm^{-1}*		*SiOSi asym. str. 1102 cm^{-1}*		*SiOSi sym. str. 1013 cm^{-1}*	
			(A_i)	*c_i*	*(A_i)*	*c_i*	*(A_i)*	*c_i*	*(A')*	*c_i*
99wt% PP/1wt% A174	0.48	0.430	0.031	0.401	0.029	0.403	0.055	0.162	0.064	0.106
98wt% PP/2wt% A174	1.01	0.546	0.127	0.532	0.127	0.526	0.192	0.207	0.177	0.193
97wt% PP/3wt% A174	1.17	0.423	0.062	0.637	0.074	0.604	0.067	0.124	0.085	0.154
95wt% PP/5wt% A174	0.99	0.545	0.113	0.562	0.112	0.562	0.138	0.161	0.193	0.208
90wt% PP/10wt % A174	1.31	0.477	0.063	0.549	0.067	0.556	0.214	0.192	0.235	0.206

concentration has little effect upon the proposed reaction. The Si-O-Si concentration in the hydrolysed material increases with the amount of silane present, where the reaction is occurring at the surface only. If it is the case that excess silane is present at 10wt%, silane precipitation might be expected to occur in the PP matrix. Hence, the 100wt% silane and the 90wt% PP/10wt% A174 material were examined by fluorescence LM. The pure silane showed no fluorescence, however, the 10wt% silane material was fluorescing, most likely due to the excess ungrafted material.

The exponential behaviour dependence in Figures, 76, 77, and 80 for A174 silanated PP is similar to that shown in other work for the dependence of oxygen permeability on

increasing crystallinity and hence density of HDPE[42]. Increasing the density above ≈ 0.92 kg/m^3 greatly decreases the permeability, from 125 cm^3 mm/m^2/day/bar at 0.92 kg/m^3 to 18 cm^3 mm/m^2/day/bar at 0.98 kg/m^3 density. However, above the higher density, the curve is asymptotic. The length of the polymeric chains is also a factor, and a profound effect of the polymer thermal history, since this can modify the number and size of the crystallites (spherulites) present.

4.7 Free Volume Effect on Permeability

4.7.1 Volume Thermal Expansion Determination

When the temperature T increases, the amorphous polymer volume, V(T) increases, because of thermal expansion. The surface tension, τ(T), however, decreases as a result of its dependence on $1/V^4(T)$[43,21]. The equation below shows that the rate of decrease of τ with increasing temperature mainly comes from a factor proportional to the coefficient of volumetric thermal expansion α :

$$d\tau(T)/dT = -4\ \alpha(T)\ \tau(T) \text{ ---------- [70]}$$

α changes only slowly with temperature and manifests a discontinuous increase when a material undergoes the glass transition. The amount of free volume can be frozen into a material as a result of the slowing down of the molecular-level relaxation processes as T decreases significantly below T_g. In addition, the free volume increases with increasing T as a result of thermal expansion. The free volume can therefore play a vital role in thermal expansion processes both at low and high temperatures. Robertson's excellent review article[44] gives a thorough discussion of this concept. A good approximation for the coefficient of thermal expansion over the temperature range $150K \leq T \leq T_g$[45] is obtained from :

$$\alpha(T) = 1/(T + 9.47T_g) \text{ ---------- [71]}$$

In this work, the volume thermal expansion coefficient, was determined experimentally for, PP, PA6(A23), PA6(B5), XLPP(2wt% A174 Silanes), Orgalloy R6000, 70wt% PP/26wt% B5/4wt% PB3002, and 56wt% A23/36wt% PP/8wt% BMAcoMAgPP, as discussed in Section 3b.2.1, and the values obtained are shown in Table 12. The published value for α of PP is 42 x 10^{-5} °K^{-1} [46] and for PA6, 0.31[47], both in the range 20-100 °C.

Samples were selected which had been treated with similar heating rates, residual molding stresses, and the same loads. Through eliminating creep effects by keeping the time of the test similar for each sample, the high resolution of this method can be utilised. The temperature range is from room temperature to 100 °C. It was thought that the coefficient would be linear in this range, well above the T_g and also below the softening point of the polymers under investigation, in order to protect the instrument from the danger of melting the polymers. The parameter actually measured by the TMS I was the linear thermal expansion coefficient β, from which α, the volume thermal expansion coefficient, was calculated, since α is 3 x β.

The values obtained for homopolymers and alloys, are shown in Table 12 below, and are of the same order of magnitude as the quoted literature values, with that of Orgalloy R6000 being closer to PP than PA6. With a PA6 matrix, this is an unexpected result but indicates that at a low molecular weight PA6 with a low viscosity, is possibly made by polymerising the monomer with PP in a reactive extrusion process. The B5 and A23 blends were chosen since the former has a fine microstructure and the latter is coarse.

4.7.2 Temperature effects

Polymer chain segmental motion is affected by both temperature and concentration of sorbed permeant in the matrix. One effect of temperature on polymer chain segmental motion is a free volume increase, directly related to the bulk expansion of the polymer, due to the increased segmental motions. The sorbed permeant also increases the free volume to a similar amount as a corresponding temperature increase, providing there is no component interaction. Therefore, there is a temperature-concentration equivalence for transport phenomena, which is similar to the temperature-time equivalence for viscoelastic behaviour. This implies that there is also a concentration-time equivalence relationship[48]. The shape of the $\log_n$ complex modulus (G*) curve vs. temperature or angular velocity, ω (shear rate) is maintained when there is an increase in any of the three variables for both viscoelastic and transport phenomena. It is simply shifted to a lower temperature, corresponding to the change in T_g, without any change in shape when a constant permeant concentration is sorbed as an ideal solution. Changes in water vapour permeability with temperature were investigated in this work as shown in Figure 81, which reinforces the above theories, since the curves of permeability as a function of

Table 13 : Volume Thermal Expansion Coefficient for selected polymers

Polymer	*Volume Thermal Expansion Coefficient, $\alpha \times 10^{-5}$, $°K^{-1}$*
PP	57.9
XLPP(2wt% A174 Silanes)	46.8
PA6(Ultramid B5)	0.23
PA6(Grilon A23)	0.29
Orgalloy R6000	59.1
70wt% PP/ 26wt% B5/ 4wt%PB3002	35.4
56wt% A23/ 36wt% PP/ 8wt%BMAco MAgPP	42.7

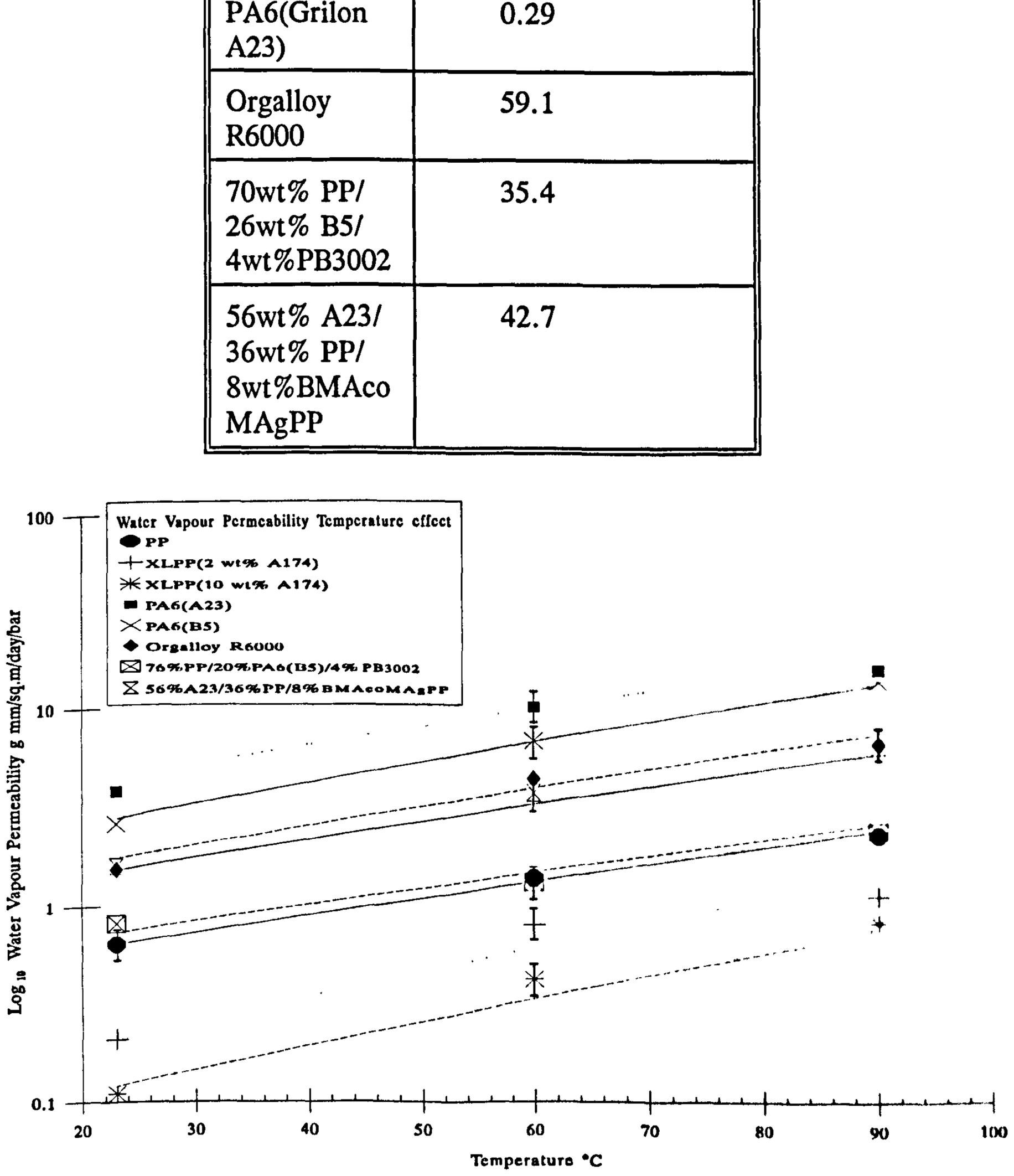

Figure 81 : Polymer Water Vapour Permeability as a function of temperature

PA6 concentration are simply shifted towards higher permeability, with increasing temperature.

4.7.3 Permeant Concentration Effects

The mechanism of water vapour permeability through a polymer blend film is a gradual increase of water molecule concentration in the matrix, which can be enhanced or suppressed by the dispersed phase. If the latter is more hydrophillic than the matrix then the maximum concentration in the film will be higher and the permeability will be higher, and vice versa. Interaction forces between the permeant molecule and polymer, of varying magnitude and nature result in the permeant molecule being localised at an active site or entrapped by a volume element for more than unit time for a diffusion step. Hence immobilisation occurs, without contribution to the overall flux. Strong interactions result in solvation clusters, chemisorption modes, or chemical reaction, and a greater clustering results. Inside a cluster, a molecule will be less mobile than an isolated one. The study of diffusion data for water and alcohols in PA6[49] showed little effect of clustering for water transport but a marked effect on alcohol transport. Dynamic mechanical properties were significantly affected by the clustering of all components, having different relaxation times than the diffusion process.

PA6 will need to be made more hydrophobic, to improve the water vapour barrier. This certainly is the case for compatibilized blends, since these show lower water vapour permeability than the binary blends. Hence, it is not surprising that the water vapour permeability of the binary blends containing 8wt% compatibilizers with PA6's were prepared, to test this theory. Not only was the PA6 viscosity, for both the low and high molecular weight materials increased, except where free MA was present, but also the water vapour barrier of the PA6 was improved. The results below in Table 14 show that the increase in water vapour permeability for XLPP is greater than that of PP, taken as an arithmetic mean of four determinations within a standard deviation of $\pm 10\%$. This is because of the very low mass increases involved. PA6 increases are naturally greater than for the PP's, with surprisingly B5, with a greater molecular weight and melt viscosity,

Table 14 : Molecular Concentration Dependence of Water Permeability

Polymer	*Water permeability, g mm/m²/day/bar*	*Percentage increase for liquid in contact with film*
PP	0.64(vapour)	———
PP in contact with liquid	0.66	3.1
XLPP(2wt% A174 Silanes)	0.21(vapour)	———
XLPP(2wt% A174 Silanes)in contact with liquid	0.22	6.6
PA6(B5)	2.65(vapour)	———
PA6(B5) in contact with liquid	6.59	148.7
PA6(A23)	2.83(vapour)	———
PA6(A23) in contact with liquid	3.85	36.0
Orgalloy R6000	1.55(vapour)	———
Orgalloy R6000 in contact with liquid	2.67	72.3
70wt% PP/26wt% B5/4wt% PB3002	0.82(vapour)	———
70wt% PP/26wt% B5/4wt% PB3002 in contact with liquid	1.41	71.4
56wt% A23/36wt% PP/8wt% BMAcoMAgPP	1.61(vapour)	———
56wt% A23/36wt% PP/8wt% BMAcoMAgPP in contact with liquid	2.61	62.2

showing a larger increase than that for A23. With a PA6 matrix, the R6000 value lies intermediate between the PP and PA6. With a similar PA6 concentration, the A23 blend has a lower percentage increase than R6000. In all probability, the matrix PA6 of R6000 has a similar lower viscosity to that of the A23 blend. It is interesting to note that the B5 blend has a fine phase dispersion but that of the A23 blend is coarse. Despite that, the percentage increase for the B5 material is greater, although the PA6 concentration is

lower, reflecting the greater increase of the B5 homopolymer, as compared to that of A23.

4.7.4 Summary of Free Volume effect on permeability

For the systems investigated, the thermal expansion coefficient data could be correlated with that of surface tension, through equ'n.[70] and also with the uptake data through equ'n.[73].

4.8 Oxygen Permeability

Some oxygen permeability tests were conducted using Oxtran equipment at the CarnaudMetalbox laboratories and the results are shown in Table 15. The creation of ternary blend systems by compatibilizer addition is an example of new functional group influence, also present in two phase PP/silane systems. For the latter systems, the oxygen permeability of PP been reduced by the addition of silane functional groups, an improvement observed in two separate PP/silane systems. Silane A174 is more effective,

Table 15 : Oxygen Permeability for selected polymers

Polymer	Oxygen Permeability, cm^3 $mm/m^2/day/bar$
PP (48M10)	68.1
PA6(B5)	1.1
PA6(A23)	1.7
Orgalloy R6000(pellets)	2.2
Orgalloy R6000(Inj. Molded)	2.6
XLPP (2wt% A174 Silanes)	19.0 (72.2 μm)
XLPP (10wt% Z6082 Silanes)	40.5

but less effective than R6000. The latter has an oxygen permeability of approximately 25% that of PP and the oxygen permeability of PA6(B5) is 50% that of R6000 and

PA6(A23) oxygen permeability is 77% that of R6000.

The silanated PP materials show an improvement in oxygen permeability when compared with PP, but do not approach the oxygen permeability of the PA6's. Orgalloy R6000 has an excellant oxygen barrier for a material which contains ≈ 48wt% PA6. The silane A174/PP results are encouraging and better than expected, for the addition of a small amount of A174 silane.

4.9 Organic Solvent/Natural Gas Permeability and Uptake Determinations

4.9.1 Introduction

Chlorinated solvents such as dichloromethane (DCM), used as an ingredient of paint stripper with methanol, are frequently packaged in polymeric containers and alkane gases such as methane and propane are often used as propellants in aerosol canisters. Therefore, the relationship between the number of chlorine atoms in methane and its chlorinated derivatives was investigated, for polyolefins, PA6 and R6000. Tests were also conducted with methanol as the penetrant, since it is also a paint stripper ingredient, and to investigate steric hinderance, with xylene. The inert Poly(tetrafluoroethylene) (PTFE) was also tested for DCM permeability. Uptake determinations gave some indication for the selected polymers of their suitability as storage containers of the selected polymers.

4.9.2 Organic Vapour Permeability Determination

Organic Solvent Vapour permeabilities were determined gravimetrically, as discussed in Section 3b.4.2, using the same gravimetric method as that used for water vapour permeability. The results of these determinations are included in Table 16, alongside the liquid permeability results, for the same penetrants, the latter determined using a Differential Pressure Transducer Constant Volume Manometric cell. Each value represents the arithmetic mean of three determinations, within a standard deviation of ± 10%.

4.9.3 Natural Gas Permeability Determination

For natural gas permeability, the Differential Pressure Transducer Constant Volume Manometric cell method was used and equ'ns.[45]-[49] from Section 3b.4.2, to calculate the permeability coefficient, but Δp is now equal to an arithmetic mean of the natural gas

supply pressure, measured at the beginning and end of the test, minus the initial evacuated pressure. The values obtained for PP, PA6(B5), and XLPP are included in Table 16 below. For natural gas permeation through PP and XLPP, the situation is less clear, but appears to depend on the relative film thicknesses. For natural gas through PA6(B5), the plateau saturation pressure is equivalent to the natural gas supply pressure value. The Methane permeability value[50] for BOPP 0.255 cm^3 mm m^{-2} day^{-1} bar^{-1} and published values for CCl_4 and methanol permeabilities[51] of PP are 181 and 0.80 g mm m^{-2} day^{-1} bar^{-1} at 22.8 °C, respectively. These compare with the values obtained in this work of 170.1 and 2.83 g mm m^{-2} day^{-1} bar^{-1}. Stannett and Szwarc[52], Rogers et al[53], and Frisch[54], reported a correlation between the ratios of the permeabilities, in consistent units, of various gases through two polymers, and also the ratio between two gases through various polymers, with the value for nitrogen being taken as unity. The

Table 16 : Organic Solvent and Natural Gas Permeability of selected polymers

Polymer	**Permeability, cm^3 mm/m^2/day/bar**						
	Natural Gas	*Methanol*	*DCM*		*Chloroform*	*Carbon Tetrachloride*	*Xylene*
		Gravimetric Vapour	*Gravimetric Vapour*	*Liquid*	*Gravimetric Vapour*	*Gravimetric Vapour*	*Gravimetric Vapour*
PP DSM 48M10 co-polymer	91.2	3.5	144.2	423.1	111.09	71.5	1.27
HDPE	56(Methane) *	———	106.1	—	19.0	14.2	———
LLDPE	———	———	97.7	—	43.3	14.3	———
LDPE	———	———	106.9	—	42.5	35.6	———
XLPP (2wt% A174 Silanes)	35.6	1.2	28.7	208.5	38.1	23.7	1.10
XLPP (10wt% A174 Silanes)	———	1.0	63.1	—	———	———	0.83
XLPP (3wt% Z6082 Silanes)	———	3.4	26.5	—	———	———	1.48
XLPP (10wt% Z6082 Silanes)	———	1.5	62.2	—	———	———	0.48
PA6(Ultramid B5)	21.3	8.7	24.2	—	18.1	4.6	1.07
PA6(EMS-Chemie Grilon A23)	———	29.6	63.0	—	46.8	7.2	0.79
Orgalloy R6000 (pellets)	———	1.1	79.8	—	61.1	43.4	1.13
PTFE (Virgin)	———	———	14.8	—	———	———	———

* = Value from British Gas

ratio's for oxygen and methane to nitrogen are 3.4 and 3.8 respectively, giving their ratio to each other is 0.89. In this work, for PP the ratio of oxygen (68.1 cm^3 $mm/m^2/day/bar$), obtained from an Oxtran, to methane is 7.47. For XLPP (oxygen permeability 19.03 cm^3 $mm/m^2/day/bar$), obtained from an Oxtran, the ratio is 5.35, and for PA6(B5), with an oxygen permeability of 1.1 cm^3 $mm/m^2/day/bar$[55] at 23 °C and 50% RH, the ratio is 0.47. The published oxygen permeability value for BOPP is 10.43 cm^3 $mm/m^2/day/bar$ at 23 °C and 0-90% RH[50]which will give the ratio of O_2:CH_4 permeabilities as 4.09.

The natural gas average methane composition in the North Thames Region is 91.96 vol% and the British Gas quoted methane permeability of HDPE, 54 cm^3 $mm/m^2/day/bar$[56], is included in Table 16 and also the Figures 82 and 83 below. The British Gas quoted

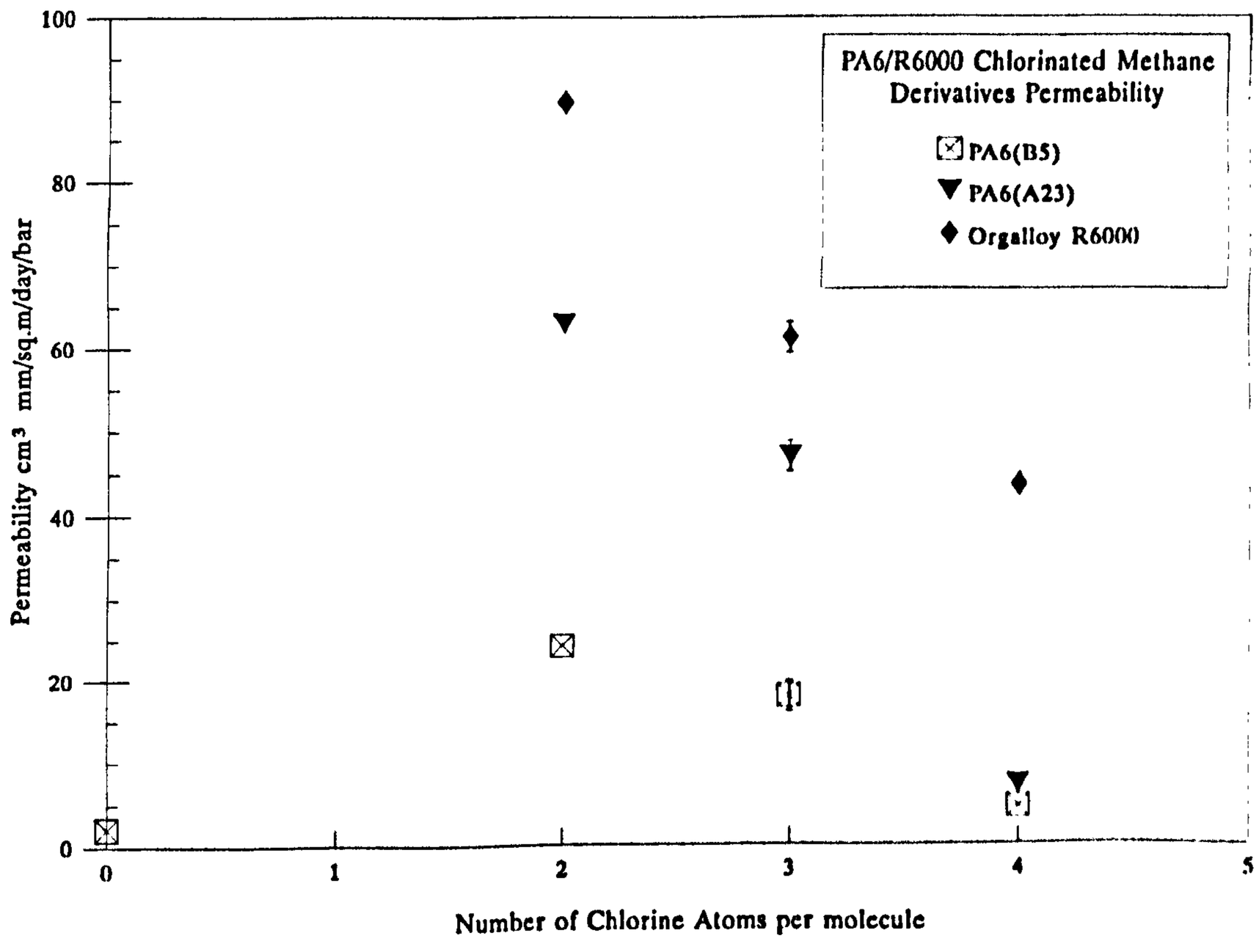

Figure 87 : PA6/R6000 Chlorinated Methane Derivatives Permeability

values for nitrogen and oxygen permeability of HDPE are 18 and 72 cm^3 $mm/m^2/day/bar$ respectively, which from the data of references [47],[48] and [49] gives O_2:N_2 and CH_4:N_2 ratios of 4.0 and 3.1 respectively, and their ratio to each other of 1.29.

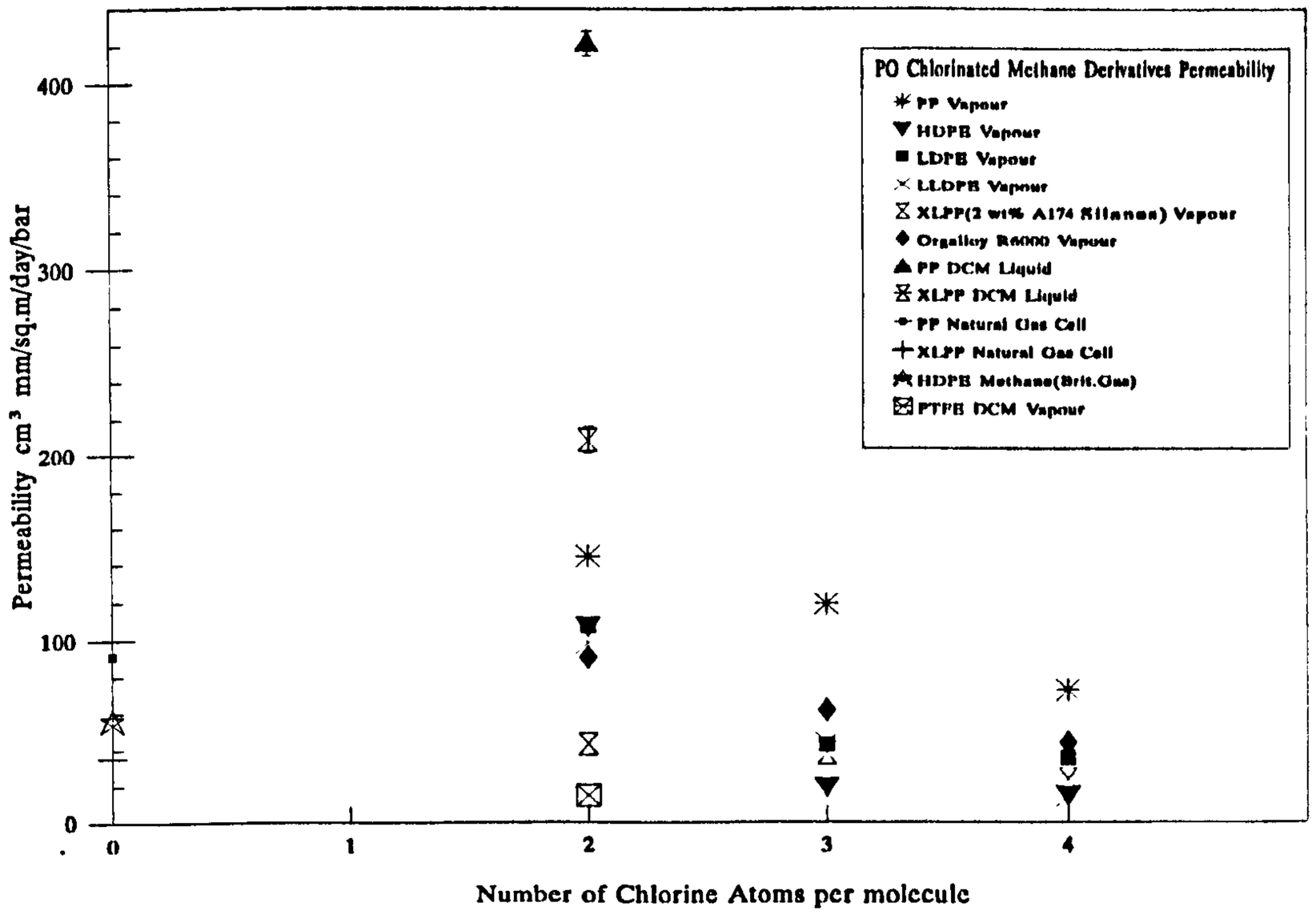

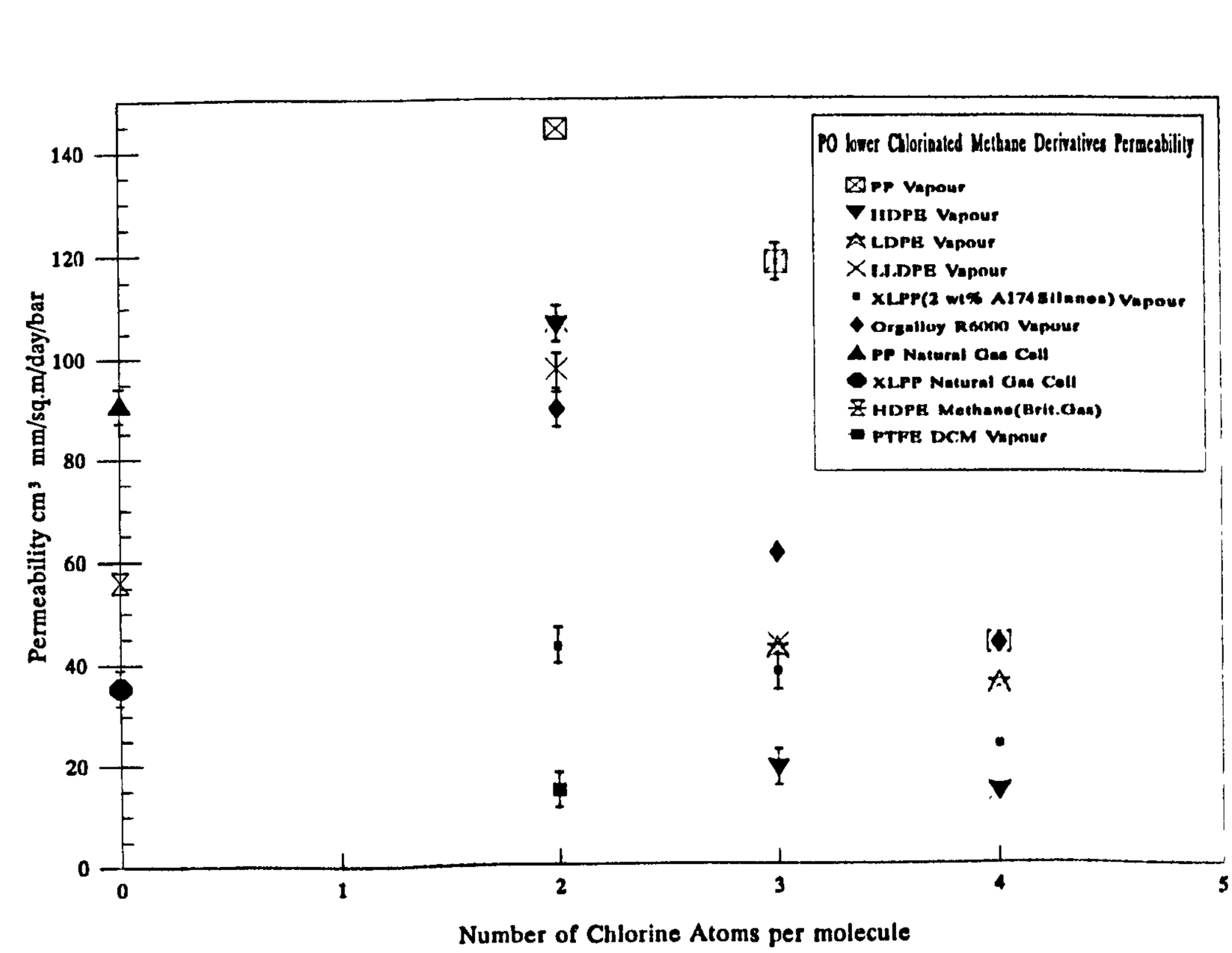

Figure 83 : Polyolefin(PO) and Orgalloy R6000 Chlorinated Methane derivative permeabilities

4.9.4 Liquid Permeability Determination

The Differential Pressure Transducer Constant Volume Manometric (DPTCVM) cell method was used to determine DCM liquid permeabilities, as discussed in Section 3b.4.2. The liquid permeabilities are calculated from equ'n.[56], Section 3b.4.1, using the slope of the graphs for the increasing value of p_2 as a function of time (not shown in this work). The liquid and vapour permeabilities, the latter obtained gravimetrically, are tabulated in Table 16 and are plotted as a function of number of chlorine atoms per permeant molecule in Figures 82 and 83. The gravimetric method is unsuitable for liquid permeability determination because the liquid DCM will find leakage paths through the sealant. Similarly, the DPTCVM cell is not suitable for vapour permeability determinations with DCM, since although DCM is volatile, it is normally a liquid at ambient temperatures and pressures.

For completion, it would have been beneficial to investigate monochloromethane (methyl chloride) permeability, for the increasing chlorine concentration per molecule. It is however a very hazardous substance not only because of high toxicity but also because of flammability, and volatility. The recommended safety procedures for working with it are extremely stringent, hence permeability tests could not be conducted with the existing equipment.

The saturation plateau of the p_2 as a function of time plot for DCM is equivalent to the saturated vapour pressure under the test conditions. The gravimetric results have been converted to cm^3 $mm/m^2/day/bar$, for consistency. The increase in permeability of PP to DCM liquid as compared to vapour is 293% and for XLPP is 330%. Only negligible swelling of the PP film with DCM was measured, 1.18 vol%, compared to that for XLPP of 31.0 vol%. A possible explanation is reaction of excess uncoupled silane with the DCM, which changes the film geometry.

4.9.5 Organic Solvent Uptake Determination

Figures 84-88, below show the organic solvent uptake results for selected polymers, using chlorinated solvents based on methane, methanol, and xylene. It can be shown that for cubic polymer samples[57], the solvent uptake, for one and two component systems (with acetone, acetic acid, lactic acid, chloroform, and water), will proceed as a diffusion

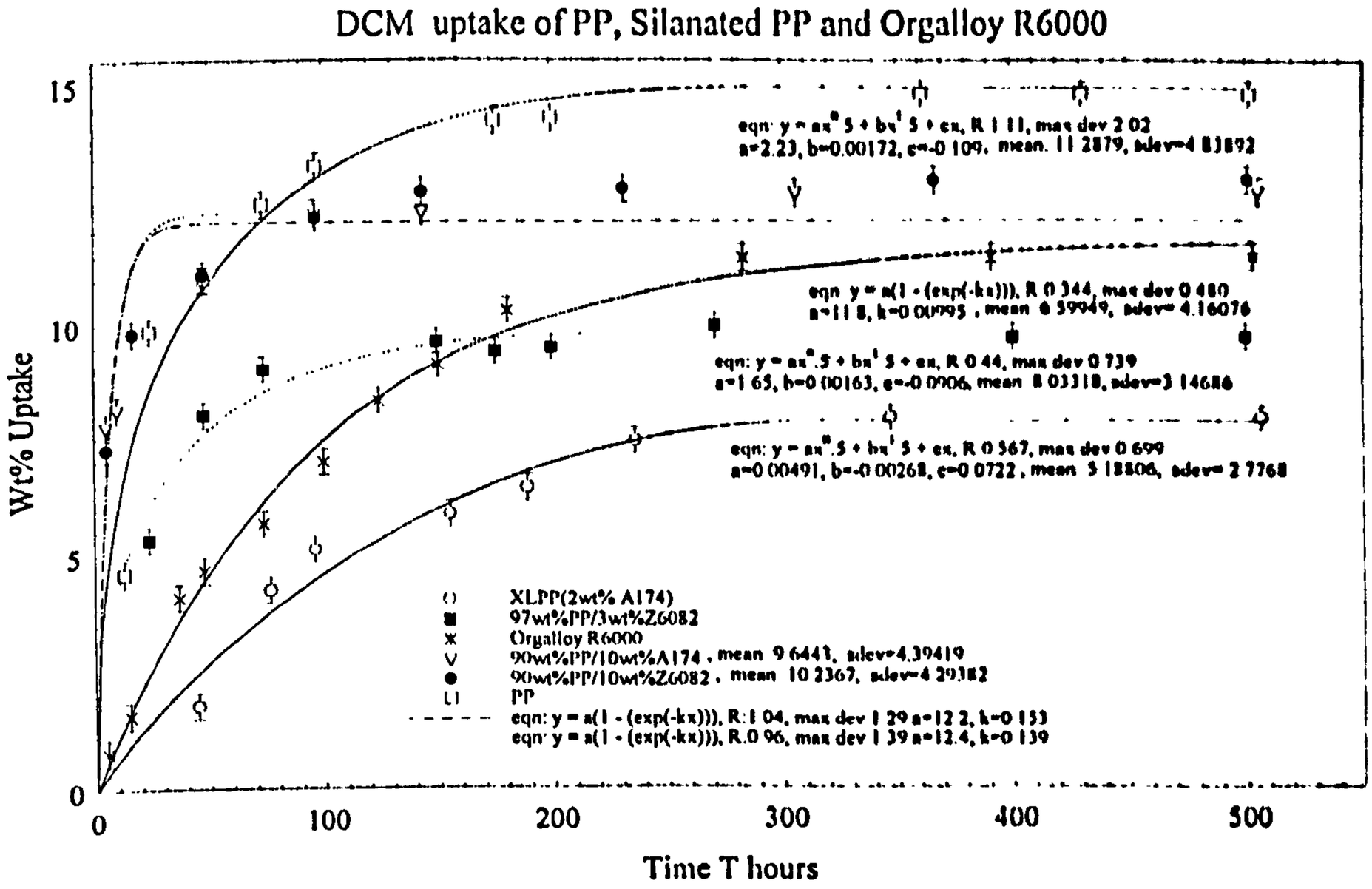

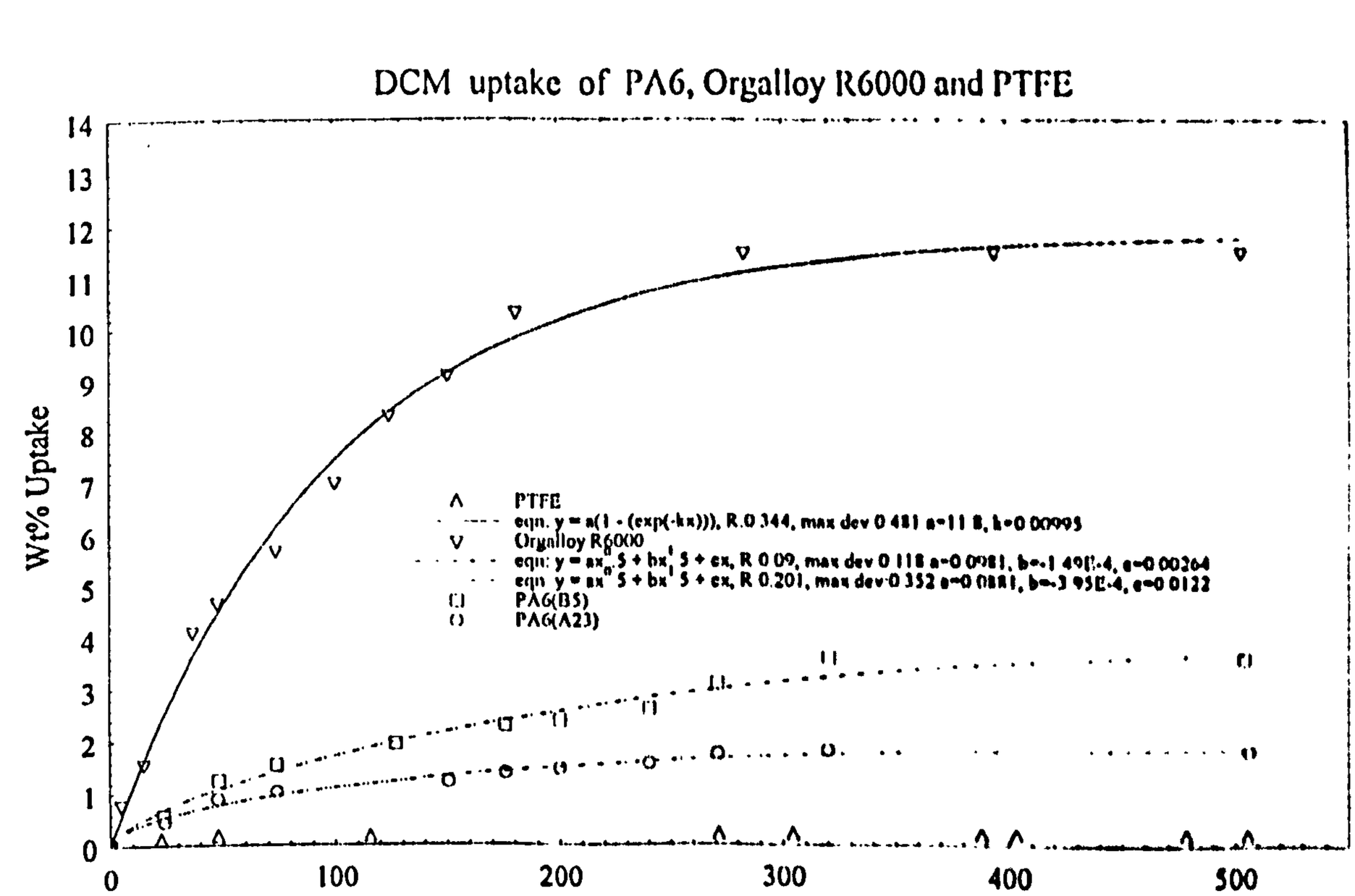

Figure 84 : Dichloromethane uptake of PP, silanated PP, PA6, and Orgalloy R6000

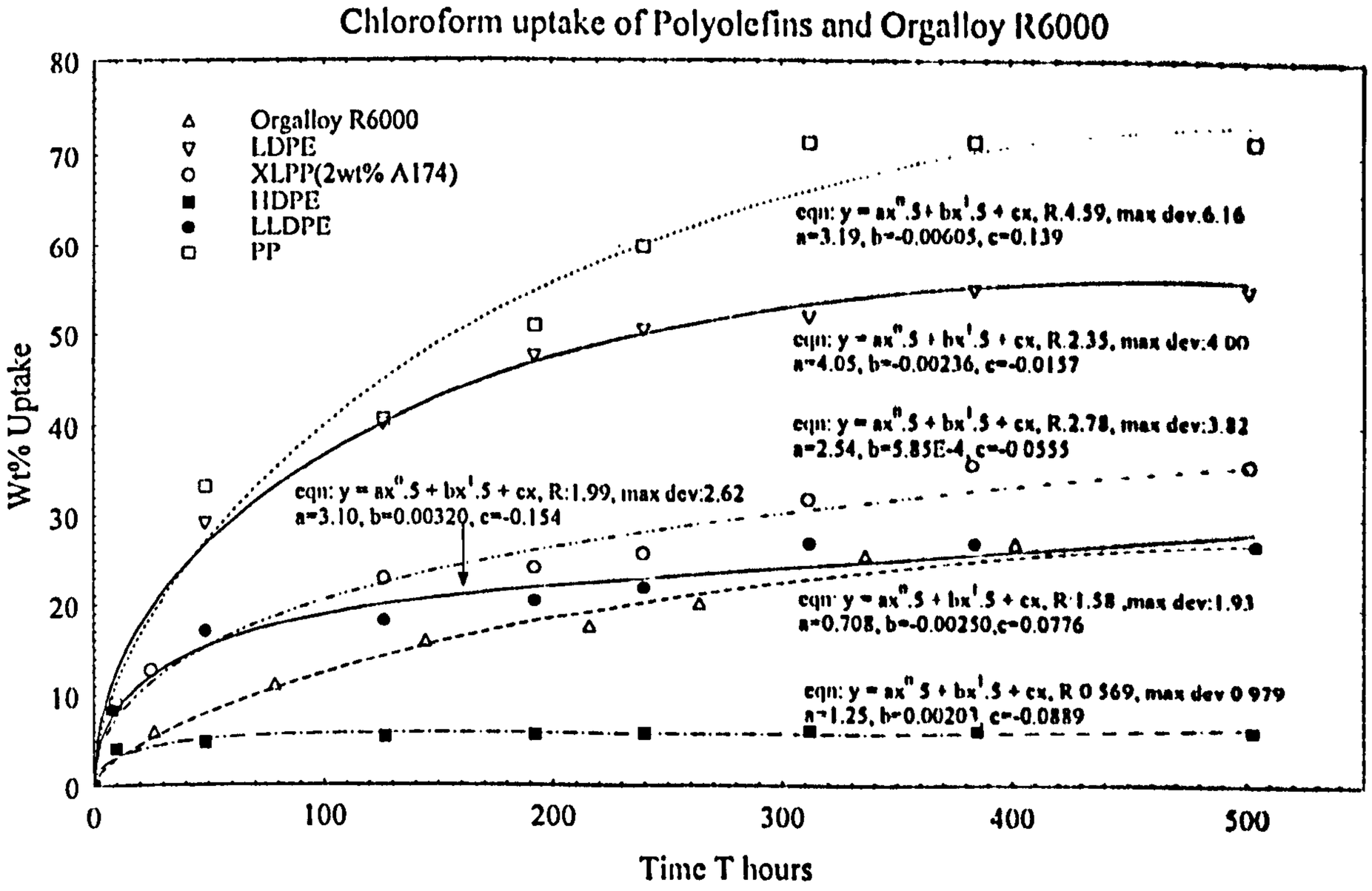

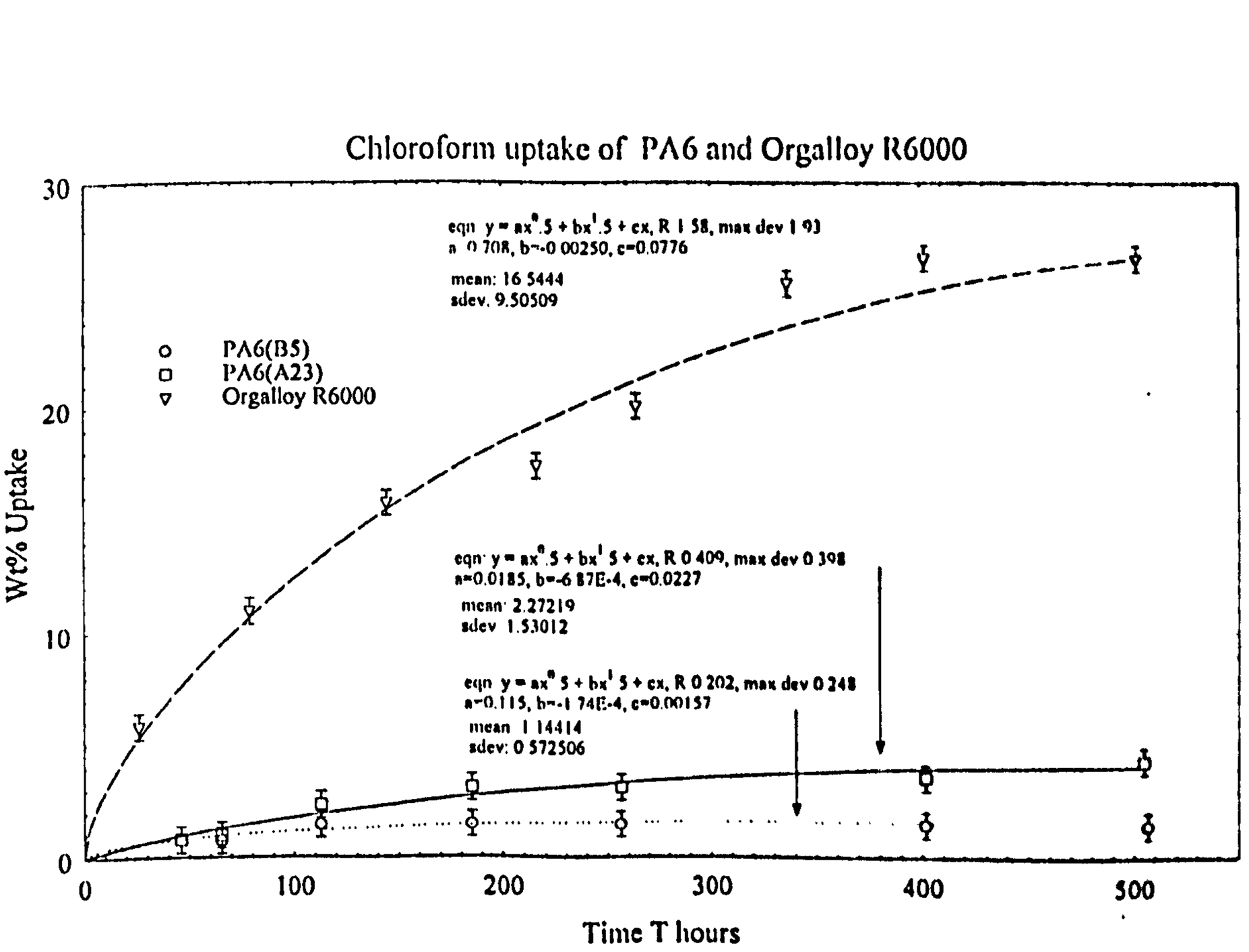

Figure 85 : Chloroform uptake of polyolefins, PA6, and Orgalloy R6000

front through each cube face, with a cross section which is the same shape as the face. The area into which the solvent has not diffused will gradually decrease and therefore the diffusion rate will diminish with the approach to saturation. From these physical phenomena, the change in mass ΔW of the polymeric sample with time t are related through equ'n.[72] :

$$\Delta W = 6\rho S(Ba^2t^{0.5} - 2B^2at + 1.33B^3t^{1.5}) \text{ ---------- [72]}$$

where, a is the face length of the cube

ρ is the penetrant density

S is the fractional solubility of the penetrant in the matrix

B is the constant of diffusion (different from the Fickian diffusion coefficient)

where, B is related to the penetrated distance z by :

$$(1\text{-}b)z = Bt^{0.5} \text{ ---------- [73]}$$

derived from[58] the relationship :

$$z = Bt^{0.5} \text{ ---------- [74]}$$

where, b is a constant related to the volume expansion of the sample.

The first term in equ'n.[72] was shown to be the predominant one.

For the rectangular shaped samples of the current work, when equ'n.[72] was applied to the methanol/PA6 systems, the relationship was not found to be valid. The corresponding relationship, however, found to fit the majority of experimental data is :

$$\Delta W = Dt^{1.5} + Ct^{1.0} + At^{0.5} \text{ ---------- [75]}$$

D, C, and A are the empirical correlation coefficients, related to sample geometry, penetration distance, penetrant/matrix interaction, solubility, and penetrant density. t is the time elapsed from the start of the experiment. For the majority of the uptake data obtained from this work, equ'n.[75] has been found to be valid.

In relation to the possible reaction between the penetrant and polymer, the following equation was found to fit some of the experimental uptake data :

$$\Delta W = A(1 - e^{-kt}) \text{ ---------- [76]}$$

where k is the slope of the linear portion of the fitted curve, t is the time elapsed from the start of start of the experiment and A is the maximum mass uptake plateau value. where the shape of the curve obtained with equ'n.[76] exhibits a transition from the linear portion to the saturation plateau value. This could also indicate that the sample geometry is similar to a cube. Two uptake rates also exist in some cases, where clear

discontinuity is clearly seen in the uptake experimental data, possibly indicating two phases are present.

Systems where equ'n.[76] described the uptake behaviour are, methanol in 97wt% PP/3wt% Z6082, xylene in LDPE and HDPE, and DCM in 90wt% PP/10wt% A174 silane, 90wt% PP/10wt% Z6082 silane, and in R6000. Xylene is a well known solvent for HDPE and LDPE, hence it is not surprising that equ'n.[76] is valid in these cases. PP/xylene uptake behaviour is not described by equ'n.[76] because of the methyl side groups on the polymer chain and LLDPE/xylene uptake behaviour is not described by equ'n.[76] because of the lack of branching in LLDPE molecular structure as compared to LDPE.

The DCM uptake behaviour of PP and XLPP, Figure 84, both show the equ'n.[75] dependency with each of them taking up more than either of the two PA6's. The Orgalloy R6000 shows a typical behaviour up to the saturation uptake plateau, where the higher uptake of DCM into the PP phase is the controlling factor. The rate of swelling is much greater for the silanated PP and the degree of swelling is dependent on the relative amounts of PP and silane in the material, or in the case of R6000, the relative amounts of PP/PA6. Both the PA6's show lower DCM uptake rate and maximum value than the polyolefins, including the silanated PP, each showing the equ'n.[75] dependency behaviour. The lower viscosity material A23 shows greater resistance than the higher viscosity B5.

The chloroform uptake determinations, Figure 85, with polyolefins shows that both R6000 and HDPE are more resistant than XLPP(2wt% A174 Silanes), and all exhibiting equ'n.[75] behaviour, with the R6000 curve being similar to LLDPE. However, since PP shows an even lower resistance behaviour than LDPE, the XLPP, based on the same PP, has an improved maximum uptake of $\approx$ 50% over that of PP.

HDPE does show similar low uptake behaviour to the two PA6's with chloroform with the higher viscosity B5 being more resistant than A23. Despite R6000 having a PA6 matrix, the uptake behaviour is similar to HDPE. Note that the shape of the R6000 and

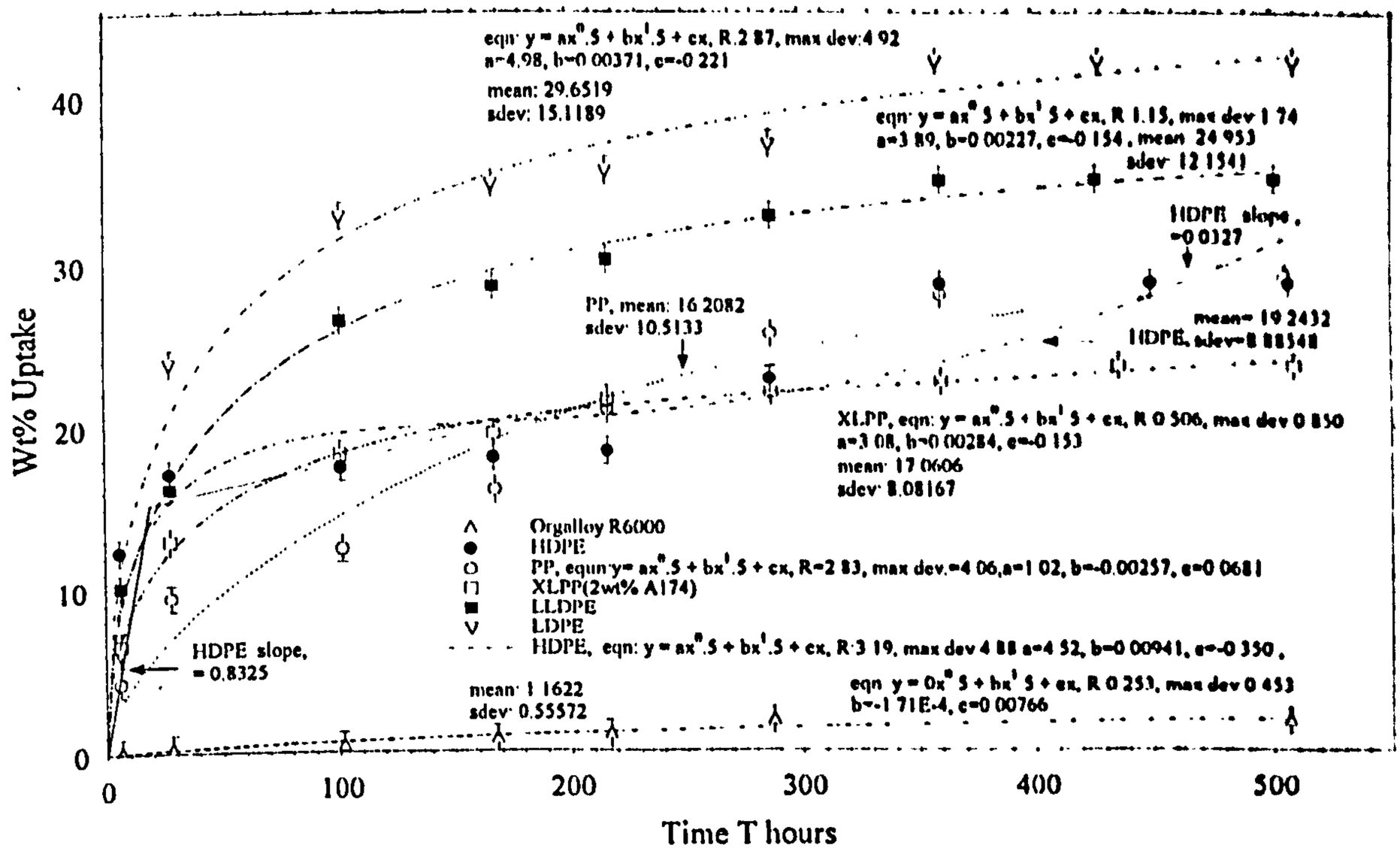

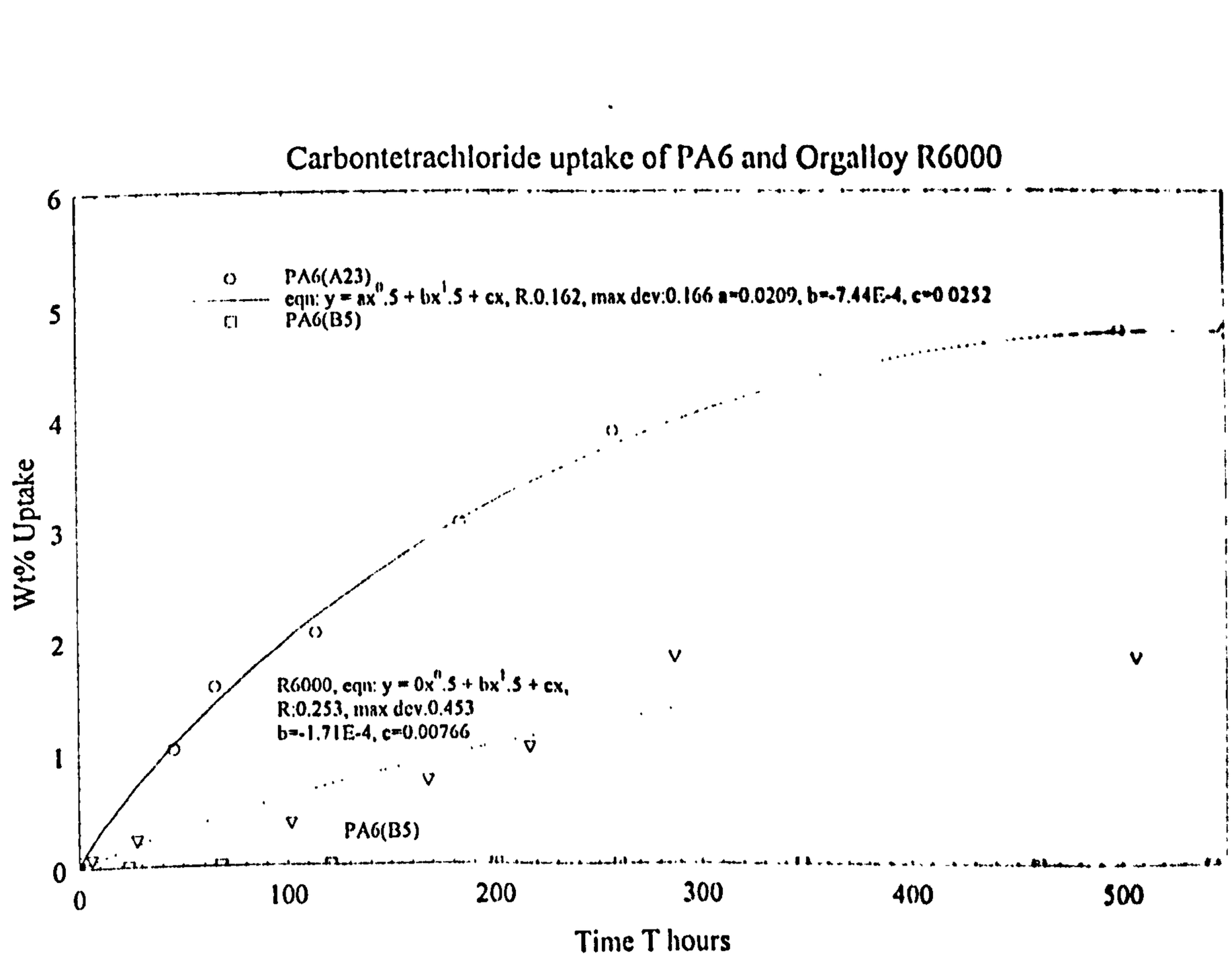

Figure 86 : Carbon tetrachloride uptake of polyolefins, PA6, and Orgalloy R6000

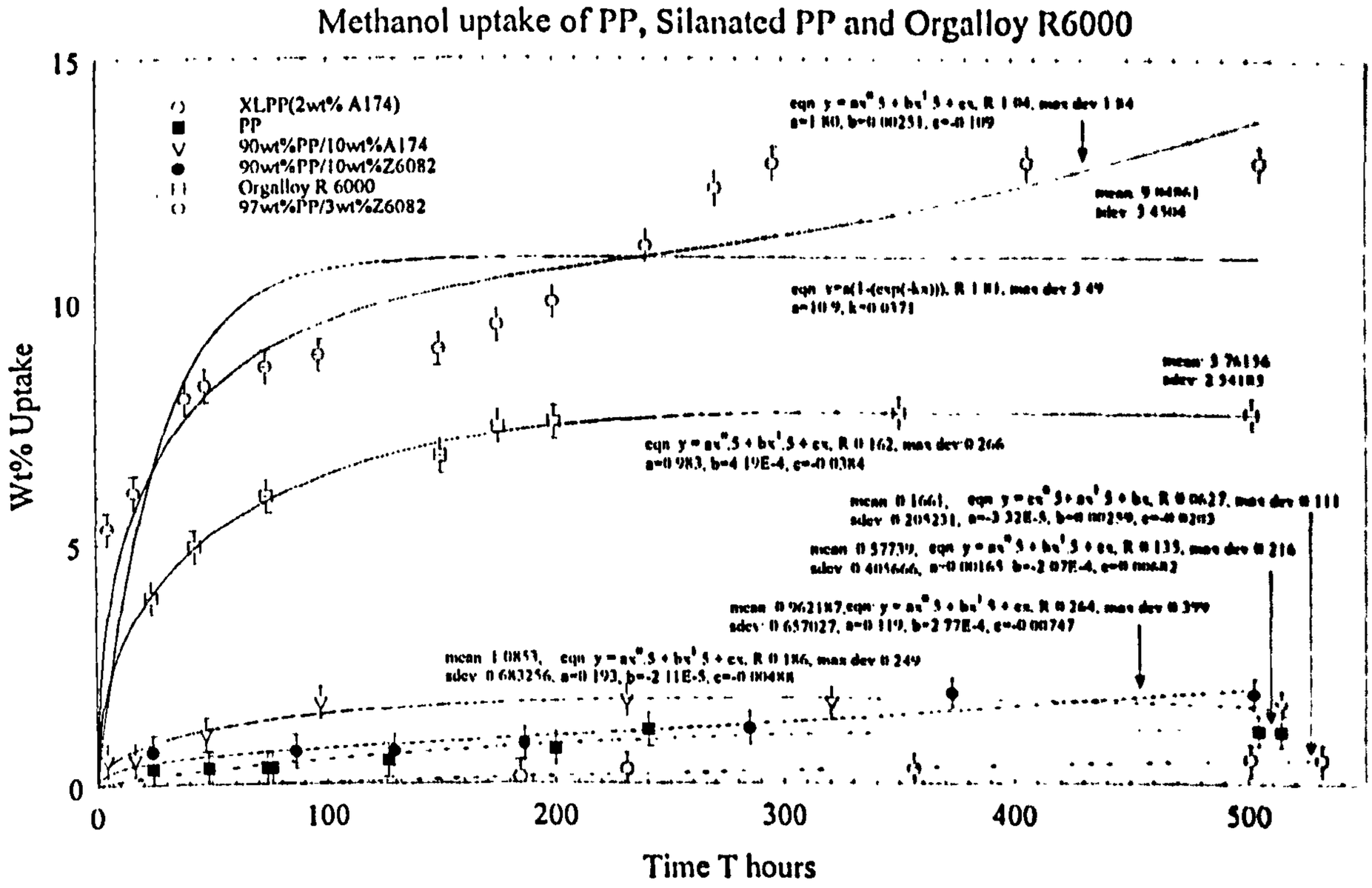

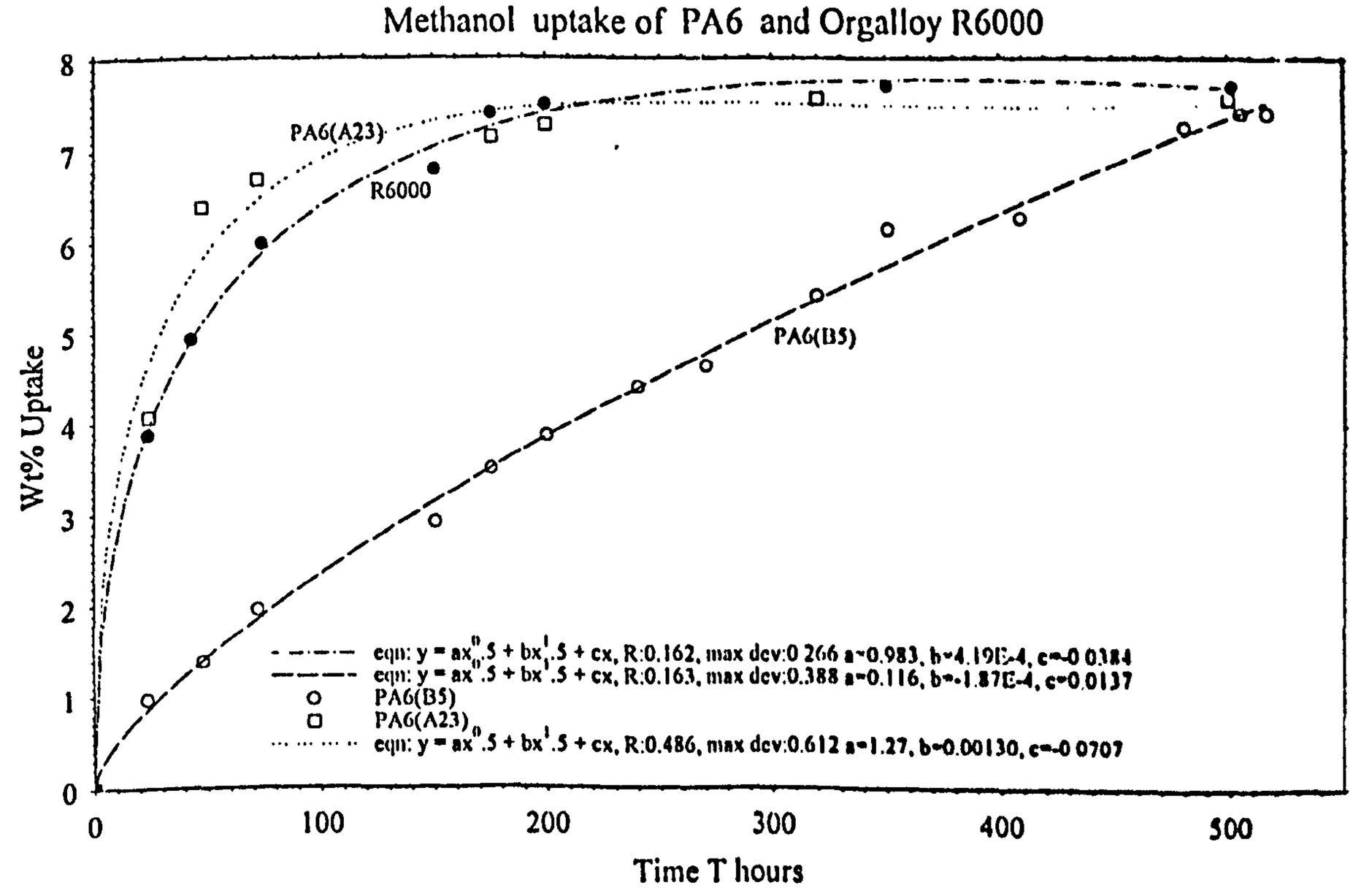

Figure 87 : Methanol uptake of PP, silanated PP, PA6, and Orgalloy R6000

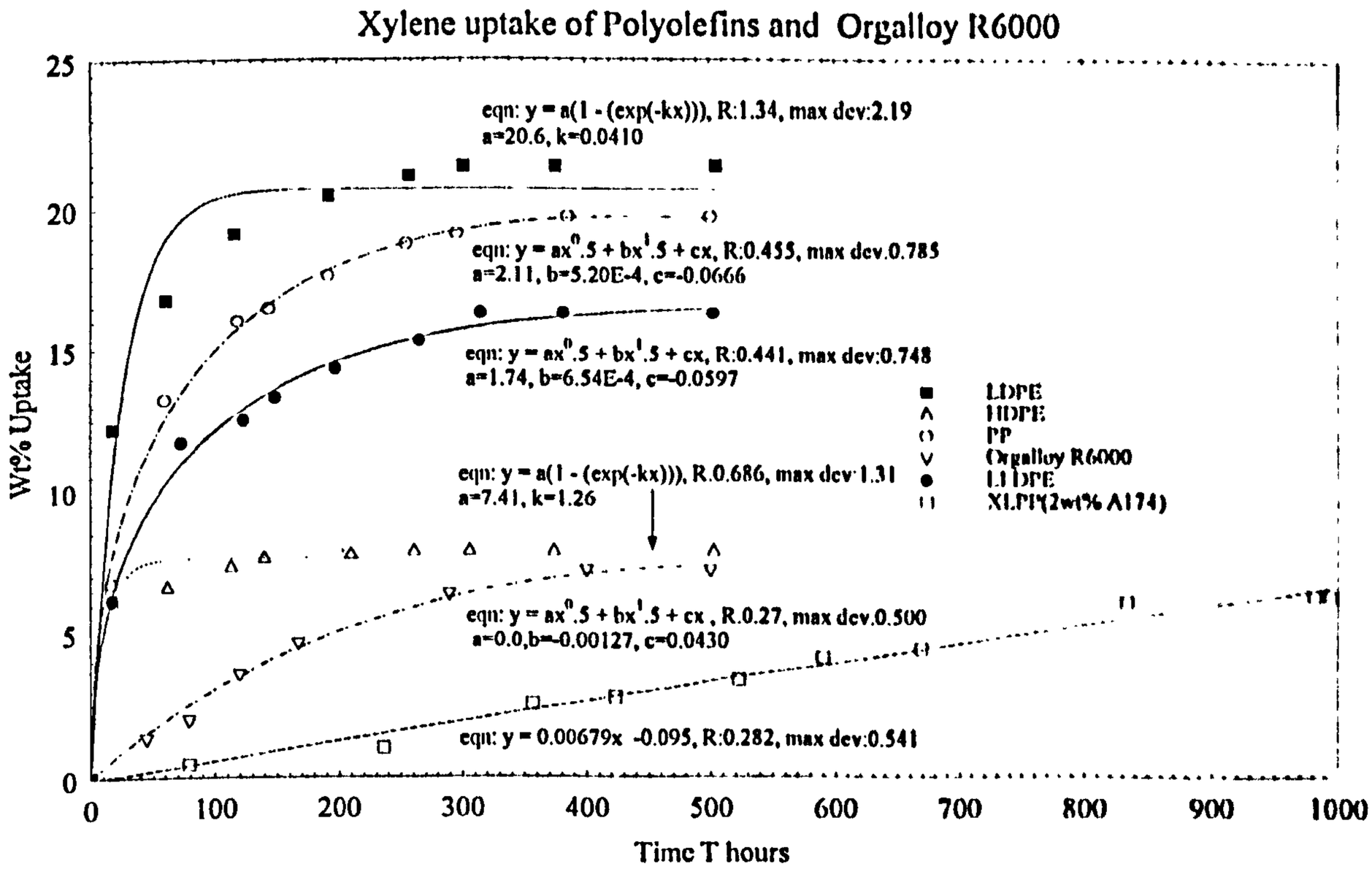

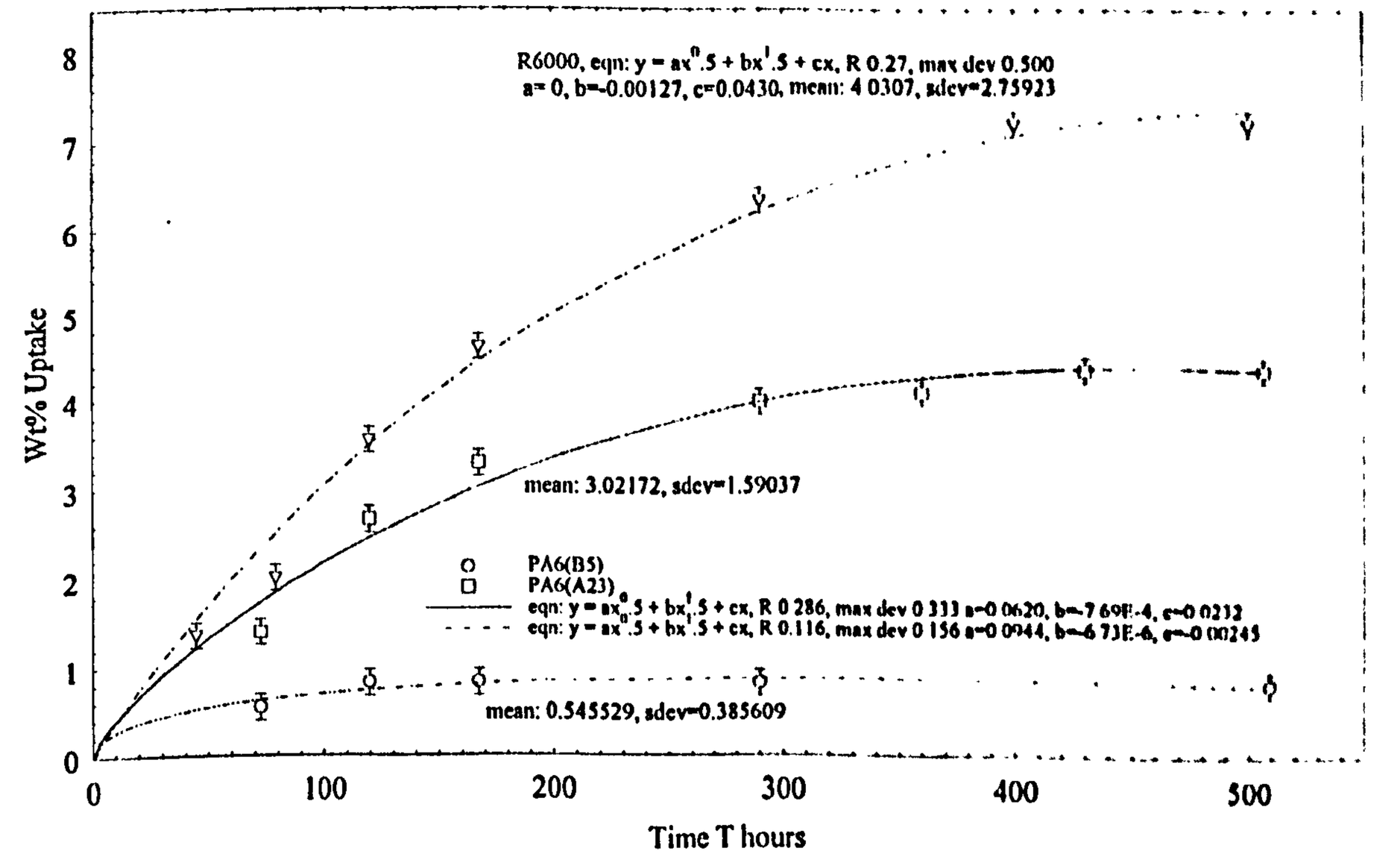

Figure 88 : Xylene uptake of polyolefins, PA6, and Orgalloy R6000

XLPP experimental data behaviour is similar, which for the former reinforces the two phase structure, and for the latter, the two phase silanated amorphous portion and crystalline portions. The R6000 and LLDPE fitted data both appear not to have reached the saturation plateau, whereas the other materials fitted data has. All the materials show the polynomial uptake behaviour of equ'n.[75] with $CHCl_3$.

The symmetrical carbontetrachloride (CCl_4) molecule again is taken up more rapidly and to a greater degree in LDPE (Figure 86) closely followed by the LLDPE. The PP maximum value is of the same order, but the initial uptake rate is much slower. R6000 is in fact lower than PA6(A23), the latter showing a much slower uptake rate than any polyolefins. The uptake of CCl_4 by B5 was very low. The shape of all the CCl_4 curves is not smooth, ie. the rate of uptake varies with time, with the exceptions being the PA6's. A point of inflexion is observed in the HDPE experimental data and that fitted using equ'n.[75]. As an alternative model, two straight lines can be drawn, intersecting as shown, where the rate is dramatically reduced, in less than 72 hours. This behaviour is generally exhibited by a sample with a surface area much greater than the thickness. The HDPE uptake behaviour is not easy to explain, showing two different uptake rates, possibly due to chemical interaction of CCl_4 and additives, such as antioxidants.

Xylene uptake is at a much higher rate, Figure 88, and the maximum value for the polyolefins is greater than for the PA6's, with the exception of XLPP, which shows similar maximum value as A23, but at a much slower linear behaviour uptake rate. R6000 is approximately intermediate between the two types of materials, exhibiting the same shape of uptake curve as the PA6's. Hence, in this case, the PA6 matrix is the controlling factor. For the more polar PA6's, it is not surprising that they exhibit more resistance to the non-polar xylene than the polyolefins, since xylene is a well known solvent for supporting polyolefin grafting reactions. Exceptionally, HDPE does not follow equ'n.[75] where a different polynomial relationship closely follows the experimental data. The curve from equ'n.[75] however shows an inflexion point in a similar way as carbontetrachloride uptake into HDPE and the two straight line portions have been fitted to represent two different linear uptake rates.

Steric hinderance of the xylene molecule, as compared to the smaller DCM and methanol

molecules is a significant factor for PA6's, as shown by comparing the uptake behaviour of xylene with that of methanol, but also note that R6000 shows similar uptake behaviour with both penetrants. Similar comparisons can be made for XLPP and PP, where in both cases, the rates and maximum values for methanol uptake are considerably lower than for xylene. For the other polyolefins, HDPE shows the equ'n.[75] behaviour with xylene, as does LLDPE, which uptakes approximately twice as much, but less than both LDPE and PP.

Methanol uptake, Figure 87, in PP and silanated PP, contrary to the DCM uptake behaviour, for the 3wt% Z6082 material shows much less resistance to methanol than the 10wt% material, and the shape of the curves fitted to equ'n.[75] is a different shape. The 3wt% Z6082 material shows two phase behaviour characteristics, with point of inflexion for the change in uptake rate. A different polynomial equation can be fitted to the data and for pre inflexion point, equ'n.[75] can be fitted. Both Z6082 silanated materials are in fact inferior to 100wt% PP, probably making them unsuitable for this application.

For the A174 silanated materials, only the 2wt% material shows superior uptake behaviour to PP, but the 10wt% material shows a similar maximum value to 10wt% Z6082 material, but reaching the maximum value in a much shorter time scale, of 100 hours, and then showing dimensional stability. Both show the 2nd order polynomial behaviour of equ'n.[75]. R6000 shows a sharp uptake of methanol to 125 hours, reaching then a maximum of approximately 7wt%, which is similar to that of the PA6's. The uptake rate, as displayed by the curve is similar to the lower viscosity A23. This is surprising since the blend consists of 40wt% PP, and yet clearly the matrix PA6 uptake in this material is dominant. The B5 reaches the maximum value after approximately 500 hours, again fitting equ'n.[75], but at an almost linear rate.

The statistical terms shown with the appropriate mathematical functions in Figures 84-88, are as follows :

R = the coefficient of correlation = $\Sigma xy/[(\Sigma x^2)\ (\Sigma y^2)]^{0.5}$,

defined as the sum of product of deviation of the means/sum of product of the standard deviations, where, standard deviation, $\sigma = [\Sigma(Np - N)^2/n\text{-}1]^{0.5}$,

and where, Np = population member, N = arithmetic mean of population members,

n = number of population members and maximum deviation = maximum difference of an experimental value from the fitted curve value.

4.9.6 Correlation of Uptake with Organic Solvent Permeability

All data for polymers which had been previously selected for uptake and permeability determination, using DCM(Dichloro-Methane) and Methanol as penetrants, was examined for possible correlation of these two parameters. The maximum uptake values were taken from Figures 84-88. The mass percentage uptake was plotted as a function of permeability on a mass basis. No correlation was found between these transport properties but possibly a correlation could exist for a particular class of polymers.

4.9.7 Organic solvent uptake and permeability results summary

As a barrier to dichloromethane, the silanated PP (2wt% A174 and 3wt% Z6082 silanes) has a permeability twice that of PTFE and the 2wt% A174 material has 50% the PP maximum uptake of DCM. Note that increasing the degree of silanation to 10wt%, increases the DCM permeability with both silanes, indicating some interaction between silane functional groups and the DCM. PTFE has a negligible DCM uptake, which the experimental results show, see Figure 84. For the PA6 permeability of the chlorinated methane derivatives, clear trends are observed in that PA6 is a better barrier to the chlorinated solvents than the polyolefins. R6000 is an inferior barrier to the chlorinated solvents than XLPP, where for all materials a clear trend of better permeability with the larger permeant molecules exists.

The trend clearly for both PA6 materials and R6000 chlorinated solvent permeabilities is for higher permeability with higher dipole. This trend is similar for 2wt% A174 silanated PP, and PP. HDPE has a suprisingly low permeability to carbon tetrachloride and chloroform.

CHAPTER 5 - CONCLUSIONS and FURTHER WORK

5.1 Conclusions

In this work an attempt has been made to understand the formation of microstructure in PA6 and PP blends, using a range of compatibilizers. The blend water vapour permeabilities were studied and correlated with composition and also compared with the water vapour permeability of laminates, for a polymer packaging barrier application. It has been shown that :

(1) The viscosity ratio cannot alone explain the phase dispersion in the systems investigated, see Figure 17, where d is plotted against the blend viscosity ratio for both binary and ternary systems. The reciprocal log dependency of viscosity on d showed linear behaviour only for some blends.

(2) The dispersed phase size of the binary B5/PP blends showed a minimum at low dispersed phase concentrations and near the phase inversion. When the viscosity ratio and volume fraction ratio were considered (Z factor), an exponential relationship describes the phase dispersion in binary B5/PP blends, dual phase morphology, and the onset of phase inversion. The interfacial slip factor calculations showed for binary blends as a function of component concentration has minimum values for concentrations near the phase inversion. For compatibilized systems, eg. BMAcoMAgPP and PB1001, values approach unity near the phase inversion concentration, ie. the deviation from linearity is diminishing.

(3) Interfacial interaction is therefore considered to be a significant parameter, but is very difficult to measure. Simple dynamic surface tension experiments at ambient temperature with low molecular weight liquids confirmed the literature values for the homopolymers but these data did not explain phase formation (dispersion) in the polymer melt . Nonetheless, the surface tension can be related to the volume thermal expansion coefficient through equ'n.[72] of Section 4.8.1, which is in turn related to the free volume, occupied by the penetrant during the swelling of the polymer matrix, as exhibited in equ'n.[75].

(4) The compatibilizer which had the most significant effect on reducing the phase size was PB3002, a Maleic Anhydride grafted onto PP material, despite having a low grafting

level of < 1.0wt%. FTIR spectroscopy of materials containing the higher level of grafting, in house prepared, MAgPP compatibilizer, revealed chemical reactions during blending by the production of a chemical bond between the components, forming a block co-polymer of PP-MAgPP-PA6.

(5) A relationship between phase size and water vapour permeability was not found and it is therefore concluded that the chemical modification of the matrix is more important than dispersed phase size for controlling water vapour permeability.

(6) The water vapour permeability of ternary compatibilized systems is lower as compared to the binary systems, and are better than R6000. In fact the water vapour permeability of injection moulded R6000 is similar to that of binary B5 and A23 blends, see Figure 65a. FTIR spectral subtraction identified functional groups present in the R6000, which are not present in the homopolymers and the phase dispersion has been shown to be destabilised by injection molding.

(7) In the present work, the investigations by Robeson et al[1] showing the sharp change in oxygen permeabilities at the phase transition have not been confirmed. The transition at inversion is negligible, possibly because of the relatively small differences in the homopolymer water vapour permeabilities. In addition, at constant PA6 concentration, only a relatively small difference in water vapour permeability is observed for laminate and blend permeabilities.

(8) Functional groups present in the matrix are the most important parameters controlling permeability, providing active sites for permeant molecular transport. The OH functional groups, which do not interact with oxygen significantly below 70% RH, were identified by spectral subtraction in silanated PP. Their presence in silanated PP decreased the oxygen permeability of PP. The SiOSi groups on the other hand, will reduce water vapour permeability.

(9) Hence the change in the oxygen permeability of a hydrophillic oxygen barrier materials such as EVOH or PA6, as a function of polymer moisture content is mostly controlled by the change in oxygen solubility.

(10) The water vapour barrier performance of the compatibilized blends and ternary "compatibilized" laminates compared to the corresponding binary blends and laminates is as follows :

(i) The PA6/BMAcoMAgPP/PP ternary systems with PP down, and a thin PA6 layer, show superior barrier to binary laminates, and the converse with a thinner PP layer. The B5/BMAcoMAgPP blends show a negative deviation significantly towards better permeability than binary blends. The BMAcoMAgPP/PA6(B5) down laminates show an inferior dependency on PA6 concentration than the corresponding binary laminates and show a similar dependency to the blends.

(ii) The PA6(A23)/BMAcoMAgPP PP down laminates are significantly better than corresponding binary systems or blends. The PP/BMAcoMAgPP/PA6(A23) laminates and blends dependency curve is similar to that of the A23 and PP down binary laminates.

(iii) Both the B5/PB1001 ternary laminates are inferior to the binary systems, and binary and ternary blends show similar water vapour barrier.

(iv) The PP down PB1001/A23 laminates are superior to binary ones, whereas and PB1001/A23 blends and PB1001/A23 down laminates are slightly inferior to the binary systems.

(v) The PP down MAgPP/B5 laminates are superior at low PA6 concentration but inferior at high concentrations to the binary systems but superior to the blends, which in turn show negative deviation compared to the binary blends, ie. the compatibilizer gives significantly better water vapour barrier. The MAgPP/B5 down laminates show a similar dependency on PA6 concentration as the binary B5 down laminates.

(vi) The MAgPP/A23 down laminates are inferior when compared to the corresponding binary systems but the PP down ternary systems are marginally better than binary materials. No blends were made for these materials.

(vii) The PP down PB3002/B5 systems are superior at low PA6 concentrations than binary systems, but worse at high PA6 concentrations. The PB3002/B5 compatibilized blends have significantly better barrier than the binary blends and are better than the Pa6 down laminates. The binary B5 down laminates are also better than the PB3002/PA6 down laminates.

(viii) Both the A23/PB3002 PP down and PA6 down laminate systems have inferior barrier when compared to the corresponding binary laminates. No blends were prepared for these materials.

(ix) XLPP/B5 binary laminates, both XLPP and B5 down, are superior to the corresponding PP/B5 laminates and likewise for the blends. The XLPP/Plast.B5 blends are also superior to the corresponding PP/Plast.B5 blends.
(x) XLPP/A23 down laminates are superior to the A23/PP blends and the PP/A23 down laminates. No A23/XLPP blends were prepared.

(11) The water vapour barrier performance of the tie-layer adhesive laminates as compared to the corresponding binary systems is as follows :
(i) With a thicker B5 layer, PP down laminate Scotchgrip systems, the laminates show lower permeabilities, but at intermediate B5 thickness, Fastbond systems are superior. All the B5 PP down tied systems show very similar behaviour to binary laminates. For PA6 down and PP down B5 systems, little improvement is shown for the latter with Fastbond and these systems are again superior to the other tied laminates and binaries.
(ii) Both with the PP and PA6 down, the A23 non-tied systems are superior, with thicker A23 layers, to the tied ones, but the Fastbond systems are superior for thinner A23 layers. Thicker PA6 layer, A23 down systems show Scotchgrip tied laminates as superior. Durotak appears not to be effective for A23 laminates, either PP or A23 down.
(iii) Durotak/B5 PP down systems show higher permeability than the binary systems. However, when the B5 is down, the Durotak system then shows lower permeabilities. The hydrophilicity of the toluene based Durotak displays a synergism with the water vapour plasticised B5, which is not possible when the PP is nearer to the penetrant.
(iv) The dependency of the tie-layer systems water vapour permeabilities on a component concentration (thickness) have been shown to be largely empirical non-linear equations, showing negative deviations largely from the linear additivity rule.

The effect of morphology on water vapour permeability has been most clearly demonstrated by experiments with laminates. The group of laminates formed by sandwiching a compatibilizer between layers of PP and PA6 showed the lowest permeability when the PP was facing the penetrant. The compatibilizer also had a pronounced effect on the improvement of the barrier properties. However, their contribution was not purely additive and the chemical interaction across the interface seemed to have a decisive effect on the barrier performance of the laminates. The best results were obtained with the BMAcoMAgPP/PA6(A23) and PB3002/PA6(B5) systems.

The tie-layer adhesive permeabilities were similar to or slightly higher than that of the compatibilizers, see Table 10. The performance of these laminates was in some cases better than that of binary laminates, with Fastbond having the most significant overall effect on the permeability improvement. Durotak was only effective with PA6(B5).

5.2 Conclusions Summary

The most important conclusion from this work therefore is that functional group interaction with the permeant is unambiguously more important than any morphological changes in the blends, since it has been shown that, the level of dispersion, the viscosity ratio, the overall viscosity, interfacial properties and uptake behaviour are less important for polymer water vapour and organic solvent permeability control, for the systems investigated, than functional group interactions. Indeed, upon injection molding a commercial PP/PA6 blend, Orgalloy R6000, the dispersed phase size increased by 100%, from 0.6 to 1.2 μm, but the water vapour permeability increased by only 11%, and the oxygen permeability by 21.7%.

Uniquely, water vapour permeability for polymer laminated multiphase was compared with that of blends made of the same components, which showed in this work that the laminates were superior to the corresponding blends, with and without the tie-layer adhesives or compatibilizers. In addition, the sensitivity of water vapour permeability for PP/PA6 laminates as to which component was closest to the penetrant was demonstrated.

5.3 Suggestions For Further Work

(i) Oxygen permeability determinations of blends and laminates using commercially available equipment.

(ii) Investigate thermal stabilisation of blends by annealing/coalescence.

(iii) Investigate a masterbatch di-block co-polymer compatibilizer made from a low molecular weight PA6, low molecular weight PP and MAgPP.

(iv) Higher PA6 concentration compatibilized blend preparation, and characterization, to determine phase inversion permeability discontinuities.

(v) Further silanated PP/PA6 blends, using higher concentrations of silane with PP and different PA6 concentrations, for investigation of the silane additionally as a blend coupling agent.

(vi) FTIR microscopy for penetrant diffusion front concentration profile tracking in organic solvent uptake experiments.

(vii) Organic solvent permeability determination of blends.

(viii) Water vapour and oxygen permeability determinations of Tufloc cyanoacrylate tied laminates.

(ix) The effect of humidity on the oxygen barrier of silanated PP.

(x) The correlation of blend microstructure and blend mechanical properties, such as tensile strength, impact resistance, elongation, and tear resistance.

(xi) The correlation of dynamic mechanical testing data, such as T_g, with microstructure.

(xii) An in depth study of blend interfaces using Transmission Electron Microscopy.

(xiii) Getting the functionality of the matrix right - investigation of the effect functional groups have on permeability.

CHAPTER 6 - REFERENCES

6.1 Chapter 1 References

[1] Jenkins, W. A., and K. R. Osborne, "Plastic Films Technology and Packaging Applications", Technomic, p255, (1992).
[2] Ibid, p9.
[3] Rogers, C.E., "Permeation of gases and vapours in polymers", in "Polymer Permeability", ed. J. Comyn, p28, (1985).
[4] Ashley, R.J., "Permeability and Plastics Packaging", in "Polymer Permeability", ed. J. Comyn, p284, (1985).
[5] Jenkins, W.A., and K.R. Osbourne, "Plastic Films Technology and Packaging Applications", Technomic, p124, (1992).
[6] Barrer, R.M., "Diffusion In and Through Solids", C.U.P., Cambridge, (1941).
[7] Corish, P.J. (ed.), "Concise Encyclopaedia of Polymer Processing & Applications", p493, Pergamon, (1992).
[8] Eur. Plast. News., p14, December, (1995).
[9] Private Communication with CarnaudMetalbox plc., Jan., (1996).
[10] Wu S., Polym. Eng. Sci., 27, p335 (1987).
[11] Favis B. D., and J. P. Chalifoux, Polym. Eng. Sci., 27, p1591, (1987).
[12] Vesely D. and M. A. Parker, 3rd Europ.Symp.Polym.Blends, Cambridge(PRI-publ.),D2/1 (1990).

6.2 Chapter 2 References

6.2.1 Polymer Blend Literature

[1] Utracki, L.A., "Polymer Alloys and Blends", p31, Hanser Verlag (1989).
[2] Vesely, D., and A.M.Parker, Jour. Polym. Sci., Polymer Phys., 24, p1869, (1986).
[3] Frisch, H.L., Jour. Polym. Sci., 16, p1657, (1978).
[4] Hopfenburg, H.B., L.Nicolais, and E.Drioli, Polymer, 17, p195, (1966).
[5] Robeson, L.M., in "Polymer Compatibility and Incompatibility", K.Solc (Ed.), Harwood Academic Publ., New York (1980).
[6] Robeson, L.M., private communications, to L. A. Utracki (1989).
[7] Bucknall, C.B., "Toughened Plastics", Appl.Sci.Publ., London, (1977).
[8] Bucknall, C.B., and W.W.Stevens, Jour.Mater.Sci., 15, p2950 (1980).
[9] Bucknall, C.B., and C.J.Page, Jour.Mater. Sci., 17, p808, (1982).
[10] Juliano, P. Polymer Eng. Sci., 24, p1359, (1984).
[11] Bucknall, C.B., and I.K.Partridge, in "Toughening of Plastics", PRI, London (1985).
[12] Bauer, R.F., Polym. Eng. Sci., 22, p130, (1982).
[13] Krause, S., 5th Conven., Ital. Sci. Macromol., (1981).
[14] Eisenburg, A., M.Hara, Polym. Sci.Eng., 24, p1306, (1984).
[15] Smith, P, M.Hara, and A. Eisenburg, in "Current Topics in Polymer Science", R.M.Ottenbrite, L.A.Utracki and S.Inoue, Eds., Hanser-Verlag, Munchen, (1987).
[16] Siegfried, D.L., D.A.Thomas and L.H. Sperling, Jour. Appl. Polymer Sci., 26, p177, (1981).
[17] Sperling, L.H., "Interpenetrating Polymer Networks and Related Materials", Plenum Press, New York, 1981.
[18] Siegfried, D.L., Polymer Eng. Sci., 21, p39, (1982).
[19] Djomo, H., R. Colemanares and G.Meyer, Eur. Polym. Jour., 17, p521, (1981).
[20] Adachi, H., S.Nishi, and T. Kotaka, Polym. Jour., 14, p985, (1982).
[21] Frisch, K. C., D. Klempner, and H.L.Frisch, Polym. Eng. Sci., 22, p143 (1982).
[22] Sperling, L.H., and J.M.Weidermaier, Polym. Sci.Technol., 20, p191, (1983).

[23] Yeo, J.K., L.H. Sperling, and D.A. Thomas, Polymer, 24, p307, (1983).
[24] Sperling, L.H., J.M.Weidermaier, J.K. Yeo, and J. Michel, Polym. Sci. Technol., 20, p191, (1983).
[25] Hage, E., Jnr., Ph. D. thesis, North Carolina State University., Raleigh, NC, (1983).
[26] Lipatov, Yu. S., A. Ye.Nestorov, T.D. Ignatova, N.P.Gudima, and O.T. Gritsenko, Eur. Polym. Jour., 22, p83, (1986a).
[27] Newman, S., and D.R. Paul, "Polymer Blends", Academic Press, New York, (1978).
[28] Dagli, S.S., and M.Xanthos, Polym. Eng. Sci., 31, 13, p929, (1991).
[29] Xanthos, M., Polym. Eng. Sci., 28, 21, p1392, (1988).
[30] Gaylord, N.G., Macromol.Sci.-Chem., A26, 8, p1211, (1989).
[31] Rizzo, G., G. Spadaro, D.Acierno and E.Calderaro, Radiat.Phys.Chem., 21, p349, (1983).
[32] Paul, D.R. and J.W. Barlow, J. Macromol. Sci., Rev. Macromol. Chem., C18, p109, (1980).
[33] Olabisi, O., Polyblends, in "Kirk-Othmer Encyclopaedia of Chem.Technol.", Third Edition, J.Wiley and Sons, New York, (1982).
[34] Fox, D.W., R.B. Allen, J.I.Kroschwitz, Compatibility, in "Encyclop. Polym. Sci. Eng.", J. Wiley and Sons, New York, (1985).
[35] Walsh, D.J., and S.Rostami, Adv. Polym. Sci. 70, p119, (1985).
[36] Brooks, N.M., Jour. Ind. Irradiat. Technol., 1, p237, (1983).
[37] Nakamura, Y., A.Watanabe, K. Mori, K.Tamura, and H.Miyazaki, Jour.Polym. Sci., Part C, Polym. Let., 25, p127, (1987).
[38] Rudin, A., D.A. Loucks, and J.M. Goldwasser, Polym. Eng. Sci., 20, p741, (1980).
[39] Padwa, Allen R., Polym. Eng. Sci., 32, 22, p1703, (1992).
[40] Van Duin, M., Aussems, M.P.T., and Borggreve, R.J.M., Polym. Proc. Soc. IX Meet., Manchester, April, 09-02, p275 (1993).
[41] Ide, F., and Hasegawa, A., Jour.Appl. Polym. Sci., 18, p963, (1974).
[42] Nishio, T., et al, Polym. Proc. Soc. IX Meet., Manchester, April, 09-04, p279, (1993).
[43] Lambla, M., A.C.S. Polym. Mater. Sci. Eng. Div. Preparings, 58, p879, (1988).
[44] Ward, I.M., "Developments in Oriented Polymers-1", Appl.Sci.Publ., Barking, U.K., (1982).
[45] Ward, I.M., Adv. Polym. Sci., 70, p1, (1985).
[46] Illing, W., Kunstoffe, 80, 7, p838, (1990).
[47] Green, P.F., P.J.Mills, and E.J. Kramer, Polymer, 27, p1063, (1986).
[48] Fleischer, G., Coll. Polym. Sci., 265, p89, (1987).
[49] Kausch, H.H., and M.Tirrell, Ann. Rev. Mater. Sci., 19, p341, (1989).
[50] Dimov, K., and M. Savov, Vysokomol. Soed., A22, p65, (1980).
[51] Yakovlev, K.V., R.I. Zhitomirets, O.V. Romankevich, S.E. Zabello A.V. Yudin, Khim. teknol. (Kiev), 5, p14, (1984).
[52] DiPaola-Barayani, G., in ACS Symp. Ser. 391, Inv. Gas Chrom., eds. D. R. Lloyd, T.C. Ward, H.P. Schrieber, C.C. Pizana, p109, (1989).
[53] Kammer, H.W., Acta Polymerica, 42, 11, p571, (1991).
[54] Paul, D.R., and J.W. Barlow, Polymer, 25, p487, (1984).
[55] Mendelson, R.A., Jour. Polym.Sci., Polym. Phys. Ed., 23, p1975, (1985).
[56] Fowler, M.E., J.W. Barlow, and D.R. Paul, Polymer, 28, p1177, (1987).

[57] Goh, S.H., S.Y.Lee, K.S. Siow, and C.L.Pua, Jour. Appl. Polym. Sci., 33, p353, (1987).
[58] Wu, S., Polymer, 28, p1144, (1987).
[59] Graebling, D.,R. Muller, and J.F. Palierne, Macromolecules, 26, p320, (1993).
[60] Scholtz, P., D.Froelich and R.Muller, Jour. Rheol., 33(3), p481, (1989).
[61] Utracki, L.A., Adv. Polym. Techn., 5, p41, (1985).
[62] Okoroafor, E.U. et al, Polym., 33, 24, p5264, (1992).
[63] Han, C.D. and Yang, H.H., Jour. Appl. Polym. Sci., 33, p1221, (1987).
[64] Han, C.D., and Chuang, H.H., Jour. Appl. Polym. Sci., 30, p2431, (1985).
[65] Utracki, L.A., Adv. Polym. Technol., 5, p41, (1985).
[66] Utracki, L.A., in "Multiphase Polymeric Materials", L.A.Utracki, and R.A.Weiss, Eds., ACS Books, Washington DC, (1989).
[67] Willis, J.M., and B.D. Favis, Polym. Eng. Sci., 28, p1416, (1988).
[68] Lin, C.C., Polym. Jour., 11, p185, (1979).
[69] Utracki, L.A., "Polymer Alloys and Blends", Hanser, p179, (1989).
[70] Utracki, L.A., Jour. Rheol., 35, 8, p1615, (1991).
[71] Lyngaae-Jφrgensen, J., "Rheology of Polymer Blends", in ""Polymer Blends and Alloys", eds., M. J. Folkes and P.S. Hope, p90, (1993).
[72] Paul, D.R., and J.W.Barlow, Polym. Eng. Sci., 24, 8, p525, (1984).
[73] Plochocki, A.P. in "Polymer Blends", D.R. Paul and S. Newman, Eds., Academic Press, New York, (1978).
[74] Plochocki, A.P.,Polym. Eng. Sci., 22, p1153, (1982).
[75] Plochocki, A.P.,Polym. Eng.Sci., 26, p82, (1986).
[76] Utracki, L.A., Proceed., Int. Chem. Cong. Pacific Basin Socs., Honolulu, Dec.16-21, (1984).
[77] Utracki, L.A.,Adv. Polym. Technol.,5, p41, (1985).
[78] Deanin, R.D., and G.E. D'Isadoro, A.C.S. Div. Org. Coat. Plast. Prepr., 43, p19, (1980).
[79] Utracki,L.A., in "Multiphase Polymeric Materials", L.A.Utracki, & R.A.Weiss,Eds., ACS Books, Washington DC, (1989).
[80] Ho, W.J. and R.J. Salovey, Polym. Eng. Sci., 21, p839, (1981).
[81] Bartlett, D.W., J.W.Barlow, and D.R. Paul, Jour. Appl. Polym. Sci., 27, p2351, (1982).
[82] Olabisi, O., L.M.Robeson, and M.T.Shaw, "Polymer-Polymer Miscibility", Academic Press, New York, (1979).
[83] Raval, H., Polym.Int., 26, p105, (1991).
[84] Park, S.J., B.K.Kim, H.M.Jeong, Eng. Polym. Jour., 26, 2, p131, (1990).
[85] Subramanium, N., and T.J. Nelson, Polym.-Plast. Technol., 32(6), p635, (1993).
[86] Germain Y. et al, Jour. Rheol., 38,3, p681, (1994).
[87] Oldroyd, J.G., Proc. Royal. Soc., London Ser. A,218, p122, (1953).
[88] Raval, H. et al, Polym.Int., 24, p99, (1991).
[89] Alberts, H. et al, "Co-polymers, Polyblends, and Composites", Acad. Press, N.Y., N.Y.,(1980).
[90] Raval, H., Polym., 32, 3, p493, (1991).
[91] Lindberg, K.A.H., and M.Johansson, Plast. Rubb. Proc.Appl., 14, p195.(1990).
[92] Speroni, F., Macromol. Symp., 78, pp299-311, (1994).
[93] Cheng, C.C., and J.L.White, Polym. Eng. Sci., 33, 14, p923, (1983).
[94] Lindberg, K.A.H., and H.E. Bertiilsson, Jour. Mats. Sci., 26, pp4383-4388, (1991).

[95] Chang, D.H., and H.K. Chuang, Jour.Appl.Sci., 30, p2431, (1985).
[96] Duschek, T., R. Mulhaupt, B.Reiger, Makromol.Chem., Macromol.Symp., 48/49, p317, (1991).
[97] Chen, C.C., E.Fontan, K.Min, and J.L.White, Polym. Eng.Sci., 28, p2, 69, (1988).
[98] Utracki, L.A., P.Sammut, Plast.Rubb. Comp. Proc.App., 16, 4, p221, (1991).
[99] Ibid, Polym. Netw. Blends,2(1), p23, (1992).
[100] Glotin, M., R.Parsy, and P.Abadie, FR. Appl.N.003877, 24.03.88 to ATOCHEM.
[101] Aharoni, S., "Analysis of N6/PP blend ORGALLOY R-6000", Report to VAMAS TWP-PB, Sept.(1989).
[102] Cook, B.W., and K. Jones, "A Programmed Introduction to Infrared Spectroscopy", p112, Heyden, 1972.
[103] Messerschmidt, R.G., and M. A. Harthcock, (eds.), "Infrared Microscopy", Dekker, New York, 1988.
[104] Tabb, D.L., Sevcik, J.J., Koenig, J.L., Jour. Polym. Sci., 13, pp815-824, 1975.
[105] Garton, A., Polym. Eng. Sci., 24, p112, 1984.
[106] Coleman, M.M., and P.C. Painter, Applied Spectroscopy Reviews, 20, p255, 1984.
[107] Garton, G., Bamji, S.,Bulinski, J., Densley, R.J., IEEE Trans. Elec. Ins. EI-22, p405, 1987.
[108] Ishida, H., Ishitani,A., Chpt.7, "Practical FTIR Spectroscopy", Ferraro, J.R., Krishnan, K.,eds., Acad.Press, N.Y., N.Y., 1990.
[109] Yang, J., Garton, G., Proc. Amer. Chem. Soc., PMSE, 62, pp916-9, 1990.
[110] Ross, R., Guerts, W.S.M., Smit, J., IEE Conf. Pub. no.259, Diel.Mats.Meas.Apps., pp313-7, 1988.
[111] Garton, A., Polym. Compos., 5, p258, (1984).
[112] Garton A., and J.H. Daly, Canadian Aeronautics Space Inst. Conf., Ottawa, Canada, June, 1984.
[113] Koenig, J.L.Adv. Polym. Serv., 54, p87, (1983).
[114] Harthcock, M.A., and S.C. Atkin, Infrared Microspectroscopy:Development and Applications of Imaging Capabilities, in, "Infrared Microspectroscopy Theory and Applications", 21, ed. R.G.Messerschmidt and M.A.Harthcock, Marcel Dekker, N.Y., (1988).
[115] Coleman, M.M., D.F. Varnell, and J.P. Runt, in "Polymer Alloys III", D.Klempner and K.C. Frisch, Eds., Plenum Press, New York,(1981).
[116] Coleman, M.M., P.C. Painter, Appl. Spectroscopy Rev., 20, p255, (1984).
[117] Coleman M.M., J.L.Koenig, and P.C.Painter, "Theory of Vibrational Spectra and its Application to Polymeric Materials", J.W.Wiley, New York, (1982).
[118] Coleman, M.M., P.C.Painter, and J.L.Koenig, "Specific Interactions and the Miscibility of Polymer Blends", Technomic Publishing Company Inc., Lancaster, USA, (1991).
[119] Klopffer, W., "Introduction to Polymer Spectroscopy", Springer Verlag, (1984).
[120] Allara, D.L., Applied Spectroscopy, 33, p358, (1979).
[121] "Infrared Spectroscopy of Polymer Blends, Composites, and Surfaces", by A. Garton(ed.), Hanser, p126, (1992).
[122] Ting, S.P., E.M. Pearce,and T.K. Kwei, Jour.Polym. Sci., Polym. Lett. Ed., 18, p201, (1980).
[123] Cangelosi, F., Ph.D. thesis, Univ. Of Connecticut, Storrs, (1982).

[124] Moskala, E.J., Ph. D. thesis, Penn. State University, (1984).
[125] Moskala, E.J., D.F.Varnell, and M.M.Coleman, Polym. Comms., 24, p206, (1983).
[126] Pennacchia, J., Ph.D. thesis, Polytechnic Inst., New York, (1986).
[127] Coleman, M.M., D.J. Skrovanek, J. Hu. and P.C. Painter, Macromolecules, 21, p59, (1988).
[128] Painter, P.C., Y.Park, and M.M. Coleman, Macromolecules, 21, p66,(1988).
[129] Hemsley, D.A., "Applied Polymer Light Microscopy", Elsevier Applied Science, (1989).
[130] Karger-Kocis, J., A. Kalo, and V.N.Kuleznev, Polymer, 25, p279,(1984a).
[131] Dumoulin, M.M., L.A.Utracki, and C.Farha, S.P.E. Technical Paper, 30, p443, (1984).
[132] Vesely D. and M. A. Parker, 3rd Europ.Symp.Polym.Blends,Cambridge(PRI-publ.),D2/1 (1990).
[133] Thomas, D.A., Jour.Polym.Sci., Polym. Symp., 60, p189, (1977).
[134] Roche, E.J., and E.L. Thomas, Polymer, 22, p333, (1981).
[135] Vesely, D., and H.Lindberg, Inst. Phys. Conf. Ser., 61, p7,(1982).
[136] Michler, G.H., Ultramicroscopy, 15, p81, (1984).
[137] White, J.R., E.L.Thomas, Rubber Chem. Technol., 57, p457,(1984).
[138] Shaw, M.T., in "Polymer Blends and Mixtures", eds. D.J. Walsh, J.S. Higgins, and A. Maconnachie, NATO Series E No.89, Martins Nijhoff publ. Dordrecht, (1985).
[139] Kamal, M.R., and P.G. Lafleur, Polym. Eng. Sci., 24, p692, (1984).
[140] Dumoulin, M.M., P.Toma, L.A.Utracki, I.A. Jinnah, M.R.Kamal, S.P.E. Technical Papers, 31, p534, (1985).
[141] Utracki, L.A., M.M.Dumoulin, and P.Toma, Polym. Eng. Sci., 26, 1, p34,(1986).
[142] Pillon, L.Z. and L.A.Utracki, NRCC/IMRI Symp. Polyblends-'85, Boucherville, Canada, April 16, (1985).
[143] Pillon, L.Z., and L.A. Utracki, Polym. Proc. Eng., 4, p375, (1986).
[144] Noel, O.F.I., and J.E.Carley, Polym.Eng.Sci., 24, p488,(1984).
[145] Elemans, P.H.M., J.G.M. van Gisbergen, and H.E.M. Meijer, in "Integration of Fundamental Polymer Science and Technology-2", P.J.Lemstra, and L.A. Kleintjens, Eds., Elsevier Appl. Sci., London, (1988).
[146] Meijer, H.E.M., P.J.Lemstra, and P.H.M. Elemans, Makromol.Chem., Macromol. Symp., 16, p113, (1988).
[147] Valsamis, L.N., M.R.Kearney, S.S.Dagli, D.D.Merhta, and A.P.Plochocki, Adv. Polym. Technol., 8, p115,(1988).
[148] Rybnikar, F., Jour. Appl. Polym. Sci., 30, p1949, (1985).
[149] Eastmond, G.C., and D.G. Phillips, Polym. Commun., 26, p98, (1985).
[150] Lars, G., J.Bohse, R.Stephan, and J. Sachse, Plast.Kautsch., 30, p458, (1983).
[151] Yang, D., B.Zhang, Y.Yang, Zh. Fang, G.Sun, and Zh. Feng, Polym. Eng.Sci. 24, p612, (1984).
[152] Karger-Kocis, J., L.Kiss, and V.N. Kuleznev, Polym.Commun., 25, p122, (1984b).
[153] Kyotani, M., and H.Kanetsuna, Jour. Macromol.Sci.Phys., B26, p325, (1987).
[154] Hsu, C.C., and P.H.Geil, Polym. Eng. Sci., 27, p1542, (1987).
[155] Tung, M.A., and L.Jones, Scanning Electron Microscopy, 3, p523, (1981).
[156] Holsti-Miettinen, R.M. and J.V. Seppala, Polym. Eng. Sci., 34, 5, p395,(1994).
[157] Parker, M.A., and D. Vesely, Micro. Res. and Tech., 24, p333, (1993).

[158] Jinnah, I. A., Kamal, M. R., Utracki, L. A., Polym. Eng. Sci., 24, 17, p1337, (1984).
[159] Handlin, D.L., W.J. MacKnight, and E.L.Thomas, Macromolecules, 14, p795, (1980).
[160] Vesely, D., D.S.Finch, Makromol. Chem., Macromol. Symp., 16, p329, (1988).
[161] Krause, S., Pure Appl.Chem., 58, p1553, (1986).
[162] Hayashida, K., and T. Yoshida, Bull. Faculty Textile Sci., Kyoto Univ., 9, p65, (1979).
[163] Han, C.D., "Multiphase Flow in Polymer Processing", Academic Press, New York, (1981).
[164] Liang, B.R., J.L. White, J.E. Spruiell and B.C. Goswami, Jour. Appl. Polym. Sci., 28, p2011, (1983).
[165] Subramanian, P.M., Polym. Eng. Sci., 25, 8, p483, (1985).
[166] Kuraray Co. Ltd., Kuraray EVAL Resin, (1986).
[167] Sadova, L.P., B.V. Yarlykov, M.L.Kerber, M.S. Akutin, T.I.Saglova and T.V. Babkina, Izv. Viz., Khim. Tekhn.,4, p540, (1977).
[168] Danesi, S., and R.S. Porter, Polymer, 19, p890, (1978).
[169] Akhtar, S., B.Kuriakose, P.P. De. and S.K. De, Plast. Rubber Process. Appl., 7, p11, (1987).
[170] Subramanian, P.M., and V.Mehra, Polym. Eng. Sci.27, 9, p663, (1987).
[171] Dupont Corporation, Selar Barrier Resins, Bulletins E73971, E73973, E73974.
[172] Bataille P., Boisse S., and H.P. Schreiber, Polym. Eng.Sci., 27, 9, p622, (1987).
[173] Biesenberger, J.A., M.Xanthos, M.W.Young, Polym. Eng. Sci., 30, 6, p355, (1990).
[174] F.P. La Mantia, and Curto, D., Polym. Degrad. and Stab., 36, pp131-135, (1992).
[175] Curto, D., A.Valenza, and F.P. La Mantia, Jour. Appl.Polym. Sci.,39, p865, (1990).
[176] Nir, M.M., A. Ram, and J. Miltz,Polym. Mats. Sci. Eng.,Proc. ACS Div. Polym. Mats.Sci. Eng., 67, p405, (1992).
[177] Utracki, L.A., "Polymer Alloys and Blends", p34, Hanser Verlag (1989).
[178] Fernandez, M.L., Sci.Progress Oxford, 74, p257, (1990).
[179] Mark, H.F. et al (eds.), Polymer Blends in "Encyclopedia of Polymer Science and Engineering", vol. 12, p402, (1988).
[180] Utracki, L.A., "Polymer Alloys and Blends", p36, Hanser Verlag (1989).
[181] Utracki, L.A., "Polymer Alloys and Blends", p37, Hanser Verlag (1989).
[182] Utracki, L.A., "Polymer Alloys and Blends", p39, Hanser Verlag (1989).
[183] Walsh, D.J., S.Rostami, and V.B. Singh, Makromol. Chem., 186, p145, (1985).

6.2.2 Polymer Permeability Literature

[1] Crank, J., "The Mathematics of Diffusion", 2nd. ed. p45, (1993).
[2] Barrer, R.M., "Permeation, Diffusion, and Solution of Gases in Organic Polymers", Trans. Farad. Soc., 35, p628, (1939).
[3] Aithal, U. S., T. M. Aminabhavi, and S. S. Shukla, Polym.- Plast., Technol.-Eng., 28(5&6), p567, (1989).
[4] Aithal, U. S.,T. M. Aminbhavi, R. H. Balundgi, and S. S. Shukla, Polym. Plast. Technol. Eng., in press.
[5] Aminabhavi, T.M., U. S. Aithal, and S. S. Shukla, Jour. Macromol. Sci.-Rev. Macromol. Chem. Phys., C29(2&3), p319, (1989).

[6] Pollack, H. D., and H. L Frisch, Jour. Phys. Chem., 63, p1022, (1959).
[7] Kawakami, Y., and Y. Yamashita, Mem. Fac. Eng., Nagoya Univ., 39(1), p62 (1987).
[8] Cassidy, P. E., T. M. Aminbhavi, and C. M. Thompson, Rubber Chem. Technol., Rubber Rev., 56, p594, (1983).
[9] Lebovits, A., Mod. Plast., March, p139, (1966).
[10] Frisch, H.L., Jour. Phys. Chem., 62, p401, (1958).
[11] Laidler, K.J., and K. E. Shuler, J. Chem. Phys., 17, p851, (1949).
[12] Baddeur, R. F., et al, A.C.S. Div. Ind. Eng. Chem., 143rd meeting, Los Angeles, Mar.,(1963).
[13] Barrer, R.M., Jour. Phys. Chem., 61, p178, (1957).
[14] Crank, J., and G. S. Park, Trans. Faraday Soc., 47, p1073, (1951).
[15] Li. N. N., R.B.Long, and E. J. Henley, Ind. Eng. Chem., 57, p18, Mar., (1965).
[16] Kokes, R. J., and F. A. Long, J. Am. Chem. Soc., 75, p6142, (1953).
[17] Barrer, R. M., Trans. Farad. Soc., 35, 628, p644, (1939).
[18] Rogers, C.E., et al, Rec. Dev. Sep. Sci.,2, p107, (1972).
[19] Li N.N., and E. J. Henley, A. I. Ch. E. Jour., 10, p666, (1964).
[20] Kulkarni, P. V., S. B. Rajur, P. Antich, T. M. Aminabhavi, and M.I. Aralaguppi, Jour. Macromol. Sci.-Rev. Macromol. Chem. Phys., C30(3&4), p441, (1990).
[21] Marcandelli, B., E.Martuscelli, G.Testa, A.Seves, Polymer, 34, 10, p2202, (1993).
[22] Baker, R. W., and I. Blume, Chemtech, 16, p232, (1986).
[23] Preston, W. E., J. W. Barlow, and D. R. Paul, Jour. Appl. Polym. Sci., 29, p2251, (1984).
[24] Felder, R. M., and G. S. Huvard, Methods Exp. Phys.,16, p315, (1980).
[25] Ashley, R. J., in "Plastic Materials", Illiffe, London, Chap. 7, (1966).
[26] Bal, R. K., M. Y. Huang,and Y. Y. Ziang, Polym. Bull., 20, p83, (1988).
[27] Marcellin, P., Chim. Ind., Genie Chim., 104, 17, p2141, (1971).
[28] Yun, Z., M. Y. Huang, and Y. Y. Ziang, Polym. Bull., 20, p3, (1988).
[29] Park, G. S., Nato Adv. Study Inst. Ser., Ser. C.181(Synth. Membr. Sci. Eng. Appl.), p57, (1986).
[30] Mears, P., Ibid., p155, (1986).
[31] Ward, W. Jour. III,Ibid.,p389, (1986).
[32] Schultz, S., Ibid., p523, (1986).
[33] Koros, W. J., B. J. Story, S. M. Jordon, K. O'Brien, and G. R. Husk, Polym. Eng. Sci., 27(8), p603, (1987).
[34] Chao, R. R., and S. S. H. Rizvi, AM. Chem. Soc.,Symp. Ser.,365,(Food Packag. Interact.), p217, (1988)
[35] Chiou, J. S., and D. R. Paul, Jour. Appl. Polym. Sci., 32, p4793, (1986).
[36] Min, K. E., and D. R. Paul, Jour. Appl. Polym. Sci., Part B, Polym. Phys., 26, p1201, (1988).
[37] Haraya, K., K. Obata, T. Hakuta, and H. Yoshitome, Maku, 11, p48, (1986).
[38] Haraya, K.,K. Obata, N. Itoh, Y. Shindo, T. Hakuta, and H. Yoshitome, Jour. Membr. Sci.,41, p23, (1989).
[39] Bawer, R. M., and H. T. Chio, Jour. Polym. Sci., Part C, 10, p111, (1966).
[40] Weinkauf, D. H., and D. R. Paul, Polym. Prepr., Am. Chem. Soc., Div. Polym. Chem., 30, p3, (1989).
[41] Slee, J. A., G. A. J. Orchard, D. I. Bower, and I. M. Ward, Jour. Polym. Sci., Part B, Polym . Phys.,27, p71, (1989).
[42] Ward, I.M., 3rd Int.Conf. Diffusion in Polymers, York, UK, Feb.13-15, 1/1,

P.R.I., (1991).
[43] Vittoria, V., A. R.Filho, Jour. Appl. Polym. Sci., 40, 12, p2127, (1992).
[44] Vittoria, V., A. R.Filho, Jour. Appl. Polym. Sci., 49, 2, p253, (1993).
[45] Vittoria, V. A., R. H. Olley, D. C. Basset, Coll. Polym. Sci., 267, p661, (1989).
[46] Courtaulds Films, Interim Technical Data Sheet SPC 40, (1994).
[47] Michaels, A. S., and R. B. Parker Jr., Jour. Polym .Sci., XLI, 53, (1959).
[48] Marcus, S. A., Multilayer Plastics Food Containers, Foods and Drug Packaging, August, (1982).
[49] Dong, J. H., C. K. Huang and Y. Y. Ziang,Polym. Bull.,20, p521, (1988).
[50] Fujita, H., A. Kishimoto, and K. Masumoto, Trans. Faraday Soc., 56, p424, (1960).
[51] Michaels, A. S., and R. B. Parker Jr., Jour. Phys. Chem., 62, p1604, (1958).
[52] ASTM D-1434, "Oxygen Gas Transmission Rate through Plastic Film and Sheeting using a Manometric Cell", (1987).
[53] Lomax, L., Polym. Test., 1, p105, (1980).
[54] Rogers, W. A., R. S. Burity and D. Alpert, Jour. Appl. Phys.,25, p868, (1954).
[55] Ziegel, K. D., and F. R. Eirich, Jour. Polym. Sci., Part A-2, 8, p2015, (1970).
[56] ASTM D-3985, "Oxygen Gas Transmission Rate through Plastic Film and Sheeting using a Coulometric Sensor", (1987).
[57] Spalding M. A., Delassus, P. T., Jour., Plast. Film Sheet, Oct., 6, 4, p292, (1990).
[58] Hori, Y., Z. Fukunaga, S. Shimada, and H. Kashiwara, Polymer, 20, p181, (1979).
[59] Orsat V., B.Panneton, Vigneault C., Canad. Agric. Eng., 34, 2, p183, (1992).
[60] Zhang, W. Z., A. Noderao, M. Satoh, and J. Komiyama, Jour. Membr. Sci., 35, p311, (1988).
[61] Speas, C. A., Pack.Eng., Oct., p78, (1972).
[62] Baysal, B. M., Erbil, H. Y., Jour. Memb. Sci., 26, p199, (1986).
[63] Miltz, J. and S. Ulitzur, Jour. Food Technol., 15, p389, (1980).
[64] Mellwrick, C. R., and C. S. G. Phillips, Jour. Phys. E:Sci. Insts. 6, p1208 (1973).
[65] Clement, C. et al, Polymer Testing, 12, p195, (1993).
[66] Petrak, K. L., and T. J. Bumfrey, Polym. Bull., 3, p311, (1980).
[67] Petrak, K., Jour. Appl. Polym. Sci., 23, p2365, (1979).
[68] Petrak, K. and E. Pitts, Ibid, 25, p879, (1980).
[69] Mercea, P.V., and M. Bartan, Jour. Memb. Sci., 59, 353, (1991).
[70] Major, C. J., and K. Kammermeyer, Mod. Plast., July, p135, (1962).
[71] Peterson, C. M., Jour. App. Polym. Sci., 12, pp2669-2674, (1968).
[72] Garbassi F., Morra, M., and E.Occhiello, Jour. Appl. Polym. Sci., 48,p1331, (1993).
[73] Lyssy, G. H., "Analytic Gas Permeation Fractioner Mod. GPM 200", (1991).
[74] Kaptan Y., O. Pekan, and O. Guven, Jour. Appl. Polym. Sci., 44, p1595, (1992).
[75] Li D., and A. E. Hamielec, Polymer, 34, 7, p1383, (1993).
[76] Alger, A. A., and T. J. Stanley, Polymer, 36, p1501, (1988).
[77] Li, D., S. Zhu, and A. E. Hamielec, Polym. 34, 7, pp1383-1387, (1993).
[78] Marcandalli, B., et al, Desal., 51, p113, (1984).
[79] Kaplan, W.A., Tabor, R.L., Cell.Polym., 12, 2, p102, (1993).
[80] Schlotter, N. E., and P. Y. Furlan, Polym., 33, 16, p3323, (1992).
[81] ASTM F-372-73, "Water Vapour Transmission Rate of Flexible Barrier Materials using an Infrared Detection Technique" (Reapproved 1978).
[82] ASTM Standard E96-80, ASTM (1983).
[83] Banker, G. S., A.Y.Gore, J.Swarbrick, Jour.Pharm., 18, p457, (1966).

[84] Patel, M., J.Patel,A. P.Lemberger, Jour. Pharm. Sci.,53, p286, (1964).
[85] Sfirakis, A., and C. E. Rogers, Polym. Eng. and Sci., 20, 4, p294, (1980).
[86] McCall, D. M., et al, Macromol., 17, pp1644-1649, (1984).
[87] Rogers, C. E., et al, Polym. Sci. and Technol.,1, p297, (1973).
[88] Romero, M.A., et al, Polym., 34, 14, p3004,(1993).
[89] Campion, R. P., "Additional Notes on High Pressure Testing at MERL", 25th March (1993).
[90] Murray, L.J., Pack. Eng., Mar., p76, (1983).
[91] Zobel, M.G.R., Polym. Test., 5, p153, (1985).
[92] De Lassus, P., TAPPI Proceedings, "Polymers, Laminations and Coating Conference", p445, (1985).
[93] Baner, A. L., "Diffusion and Solubility of Toluene Vapour in Polymer Films", 13th Ann. IAPRI Symp., Oslo, May, (1986).
[94] Caldecourt, V., and J. Tou, TAPPI Proceedings, "Polymers, Laminations and Coating Conference", p441, (1985).
[95] Hernandez, R. J., M.S. Thesis, Michigan State Uni., (1984).
[96] Baner, A. L., et al, Curr. Technol. in Flex. Pack., ASTM STP 912, (1986).
[97] Hernandez, R. J., J. R. Giacin, and A. L. Baner, Jour. Plast. Film Sheet, 2, July, p187, (1986).
[98] Franz, R., Pack. Technol. Sci., 6, pp91-102, (1993).
[99] Gilbert, S. G., J. Miltz, and J. R. Giacin, Jour. Food Proc. & Pres., 4, pp27-49, (1980).
[100] Vittoria. V., Jour. Polym. Sci., Polym. Phys. Ed., 24, p451,(1986).
[101] de Candia, F., V. Capodanno and V. Vittoria, Polym. Comm., 29, Sept., p255, (1988).
[102] Wycisk, R., and W. Trochimczuk, Jour. Polym. Sci. Part B:Polym. Phys., 32, p585, (1994).
[103] Meyers, A. W., C. E. Rogers, V. Stannet, and M. Szwarc, "Permeability of Plastic Films and coated Papers to Gases and Vapours", Tappi Monograph Series, 23, p49., (1962).
[104] Bissot, T. C., ACS Symposium Series, vol. 423, p225, (1990).
[105] Cussler, E.L., et al, Jour. Memb. Sci., 38, p161,(1988).
[106] Europ. Plast. News, November, p43, (1995).
[107] Wachtel, J. A. et al, Plast. Eng., Feb., p41, (1985).
[108] Kamal, M. A., et al, Polym. Eng. Sci., 24, 17, pp1337-1347.
[109] Subramanium, P.M., and V. Mehra, Polym. Eng. Sci., 27, 9, p663, (1987).
[110] Granger, V.M., and M.A. Tigani, Tappi Jour., May, p98, (1993).
[111] Lohfink, G.W., and M.R. Kamal, Polym. Eng. Sci., 33, 21, p1404,(1993).
[112] Ryder, L. B., Plast. Eng., May, p41, (1984).
[113] Eur. Plast. News., May, p18, (1994).
[114] Chiou, J. S., and D. R. Paul, Jour. Appl. Polym. Sci., 32, p2897, (1986).
[115] Pappas, N.A., and R. Khanna, Polym. Eng. Sci., 20, 17, p1147, (1980).
[116] Smith, J.S., and N.A. Pappas, Jour. Appl. Polym. Sci., 43, p1219, (1991).
[117] Howsman, G. J., and N. A. Pappas, Jour. Appl. Polym. Sci., 31, p2071, (1986).
[118] Iter, M., M. Ozilgen, and N. Orbey, Polym. Int., 25, p211, (1991).
[119] Kusanagi, K., and S. Yukawa, Polym., 35, 26, p5637, (1994).
[120] Wycisk, R. and W. Trochimczuk, Jour. Polym. Sci., Part B, Rap. Com., 32, p585, (1994).
[121] Brown, W. E., and P. T. DeLassus, Polym. Plast. Technol. Eng., 14, p171,

(1980).
[122] Robeson, L. M., G. A. Nosha, and M. Patzner, Die Angew, Makromol. Chem., 29/30, p47, (1973).
[123] Subramanium, P.M., Polym. Eng. Sci., 25, 8, p483, (1985).
[124] Peterson, C. M., Jour. Appl. Polym. Sci., 12, p2649, (1968).
[125] Hayes, R.A., Jour. Appl. Polym. Sci., 5, p318, (1961).
[126] Ottino, J. M., Sax, J., Polym. Eng. Sci., Feb., 23, 3, p165, (1983).
[127] Vesely, D., 2nd. Int. Conf. on Barrier Packaging Developments, LONDON,10-11 June, paper 22, p1, (1991).
[128] Schwartzenberg, H. G., "Modelling of Gas and Vapour Transport through Hydrophillic Films", p115, in "Food Packaging and Preservation Theory and Practice", ed. M. Mathlouthi, Elsevier, (1986).
[129] Middleman, S., "Principles of Polymer Polymer Processing", McGraw-Hill, pp363-7, (1977).
[130] de Leiris, J. P., "Water Activity and Permeability", p213, in "Food Packaging and Preservation Theory and Practice", ed. M. Mathlouthi, Elsevier, (1986).
[131] Luikov, A. V., "Heat and Mass Transfer", MIR Publ., Moscow, (1980).
[132] Wilmar, O., Proc. Internat. Conf.Spacecraft Structures and Mechanical Testing, Neth., 24-26 April (1991).
[133] Sok, R. M., and H. Berendsen, Jour. Chem .Phys., 6, 15 March, p4699, (1992).
[134] Salame, M., Polym. Eng. Sci. 26, 22, p1543, (1986).
[135] Stannett, V., and Szwarc,M., Jour. Polym. Sci.,16, p89, (1955).
[136] Rogers, C., J. A. Meyer, V. Stannett, and M. Szwarc, Tappi,39, p741, (1956).
[137] Frisch, H. L., Polym. Lett.,1, p581, (1963). [120] Pike, L. and G. D. Wofford, Jour. Plast. Film Sheet, 2, p242, (1986).
[138] Salame, M., private communication to D. W. Van Krevelen, (1987).
[139] Salame, M., private communication from author, (1992).
[140] Bicerano, Jozef, "Prediction of Polymer Properties", p325, Marcel Dekker, (1993).
[141] Fedors, R.F., Polym. Eng. Sci., 14, p147-154, (1974).
[142] Ibid, p472, (1974).
[143] Surgi, M. R., A. J. Polak, and R. C. Sundahl, Jour. Polym. Sci., Pt. A, Polym. Chem.,27, p2761, (1989).
[144] Miltz, J., and S. Eichler, Jour. Appl. Polym. Sci., 50, p2095, (1993).
[145] Van Krevelen, D.W., Properties of Polymers, Chpt.7, Elsevier, Amsterdam,(1990).
[146] Salame, M., private communication to J. Miltz, (1990).

6.3 Chapter 3 References

6.3.1 Multiphase systems preparation references

[1] Wu S., Polym. Eng. Sci., 27, p335 (1987).
[2] Vesely D. and M.A.Parker, 3rd Europ.Symp. Polymer Blends, Cambridge(PRI-publ.), D2/1 (1990).
[3] Olssen, H., Eur. Plast. News, April, 32, (1992).
[4] Favis B.D., and J.P.Chalifoux, Poly. Eng. Sci., 27, p1591, (1987).
[5] Albert H., H. Bartl, Kuhn R., "Co-polymers, Polyblends, and Composites", Academic Press, New York, (1980).
[6] Kuraray EVAL Resins, Kuraray Ltd., Düesseldorf, Dec., pp110-12, (1986).
[7] Raval H., Y.P.Singh, M.H.Mehta and S. Devi, Polym. Int., 24, pp99-104, (1991).

[8] Domingue, J., "Probing the Chemistry of the solid/liquid interface", Amer. Laboratory, Oct., (1990).
[9] ASTM D4440-90, Annual Book of ASTM Standards, p.484-486, March 30th 1990.
[10] Folkes, M. J., and P. S. Hope eds., "Polymer Blends and Alloys", Blackie, p86, (1993).
[11] Park, S.J., B.K.Kim, H.M.Jeong, Eur. Polym. Jour., 26, 2, p131, (1990).
[12] Raval H., Y.P.Singh, M.H.Mehta and S. Devi, Polym. Int., 24, pp105-113, (1991).
[13] Raval H., Y.P.Singh, M.H.Mehta and S. Devi, Polym., 32, 3, pp493-500, (1991).
[14] Cameron R., BP Chemicals, London, Private communication, (1992).
[15] Utracki L.A., P.Sammut, Polym. Networks Blends, 2(1), pp23-29,(1992).
[16] Romero, M., A. Domard, and D. Petit, Polym., 34, 14, p3004, (1993).
[17] Arkles, B., "Silane Coupling Agent Chemistry" in " Silicon Compounds Register and Review", Anderson, R. Arkles, B. Larson, G.L. Petarch Systems Inc., publ. Hüls America Inc., p54, (1987).
[18] Dow Corning Product Information Data Sheet N° 22-1054A-01
[19] Akay, A., N.Batmaz, T.Tincer, Radiat.Phys.Chem., 36, 3, pp345-351, (1990).
[20] Abdul Khadir Z., I.Ishigaki, K.Makuuchi, F.Yoshii, Polymer, 30, p1425, (1989).
[21] Ambrovic, P., E.Borsig, M.Klimova, J. Tino, Jour.Polym.Sci., Polym.Phys., 23, pp105-111, (1985).
[22] Gaylord, N., M.K.Mishra, Jour.Polym.Sci., Polym.Lett.Ed., 21, p23, (1983).
[23] Fowler, R., Plast. Rubb. Today, Jan./Feb.,p8, (1992).
[24] Plazek,D.J., "Viscoelastic and Steady-State Rheological Response", p48, in "Methods of Experimental Physics", vol. 16-Part C, Polymers Physical Properties, ed. R.A.Fava, Academic Press, 1980.

6.3.2 Barrier properties determination references

[1] ASTM E 96-80, Water Vapour Transmission of Materials,Feb.,(1983).
[2] Vrentas, J.S., and J.L. Duda, Jour. Polym. Sci., 21, pp1715-1728, (1977).
[3] Ju, S. T., J.L. Duda, and J.S. Vrentas, Ind. Eng. Chem.Prod. Res. Dev., 20, pp330-335, (1981).
[4] Vrentas, J.S., J.L. Duda, H.C. Ling., and A.C. Hou, Jour. Polym. Sci., Polym.Phys. Ed.,23, pp2469-2475, (1985).
[5] Vrentas, J.S., J.L. Duda, and H.C. Ling., Jour. Appl.Polym. Sci., 33, pp2581-2586, (1987).
[6] Rogers, C.E., "Permeation of gases and vapours in polymers", p36, in "Polymer Permeability",ed. J.Comyn, Elsevier, (1985).
[7] Lomax, M., Polym. Test., 1, p112, (1980).
[8] ASTM D952-90, Annual Book of ASTM Standards,p.336-337, March 30th 1990.
[9] Major, C. J., and K. Kammermeyer, Mod. Plast., July, p179, (1962).
[10] Schlessinger, G.G., in "Handbook of Chemistry and Physics", 52nd edition, ed. R.C. Weast, D-151, (1971).

6.4 Chapter 4 References

[1] Wu S., Polym. Eng. Sci., 27, p335 (1987).
[2] Favis B. D., and J. P. Chalifoux, Polym. Eng. Sci., 27, p1591, (1987).
[3] Vesely D. and M. A. Parker, 3rd Europ.Symp.Polym.Blends, Cambridge(PRI-publ.),D2/1 (1990).
[4] Utracki, L.A., and P.Sammut, Plast.Rubb.Comp. Proc.App.,16, 4, pp221-229, (1991).

[41] Colthup, N. B., L.H. Daly and S. E. Wiberley, "Introduction to Infrared and Raman Spectroscopy", 3rd edn., Academic Press, p100, (1990).
[42] Salame, M., and J. Steingiser, Polym. Plast. Techn. Eng.,8, 2, p155, (1977).
[43] Wu, S., "Polymer Interface and Adhesion", Marcel Dekker, New York, (1982).
[44] Robertson, R.E., in "Computational Modelling of Polymers", J. Bicerano, ed., Dekker, NY NY, Chpt.6.
[45] Seitz, J. T., Jour. Appl. Polym. Sci., submitted for publication.
[46] Polymer Handbook, 3rd ed., V, 414, (1989).
[47] Polymer Handbook, 3rd ed., V, 113, (1989).
[48] Rogers, C. E., "Permeation of gases and vapours in polymers", in "Polymer Permeability", Elsevier, ed. J.Comyn, p28, (1985).
[49] Sfirakis, A., and C. E. Rogers, Polym. Eng. and Sci., 20, 4, p294, (1980).
[50] Zobel, M.G.R., BCL R. and D. Dept., "Determination of odour barrier performance of co-extruded packaging films", Coex '84, Princeton, USA, Oct. (1984).
[51] Salame, M., S.P.E. Transactions, 1, p153, (1961).
[52] Stannett, V., and M. Szwarc, Jour. Polym. Sci., 16, p89, (1955).
[53] Rogers, C. E., et al, Tappi Jour., 39, p741, (1956).
[54] Frisch, H. L., Polym. Lett., 1, p581, (1963).
[55] Corish, P.J. (ed.), Concise Encyclopedia of Polymer Processing & Applications, p493, Pergamon Press, (1992).
[56] Stafford, T., British Gas Scientific Services, North Thames Region, Private Communication, 10th June, (1994).
[57] Dutheillet, Y. and D. Vesely, Proc. Polymat '94, Imp. Coll, London, 151, 22nd Sept. (1994).
[58] Parker, M.A., D. Vesely, Jour. Polym. Sci.(B), 24, pp1869-78, (1986).

6.5 Conclusions and Further Work References

[1] Robeson, L. M., G. A. Nosha, and M. Patzner, Die Angew, Makromol. Chem., 29/30, p47, (1973).

6.6 Appendices References

[1] Utracki L.A., P.Sammut, Polym. Networks Blends, 2(1), pp23-29,(1992).

APPENDIX I

Table 18 : Volume-Concentration Z factor for PP/PA6 blends

Blend wt%	Blend No.	Blend volume fractions ϕ_1 & ϕ_2	$q = \phi_2/\phi_1$	η^*_1 Pa.s	η^*_2 Pa.s	$\lambda = \eta^*_1/\eta^*_2$	$Z = \lambda \times q$	d µm
95% PP/5% B5	1	0.04 & 0.96	23.81	2642	375	7.04	167.6	2.4
85% PP/15% B5	2	0.12 & 0.88	7.13	"	"	7.04	50.2	3.7
70% PP/30% B5	3	0.26 & 0.74	2.92	"	"	7.04	20.6	4.1
60% B5/40% PP	4	0.46 & 0.54	1.20	375	2642	0.142	0.17	1.5
70% B5/30% PP	5	0.35 & 0.65	1.86	"	"	"	0.26	2.9
80% B5/20% PP	6	0.24 & 0.76	3.19	"	"	"	0.45	2.6
90% B5/10% PP	7	0.12 & 0.88	7.18	"	"	"	1.02	2.0
60% A23/40% PP	8	0.44 & 0.56	1.29	"	202	1.856	2.39	3.2
70% PP/30% A23	9	0.25 & 0.75	3.01	202	375	0.539	1.62	2.7
R6000 pellets(≈ 48% PA6/40% PP/12% compatibilizer[1]	10	0.42/0.58[1]	0.717[1]	1.052 (η_0)	0.752 (η_0)	1.402	1.01	0.6
60% B5/40% XLPP	11	0.47 & 0.53	1.14	1268	2642	0.450	0.51	2.5
70% XLPP/30% B5	12	0.25 & 0.75	3.06	2642	1268	2.084	6.38	2.2
60% Plast.B5/40% PP	13	0.38 & 0.62	1.66	375	498	0.753	1.25	3.2
70% PP/30% Plast.B5	14	0.32 & 0.68	2.11	498	375	1.328	2.80	3.9
70% XLPP/30% Plast.B5	15	0.31 & 0.69	2.21	498	1268	0.393	0.87	3.5
60% Plast.B5/40% XLPP	16	0.39 & 0.61	1.58	1268	498	2.546	4.02	2.7
70% PP/26% B5/4% PB3002	17	0.22 & 0.78	3.57	2642	390.7	6.76	24.1	1.6
70% PP/26% B5/4% MAgPP	18	0.22 & 0.78	3.56	"	358.6	7.37	26.2	2.6
70% PP/26% B5/4%(BMAcoMA)gPP	19	0.22 & 0.78	3.57	"	358.4	7.37	26.3	2.1
62% PP/30% B5/8% PB1001	20	0.26 & 0.74	2.92	"	367.5	7.389	21.6	2.9
56% B5/36% PP/8%PB1001	21	0.59 & 0.41	0.69	317.4	2642	0.120	0.18	2.8
62%PP/30% B5/8% (BMAcoMA)gPP	22	0.25 & 0.75	2.92	2642	306.3	8.628	25.2	2.4
56% B5/36% PP/8% (BMAcoMA)gPP	23	0.41 & 0.59	1.46	319.2	2642	0.121	0.18	2.7
66% PP/26% A23/8% PB1001	24	0.21 & 0.79	3.66	202	340.7	0.593	2.17	2.3
56% A23/36% PP/8% PB1001	25	0.41 & 0.59	1.43	202	317.3	0.637	0.44	2.4
66% PP/26% A23/8% (BMAcoMA)gPP	26	0.21 & 0.79	3.67	202	341.81	0.591	2.17	1.7
56% A23/36%PP/8% (BMAcoMA)gPP	27	0.41 & 0.59	1.43	319.2	202	1.58	2.26	3.2

APPENDIX II

Table 19 : Interfacial Slip Factor β for PP/PA6 blends

w_1	w_2	w_3	η_1	η_2	η_3	η^*	G"	β_{12}	$\beta_{1,2}$
0.05(B5)	0.95	———	2642	375	—	803	244.4	0.4879	574 38
0.15(B5)	0.85	———	"	"	—	931	371.58	0.4623	559.51
0.30(B5)	0.70	———	"	"	—	554	636	1.2034	-283 34
0.40	0.60(B5)	———	"	"	—	695	494	1.1122	-113.13
0.30	0.70(B5)	———	"	"	—	1212	118	0 9868	3 8731
0.20	0.80(B5)	———	"	"	—	1152	726	0.8151	292.75
0.10	0.90(B5)	———	"	"	—	1861	2687	0 8849	1031 04
0.30(Plast. B5)	0.70	———	498	"	—	385	1063	1.3966	-919 59
0.30(B5)	0.70(XLPP)	———	2642	1268	—	465	817	2.4917	-2659 5
0.30(Plast.B5)	"	———	498	1268	—	380	1150	2 2795	-2118 4
0.40(XLPP)	0.60(B5)	———	1268	2642	—	603	817	2 4917	-6842 8
0.40	0.60(Plast.B5)	———	375	498	—	391	1663	2.3797	-3210 3
0.40(XLPP)	0.60(Plast.B5)	———	1268	498	—	380	565	2.7182	-4683.5
0.30(A23)	0.70	———	202	375	—	236	260	1.2642	-149 67
0.40	0.60(A23)	———	375	202	—	200	186.1	1.2386	-90 61
0.08(PB3002)	0.92(PP)	———	665	375	—	1089	983	0.2511	2713.32
0.26(B5)	0.70	0.04(PB3002)	2642	375	665	630	1003	0.7838	1535 04
0.08(PB3002)	0.92(B5)	———	665	2642	—	4153	1767	0.5139	1480
0.08(MA-g-PP)	0.92(PP)	———	67.5	375	—	514	826	0.7565	698 4
0.26(B5)	0.70	0.04(MA-g-PP)	2642	375	67.5	633	1376	0.6206	1963.56
0.08(MA-g-PP)	0.92(B5)	———	67.5	2642	—	1721	778	0.2259	2219.78
0.08(PB1001)	0.92(PP)	———	57.9	375	—	515.5	692	0.7485	641.37
0.30(B5)	0.26	0.08(PB1001)	2642	375	57.9	562	918 87	0 8986	378 82
0.36	0.56(B5)	0.08(PB1001)	375	2642	57.9	562	271.41	0.6968	325 64
0.08(PB1001)	0.92(B5)	———	57.9	2642	—	5498	1821	0.3739	55 6
0.08((BMAcoMA)gPP))	0.92(PP)	———	68	375	—	887	965	0.3106	2452.18
0.26(B5)	0.70	0.04((BMAcoMA)gPP))	2642	375	68	1013	1190	0.1934	1187.3
0.36(B5)	0.56	0.08((BMAcoMA)gPP))	2642	375	68	499	571	0 6534	804 60
0.36	0.56(B5)	0.08((BMAcoMA)gPP))	375	2642	68	520	321.71	0 6655	425 82
0.08((BMAcoMA)gPP))	0.92(B5)	———	68	2642	—	4128	1763	0.1589	1044 81
0.08(MA-g-PP)	0.92(A23)	———	67.5	202	—	302	337	0.5769	525 55
0.08(PB3002)	0.92(A23)	———	665	202	—	254	117	0.8422	68 06
0.26(A23)	0.66	0.08(PB1001)	202	375	57.9	493	508.93	0.458	973 5
0.36	0.56(A23)	0.08(PB1001)	375	202	57.9	232	311.35	0 8429	193 62
0.08(PB1001)	0.92(A23)	———	57.9	202	—	459	236	0.367	4202.15
0.36(A23)	0.56	0.08((BMAcoMA)gPP))	202	375	68	461	416.15	0.5136	845.36
0.36	0.56(A23)	0.08((BMAcoMA)gPP))	375	202	68	184	163.11	0.1072	-69.224
0.08((BMAcoMA)gPP))	0.92(A23)	———	68	202	—	489	403	0.3568	955.38

APPENDIX III

Relevant research work presented at technical conferences

(i) "Chemical Interaction in Nylon-6/Polypropylene Blends" - Poster presented at the Fourth European Symposium on Polymer Blends, Capri, Italy, May 1993.

(ii) "Phase Dispersion in Immiscible Blends" - Paper presented at Polymat '94, Imperial College, London, September 1994.